

PROBABILISTIC SEISMIC HAZARD ANALYSIS: A SENSITIVITY
STUDY WITH RESPECT TO DIFFERENT MODELS

A THESIS SUBMITTED TO
THE GRADUATE SCHOOL OF NATURAL AND APPLIED SCIENCES
OF
MIDDLE EAST TECHNICAL UNIVERSITY

BY

NAZAN YILMAZ ÖZTÜRK

IN PARTIAL FULFILLMENT OF THE REQUIREMENTS
FOR
THE DEGREE OF DOCTOR OF PHILOSOPHY
IN
CIVIL ENGINEERING

FEBRUARY 2008

Approval of the thesis:

**PROBABILISTIC SEISMIC HAZARD ANALYSIS: A SENSITIVITY
STUDY WITH RESPECT TO DIFFERENT MODELS**

submitted by **NAZAN YILMAZ ÖZTÜRK** in partial fulfillment of the requirements for the degree of **Doctor of Philosophy in Civil Engineering Department, Middle East Technical University** by,

Prof. Dr. Canan Özgen _____
Dean, Graduate School of **Natural and Applied Sciences**

Prof. Dr. Güney Özcebe _____
Head of Department, **Civil Engineering**

Prof. Dr. M. Semih Yüçemen _____
Supervisor, **Civil Engineering Dept., METU**

Examining Committee Members:

Prof. Dr. Ali Koçyiğit _____
Geological Engineering Dept., METU

Prof. Dr. M. Semih Yüçemen _____
Civil Engineering Dept., METU

Prof. Dr. Reşat Ulusay _____
Geological Engineering Dept., Hacettepe University

Assoc. Prof. Dr. Ahmet Yakut _____
Civil Engineering Dept., METU

Assoc. Prof. H. Şebnem Düzgün _____
Mining Engineering Dept., METU

Date: _____ 08.02.2008

I hereby declare that all information in this document has been obtained and presented in accordance with academic rules and ethical conduct. I also declare that, as required by these rules and conduct, I have fully cited and referenced all material and results that are not original to this work.

Name, Last name : Nazan Yılmaz Öztürk

Signature :

ABSTRACT

PROBABILISTIC SEISMIC HAZARD ANALYSIS: A SENSITIVITY STUDY WITH RESPECT TO DIFFERENT MODELS

Yılmaz Öztürk, Nazan

Ph.D., Department of Civil Engineering

Supervisor: Prof. Dr. M. Semih Yüçemen

February 2008, 253 pages

Due to the randomness inherent in the occurrence of earthquakes with respect to time, space and magnitude as well as other various sources of uncertainties, seismic hazard assessment should be carried out in a probabilistic manner.

Basic steps of probabilistic seismic hazard analysis are the delineation of seismic sources, assessment of the earthquake occurrence characteristics for each seismic source, selection of the appropriate ground motion attenuation relationship and identification of the site characteristics. Seismic sources can be modeled as area and line sources. Also, the seismic activity that can not be related with any major seismic sources can be treated as background source in which the seismicity is assumed to be uniform or spatially smoothed. Exponentially distributed magnitude and characteristic earthquake models are often used to describe the magnitude recurrence relationship. Poisson and renewal models are used to model the occurrence of earthquakes in the time domain.

In this study, the sensitivity of seismic hazard results to the models associated with the different assumptions mentioned above is investigated. The effects of different sources of uncertainties involved in probabilistic seismic hazard analysis methodology to the results are investigated for a number of sites with different distances to a single fault. Two case studies are carried out to examine the influence of different assumptions on the final results based on real data as well as to illustrate the implementation of probabilistic seismic hazard analysis methodology for a large region (e.g. a country) and a smaller region (e.g. a province).

Keywords: Seismic Hazard, Seismic Source, Magnitude Distribution, Renewal, Poisson, Earthquake.

ÖZ

OLASILIKSAL SİSMİK TEHLİKE ANALİZİ: DEĞİŞİK MODELLERE GÖRE DUYARLILIK ÇALIŞMASI

Yılmaz Öztürk, Nazan

Doktora, İnşaat Mühendisliği Bölümü

Tez Yöneticisi: Prof. Dr. M. Semih Yüçemen

Şubat 2008, 253 sayfa

Deprem oluşumlarının zaman, yer ve büyüklük bakımından gösterdikleri rassallık ve diğer çeşitli belirsizlikler nedeniyle sismik tehlikenin belirlenmesi olasılığa dayanan yöntemlerle yapılmalıdır.

Olasılıksal sismik tehlike analizinin başlıca adımları sismik kaynakların ve bu kaynakların her biri için deprem oluşum özelliklerinin belirlenmesi, uygun azalım ilişkisinin seçilmesi ve sahadaki zemin özelliklerinin saptanmasıdır. Sismik kaynaklar alan ve çizgi kaynaklar olarak modellenebilir. Ayrıca, herhangi bir ana sismik kaynak ile ilişkilendirilemeyen sismik etkinlik, deprenselliğin bir biçimli ya da mekansal olarak yaygınlaştırılmış olduğu kabul edilen arka plan kaynak olarak incelenebilir. Üstel dağılımlı büyüklük ve karakteristik deprem modelleri büyüklük-tekrarlanma ilişkilerini tanımlamak için en sık kullanılanlardır. Poisson ve yinelenme modelleri depremlerin zaman uzayıdaki oluşumlarını modellemek için kullanılmaktadır.

Bu alıřmada sismik tehlike sonularının yukarıda bahsedilen deęiřik varsayımlarla iliřkilendirilen modellere duyarlılıęı arařtırılmıřtır. Olasılıksal sismik tehlike analizindeki deęiřik belirsizliklerin sonulara etkileri bir faydan oluřan sismik kaynaęa deęiřik uzaklıklarda yer alan birkaç saha iin arařtırılmıřtır. Deęiřik varsayımların nihai sonulara olan etkisini gerek veriye dayalı olarak incelemek ve olasılıksal sismik tehlike ynteminin byk (bir lke gibi) ve daha kk bir blgenin (bir kent gibi) sismik tehlikesinin belirlenmesi iin uygulanmasını gstermek amacıyla iki rnek alıřma yapılmıřtır.

Anahtar Kelimeler: Sismik Tehlike, Sismik Kaynak, Byklk Daęılımı, Yinelenme, Poisson, Deprem.

to my family...

ACKNOWLEDGEMENTS

This study was accomplished under the supervision of Prof. Dr. M. Semih Yücemem. I would like to thank him for his continuous guidance, advice, patience, and support throughout the period of this study. His supervision made my biggest academic achievement possible. I am grateful to him for making my way to the academic world.

I want to thank Assoc. Prof. Dr. Ahmet Yakut and Assoc. Prof. Dr. H. Şebnem Düzgün for their valuable suggestions and encouraging comments during the progress of this dissertation.

I would like to thank Prof. Dr. Ali Koçyiğit from the Geological Engineering Department, for his contributions towards my understanding of tectonics and in particular, sharing his knowledge on the faults located in Turkey with me.

I want to thank Prof. Dr. Reşat Ulusay for his detailed review of the manuscript of this dissertation and his valuable suggestions.

This thesis started in the structural mechanics laboratory of Civil Engineering Department. I would like to thank all my friends from the lab for their help and support.

The majority of this study is carried at the Earthquake Engineering Research Center (EERC) at METU. I want to thank to Prof. Dr. M. Semih Yücemem once again for providing the office there and Asst. Prof. Dr. Altuğ Erberik and İlker Kazaz for their supports during all stages of this dissertation.

Special thanks go to my lifelong friend (or my little sister) Dr. Ayşegül Askan-Gündoğan for being nearby in the beginning of this study as well as catching up in

the end. In the mean time, via long-distance phone calls, she proved me that distances do not matter in friendships.

I would like to thank Dr. Erol Kalkan for devoting his time and sharing the documents on the subject of this study and the code for spatially smoothed seismicity model.

My good friends; Eser Tosun, Selim Günay, Berna Unutmaz, Emriye Kazaz, Sermin Oğuz Topkaya, Sergen Bayram and Altuğ Bayram, deserve thanks for their support and patience.

I also would like to extend my thanks to the staff of the Earthquake Research Department at the General Directorate of Disaster Affairs, especially Dr. Murat Nurlu, current director of the Laboratory Division, for his support and understandings. I owe thanks to Cenk Erkmen, Hakan Albayrak, Tülay Uran, Tuğbay Kılıç and Ulubey Çeken for their theoretical and technical supports.

I would like to thank my father, mother, sister and brother for their love, understanding and encouragement throughout my life and for forgiving me for all the postponed get-togethers with them. I promise to make up for those times after I finish.

Finally, I would like to give my thanks to my husband for his invaluable support during this long period.

TABLE OF CONTENTS

ABSTRACT.....	iv
ÖZ.....	vi
ACKNOWLEDGEMENTS.....	ix
TABLE OF CONTENTS.....	xi
LIST OF TABLES.....	xv
LIST OF FIGURES.....	xvii
CHAPTER	
1. INTRODUCTION.....	1
1.1 GENERAL.....	1
1.2 LITERATURE SURVEY.....	2
1.3 OBJECTIVES AND SCOPE OF THE STUDY.....	6
2. ALTERNATIVE MODELS APPLIED IN SEISMIC HAZARD ANALYSIS.....	8
2.1 INTRODUCTION.....	8
2.2 DETERMINISTIC SEISMIC HAZARD ANALYSIS.....	9
2.3 PROBABILISTIC SEISMIC HAZARD ANALYSIS.....	13
2.3.1 Seismic Sources.....	14
2.3.2 Magnitude Recurrence Relationship.....	20
2.3.3 Modeling of Earthquake Occurrences.....	25
2.3.4 Attenuation Relationships (Ground Motion Prediction Equations).....	30
2.3.4.1 Attenuation Models Developed for Other Countries....	31
2.3.4.1.1 <i>Abrahamson and Silva (1997)</i>	31
2.3.4.1.2 <i>Boore et al. (1997)</i>	34
2.3.4.1.3 <i>Sadigh et al. (1997)</i>	36
2.3.4.1.4 <i>Ambraseys et al. (1996)</i>	41

2.3.4.2	Attenuation Models Developed for Turkey.....	43
2.3.4.2.1	<i>Inan et al. (1996)</i>	43
2.3.4.2.2	<i>Aydan et al. (1996) and Aydan (2001)</i>	43
2.3.4.2.3	<i>Gülkan and Kalkan (2002), Kalkan and Gülkan (2004)</i>	44
2.3.4.2.4	<i>Özbey et al. (2004)</i>	47
2.3.4.2.5	<i>Ulusay et al. (2004)</i>	48
2.3.5	Seismic Hazard Calculations.....	50
2.3.6	Consideration of Uncertainties.....	51
2.3.6.1	Uncertainty Due to Attenuation Equation.....	52
2.3.6.2	Uncertainty in the Spatial Distribution of Earthquakes..	60
2.3.6.3	Uncertainty in the Magnitude Distribution.....	77
2.3.6.4	Uncertainty in the Temporal Distribution of Earthquakes.....	80
2.3.6.5	Uncertainties in Earthquake Catalogs.....	87
2.3.7	Logic Tree Methodology.....	87
2.3.8	Deaggregation of Seismic Hazard.....	90
3.	CASE STUDY FOR A COUNTRY: SEISMIC HAZARD MAPPING FOR JORDAN.....	93
3.1	INTRODUCTION.....	93
3.2	PREVIOUS PROBABILISTIC SEISMIC HAZARD ASSESSMENT STUDIES FOR JORDAN.....	94
3.3	ASSESSMENT OF SEISMIC HAZARD FOR JORDAN.....	96
3.3.1	Seismic Database and Seismic Sources.....	96
3.3.1.1	Seismic Database.....	96
3.3.1.2	Seismic Sources.....	99
3.3.2	Alternative Models.....	103
3.3.2.1	Model 1.....	103
3.3.2.2	Model 2 and Model 3.....	104
3.3.2.3	Model 4.....	105
3.3.3	Seismic Hazard Computations.....	110

3.3.4 “Best Estimate” Seismic Hazard Maps for Jordan.....	135
4. CASE STUDY FOR A REGION: SEISMIC HAZARD MAPPING FOR THE BURSA PROVINCE.....	145
4.1 INTRODUCTION.....	145
4.2 PREVIOUS PROBABILISTIC SEISMIC HAZARD ASSESSMENT STUDIES FOR BURSA.....	146
4.3 ASSESSMENT OF SEISMIC HAZARD FOR BURSA.....	147
4.3.1 Seismic Database and Seismic Sources.....	147
4.3.1.1 Seismic Database.....	147
4.3.1.2 Seismic Sources.....	150
4.3.2 Methodology.....	151
4.3.2.1 Seismic Hazard Resulting From Background Seismic Activity.....	154
4.3.2.2 Seismic Hazard Resulting From Faults.....	173
4.3.3 “Best Estimate” of Seismic Hazard for the Bursa Province.....	187
5. SUMMARY AND CONCLUSIONS.....	196
5.1 SUMMARY.....	196
5.2 DISCUSSION OF RESULTS AND MAIN CONCLUSIONS.....	197
5.3 RECOMMENDATIONS FOR FUTURE STUDIES.....	202
REFERENCES.....	205
APPENDICES	
A. GRAPHS SHOWING THE DIFFERENCE BETWEEN THE SEISMIC HAZARD RESULTS OBTAINED BY IGNORING AND CONSIDERING RUPTURE LENGTH UNCERTAINTY.....	217
B. EARTHQUAKE CATALOG PREPARED FOR JORDAN.....	225
C. SEISMIC HAZARD MAPS FOR JORDAN BASED ON DIFFERENT MODELS.....	230
D. MAIN SEISMIC DATABASE COMPILED FOR BURSA FROM THE CATALOGS OF EARTHQUAKE RESEARCH DEPARTMENT, GENERAL DIRECTORATE OF DISASTER AFFAIRS.....	237

E. MAIN SHOCK SEISMIC DATABASE COMPILED FOR BURSA
FROM THE CATALOGS OF EARTHQUAKE RESEARCH
DEPARTMENT, GENERAL DIRECTORATE OF DISASTER
AFFAIRS..... 246
CURRICULUM VITAE 251

LIST OF TABLES

TABLES

Table 2.1	Parameters of the Fault and the Scenario Earthquake Model Used for İstanbul in This Study (JICA, 2002).....	11
Table 2.2	Mean and Median PGA Values Estimated at the Site by Using Different Attenuation Relationships for Rock Site Condition in DSHA.....	12
Table 2.3	Coefficients for the Average Horizontal Component (Abrahamson and Silva, 1997).....	35
Table 2.4	Smoothed Coefficients for Pseudo-Acceleration Response Spectra (g) (Boore et al., 1997).....	37
Table 2.5	Coefficients for Rock Sites with $M_w \leq 6.5$ (Sadigh et al., 1997).....	39
Table 2.6	Coefficients for Rock Sites with $M_w > 6.5$ (Sadigh et al., 1997).....	39
Table 2.7	Dispersion Relationships for Horizontal Rock Motion (Sadigh et al., 1997).....	40
Table 2.8	Coefficients for Deep Soil Sites (Sadigh et al., 1997).....	40
Table 2.9	Coefficients of the Attenuation Relationship Proposed by Ambraseys et al. (1996).....	42
Table 2.10	Coefficients of Attenuation Relationships Developed by Gülkan and Kalkan (2002).....	45
Table 2.11	Coefficients of Attenuation Relationships Developed by Kalkan and Gülkan (2004).....	46
Table 2.12	Site Class Definitions Used by Özbey et al. (2004).....	48
Table 2.13	Attenuation Coefficients in the Equation Proposed by Özbey et al. (2004).....	49
Table 2.14	Examples of Uncertainties in Seismic Hazard Analysis (McGuire, 2004).....	52

Table 2.15	Relationships between Magnitude and Rupture Length.....	61
Table 2.16	Parameters of the Darıca, Adalar, Yeşilköy and Kumburgaz Segments.....	68
Table 2.17	Calculations of Multi-Segment and Individual Segment Probabilities According to the Cascade Methodology Defined by Cramer et al. (2000).....	71
Table 3.1	Space and Time Windows to Identify Secondary Events (After Deniz and Yüçemen, 2005).....	98
Table 3.2	Parameters of Seismic Sources Considered in Model 1.....	104
Table 3.3	Parameters of Seismic Sources Considered in Model 2 and Model 3.....	105
Table 3.4	Parameters of Seismic Sources Considered in Model 4.....	108
Table 3.5	PGA and SA (0.2 sec and 1.0 sec) Values Corresponding to Different Return Periods for the Four Sites According to Different Assumptions (in g).....	123
Table 4.1	b, β and ν Values Computed According to Alternative Assumptions for the Background Seismic Activity.....	154
Table 4.2	Maximum PGA Values (in g) Obtained from Background Area Source with Uniform Seismicity.....	156
Table 4.3	Parameters of the Fault Segments Used in This Study (Koçyiğit, 2005; Yüçemen et al., 2006).....	174
Table 4.4	Subjective Probabilities Assigned to Different Assumptions.....	187
Table B.1	Main Shocks in the Earthquake Catalog Prepared for Jordan.....	225
Table D.1	All Earthquakes in the Seismic Database Compiled for Bursa.....	237
Table E.1	Mainshocks in the Seismic Database Compiled for Bursa.....	246

LIST OF FIGURES

FIGURES

Figure 2.1	Schematic Description of DSHA for a Site.....	10
Figure 2.2	Map Showing the Location of the Fault (F) Forming the Basis for the Scenario Earthquake Model Used for İstanbul in This Study (JICA, 2002).....	11
Figure 2.3	Schematic Description of the Classical PSHA Methodology.....	15
Figure 2.4	Linear, Bilinear and Parabolic Magnitude Recurrence Relationships (Yüçemen, 1982).....	23
Figure 2.5	Characteristic Earthquake Model Proposed by Youngs and Coppersmith (1985).....	24
Figure 2.6	Hazard Rate Functions for Different Inter-Event Time Distributions (Matthews et al., 2002).....	28
Figure 2.7	Median Peak Ground Acceleration (PGA) Curve Predicted for Kocaeli, 1999 Earthquake by Using Kalkan and Gülkan (2004) Attenuation Relationship at Rock Sites; Distribution of PGA Values at 1 km Distance and the Recorded Data.....	53
Figure 2.8	(a) Probability Density Function of Ground Motion Parameter, Y, for a Single Scenario, (b) Complementary Cumulative Distribution Function Describing the Probability of Ground Motion Parameter Exceeding the Level, Y, for a Single Scenario.....	54
Figure 2.9	Probability Density Functions Corresponding to Different Values of $\sigma_{\ln(\text{PGA})}$	55
Figure 2.10	Hazard Curves Corresponding to Different Values of $\sigma_{\ln(\text{PGA})}$	56
Figure 2.11	Probability Density Functions of PGA Truncated at Different Levels.....	58

Figure 2.12	Hazard Curves Corresponding to Truncation of Attenuation Residuals at Different Levels.....	58
Figure 2.13	Hazard Curves Obtained by Using Different Attenuation Relationships.....	59
Figure 2.14	Locations of Fault and Sites Considered in the Analyses Performed to Investigate the Effect of Rupture Length Uncertainty on Seismic Hazard Results.....	63
Figure 2.15	Differences in Seismic Hazard Values Obtained for Site 1c by Using Different Values of Standard Deviation for Logarithm of Rupture Length.....	65
Figure 2.16	Variation of Rupture Length as a Function of Earthquake Magnitude According to the Relationships Proposed by Wells and Coppersmith (1994), Bonilla, et al. (1984) and Ambraseys and Jackson(1998).....	66
Figure 2.17	Seismic Hazard Curves Obtained for Site 1c by Using Different Rupture Length Estimation Equations for Magnitude 5 Earthquake...	66
Figure 2.18	Locations of Darıca (D), Adalar (A), Yeşilköy (Y) and Kumburgaz (K) Segments (Yüçemen et al., 2006).....	67
Figure 2.19	Seismic Hazard Curves Obtained by Considering Segmentation Concept and Fault-Rupture Model.....	69
Figure 2.20	Seismic Hazard Curves Obtained for the Three Sites by Using Cascade and Fault Segmentation Models.....	72
Figure 2.21	Locations of Sites, Line (Fault) Source and Area Source Representing the Fault.....	73
Figure 2.22	Seismic Hazard Curves Obtained by Using Area and Line (Fault) Source Models.....	74
Figure 2.23	Probability Density Functions Corresponding to Truncated Exponential Distribution (TED) and Characteristic Earthquake Model (CEM) with Varying Δm values.....	78

Figure 2.24	Probability Density Functions Corresponding to Purely Characteristic Earthquake Model (PCEM) and Truncated Gaussian Distribution (TGD) for Characteristic Magnitudes and Truncated Exponential Distribution (TED) for Smaller Magnitudes.....	79
Figure 2.25	Seismic Hazard Curves for Site 4 Corresponding to: Truncated Exponential Distributions for $4.5 < m < 7.5$ (TED); Characteristic Earthquake Model (CEM) with Varying Δm values; Purely Characteristic Earthquake Model Combined with Exponential Distribution for Smaller Magnitudes ($4.5 \leq m \leq 7.0$) (PCEM&TED); Truncated Gaussian Distribution for Characteristic Magnitudes ($7.22 \leq m \leq 7.78$) Combined with Exponential Distribution for Smaller magnitudes ($4.5 \leq m \leq 7.0$) (TGD&TED).....	80
Figure 2.26	Estimated Ruptures (Thick Dashed Green Lines), Modified Mercalli Intensity (MMI) Values (Yellow Dots), Sites of Damage Potentially Enhanced by Soft Sediments (Red Dots), Moment Magnitude M Needed to Satisfy the Observations for a Given Location (Red Dashed Contours) for Large Earthquakes Occurred between A.D. 1500 and 2000 (After Parsons, 2004).....	82
Figure 2.27	Probability Density Functions Corresponding to the BPT and LN Distributions Based on the Mean Inter-Event Time of $\mu_T = 54$ years and $\alpha = \text{cov} = 0.5$	83
Figure 2.28	Hazard Functions Corresponding to the BPT and LN Distributions Based on the Mean Inter-Event Time of $\mu_T = 54$ years and $\alpha = \text{cov} = 0.5$	83
Figure 2.29	Variation of Equivalent Mean Rate of Characteristic Earthquakes Calculated Based on Eqs. (2.20) and (2.28) for the BPT and LN Distributions.....	85

Figure 2.30	Seismic Hazard Curves for Site 4 Corresponding to the Combinations of Renewal Model with PCEM&TED and CEM; Poisson Model with PCEM and CEM with $\Delta m=1.0$	86
Figure 2.31	A General Logic Tree (After Risk Engineering, 2006).....	89
Figure 2.32	Examples of Deaggregation Graphs Obtained from a Seismic Hazard Analysis Carried Out by Using EZ-FRISK (Risk Engineering, 2005).....	92
Figure 3.1	Map Showing the Spatial Distribution of Main Shocks in the Catalog Compiled for the Seismic Hazard Assessment of Jordan.....	100
Figure 3.2	Tectonic Setting of Dead Sea Transform Fault System (After Barazangi, 1983).....	101
Figure 3.3	Locations of Area Sources Used in This Study (After Jiménez, 2004).....	102
Figure 3.4	Locations of Line Sources Used in This Study (After Jiménez, 2004).....	102
Figure 3.5	Map Showing the Distribution of Earthquakes Used in Spatially Smoothed Seismicity Model and Locations of the Cities for Which Seismic Hazard are Computed.....	109
Figure 3.6	Magnitude-Recurrence Relationship Derived from the Data Used in Spatially Smoothed Seismicity Model.....	110
Figure 3.7	Seismic Hazard Curves Obtained for the Site Located in Amman....	112
Figure 3.8	Seismic Hazard Curves Obtained for the Site Located in Azraq.....	112
Figure 3.9	Seismic Hazard Curves Obtained for the Site Located in Aqaba.....	113
Figure 3.10	Seismic Hazard Curves Obtained for the Site Located in Irbid.....	113
Figure 3.11	Contributions of the Different Seismic Sources to the Seismic Hazard at the Site Located in Amman.....	114
Figure 3.12	Contributions of the Different Seismic Sources to the Seismic Hazard at the Site Located in Azraq.....	116
Figure 3.13	Contributions of the Different Seismic Sources to the Seismic Hazard at the Site Located in Aqaba.....	118

Figure 3.14	Contributions of the Different Seismic Sources to the Seismic Hazard at the Site Located in Irbid.....	120
Figure 3.15	Seismic Hazard Map for PGA (in g) Obtained by Using Spatially Smoothed Seismicity Model for a Return Period of 475 Years.....	127
Figure 3.16	Seismic Hazard Map for PGA (in g) Obtained by Using Spatially Smoothed Seismicity Model for a Return Period of 1000 Years.....	127
Figure 3.17	Seismic Hazard Map for PGA (in g) Obtained by Using Spatially Smoothed Seismicity Model for a Return Period of 2475 Years.....	128
Figure 3.18	Seismic Hazard Map Showing the PGA Values (in g) Obtained by Using Spatially Smoothed Seismicity Model for a Return Period of 2475 Years and Epicenters of Earthquakes Considered in the Assessment of Seismic Hazard.....	128
Figure 3.19	Map Showing the Spatial Variation of the Difference between PGA Values Obtained by Using Spatially Smoothed Seismicity Model and Background Seismic Source with Uniform Seismicity for a Return Period of 2475 Years and Epicenters of Earthquakes....	129
Figure 3.20	Map Showing the Spatial Variation of the Difference between the PGA Values Obtained from Model 2 and Model 1 for a Return Period of 475 Years.....	129
Figure 3.21	Map Showing the Spatial Variation of the Difference between the PGA Values Obtained from Model 2 and Model 1 for a Return Period of 2475 Years.....	130
Figure 3.22	Map Showing the Spatial Variation of the Difference between the PGA Values Obtained from Model 2 and Model 1 for a Return Period of 2475 Years and Locations of Area Seismic Sources (Dashed Black Lines) and Line Sources (Black Lines).....	130
Figure 3.23	Map Showing the Spatial Variation of the Difference between the PGA Values Obtained from Model 3 and Model 2 for a Return Period of 475 Years.....	131

Figure 3.24	Map Showing the Spatial Variation of the Difference between the PGA Values Obtained from Model 3 and Model 2 for a Return Period of 2475 Years.....	131
Figure 3.25	Map Showing the Spatial Variation of the Difference between the PGA Values Obtained from Model 3 and Model 2 for a Return Period of 2475 Years and Locations of Line Sources (Black Lines)..	132
Figure 3.26	Map Showing the Spatial Variation of the Difference between the PGA Values Obtained from Model 4 and Model 3 for a Return Period of 475 Years.....	132
Figure 3.27	Map Showing the Spatial Variation of the Difference between the PGA Values Obtained from Model 4 and Model 3 for a Return Period of 2475 Years.....	133
Figure 3.28	Map Showing the Spatial Variation of the Difference between the PGA Values Obtained from Model 4 and Model 3 for a Return Period of 2475 Years and Locations of Line Sources (Black Lines) and Epicenters of Earthquakes Considered in Spatially Smoothed Seismicity Model.....	133
Figure 3.29	Logic Tree Formulation for the Combinations of Different Assumptions (The values given in the parentheses are the subjective probabilities assigned to the corresponding assumptions.).....	136
Figure 3.30	Best Estimate Seismic Hazard Map of Jordan for PGA (in g) Corresponding to 10% Probability of Exceedance in 50 Years (475 Years Return Period).....	137
Figure 3.31	Best Estimate Seismic Hazard Map of Jordan for PGA (in g) Corresponding to 5% Probability of Exceedance in 50 Years (1000 Years Return Period).....	137
Figure 3.32	Best Estimate Seismic Hazard Map of Jordan for PGA (in g) Corresponding to 2% Probability of Exceedance in 50 Years (2475 Years Return Period).....	138

Figure 3.33	Best Estimate Seismic Hazard Map of Jordan for SA at 0.2 sec (in g) Corresponding to 10% Probability of Exceedance in 50 Years (475 Years Return Period).....	138
Figure 3.34	Best Estimate Seismic Hazard Map of Jordan for SA at 0.2 sec (in g) Corresponding to 5% Probability of Exceedance in 50 Years (1000 Years Return Period).....	139
Figure 3.35	Best Estimate Seismic Hazard Map of Jordan for SA at 0.2 sec (in g) Corresponding to 2% Probability of Exceedance in 50 Years (2475 Years Return Period).....	139
Figure 3.36	Best Estimate Seismic Hazard Map of Jordan for SA at 1.0 sec (in g) Corresponding to 10% Probability of Exceedance in 50 Years (475 Years Return Period).....	140
Figure 3.37	Best Estimate Seismic Hazard Map of Jordan for SA at 1.0 sec (in g) Corresponding to 5% Probability of Exceedance in 50 Years (1000 Years Return Period).....	140
Figure 3.38	Best Estimate Seismic Hazard Map of Jordan for SA at 1.0 sec (in g) Corresponding to 2% Probability of Exceedance in 50 Years (2475 Years Return Period).....	141
Figure 3.39	Best Estimate Seismic Hazard Map of Jordan for SA at 0.2sec (in g) Corresponding to 2% Probability of Exceedance in 50 Years (2475 Years Return Period) and Locations of Faults.....	142
Figure 3.40	Seismic Hazard Maps Derived for PGA with 10% Probability of Exceedance in 50 Years by (a) Yücemem (1992) (Values are given in terms of %g) (b) Al-Tarazi and Sandvol (2007) (Values are given in terms of cm/sec ²) (c) This study (Values are given in terms of g).....	143
Figure 4.1	Map Showing the Locations of Faults (Thick Lines in Various Colors) Considered in This Study (Yücemem et al., 2006; Koçyiğit, 2005; Koçyiğit, 2006; Emre and Awata (2003), Awata et al., 2003; Şaroğlu et al. ,1992; Koçyiğit, 2007).....	152

Figure 4.2	Map Showing the Faults (Thick Black Lines) and the Spatial Distribution of All Earthquakes.....	153
Figure 4.3	Map Showing the Faults (Thick Black Lines) and the Spatial Distribution of Main Shocks.....	153
Figure 4.4	Schematic Description of the Procedure Utilized in the Assessment of Background Seismic Activity.....	157
Figure 4.5	Seismic Hazard Curves Obtained by Using Spatially Smoothed Seismicity Model with; (a) Main Shocks in the Incomplete Database, (b) All Earthquakes in the Incomplete Database, (c) Main Shocks and Adjusting for Incompleteness, (d) All Earthquakes and Adjusting for Incompleteness and by Using Uniform Seismicity with; (e) Main Shocks in the Incomplete Database, (f) All Earthquakes in the Incomplete Database, (g) Main Shocks and Adjusting for Incompleteness, (h) All Earthquakes and Adjusting for Incompleteness.....	158
Figure 4.6	Seismic Hazard Maps for PGA (in g) Corresponding to the Return Period of 475 Years Obtained by Using Spatially Smoothed Seismicity Model with Main Shocks (a) Incomplete Database (b) Database Adjusted for Incompleteness.....	159
Figure 4.7	Seismic Hazard Maps for PGA (in g) Corresponding to the Return Period of 475 Years Obtained by Using Spatially Smoothed Seismicity Model with All Earthquakes (a) Incomplete Database (b) Database Adjusted for Incompleteness.....	160
Figure 4.8	Seismic Hazard Maps for PGA (in g) Corresponding to the Return Period of 1000 years Obtained by Using Spatially Smoothed Seismicity Model with Main Shocks (a) Incomplete Database (b) Database Adjusted for Incompleteness.....	161
Figure 4.9	Seismic Hazard Maps for PGA (in g) Corresponding to the Return Period of 1000 years Obtained by Using Spatially Smoothed Seismicity Model with All Earthquakes (a) Incomplete Database (b) Database Adjusted for Incompleteness.....	162

Figure 4.10	Seismic Hazard Maps for PGA (in g) Corresponding to the Return Period of 2475 years Obtained by Using Spatially Smoothed Seismicity Model with Main Shocks (a) Incomplete Database (b) Database Adjusted for Incompleteness.....	163
Figure 4.11	Seismic Hazard Maps for PGA (in g) Corresponding to the Return Period of 2475 years Obtained by Using Spatially Smoothed Seismicity Model with All Earthquakes (a) Incomplete Database (b) Database Adjusted for Incompleteness.....	164
Figure 4.12	Map Showing the Spatial Variation of the Difference between the PGA Values Obtained from Spatially Smoothed Seismicity Model and Background Area Source with Main Shocks and Incomplete Database for a Return Period of 475 Years.....	167
Figure 4.13	Map Showing the Spatial Variation of the Difference between the PGA Values Obtained from Spatially Smoothed Seismicity Model and Background Area Source with Main Shocks and Incomplete Database for a Return Period of 2475 Years.....	167
Figure 4.14	Map Showing the Spatial Variation of the Difference between the PGA Values Obtained from Spatially Smoothed Seismicity Model and Background Area Source with Main Shocks and Incomplete Database for a Return Period of 2475 Years and Epicenters of Earthquakes Considered in Spatially Smoothed Seismicity Model.....	168
Figure 4.15	Map Showing the Spatial Variation of the Difference between the PGA Values Obtained from Spatially Smoothed Seismicity Model and Background Area Source with Main Shocks and Database Adjusted for Incompleteness for a Return Period of 475 Years.....	168

Figure 4.16	Map Showing the Spatial Variation of the Difference between the PGA Values Obtained from Spatially Smoothed Seismicity Model and Background Area Source with Main Shocks and Database Adjusted for Incompleteness for a Return Period of 2475 Years.....	169
Figure 4.17	Map Showing the Spatial Variation of the Difference between the PGA Values Obtained from Spatially Smoothed Seismicity Model and Background Area Source with Main Shocks and Database Adjusted for Incompleteness for a Return Period of 2475 Years and Epicenters of Earthquakes Considered in Spatially Smoothed Seismicity Model.....	169
Figure 4.18	Map Showing the Spatial Variation of the Difference between the PGA Values Obtained from Spatially Smoothed Seismicity Model and Background Area Source with All Earthquakes and Incomplete Database for a Return Period of 475 Years.....	170
Figure 4.19	Map Showing the Spatial Variation of the Difference between the PGA Values Obtained from Spatially Smoothed Seismicity Model and Background Area Source with All Earthquakes and Incomplete Database for a Return Period of 2475 Years.....	170
Figure 4.20	Map Showing the Spatial Variation of the Difference between the PGA Values Obtained from Spatially Smoothed Seismicity Model and Background Area Source with All Earthquakes and Incomplete Database for a Return Period of 2475 Years and Epicenters of Earthquakes Considered in Spatially Smoothed Seismicity Model.....	171
Figure 4.21	Map Showing the Spatial Variation of the Difference between the PGA Values Obtained from Spatially Smoothed Seismicity Model and Background Area Source with All Earthquakes and Database Adjusted for Incompleteness for a Return Period of 475 Years.....	171

Figure 4.22	Map Showing the Spatial Variation of the Difference between the PGA Values Obtained from Spatially Smoothed Seismicity Model and Background Area Source with All Earthquakes and Database Adjusted for Incompleteness for a Return Period of 2475 Years.....	172
Figure 4.23	Map Showing the Spatial Variation of the Difference between the PGA Values Obtained from Spatially Smoothed Seismicity Model and Background Area Source with All Earthquakes and Database Adjusted for Incompleteness for a Return Period of 2475 Years and Epicenters of Earthquakes Considered in Spatially Smoothed Seismicity Model.....	172
Figure 4.24	Seismic Hazard Curves Obtained by Using Fault Segments: with Poisson Model and Attenuation Relationships proposed by (a) Boore et al. (1997); (b) Kalkan and Gülkan (2004); and with Renewal Model and Attenuation Relationships proposed by (c) Boore et al. (1997); (d) Kalkan and Gülkan (2004).....	179
Figure 4.25	Contributions of Different Faults to Seismic Hazard under the Assumption of (a) Poisson Model and (b) Renewal Model.....	180
Figure 4.26	Seismic Hazard Map Obtained for PGA (in g) Corresponding to the Return Period of 475 Years (10% Probability of Exceedance in 50 Years) by Considering Only Faults with (a) Poisson Model, (b) Renewal Model.....	181
Figure 4.27	Seismic Hazard Map Obtained for PGA (in g) Corresponding to the Return Period of 1000 Years (5% Probability of Exceedance in 50 Years) by Considering Only Faults with (a) Poisson Model, (b) Renewal Model.....	182
Figure 4.28	Seismic Hazard Map Obtained for PGA (in g) Corresponding to a Return Period of 2475 Years (2% Probability of Exceedance in 50 Years) by Considering Only Faults with (a) Poisson Model, (b) Renewal Model.....	183

Figure 4.29	Map Showing the Spatial Variation of the Difference between the PGA Values Obtained from Renewal and Poisson Models for a Return Period of 475 Years.....	185
Figure 4.30	Map Showing the Spatial Variation of the Difference between the PGA Values Obtained from Renewal and Poisson Models for a Return Period of 2475 Years.....	185
Figure 4.31	Map Showing the Spatial Variation of the Difference between the PGA Values Obtained from Renewal and Poisson Models for a Return Period of 2475 Years and Faults (Thick Black, Dark Blue, Dark Green Lines).....	186
Figure 4.32	Seismic Hazard Curves Resulting from Background Seismic Activity and Faults and the “Best estimate” Seismic Hazard Curve for the Site (40.24° N, 29.08° E) at the City Center of Bursa.....	188
Figure 4.33	Best Estimate Seismic Hazard Map of Bursa Province for PGA (in g) Corresponding to the Return Period of 475 Years (10% Probability of Exceedance in 50 Years).....	188
Figure 4.34	Best Estimate Seismic Hazard Map of Bursa Province for PGA (in g) Corresponding to the Return Period of 1000 Years (5% Probability of Exceedance in 50 Years).....	189
Figure 4.35	Best Estimate Seismic Hazard Map of Bursa Province for PGA (in g) Corresponding to the Return Period of 2475 Years (2% Probability of Exceedance in 50 Years).....	189
Figure 4.36	Best Estimate Seismic Hazard Map of Bursa Province for SA at 0.2 sec (in g) Corresponding to the Return Period of 475 Years (10% Probability of Exceedance in 50 Years).....	190
Figure 4.37	Best Estimate Seismic Hazard Map of Bursa Province for SA at 0.2 sec (in g) Corresponding to the Return Period of 1000 Years (5% Probability of Exceedance in 50 Years).....	190
Figure 4.38	Best Estimate Seismic Hazard Map of Bursa Province for SA at 0.2 sec (in g) Corresponding to the Return Period of 2475 Years (2% Probability of Exceedance in 50 Years).....	191

Figure 4.39	Best Estimate Seismic Hazard Map of Bursa Province for SA at 1.0 sec (in g) Corresponding to the Return Period of 475 Years (10% Probability of Exceedance in 50 Years).....	191
Figure 4.40	Best Estimate Seismic Hazard Map of Bursa Province for SA at 1.0 sec (in g) Corresponding to the Return Period of 1000 Years (5% Probability of Exceedance in 50 Years).....	192
Figure 4.41	Best Estimate Seismic Hazard Map of Bursa Province for SA at 1.0 sec (in g) Corresponding to the Return Period of 2475 Years (2% Probability of Exceedance in 50 Years).....	192
Figure 4.42	Seismic Hazard Map Obtained by Yüçemen et al. (2006) for PGA Corresponding to the Return Period of 475 Years (10% Probability of Exceedance in 50 Years).....	194
Figure 4.43	Seismic Hazard Maps for Bursa Province for PGA Corresponding to the Return Period of 475 Years (10% Probability of Exceedance in 50 Years) Constructed from the Results of (a) the Study Conducted by Yüçemen et al. (2006) (Values are given in terms of g), (b) This Study (Values are given in terms of g); (c) Current Regulatory Earthquake Zoning Map for Bursa (Özmen et al., 1997).....	195
Figure A.1	The Variation of the Difference Between the Seismic Hazard Results Obtained by Ignoring Rupture Length Uncertainty and Considering it As a Function of Number of Rupture Lengths per Magnitude (Site1a).....	217
Figure A.2	The Variation of the Difference Between the Seismic Hazard Results Obtained by Ignoring Rupture Length Uncertainty and Considering it As a Function of Number of Rupture Lengths per Magnitude (Site5a).....	218
Figure A.3	The Variation of the Difference Between the Seismic Hazard Results Obtained by Ignoring Rupture Length Uncertainty and Considering it As a Function of Number of Rupture Lengths per Magnitude (Site10a).....	218

Figure A.4	The Variation of the Difference Between the Seismic Hazard Results Obtained by Ignoring Rupture Length Uncertainty and Considering it As a Function of Number of Rupture Lengths per Magnitude (Site1b).....	219
Figure A.5	The Variation of the Difference Between the Seismic Hazard Results Obtained by Ignoring Rupture Length Uncertainty and Considering it As a Function of Number of Rupture Lengths per Magnitude (Site5b).....	219
Figure A.6	The Variation of the Difference Between the Seismic Hazard Results Obtained by Ignoring Rupture Length Uncertainty and Considering it As a Function of Number of Rupture Lengths per Magnitude (Site10b).....	220
Figure A.7	The Variation of the Difference Between the Seismic Hazard Results Obtained by Ignoring Rupture Length Uncertainty and Considering it As a Function of Number of Rupture Lengths per Magnitude (Site1c).....	220
Figure A.8	The Variation of the Difference Between the Seismic Hazard Results Obtained by Ignoring Rupture Length Uncertainty and Considering it As a Function of Number of Rupture Lengths per Magnitude (Site 5c).....	221
Figure A.9	The Variation of the Difference Between the Seismic Hazard Results Obtained by Ignoring Rupture Length Uncertainty and Considering it As a Function of Number of Rupture Lengths per Magnitude (Site10c).....	221
Figure A.10	The Variation of the Difference Between the Seismic Hazard Results Obtained by Ignoring Rupture Length Uncertainty and Considering it As a Function of Number of Rupture Lengths per Magnitude (Site1d).....	222

Figure A.11	The Variation of the Difference Between the Seismic Hazard Results Obtained by Ignoring Rupture Length Uncertainty and Considering it As a Function of Number of Rupture Lengths per Magnitude (Site5d).....	222
Figure A.12	The Variation of the Difference Between the Seismic Hazard Results Obtained by Ignoring Rupture Length Uncertainty and Considering it As a Function of Number of Rupture Lengths per Magnitude (Site10d).....	223
Figure A.13	The Variation of the Difference Between the Seismic Hazard Results Obtained by Ignoring Rupture Length Uncertainty and Considering it As a Function of Number of Rupture Lengths per Magnitude (Site1e).....	223
Figure A.14	The Variation of the Difference Between the Seismic Hazard Results Obtained by Ignoring Rupture Length Uncertainty and Considering it As a Function of Number of Rupture Lengths per Magnitude (Site5e).....	224
Figure A.15	The Variation of the Difference Between the Seismic Hazard Results Obtained by Ignoring Rupture Length Uncertainty and Considering it As a Function of Number of Rupture Lengths per Magnitude (Site10e).....	224
Figure C.1	Seismic Hazard Map Obtained from Model 1 for PGA at 10% Probability of Exceedance in 50 Years (475 Years Return Period).....	230
Figure C.2	Seismic Hazard Map Obtained from Model 1 for PGA at 5% Probability of Exceedance in 50 Years (1000 Years Return Period).....	231
Figure C.3	Seismic Hazard Map Obtained from Model 1 for PGA at 2% Probability of Exceedance in 50 Years (2475 Years Return Period).....	231

Figure C.4	Seismic Hazard Map Obtained from Model 2 for PGA at 10% Probability of Exceedance in 50 Years (475 Years Return Period).....	232
Figure C.5	Seismic Hazard Map Obtained from Model 2 for PGA at 5% Probability of Exceedance in 50 Years (1000 Years Return Period).....	232
Figure C.6	Seismic Hazard Map Obtained from Model 2 for PGA at 2% Probability of Exceedance in 50 Years (2475 Years Return Period).....	233
Figure C.7	Seismic Hazard Map Obtained from Model 3 for PGA at 10% Probability of Exceedance in 50 Years (475 Years Return Period).....	233
Figure C.8	Seismic Hazard Map Obtained from Model 3 for PGA at 5% Probability of Exceedance in 50 Years (1000 Years Return Period).....	234
Figure C.9	Seismic Hazard Map Obtained from Model 3 for PGA at 2% Probability of Exceedance in 50 Years (2475 Years Return Period).....	234
Figure C.10	Seismic Hazard Map Obtained from Model 4 for PGA at 10% Probability of Exceedance in 50 Years (475 Years Return Period).....	235
Figure C.11	Seismic Hazard Map Obtained from Model 4 for PGA at 5% Probability of Exceedance in 50 Years (1000 Years Return Period).....	235
Figure C.12	Seismic Hazard Map Obtained from Model 4 for PGA at 2% Probability of Exceedance in 50 Years (2475 Years Return Period).....	236

CHAPTER 1

INTRODUCTION

1.1 GENERAL

Earthquakes are natural events with random characteristics. The potential effects of future earthquakes can not be exactly assessed but it can be predicted within the probabilistic framework. In its broad sense, seismic hazard estimation includes the investigation of the effects of future potential earthquakes at a site. These effects are the parameters which describe the severity of ground shaking. In the past, intensity was the most commonly used parameter due to lack of instrumentation to measure strong ground motion. After the instruments are developed and installed to record strong ground motion data, peak ground acceleration was started to be used in seismic hazard studies. Peak ground velocity and displacement as well as spectral acceleration at different periods are examples of the other parameters used in recent seismic hazard studies.

Seismic hazard estimation is an essential component for earthquake-resistant design, seismic risk analyses, loss estimation and premium calculations in the insurance industry. Also, it is necessary for the preparation of seismic zoning maps which provide the necessary input information for the design of ordinary structures. The design and estimation of safety of important structures, such as dams, nuclear power plants etc, are performed based on the site specific seismic hazard estimation studies.

Since earthquakes are very complicated phenomena, the assessment of future earthquake threat is not an easy task. Because, it requires characterization of future potential earthquakes as well as generation and propagation of their effects on earth

surface. Therefore, it can be carried out by the combined understanding of earthquakes in several disciplines; such as geology, geophysics, geotechnics, seismology, earthquake and structural engineering, mathematics and statistics. Studies carried out in these disciplines for understanding of earthquake phenomenon and its effects led to the development of procedures followed for seismic hazard estimations and models used in these procedures to describe location, magnitude, probability of future earthquake occurrences and the spatial distributions of their effects. Therefore, seismic hazard estimation is a dynamic work and should be updated in time.

1.2 LITERATURE SURVEY

In literature, there are two basic approaches for seismic hazard assessment: deterministic and probabilistic. Since earthquakes are random events with respect to magnitude, location and time, probabilistic seismic hazard assessment procedures are more appropriate than the deterministic ones in most of the applications.

In the past, seismic hazard was quantified deterministically from maximum earthquake intensity maps constructed by seismologists from the available data on past earthquakes. In 1968, Cornell (1968) proposed a model in which probabilistic approach to estimate seismic hazard was formulated. The results of this model gave the selected seismic hazard parameter versus exceedance probabilities or average return periods corresponding to different levels of this parameter. In the Probabilistic Seismic Hazard Analysis (PSHA) methodology introduced by Cornell (1968), the occurrences of earthquakes in time were assumed to be independent events and follow the memoryless Poisson process. In addition, randomness in the size and location of future earthquakes was also taken into consideration. For this purpose, the size of future earthquakes was assumed to be exponentially distributed. The uncertainty in the location of future earthquakes was incorporated into the analysis by assigning the seismic activity surrounding the site to seismic sources which have potential to generate earthquakes in the future. In this model, the

uncertainty in the attenuation relationship (ground motion prediction equation), which describes the decrease in the intensity of earthquake induced effects with the increase of distance between the site and the earthquake epicenter, was not taken into consideration. Later, Vanmarcke and Cornell (1969) and Cornell (1971) proposed a procedure to incorporate the scatter around the mean attenuation relationship into PSHA computations. Although Cornell (1968) developed this model for seismic hazard assessment of individual sites, it can be used in the development of regional seismic hazard maps by applying it to a grid of points.

The pioneering work of Cornell (1968) motivated researchers to develop alternative models for temporal, spatial and magnitude distribution of earthquakes and attenuation relationships as well as computer programs to perform PSHA computations. As a consequence of these developments, PSHA methodology was started to be applied for the assessment of seismic hazard at specific sites where important structures are to be constructed and preparation of seismic hazard and zoning maps in macro-scale. The studies carried out by Cornell and Merz (1974), Gülkan and Yücemem (1975, 1976) and Christian et al. (1978), are the examples of first applications of PSHA for specific sites. On the other hand, Lomnitz (1969), Shah et al. (1975), Kiremidjian and Shah (1975), Gülkan and Gürpınar (1977) and Mortgat and Shah (1978) used the PSHA methodology for seismic zoning mapping purposes. In addition, 1976 national earthquake hazard map of United States was prepared based on the PSHA methodology. Therefore, 1970's can be accepted as the beginning period in which PSHA methodology was adopted in seismic hazard estimation studies.

Many computer programs have been coded and improved later with developments in computational technology and models in PSHA methodology. EQRISK (McGuire, 1976) was the most widely used one in earlier applications of PSHA methodology. McGuire (1978) improved it under the name of FRISK. Bender and Perkins (1982) developed a computer program, SEISRISK II. It is actually a revised and improved version of the original undocumented program SEISRISK I

(Algermissen et al., 1976), developed during the preparation of the 1976 national earthquake hazard maps. Chiang et al. (1984) developed a computer program, named as STASHA, at Stanford University. Bender and Perkins (1987) revised SEISRISKII and published the improved version as SEISRISKIII. Computer programs were also developed at United States Geological Survey (USGS) by Frankel et al. (1996) during the preparation of the 1996 national seismic hazard maps. EZ-FRISK (Risk Engineering, 2005), CRISIS-2003 (Ordaz et al., 2003), FRISK88M (Risk Engineering, 2006) are the other computer programs which have been used in recent probabilistic seismic hazard estimation studies.

As an alternative to the memoryless Poisson model, time dependent models (such as; Markov, semi-Markov and renewal process models) were developed to model temporal dependence of earthquakes. In the PSHA model developed by Cornell (1968), earthquake magnitudes are assumed to be exponentially distributed based on the linear magnitude recurrence relationship of Richter (1958). Since then, researches were carried out to develop alternative magnitude distributions. The magnitude distributions based on the bilinear (Shah et al., 1975) and quadratic (Shlien and Toksöz, 1970 and Merz and Cornell, 1973) magnitude recurrence relationships were proposed since linear magnitude recurrence relationship overestimates the frequency of large magnitude earthquakes. However, linear model is widely used in probabilistic seismic hazard estimation studies due to the fact that it yields conservative seismic hazard results.

Schwartz and Coppersmith (1984) indicated that some individual faults and fault segments have a tendency to repeatedly generate characteristic earthquakes and proposed the characteristic earthquake model.

Seismic sources have been modeled as point, area and line (fault) sources. In earlier studies, seismic activity in a seismic source (line or area) was assumed to be homogeneous. Fault-rupture, segmentation and cascade models are the mostly used ones in recent seismic hazard assessment studies for earthquake occurrences along faults. On the other hand, spatially smoothed seismicity model (Frankel, 1995) is

used as an alternative to the assumption of uniform seismicity distribution over background area sources. In order to model attenuation characteristics of ground motion, different attenuation relationships (ground motion prediction equations) have been developed for different tectonic regimes and for different ground motion parameters (intensity, peak ground acceleration, peak ground velocity, spectral acceleration, etc.) over the years.

Until 1996, the seismic zoning maps for Turkey were prepared based on deterministic procedures. Gülkan et al. (1993) conducted a study for Turkey to estimate seismic hazard in terms of peak ground acceleration (PGA) for a return period of 475 years. They used area sources with exponentially distributed magnitudes and Poisson model to predict probabilities of occurrence of earthquakes in these sources. Uncertainties in the location of the boundaries of seismic sources were taken into consideration. Seismicity parameters of each source were predicted by using information in the original earthquake catalog and in the artificially completed one. They used the attenuation relationship developed by Joyner and Boore (1981) based on northern U.S. ground motion data. In order to compensate for the use of nonlocal attenuation relationship, they made different analyses by using the mean PGA values calculated by this relationship and adding variations of 0.2 or 0.3 to these values. The results of analyses made according to different assumptions with respect to uncertainty in source boundaries, seismicity parameters and attenuation characteristics of the ground motion were combined by utilizing the theorem of total probability within the framework of logic tree methodology. Regulatory earthquake zoning map of Turkey was prepared based on this study of Gülkan et al. (1993) and became effective in 1996.

Until recently, probabilistic seismic hazard assessment studies carried out for a region or a province in Turkey were limited in number. After the 1999 Kocaeli and Düzce earthquakes, researchers have been motivated on the estimation of seismic hazard for İstanbul, Marmara Region since the future earthquake is expected to occur on the segments of North Anatolian Fault beneath the Marmara Sea and near

the southern boundary of this city. Consequently, the recent investigations on the region or city based estimation of seismic hazard are focused on this region. Studies have been carried out by using different seismic hazard assessment approaches (i.e. deterministic and probabilistic), different attenuation relationships and different models for seismic sources, magnitude distribution and earthquake occurrence in time.

1.3 OBJECTIVES AND SCOPE OF THE STUDY

In this study, it is aimed to investigate the sensitivity of seismic hazard results with respect to different models adopted and assumptions made in probabilistic seismic hazard assessment methodology. In other words, this study is focused on the influence of different assumptions on seismic source modeling, magnitude distribution and stochastic models used for the temporal distribution of earthquakes on seismic hazard results. Depending on the information available, the applicability of different models and effects of them on the seismic hazard results are investigated first for a semi-hypothetical example which includes a number of sites and a single fault. Then, the spatial sensitivity of seismic hazard estimation with respect to different models are examined for a large (a country) and a smaller region (a province) based on real data. In addition, the application of logic tree methodology in the combination of different results obtained from different models and assumptions is illustrated.

After this introductory chapter, in Chapter 2, deterministic and probabilistic seismic hazard estimation procedures and the treatment of uncertainties in PSHA procedure are explained in detail. In addition, the difference in the seismic hazard results obtained by using different procedures, attenuation relationships, source, magnitude distribution and earthquake occurrence models are illustrated for a number of sites under the threat of a single fault. It is to be noted that in recent years, more attention has been paid to the assessment of seismic hazard nucleating from faults. The fact that more reliable values have been obtained for the fault parameters had a

significant effect on this. The seismic hazard assessment procedures taking into consideration the hazard nucleating from active faults and utilizing the more appropriate stochastic models have become the current trend in the development of new generation of seismic hazard maps. In view of this observation, particular emphasis is given on the assessment of seismic hazard due to active faults. For this reason, in this study particular emphasis is given to the presentation and application of various models applicable to the faults, as it is done in Chapter 2.

In Chapters 3, the case study carried out for probabilistic seismic hazard assessment for Jordan is presented. It is generally very difficult both time wise and financially to update seismic hazard maps on the country basis. Accordingly the updating of current seismic hazard maps should be carried out on region or province basis. In view of this opinion, the case study carried out for probabilistic seismic hazard assessment for Bursa province is presented in Chapter 4. Here, particular emphasis is given on the investigation of the sensitivity of results to different assumptions based on real life data.

In Chapter 5, the results obtained in this study are briefly discussed and the main conclusions drawn based on them and recommendations for future studies are presented.

CHAPTER 2

ALTERNATIVE MODELS APPLIED IN SEISMIC HAZARD ANALYSIS

2.1 INTRODUCTION

The future earthquake threat at a site is generally quantified by carrying out a seismic hazard analysis. There are two basic seismic hazard assessment methodologies, namely, deterministic and probabilistic.

In the deterministic approach, one or more critical earthquake scenario(s) (i.e. maximum possible earthquake magnitudes occurring at seismic sources with minimum distances to the site) are developed. Among them, the one that will produce the largest ground motion at the site is selected. Based on the magnitude, distance and site characteristic, the ground motion at the site is predicted for this earthquake scenario. Since single deterministic values are selected for earthquake magnitude, site to source distance and ground motion prediction equation, this method is called as the deterministic seismic hazard analysis.

Although deterministic seismic hazard analysis (DSHA) is based on the most adverse earthquake scenarios regardless of how unlikely they may be, in probabilistic seismic hazard analysis (PSHA), randomness in earthquake magnitude, location and time is taken into account by considering all probable earthquake scenarios that are capable of affecting the site of interest and frequency of their occurrences. There are also uncertainties in the attenuation of ground motion of an earthquake by distance as well as in the spatial locations of faults or boundaries of area sources. In PSHA, the uncertainties in these parameters are described by probability distributions and systematically integrated into the results via

probability theory. Therefore, instead of a single ground motion value obtained from DSHA, PSHA produces likelihoods of different ground motion values occurring at the site. In other words, the output of PSHA is a set of different ground motion levels and a probability distribution described on this set. This approach also allows the analyst to compare different alternatives quantitatively in making decisions (Reiter, 1990).

In this chapter, the basic concepts, tools and models used in seismic hazard analysis will be explained and the sensitivity of seismic hazard estimations on these assumptions will be illustrated with a semi-hypothetical example which includes a single seismic source, in the form of a fault. The selection of a fault as the seismic source is due to the fact that in the development of new generation of seismic hazard maps more attention is paid on the faults which are the main source of seismic hazard.

2.2 DETERMINISTIC SEISMIC HAZARD ANALYSIS

Deterministic seismic hazard analysis (DSHA) involves three basic steps; definition of earthquake sources, determination of earthquake potential of each source, selection of an attenuation relationship and estimation of selected ground motion parameter or other earthquake effects at the site of interest. Figure 2.1 shows these steps schematically.

First, seismic sources (faults or seismic provinces) within 250 km or larger radius, which depends on the attenuation characteristics as well as tectonic settings of the region, around the site of interest are determined. Seismic sources can be modeled as line, area, dipping plane and volumetric sources. Point source model can also be used in the case that the epicenters of past earthquakes are concentrated in a very small area and they are far away from the site. Then, earthquake potential, i.e. maximum magnitude earthquake that is assumed to occur at the closest distance from the site, of each seismic source is determined. Afterwards, the ground motion values resulted from these earthquakes at the site are estimated by using selected

empirical ground motion estimation equation. Among them, the largest ground motion value is used in the deterministic method.

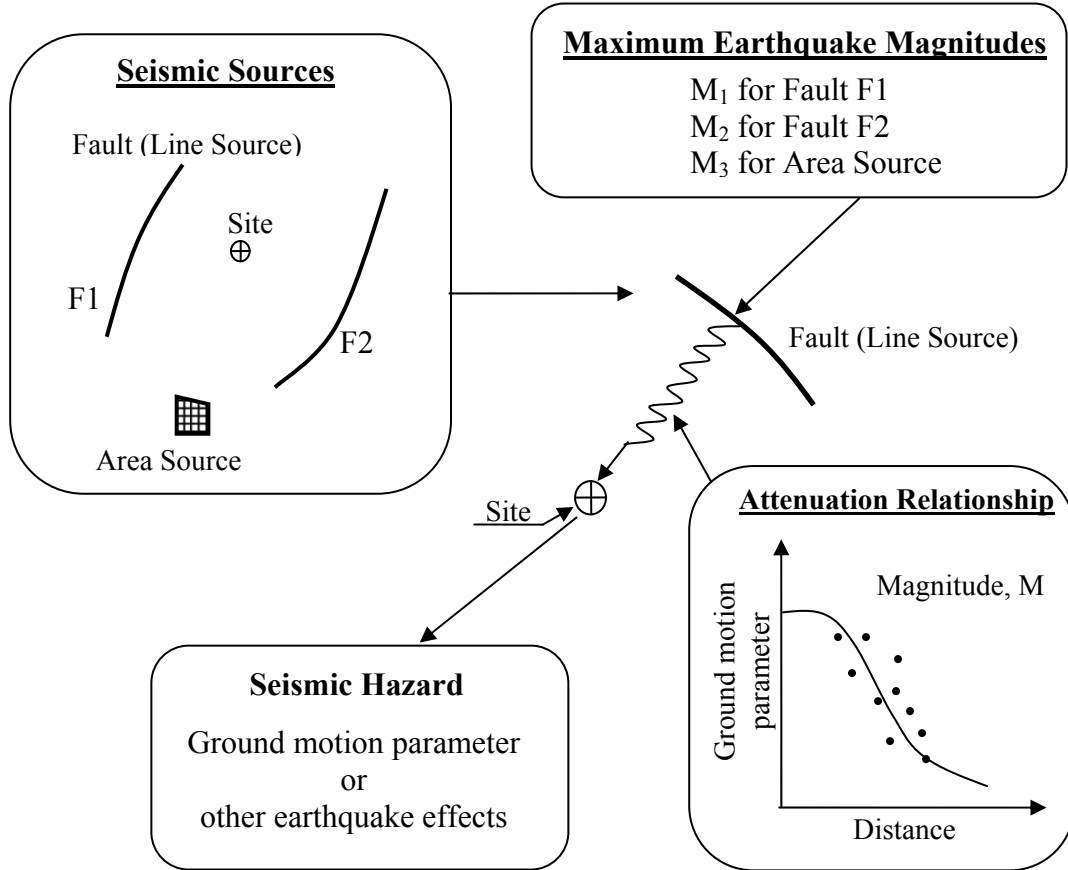


Figure 2.1 Schematic Description of DSHA for a Site

In order to illustrate the calculations performed in DSHA, a case study is carried out for a site located in İstanbul. There are several studies in literature to predict magnitude and location of potential earthquake that can cause substantial damage in İstanbul. JICA (2002) performed an extensive study in which four scenario earthquake models were described. Among them, the most probable earthquake scenario model is used in this example. This model is presented in Figure 2.2 and its parameters are given in Table 2.1.

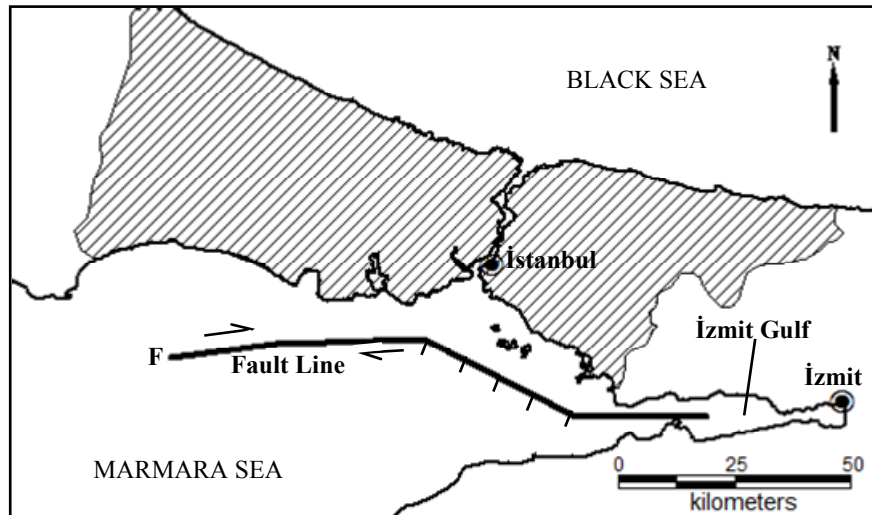


Figure 2.2 Map Showing the Location of the Fault (F) Forming the Basis for the Scenario Earthquake Model Used for İstanbul in This Study (JICA, 2002)

Table 2.1 Parameters of the Fault and the Scenario Earthquake Model Used for İstanbul in This Study (JICA, 2002)

Length (km)	119
Moment magnitude (Mw)	7.5
Dip angle (Degree)	90
Depth of upper edge (km)	0
Type	Strike Slip

A site with a closest distance to the fault of about 16 km is selected. Peak Ground Acceleration (PGA) is selected as the ground motion parameter. Four different attenuation relationships developed by Abrahamson and Silva (1997), Boore et al. (1997), Sadigh et al. (1997) and Kalkan and Gülkan (2004) for rock sites are used to predict PGA values at the site. These attenuation relationships are briefly presented in Section 2.3.4. As explained in Section 2.3.6.1, attenuation relationships are generally in the form that they predict the natural logarithm of the ground motion

parameter. Therefore, the values calculated by using these equations are median values of the ground motion parameter. Median values are converted to mean values by assuming a lognormal distribution for the ground motion parameters, Y , as follows (Risk Engineering, 2005);

$$Y_{\text{mean}} = Y_{\text{median}} \exp\left(\frac{\sigma_{\ln Y}^2}{2}\right) \quad (2.1)$$

where;

- Y_{mean} : mean value of the selected ground motion parameter
- Y_{median} : median value of the selected ground motion parameter
- $\sigma_{\ln Y}$: standard deviation of the natural logarithm of the selected ground motion parameter

Table 2.2 shows the mean and median PGA values estimated at the site by using these attenuation relationships for rock site condition.

Table 2.2 Mean and Median PGA Values Estimated at the Site by Using Different Attenuation Relationships for Rock Site Condition in DSHA

PGA (in g)	Abrahamson and Silva (1997)	Boore et al. (1997)	Sadigh et al. (1997)	Kalkan and Gülkan (2004)
Mean	0.317	0.258	0.346	0.277
Median	0.289	0.228	0.322	0.230

Compared with the probabilistic approach, DSHA approach requires less data, computational effort and time. Therefore, it is extensively used in regional seismic hazard estimates. But it is still deficient in taking into account the randomness involved in the temporal, spatial and magnitude-wise distribution of earthquakes as well as uncertainties in each step of the seismic hazard analysis. Due to these randomness and uncertainties, DSHA may not always guarantee the intended

conservatism. Furthermore, selecting the most pessimistic scenario in DSHA is not likely to represent the reality and it is not a good engineering decision (Gupta, 2002).

2.3 PROBABILISTIC SEISMIC HAZARD ANALYSIS

Considering the randomness in the occurrence of earthquakes with respect to time, space and magnitude as well as the various other sources of uncertainties, probabilistic concepts and statistical methods are the appropriate tools for the assessment of seismic hazard. PSHA methodology was first proposed by Cornell (1968) to quantify the seismic hazard at a site of interest in terms of a probability distribution. In contrast to DSHA in which seismic hazard is based on a single earthquake scenario, PSHA integrates the effects of all future earthquakes of all possible magnitudes, at all significant distances from the site. Besides, random nature of earthquake occurrences and uncertainty in attenuation of ground motion are taken into consideration in PSHA. As a result, instead of discrete, single-valued event and model used in DSHA, PSHA allows the use of continuous, multi-valued events and models.

Implementation of PSHA consists of the following basic steps: the delineation of seismic sources, assessment of the earthquake occurrence characteristics for each seismic source, selection of the appropriate ground motion attenuation relationship and identification of the site characteristics, preparation of a computational algorithm which will aggregate the seismic threat nucleating from different sources and yielding to the probability distribution for the specified ground-motion parameter at the site of interest. In addition, different sources of uncertainties are considered in PSHA and their effects are reflected to the hazard results either directly or by employing logic tree or similar statistical methods.

The basic steps of PSHA are schematically shown in Figure 2.3. They are similar to DSHA with some major differences. First, like DSHA, seismic sources that affect the site of interest are defined. Then, for each seismic source, magnitude recurrence

relationship which gives the relative frequency of different earthquake magnitudes is defined. In order to predict the probability of future earthquake occurrences, stochastic models are applied. This step of PSHA is fundamentally different from that of DSHA in which only maximum magnitude earthquake is determined for each seismic source and only this earthquake is considered in the analysis. However, in PSHA, a probability distribution is determined for earthquake magnitude and maximum magnitude is the upper bound of all earthquake magnitudes that will be used in the analysis for each source. Therefore, randomness in earthquake occurrences with respect to magnitude and time is considered in this step.

In the third step, similar to DSHA, attenuation relationship is utilized to predict the effects of all earthquakes determined in the previous step. At the last step, the effects of all earthquakes, which have different magnitudes and occur at different locations in different seismic sources are aggregated and displayed in the form of a curve that shows the probability of exceeding different levels of the selected ground motion parameter.

In the following sections, basic steps of PSHA will be explained in detail.

2.3.1 Seismic Sources

The first step in PSHA analysis is to determine the spatial distribution of potential seismic sources of future earthquakes around the site of interest. In PSHA, a seismic source is a configuration (point, line or area) in which seismicity characteristics; i.e. annual earthquake occurrence rate, attenuation characteristics and maximum earthquake magnitude value, are considered to be the same. In other words, in each seismic source, earthquakes are assumed to occur at the same rate with respect to magnitude regardless of location (Reiter, 1990). The geological and seismological data as well as present earthquake catalogs are the useful tools for the delineation of seismic sources. Expert opinion should also be consulted during this process (SSHAC, 1997).

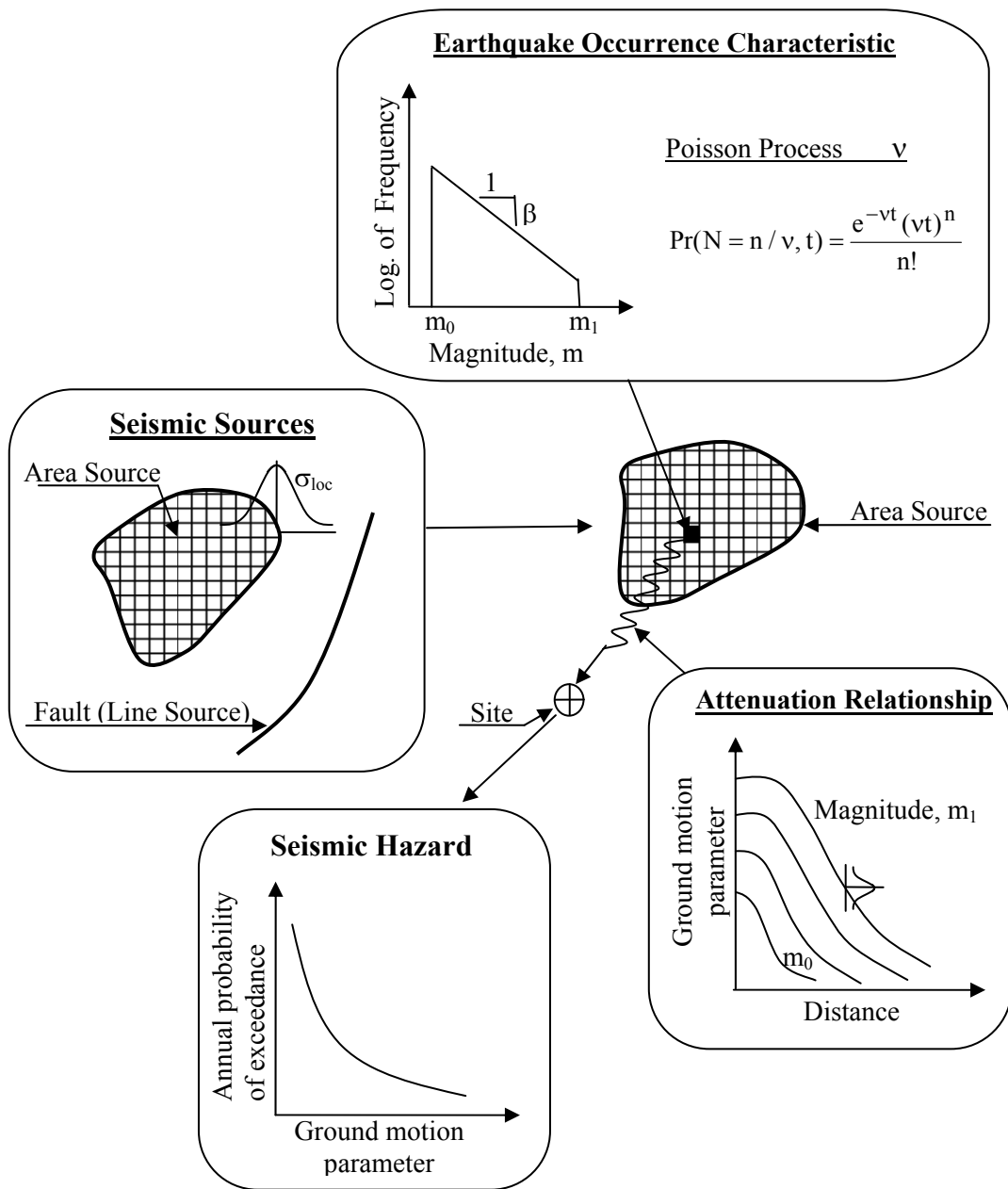


Figure 2.3 Schematic Description of the Classical PSHA Methodology

There are three general types of seismic source models; point, line (fault model) and area (source zone model). Among them, the point source model is the simplest case. When epicenters of past earthquakes are clustered in a relatively small area and they are far away from the site, they can be assumed to emanate from a point in space. Therefore, in point source model, there is no randomness with regard to the location of earthquakes and the distance of future earthquakes to the site is assumed to be same (Yüçemen, 1982).

Line sources are used to model well defined faults. This model can be imagined as map view representation of three dimensional fault planes (Thenhaus and Campbell, 2003). It is assumed that the earthquakes occur with equal probability at anywhere along the length of a line source. Therefore, line sources are divided into smaller small segments and each segment is treated as a point source in PSHA calculations.

Tectonic stresses cause the deformations or strains in the rock and earthquakes occur when some point reaches the strain level that the rock can no longer withstand. Rupture occurs along a fault and accumulated strain energy relieves or releases. Therefore, earthquakes occur as finite ruptures along the fault. Accordingly, Bender (1984) developed a fault-rupture model in which earthquakes occur as finite length ruptures along the fault and length of each rupture is the function of earthquake magnitude.

In recent studies, fault segmentation model (WGCEP, 1995, 1999) is incorporated into PSHA. In this model, a fault is divided into segments. A segment is a part of the fault with well defined end points, geometry, type and dimensions. Depending on the geometry and seismicity of the fault, there are two types of segments: seismic segment and structural segment. A seismic segment is a portion of the fault which is activated by a large magnitude (characteristic) earthquake that generates a surface rupture. On the other hand, structural segment is the part bounded by geometrical discontinuities like step-over, bifurcation and bending of the fault. These discontinuities may stop propagation of the rupture beyond these points.

Therefore, a part or whole length of a structural segment or more than one structural segment(s) may constitute a potential seismic segment (Yücemem et al., 2006). In order to predict the surface rupture due to future earthquakes, structural and seismic segments must be investigated.

In PSHA, maximum magnitude model, which will be explained in the following section, is generally applied as magnitude recurrence relationship of a segment and maximum magnitude earthquake of the segment is assigned based on the assumption that it breaks the entire segment. In order to describe the influence of earthquakes with smaller magnitudes to seismic hazard results, background area sources are incorporated into analyses.

Although segmentation concept simplifies the fault behaviour, it is important that segment boundaries do not always stop the ruptures and their positions are not constant in geological time and space. Therefore, WGCEP (1995, 1999) proposed a cascade model in which large magnitude earthquakes break multiple, contiguous segments of a fault.

Consider a fault consisting of two segments; namely, x and y. Characteristic or large magnitude earthquake can occur on this fault in three different ways: x ruptures alone or y ruptures alone or x and y rupture together. The earthquake rate of this fault is the sum of rates of these three types of events. The rupture rate of segment x is the sum of the rates of earthquakes where x ruptures alone and x and y rupture together.

In cascade model, the difficulty is that the cascade frequency can not be defined adequately by geological data unless entire earthquake history of a fault is known. In addition, the information about historical earthquakes is too uncertain to determine whether adjacent segments ruptured separately or together. Therefore, rupture rates of segments are better determined than the earthquake rates (WGCEP, 1995).

For a fault that consists of n segments, there will be $m=n(n-1)/2$ possible cascades as well as individual rupture of segments. The earthquake rates of m cascades can not be determined directly from the rupture rates of individual segments. Cramer et al. (2000) developed a methodology in which the probability of multi-segment rupture is maximized. They listed the cascades used in their study in decreasing order of their lengths. The probability of first cascade was set equal to the lowest value of the rupture probabilities of the segments participating in the cascade. Since a portion of rupture rate on each is considered to be resulted from multi-segment rupture, rupture probability of each segment must be modified. This was accomplished by using the following relation between the given segment probability, P_{si} , and multi-segment, P_{cj} , and adjusted individual segment, P_{asj} , probabilities (Cramer et al., 2000);

$$1 - P_{si} = (1 - P_{asj})(1 - P_{cj}) \quad (2.2)$$

or

$$P_{asj} = 1 - (1 - P_{si}) / (1 - P_{cj}) \quad (2.3)$$

After adjusted rupture probabilities of all segments participating in the multi-segment rupture was calculated, same calculations were repeated for the remaining cascades by using the adjusted probabilities calculated one stage before.

Area source model is generally applied in the regions where past seismic activity may not correlate with any one of the active geologic structure or the available data are not adequate to recognize a particular fault system (Yüçemen, 1982). Area sources have uniform seismicity characteristics that are different from neighboring zones and exclusive of active faults that are defined as line sources (Thenhaus and Campbell, 2003). In other words, area sources are assumed to have distributions of seismicity characteristics that do not vary in time and space (McGuire, 2004). In the simplest way, the geometry of these sources is described by using past seismic activity (McGuire, 2004). Similar to line sources, an area source can be divided into

small elements and each element can be treated as a point source in PSHA calculations.

Faults with subsurface geometry are modeled as two dimensional dipping planes and area sources with depths as three dimensional volumetric sources.

Background source model is a special type of area source model that is used to represent the seismic activity that can not be associated with the major seismic sources (McGuire, 2004). Therefore, small and moderate magnitude earthquakes can be assigned to background sources. They can be used together with fault sources in which larger earthquakes in the same region are modeled. In this case, attention should be paid to avoid overlaps in magnitude range of background sources with that of faults.

In recent PSHA applications, the spatially smoothed seismicity procedure developed by Frankel (1995) is extensively used instead of areal source zones in which seismic activity rate is homogeneous or uniformly distributed. This model assumes that future earthquakes will occur in the vicinity of past earthquakes and eliminates the subjectivity in the delineation of seismic source zones at the regions where there is no adequate seismotectonic information. In this model, earthquakes that are not assigned to major seismic sources are assumed to be potential seismic sources and spatially distributed to cells of a grid. Then, cumulative number of earthquakes, n_i , with magnitude greater than minimum magnitude is counted and converted from cumulative to incremental values. These values are spatially smoothed by multiplying them by a Gaussian function having a correlation distance, c . For each cell, the spatially smoothed values, \tilde{n}_i , is calculated by using the following equation (Frankel, 1995):

$$\tilde{n}_i = \frac{\sum_j n_j e^{-(\Delta_{ij}/c)^2}}{\sum_j e^{-(\Delta_{ij}/c)^2}} \quad (2.4)$$

where c is the correlation distance and Δ_{ij} is the distance between the i^{th} cell and j^{th} cell. The radius of smoothing is equal to $3c$.

2.3.2 Magnitude Recurrence Relationship

The seismicity of a region is characterized by an appropriate magnitude-recurrence relationship, based upon which the probability distribution of earthquake magnitudes is obtained.

In classical PSHA developed by Cornell (1968), earthquake magnitude is assumed to be exponentially distributed. Exponential magnitude distribution is derived from the linear magnitude-recurrence relationship which is recommended by Richter (1958) and proved to be valid for different regions of the world by various researchers using past earthquake data (Yüçemen, 1982). Richter (1958) proposed the following relationship between the Richter magnitude, “ m ”, and the total number of earthquakes with magnitudes equal or greater than “ m ”:

$$\log N(m) = a - bm \quad (2.5)$$

or

$$N(m) = e^{\alpha - \beta \cdot m} \quad (2.6)$$

where;

$$\alpha = a \times (\ln 10)$$

$$\beta = b \times (\ln 10)$$

$N(m)$: the number of earthquakes having magnitude equal or greater than “ m ”

a and b : constants depending on the seismic characteristic of the region considered and generally determined by fitting a least squares line to the historical earthquake data.

In seismic hazard analysis, a lower limit, “ m_0 ”, is determined for earthquake magnitude. Since the lower limit is the minimum earthquake magnitude that is

expected to generate ground motions damaging engineering structures, it changes for different types of structures. The other reason to put such a limit is that statistical data for smaller magnitude earthquakes is generally incomplete and not reliable. Although there is no consensus in the selection of an appropriate value of minimum magnitude to be used in seismic hazard analysis, a value of $m_0 = 4.0$ or 4.5 seem to be quite common. For brittle structures that are sensitive to low level of ground motion amplitudes, this value can be decreased.

There is also an upper limit, “ m_1 ”, for earthquake magnitude. The upper limit is estimated as the largest earthquake magnitude that is possible to occur in the region considered. For fault sources, maximum magnitude is assumed to rupture the entire fault or a series of its segments. This magnitude can be determined by considering the maximum historical earthquake in the earthquake catalog of the region and increasing it by some margin. But, the available earthquake catalog may not be adequate or long enough to derive a reliable estimate. In such a case, maximum magnitude can be estimated by using rupture parameters (rupture length, rupture area, displacement etc.) of the fault. In the literature, there are several investigations where relationships are developed between rupture length, “ L ” and earthquake magnitude, “ M ” generally in the following form:

$$M = a + b \log L \quad (2.7)$$

where a and b are the coefficients to be determined by the statistical analysis of empirical data.

Whenever sufficient local data are available, all of these methods should be combined to obtain the best estimate of m_1 .

Due to the truncations at both lower and upper magnitude limits, exponential magnitude distribution has to be normalized and it becomes:

$$f_M(m) = \begin{cases} k\beta e^{-\beta(m-m_0)} & m_0 \leq m \leq m_1 \\ 0 & \text{otherwise} \end{cases} \quad (2.8)$$

$$k = \left[1 - e^{-\beta(m_1 - m_0)} \right]^{-1} \quad (2.9)$$

where k is the normalizing constant, which adjusts the value of the cumulative distribution function to unity at $m = m_1$.

The linear recurrence relationship proposed by Richter (1958) is satisfactory in the estimation of small and medium magnitude earthquakes; but it gives higher values for the recurrence of large magnitude earthquakes. In other words, for large magnitude earthquakes, the recurrence rate, consequently the seismic hazard is overestimated by the linear model. To eliminate this inconsistency, bilinear and parabolic relations are recommended in the literature.

Bilinear magnitude-recurrence relationship is defined as follows (Yüçemen, 1982):

$$\log N(m) = a_1 - b_1 m \quad m \leq m^* \quad (2.10)$$

$$\log N(m) = a_2 - b_2 m \quad m > m^* \quad (2.11)$$

For magnitudes which are equal or lower than a specified magnitude level, “ m^* ”, Eq. (2.10) and for those greater than “ m^* ” Eq. (2.11) is valid.

Parabolic magnitude-recurrence relationship is given as follows (Merz and Cornell (1973), Shlien and Toksöz (1970)):

$$\log N(m) = a + b_1 m + b_2 m^2 \quad (2.12)$$

The probability density function of earthquake magnitude corresponding to parabolic magnitude recurrence relationship is given as follows (Yüçemen, 1982):

$$f_M(m) = \begin{cases} -k' \left[(\beta_1 + 2\beta_2 m) \left(e^{\beta_1(m - m_0) + \beta_2(m^2 - m_0^2)} \right) \right] & m_0 \leq m \leq m_1 \\ 0 & \text{otherwise} \end{cases} \quad (2.13)$$

where;

$$k' = \left[1 - e^{\beta_1(m_1 - m_o) + \beta_2(m_1^2 - m_o^2)} \right]^{-1} \quad (2.14)$$

$$\beta_2 = b_2 \times (\ln 10) \quad (2.15)$$

Linear, bilinear and parabolic magnitude recurrence relationships are shown in Figure 2.4. Since the linear model is simple and yields conservative hazard results compared to those obtained either from the parabolic or the bilinear models, it is widely used.

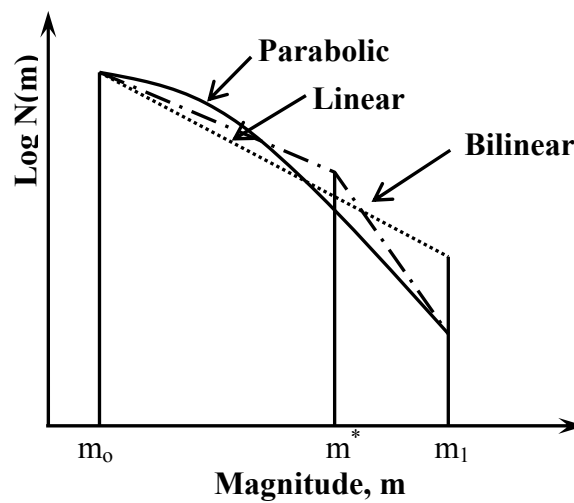


Figure 2.4 Linear, Bilinear and Parabolic Magnitude Recurrence Relationships (Yücemem, 1982)

Certain discrepancies observed between earthquake recurrence estimates based on past earthquake records and those based on seismological and geological investigations for specific regions, especially for active faults, have motivated investigators to develop alternative recurrence models to account for this discrepancy. Schwartz and Coppersmith (1984) suggested that some individual faults and fault segments have a tendency to repeatedly generate characteristic earthquakes. Characteristic earthquake is the event where magnitude is approximately equal to the maximum magnitude that a particular fault can generate

and it scatters in only a fairly narrow range (say 0.5 magnitude unit). Schwartz and Coppersmith (1984) indicated that the exponentially distributed magnitude models represent the earthquake magnitudes quite well in a large region but may underestimate the recurrence rate of large earthquakes on individual fault segments and proposed the characteristic earthquake model. Later, Youngs and Coppersmith (1985) derived a density function for magnitudes corresponding to this model. In this model, magnitudes are assumed to be exponentially distributed up to the magnitude level m' . Above this magnitude the characteristic earthquake lies with a uniform distribution between $(m_1 - \Delta m_c)$ and m_1 . Characteristic earthquake model proposed by Youngs and Coppersmith (1985) is illustrated in Figure 2.5.

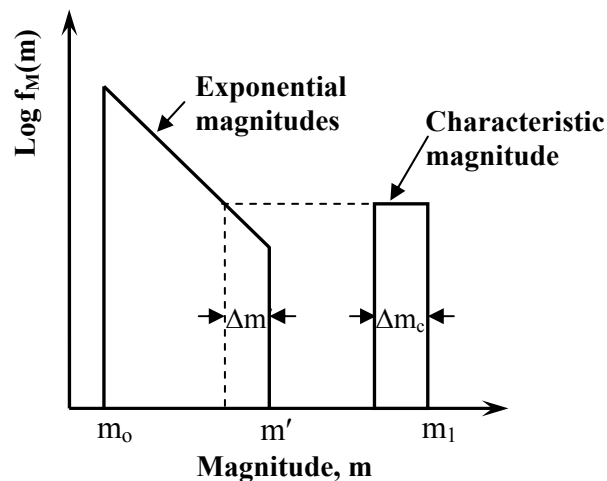


Figure 2.5 Characteristic Earthquake Model Proposed by Youngs and Coppersmith (1985)

In order to apply this model in their analysis, Youngs and Coppersmith (1985) made some simplifying assumptions. They assumed Δm_c to be equal to 0.5 magnitude unit, $m' = m_1 - \Delta m_c$ and frequency of characteristic part of the distribution equals to the frequency of the exponential part at $(m' - 1.0)$. Applying these assumptions and renormalizing the probability density function so that the total area under it equals

unity, the probability density function of the characteristic magnitude model takes the following form:

$$f_M(m) = \begin{cases} k\beta e^{-\beta(m-m_0)} & m_0 \leq m \leq m_1 - 0.5 \\ k\beta e^{-\beta\left(\left(m_1 - \frac{3}{2}\right) - m_0\right)} & m_1 - 0.5 \leq m \leq m_1 \end{cases} \quad (2.16)$$

where k is again the normalizing constant and it is expressed as follows:

$$k = \left[1 - e^{-\beta(m_1 - 0.5 - m_0)} + \beta e^{-\beta\left(m_1 - \frac{3}{2} - m_0\right)} 0.5 \right]^{-1} \quad (2.17)$$

Another form of magnitude recurrence model assumes that all energy is released by earthquakes having the maximum magnitude. If a fault is considered as truly characteristic, only a single earthquake of specified magnitude is expected to occur on the fault. In this case, this earthquake ruptures the entire fault or a series of its segments. This model is referred to as the pure characteristic or maximum magnitude model. In order to account for uncertainty in the maximum magnitude, a Gaussian distribution truncated at lower limit m^0 and upper limit m^u is also proposed in the literature. Two parameters of this distribution are the mean value of maximum magnitude and its standard deviation. To account for other earthquakes with smaller magnitudes, truncated exponential distribution is either assigned to same fault or a background seismic source is generally used with this model.

2.3.3 Modeling of Earthquake Occurrences

Since earthquakes are random events, stochastic models are applied to predict the probability of future earthquake occurrences. In the classical PSHA model, earthquake occurrences are assumed to be independent events both in time and space and modeled as a homogeneous Poisson process. According to the Poisson model, the probability that “ n ” number of earthquakes having magnitude greater than “ m_0 ” occurring in a time interval, “ t ”, is;

$$\Pr(N = n / v, t) = \frac{e^{-vt} (vt)^n}{n!} \quad (2.18)$$

where;

v : the average number of earthquakes, having magnitude equal or greater than m_0 , per unit time and it also equals to the reciprocal of the mean inter-event time (recurrence interval, mean return period).

The probability that at least one earthquake occurs in a seismic source within the time interval, “ t ”, is given as follows;

$$\Pr(N \geq 1) = 1 - e^{-v \cdot t} \quad (2.19)$$

In recent years, the renewal model has also been used in seismic hazard analysis. Renewal model is based on the assumption that the occurrence of large (characteristic) earthquakes has some periodicity. Since a characteristic earthquake ruptures the entire fault segment, it is expected to release all strain energy accumulated on the fault and earthquake cycle restarts (Wu et al., 1995). It takes time for the faults to accumulate such a large amount of energy again. Therefore, faults that are early in their earthquake cycle are less likely to generate a characteristic earthquake than those that are late in their cycle. In other words, the probability of occurrence of a characteristic earthquake increases with the elapsed time since the last characteristic earthquake (Thenhaus and Campbell, 2003).

Renewal model describes the occurrence of earthquakes as a sequence of events with independent and identically distributed inter-event times. The time dependency is taken into consideration through the hazard rate which is dependent on the assumed probability distribution of inter-event times. The hazard rate can be calculated from the hazard function given below:

$$h(t) = \frac{f_T(t)}{1 - F_T(t)} \quad (2.20)$$

where, $f_T(t)$ and $F_T(t)$, are the probability density and cumulative distribution functions of the inter-event times, respectively.

In literature, various statistical models are recommended for the probability density function of inter-event times. Esteva (1970) proposed the gamma distribution for the inter-event times. The Weibull distribution has also been used frequently to model the inter-event times (Kameda and Ozaki, 1979, Brillinger, 1982), due to the fact that the hazard rate increases with the time passed since the last event, which is consistent with the elastic rebound theory (Reid, 1910). Nishenko and Buland (1987) have shown that lognormal distribution is appropriate for inter-event times of characteristic earthquakes. Most recently the Brownian Passage Time (BPT) model has been proposed to describe the probability distribution of inter-event times (Matthews et al., 2002). The probability density function of the BPT model is expressed as follows (Matthews et al., 2002):

$$f_T(t) = \left(\frac{\mu}{2\pi\alpha^2 t^3} \right)^{1/2} e^{-\frac{(t-\mu)^2}{2\alpha^2 \mu t}} \quad (2.21)$$

where, μ is the mean inter-event time and α is aperiodicity. It is to be noted that α is the ratio of standard deviation to mean and thus it is equivalent to the coefficient of variation of the inter-event time. The hazard rate functions corresponding to different distributions proposed for the inter-event times are shown in Figure 2.6. All distributions shown in this figure have mean 1 and standard deviation 0.5, except the exponential distribution.

The conditional expected number of characteristic earthquakes, “ $\eta(w, t_0)$ ”, in the next “ w ” years, given that it has not occurred in the last “ t_0 ” years can be evaluated from hazard function, “ $h(t)$ ”, as given below;

$$\eta(w, t_0) = \int_{t_0}^{t_0+w} h(t) dt \quad (2.22)$$

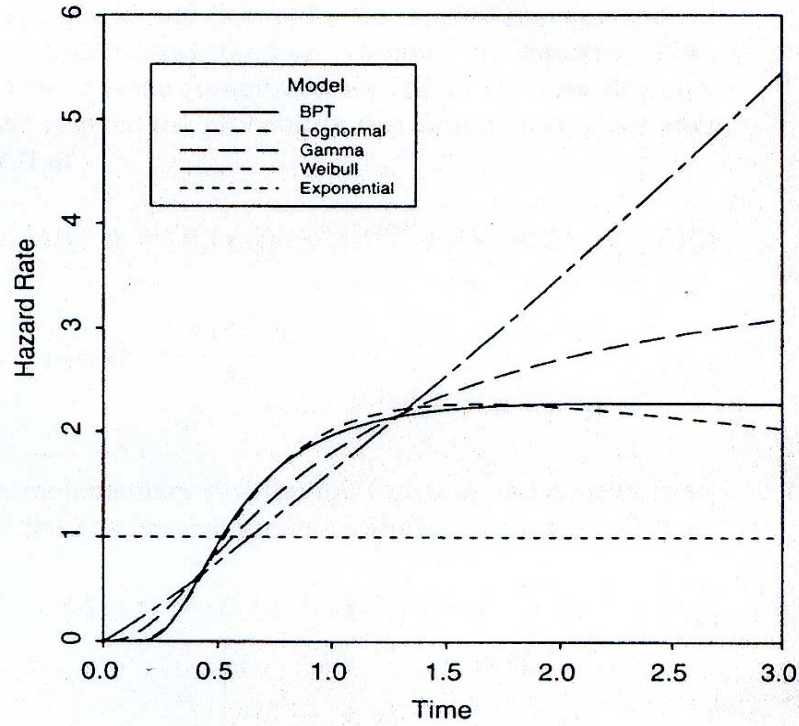


Figure 2.6 Hazard Rate Functions for Different Inter-Event Time Distributions (Matthews et al., 2002)

Most of the seismic hazard analysis programs are based on the Poisson model. In order to use these programs for non-Poissonian or characteristic earthquakes, Wu et al. (1995) proposed a renewal hybrid model where the time dependence rate of large magnitude characteristic earthquakes are considered as a renewal process together with the Poisson model for smaller earthquakes. The model aggregates the hazard stemming from both components. In other words, the probability of ground motion exceeding some specified value, “y”, during a time period, “w”, given the time since the last characteristic event, “t₀”, is expressed as follows:

$$P(Y > y/t_0) = 1 - \exp\left[-w\left(\lambda^p(Y > y) + \lambda^c(Y > y, t_0)\right)\right] \quad (2.23)$$

where $\lambda^p(Y > y)$ is the mean rate of exceedances of “y” from “smaller” Poissonian earthquakes and $\lambda^c(Y > y, t_0)$ can be imagined as the equivalent mean rate of exceedances of “y” from characteristic earthquakes.

The mean rate of exceedances of “y” from Poissonian earthquakes can be written as,

$$\lambda^P(Y > y) = v^P \cdot P[Y > y / \text{one smaller earthquake}] \quad (2.24)$$

where v^P is the mean rate of the smaller earthquakes.

The equivalent mean rate of exceedances of “y” from characteristic earthquakes is given as follows (Wu et al., 1995);

$$\lambda^C(Y > y, t_0) = \frac{1}{w} \int_{t_0}^{t_0+w} h(t) \cdot P[Y > y / \text{one characteristic earthquake}] dt \quad (2.25)$$

The terms, $P[Y > y / \text{one smaller earthquake}]$ and $P[Y > y / \text{one characteristic earthquake}]$ in Eqs. (2.24) and (2.25), are both time invariant. They can be calculated by considering the relative likelihood of different magnitudes comprising smaller or characteristic earthquakes, source to site distances and ground motion estimation equations. Therefore, equivalent mean rate of characteristic earthquakes, “ $v^C(w, t_0)$ ”, can be calculated by using “ $\eta(w, t_0)$ ” which is given in Equation (2.22) and is as follows;

$$v^C(w, t_0) = \frac{\eta(w, t_0)}{w} = \frac{1}{w} \int_{t_0}^{t_0+w} h(t) dt = \frac{1}{w} \int_{t_0}^{t_0+w} \frac{f(t)}{1-F(t)} dt \quad (2.26)$$

Since $\int \frac{F'(x)}{F(x)} = \ln|F(x)| + C$, Eq. (2.26) becomes;

$$v^C(w, t_0) = -\frac{1}{w} [\ln(G(t_0 + w)) - \ln(G(t_0))] = -\frac{1}{w} \ln \left(\frac{\int_{t_0+w}^{\infty} f(t) \cdot dt}{\int_{t_0}^{\infty} f(t) \cdot dt} \right) \quad (2.27)$$

where $G(\cdot)$ is the complementary cumulative distribution function.

In regions that have relatively low seismicity and short earthquake histories, the characteristic earthquakes may not be observed and do not appear in the earthquake catalog. Therefore, the elapsed time since the last characteristic earthquake, “ t_0 ”, can not be assessed. The only information on “ t_0 ” is that it is greater than the temporal length of the available historical earthquake record, “ L ”. In this case, Wu et al. (1995) proposed to replace “ t_0 ” in Eq. (2.25) by “ L ” and the hazard function “ $h(t)$ ” by “ $h^+(t)$ ” which is given as follows:

$$h^+(t) = \frac{G_T(t)}{\int_t^{\infty} G_T(u) du} \quad (2.28)$$

where $G_T(t)$ is the complementary cumulative distribution function of inter-event times.

2.3.4 Attenuation Relationships (Ground Motion Prediction Equations)

In seismic hazard analysis, ground motion attenuation relationships (ground motion prediction equations) are the essential tools to estimate the ground motion parameters at the site located at a distance from the source of an earthquake. When an earthquake occurs, seismic waves and consequently ground motion will propagate and attenuate with respect to distance away from its hypocenter, depending on the soil conditions. The attenuation relationship gives an estimate of ground motion parameter as a function of magnitude, distance from the site to the epicenter (or hypocenter or to a selected point on the seismic source) and other factors including type of faulting and local site conditions. Most of the attenuation relationships are derived from the statistical analyses of the strong ground motion records and they are updated as new records become available.

Although magnitude is the most acceptable scale of the earthquake severity, it can not be directly used in earthquake resistant design of structures. Peak ground acceleration (PGA), peak ground velocity (PGV) and 5 % damped elastic spectral acceleration (SA) at various frequencies at a given site are the most common parameters used in earthquake engineering. Until 1999 earthquakes, there were not adequate numbers of ground motion records to develop a reliable ground motion estimation equation for Turkey. Therefore, the attenuation relationships that were developed for other countries were used for ground motion estimations for sites in Turkey. Since 2002, a number of local attenuation models were developed based on the data recorded in Turkey. The most commonly used recent attenuation relationships are presented in the following sections.

2.3.4.1 Attenuation Models Developed for Other Countries

The attenuation relationships that are believed to be consistent with the earthquake mechanisms in our country and most widely used in seismic hazard studies carried out for Turkey can be listed as (Yücemem et al., 2006):

- Abrahamson and Silva (1997)
- Boore et al. (1997)
- Sadigh et al. (1997)
- Ambraseys et al. (1996)

Each attenuation relationship is summarized in the following sections.

2.3.4.1.1 *Abrahamson and Silva (1997)*

Abrahamson and Silva (1997) derived empirical response spectral attenuation relationships for average horizontal and vertical components of shallow earthquakes in active tectonic regions. The database used in the study consists of 655 recordings

from 58 earthquakes including Northridge earthquake. They classified the sites into two categories: deep soil and rock or shallow soil. The general functional form of the attenuation relationship is given as:

$$\ln Sa(g) = f_1(M, r_{rup}) + Ff_3(M) + HWf_4(M, r_{rup}) + Sf_5(p\hat{a}_{rock}) \quad (2.29)$$

where;

Sa(g): spectral acceleration in g

M : moment magnitude

r_{rup} : closest distance to the rupture plane in km

F : fault type (1 for reverse, 0.5 for reverse/oblique and 0 otherwise)

HW : dummy variable for hanging wall sites (1 for sites over the hanging wall, 0 otherwise)

S : dummy variable for the site class (0 for rock or shallow soil and 1 for deep soil)

The function $f_1(M, r_{rup})$ is the basic functional form of the attenuation for strike-slip events recorded at rock sites. For $f_1(M, r_{rup})$, the following form are used;

For $M \leq c_1$

$$f_1(M, r_{rup}) = a_1 + a_2(M - c_1) + a_{12}(8.5 - M)^n + [a_3 + a_{13}(M - c_1)] \ln R \quad (2.30)$$

For $M > c_1$

$$f_1(M, r_{rup}) = a_1 + a_4(M - c_1) + a_{12}(8.5 - M)^n + [a_3 + a_{13}(M - c_1)] \ln R \quad (2.31)$$

where;

$$R = \sqrt{r_{rup}^2 + c_4^2} \quad (2.32)$$

The function $f_3(M)$ that allows magnitude and period dependence of the style of faulting factor is;

$$f_3(M) = \begin{cases} a_5 & \text{for } M \leq 5.8 \\ a_5 + \frac{(a_6 - a_5)}{(c_1 - 5.8)} & \text{for } 5.8 < M < c_1 \\ a_6 & \text{for } M \geq c_1 \end{cases} \quad (2.33)$$

The functional form that takes into account the hanging wall effect, $f_4(M, r_{rup})$, is;

$$f_4(M, r_{rup}) = f_{HW}(M)f_{HW}(r_{rup}) \quad (2.34)$$

where;

$$f_{HW}(M) = \begin{cases} 0 & \text{for } M \leq 5.5 \\ M - 5.5 & \text{for } 5.5 < M < 6.5 \\ 1 & \text{for } M \geq 6.5 \end{cases} \quad (2.35)$$

and

$$f_{HW}(r_{rup}) = \begin{cases} 0 & \text{for } r_{rup} < 4 \\ a_9 \frac{r_{rup} - 4}{4} & \text{for } 4 < r_{rup} < 8 \\ a_9 & \text{for } 8 < r_{rup} < 18 \\ a_9 \left(1 - \frac{r_{rup} - 18}{7} \right) & \text{for } 18 < r_{rup} < 24 \\ 0 & \text{for } r_{rup} > 25 \end{cases} \quad (2.36)$$

The nonlinear soil response is modeled by;

$$f_5(\widehat{PGA}_{rock}) = a_{10} + a_{11} \ln(\widehat{PGA}_{rock} + c_5) \quad (2.37)$$

where \widehat{PGA}_{rock} is the expected peak acceleration on rock in g.

They gave following formula in order to calculate standard error in PGA and Sa predictions;

$$\sigma_{\text{total}}(M) = \left\{ \begin{array}{ll} b_5 & \text{for } M \leq 5.0 \\ b_5 - b_6(M - 5) & \text{for } 5.0 < M < 7.0 \\ b_5 - 2b_6 & \text{for } M \geq 7.0 \end{array} \right\} \quad (2.38)$$

The coefficients were determined by using random effects model in which the regression analysis was carried out in multiple steps and they are given for average horizontal component in Table 2.3.

2.3.4.1.2 Boore et al. (1997)

Boore et al. (1997) carried out a study on estimating peak horizontal acceleration and random horizontal component of 5 percent damped pseudo acceleration response spectra for shallow earthquakes in western North America.

They used moment magnitude as the measure of earthquake size and a distance equal to the closest horizontal distance from the station to a point on the earth's surface that lies directly above the rupture. Shear wave velocity averaged over the upper 30 m was used as a parameter to represent site effects. The ground motion estimation equation is as follows:

$$\ln Y = b_1 + b_2(M - 6) + b_3(M - 6)^2 + b_5 \ln r + b_V \ln \frac{V_s}{V_A} \quad (2.39)$$

where;

$$r = \sqrt{r_{jb}^2 + h^2}$$

Table 2.3 Coefficients for the Average Horizontal Component (Abrahamson and Silva, 1997)

Period	c ₄	a ₁	a ₃	a ₅	a ₆	a ₉	a ₁₀	a ₁₁	a ₁₂	b ₅	b ₆
0.01	5.60	1.640	-1.1450	0.610	0.260	0.370	-0.417	-0.230	0.0000	0.70	0.135
0.02	5.60	1.640	-1.1450	0.610	0.260	0.370	-0.417	-0.230	0.0000	0.70	0.135
0.03	5.60	1.690	-1.1450	0.610	0.260	0.370	-0.470	-0.230	0.0143	0.70	0.135
0.04	5.60	1.780	-1.1450	0.610	0.260	0.370	-0.555	-0.251	0.0245	0.71	0.135
0.05	5.60	1.870	-1.1450	0.610	0.260	0.370	-0.620	-0.267	0.0280	0.71	0.135
0.06	5.60	1.940	-1.1450	0.610	0.260	0.370	-0.665	-0.280	0.0300	0.72	0.135
0.08	5.58	2.037	-1.1450	0.610	0.260	0.370	-0.628	-0.280	0.0300	0.73	0.135
0.09	5.54	2.100	-1.1450	0.610	0.260	0.370	-0.609	-0.280	0.0300	0.74	0.135
0.10	5.50	2.160	-1.1450	0.610	0.260	0.370	-0.598	-0.280	0.0280	0.74	0.135
0.12	5.39	2.272	-1.1450	0.610	0.260	0.370	-0.591	-0.280	0.0180	0.75	0.135
0.15	5.27	2.407	-1.1450	0.610	0.260	0.370	-0.577	-0.280	0.0050	0.75	0.135
0.17	5.19	2.430	-1.1350	0.610	0.260	0.370	-0.522	-0.265	-0.0040	0.76	0.135
0.20	5.10	2.406	-1.1150	0.610	0.260	0.370	-0.445	-0.245	-0.0138	0.77	0.135
0.24	4.97	2.293	-1.0790	0.610	0.232	0.370	-0.350	-0.223	-0.0238	0.77	0.135
0.30	4.80	2.114	-1.0350	0.610	0.198	0.370	-0.219	-0.195	-0.0360	0.78	0.135
0.36	4.62	1.955	-1.0052	0.610	0.170	0.370	-0.123	-0.173	-0.0460	0.79	0.135
0.40	4.52	1.860	-0.9880	0.610	0.154	0.370	-0.065	-0.160	-0.0518	0.79	0.135
0.46	4.38	1.717	-0.9652	0.592	0.132	0.370	0.020	-0.136	-0.0594	0.80	0.132
0.50	4.30	1.615	-0.9515	0.581	0.119	0.370	0.085	-0.121	-0.0635	0.80	0.130
0.60	4.12	1.428	-0.9218	0.557	0.091	0.370	0.194	-0.089	-0.0740	0.81	0.127
0.75	3.90	1.160	-0.8852	0.528	0.057	0.331	0.320	-0.050	-0.0862	0.81	0.123
0.85	3.81	1.020	-0.8648	0.512	0.038	0.309	0.370	-0.028	-0.0927	0.82	0.121
1.00	3.70	0.828	-0.8383	0.490	0.013	0.281	0.423	0.000	-0.1020	0.83	0.118
1.50	3.55	0.260	-0.7721	0.438	-0.049	0.210	0.600	0.040	-0.1200	0.84	0.110
2.00	3.50	-0.150	-0.7250	0.400	-0.094	0.160	0.610	0.040	-0.1400	0.85	0.105
3.00	3.50	-0.690	-0.7250	0.400	-0.156	0.089	0.630	0.040	-0.1726	0.87	0.097
4.00	3.50	-1.130	-0.7250	0.400	-0.200	0.039	0.640	0.040	-0.1956	0.88	0.092
5.00	3.50	-1.460	-0.7250	0.400	-0.200	0.000	0.664	0.040	-0.2150	0.89	0.087

Note: Other coefficients are; a₂ = 0.512, a₄ = -0.144, a₁₃ = 0.17, c₁ = 6.4, c₅ = 0.03, n=2

and

$$b_l = \begin{cases} b_{1SS} & \text{for strike – slip earthquakes;} \\ b_{1RS} & \text{for reverse – slip earthquakes;} \\ b_{1ALL} & \text{for mechanism is not specified.} \end{cases}$$

Y: ground motion parameter (peak horizontal acceleration or pseudo acceleration response in g)

M: moment magnitude

r_{jb} : distance in km

V_s : average shear-wave velocity to 30 m in m/sec.

b_{1SS} , b_{1RS} , b_{1ALL} , b_2 , b_3 , b_5 , h , b_v and V_A : coefficients to be determined. Note that h is the fictitious depth. They used weighted, two-stage regression procedure to determine the coefficients which are given in Table 2.4.

2.3.4.1.3 Sadigh et al. (1997)

Sadigh et al. (1997) developed attenuation relationships for peak accelerations and response spectral accelerations from strong motion data recorded primarily in California earthquakes. They characterized the earthquake size by moment magnitude, M , and defined distance as minimum distance to rupture surface, r_{rup} . Attenuation relationships were developed for two general site categories: rock and deep soil. Firstly, they developed attenuation relationship for PGA by carried out regression analysis using the following general form;

$$\ln(\text{PGA}) = c_1 + c_2 M + c_3 \ln\left(r_{rup} + c_4 e^{c_5 M}\right) + c_6 Z_T \quad (2.40)$$

where Z_T is an indicator variable taking the value 1 for reverse events and 0 for strike slip events. Different coefficients are defined for events larger and smaller than $M \approx 6^{1/2}$ in order to consider near field saturation effects.

Table 2.4 Smoothed Coefficients for Pseudo-Acceleration Response Spectra (g)
(Boore et al., 1997)

Period	b _{ISS}	b _{IRV}	b _{IALL}	b ₂	b ₃	b ₅	b _v	V _A	h	σ _{ln(Y)}
0.000	-0.313	-0.117	-0.242	0.527	0.000	-0.778	-0.371	1396	5.57	0.495
0.100	1.006	1.087	1.059	0.753	-0.226	-0.934	-0.212	1112	6.27	0.460
0.110	1.072	1.164	1.130	0.732	-0.230	-0.937	-0.211	1291	6.65	0.459
0.120	1.109	1.215	1.174	0.721	-0.233	-0.939	-0.215	1452	6.91	0.462
0.130	1.128	1.246	1.200	0.711	-0.233	-0.939	-0.221	1596	7.08	0.461
0.140	1.135	1.261	1.208	0.707	-0.230	-0.938	-0.228	1718	7.18	0.463
0.150	1.128	1.264	1.204	0.702	-0.228	-0.937	-0.238	1820	7.23	0.464
0.160	1.112	1.257	1.192	0.702	-0.226	-0.935	-0.248	1910	7.24	0.466
0.170	1.090	1.242	1.173	0.702	-0.221	-0.933	-0.258	1977	7.21	0.467
0.180	1.063	1.222	1.151	0.705	-0.216	-0.930	-0.270	2037	7.16	0.468
0.190	1.032	1.198	1.122	0.709	-0.212	-0.927	-0.281	2080	7.10	0.469
0.200	0.999	1.170	1.089	0.711	-0.207	-0.924	-0.292	2118	7.02	0.470
0.220	0.925	1.104	1.019	0.721	-0.198	-0.918	-0.315	2158	6.83	0.474
0.240	0.847	1.033	0.941	0.732	-0.189	-0.912	-0.338	2178	6.62	0.475
0.260	0.764	0.958	0.861	0.744	-0.180	-0.906	-0.360	2173	6.39	0.477
0.280	0.681	0.881	0.780	0.758	-0.168	-0.899	-0.381	2158	6.17	0.482
0.300	0.598	0.803	0.700	0.769	-0.161	-0.893	-0.401	2133	5.94	0.484
0.320	0.518	0.725	0.619	0.783	-0.152	-0.888	-0.420	2104	5.72	0.487
0.340	0.439	0.648	0.540	0.794	-0.143	-0.882	-0.438	2070	5.50	0.491
0.360	0.361	0.570	0.462	0.806	-0.136	-0.877	-0.456	2032	5.30	0.492
0.380	0.286	0.495	0.385	0.820	-0.127	-0.872	-0.472	1995	5.10	0.497
0.400	0.212	0.423	0.311	0.831	-0.120	-0.867	-0.487	1954	4.91	0.499
0.420	0.140	0.352	0.239	0.840	-0.113	-0.862	-0.502	1919	4.74	0.502
0.440	0.073	0.282	0.169	0.852	-0.108	-0.858	-0.516	1884	4.57	0.504
0.460	0.005	0.217	0.102	0.863	-0.101	-0.854	-0.529	1849	4.41	0.508
0.480	-0.058	0.151	0.036	0.873	-0.097	-0.850	-0.541	1816	4.26	0.510
0.500	-0.122	0.087	-0.025	0.884	-0.090	-0.846	-0.553	1782	4.13	0.514
0.550	-0.268	-0.063	-0.176	0.907	-0.078	-0.837	-0.579	1710	3.82	0.520
0.600	-0.401	-0.203	-0.314	0.928	-0.069	-0.830	-0.602	1644	3.57	0.526
0.650	-0.523	-0.331	-0.440	0.946	-0.060	-0.823	-0.622	1592	3.36	0.533
0.700	-0.634	-0.452	-0.555	0.962	-0.053	-0.818	-0.639	1545	3.20	0.539
0.750	-0.737	-0.562	-0.661	0.979	-0.046	-0.813	-0.653	1507	3.07	0.544
0.800	-0.829	-0.666	-0.760	0.992	-0.041	-0.809	-0.666	1476	2.98	0.549
0.850	-0.915	-0.761	-0.851	1.006	-0.037	-0.805	-0.676	1452	2.92	0.553
0.900	-0.993	-0.848	-0.933	1.018	-0.035	-0.802	-0.685	1432	2.89	0.559
0.950	-1.066	-0.932	-1.010	1.027	-0.032	-0.800	-0.692	1416	2.88	0.564
1.000	-1.133	-1.009	-1.080	1.036	-0.032	-0.798	-0.698	1406	2.90	0.569
1.100	-1.249	-1.145	-1.208	1.052	-0.030	-0.795	-0.706	1396	2.99	0.577
1.200	-1.345	-1.265	-1.315	1.064	-0.032	-0.794	-0.710	1400	3.14	0.583
1.300	-1.428	-1.370	-1.407	1.073	-0.035	-0.793	-0.711	1416	3.36	0.590
1.400	-1.495	-1.460	-1.483	1.080	-0.039	-0.794	-0.709	1442	3.62	0.596
1.500	-1.552	-1.538	-1.550	1.085	-0.044	-0.796	-0.704	1479	3.92	0.601
1.600	-1.598	-1.608	-1.605	1.087	-0.051	-0.798	-0.697	1524	4.26	0.606
1.700	-1.634	-1.668	-1.652	1.089	-0.058	-0.801	-0.689	1581	4.62	0.611
1.800	-1.663	-1.718	-1.689	1.087	-0.067	-0.804	-0.679	1644	5.01	0.615
1.900	-1.685	-1.763	-1.720	1.087	-0.074	-0.808	-0.667	1714	5.42	0.619
2.000	-1.699	-1.801	-1.743	1.085	-0.085	-0.812	-0.655	1795	5.85	0.622

Secondly, they performed analyses for spectral amplification (SA/PGA) by using the following form;

$$\ln(\text{SA} / \text{PGA}) = c_7 + c_8(8.5 - M)^{2.5} + c_9 \ln(r_{\text{rup}} + c_4 e^{c_5 M}) + c_6 Z_T \quad (2.41)$$

Finally, they combined Eqs. (2.40) and (2.41) and smoothed parameters to obtain attenuation relationships that predict smooth response spectra for earthquakes having a moment magnitude from 4 and 8+ as well as at distances less than 100 km.

The attenuation model developed for rock is given as;

$$\ln Y = c_1 + c_2 M_w + c_3 (8.5 - M_w)^{2.5} + c_4 \ln(r_{\text{rup}} + e^{(c_5 + c_6 M_w)}) + c_7 \ln(r_{\text{rup}} + 2) \quad (2.42)$$

where;

Y : ground motion parameter (PGA, SA) in g

M_w : moment magnitude

r_{rup} : the closest distance to the rupture surface in km

Note that in case of reverse/thrust faulting, the above strike-slip amplitudes are to be multiplied by 1.2 for rock sites. The coefficients in Eq. (2.42) are given in Table 2.5 and Table 2.6 for $M_w \leq 6.5$ and $M_w > 6.5$, respectively. Besides, Table 2.7 presents dispersion relationships for horizontal rock motion.

Attenuation model proposed for deep soil site is given as follows;

$$\ln Y = c_1 + c_2 M_w - c_3 \ln(r_{\text{rup}} + c_4 e^{c_5 M_w}) + c_6 + c_7 (8.5 - M_w)^{2.5} \quad (2.43)$$

where;

Y : ground motion parameter (PGA, SA) in g

M_w : moment magnitude

r_{rup} : the closest distance to the rupture surface in km

$c_1 = -2.17$ for strike-slip, -1.92 for reverse and thrust earthquakes

$c_2 = 1.0$

$$c_3 = 1.70$$

$$c_4 = 2.1863, c_5 = 0.32 \text{ for } M \leq 6.5$$

$$c_4 = 0.3825, c_5 = 0.5882 \text{ for } M > 6.5$$

c_6, c_7 and standard error are given in Table 2.8.

Table 2.5 Coefficients for Rock Sites with $M_w \leq 6.5$ (Sadigh et al., 1997)

Period	c_1	c_2	c_3	c_4	c_5	c_6	c_7
0	-0.624	1.0	0.000	-2.100	1.29649	0.250	0.0
0.07	0.110	1.0	0.006	-2.128	1.29649	0.250	-0.082
0.1	0.275	1.0	0.006	-2.148	1.29649	0.250	-0.041
0.2	0.153	1.0	-0.004	-2.08	1.29649	0.250	0.0
0.3	-0.057	1.0	-0.017	-2.028	1.29649	0.250	0.0
0.4	-0.298	1.0	-0.028	-1.990	1.29649	0.250	0.0
0.5	-0.588	1.0	-0.040	-1.945	1.29649	0.250	0.0
0.75	-1.208	1.0	-0.050	-1.865	1.29649	0.250	0.0
1	-1.705	1.0	-0.055	-1.800	1.29649	0.250	0.0
1.5	-2.407	1.0	-0.065	-1.725	1.29649	0.250	0.0
2	-2.945	1.0	-0.070	-1.670	1.29649	0.250	0.0
3	-3.700	1.0	-0.080	-1.610	1.29649	0.250	0.0
4	-4.230	1.0	-0.100	-1.570	1.29649	0.250	0.0

Table 2.6 Coefficients for Rock Sites with $M_w > 6.5$ (Sadigh et al., 1997)

Period	c_1	c_2	c_3	c_4	c_5	c_6	c_7
0	-1.274	1.1	0.000	-2.100	-0.48451	0.524	0.0
0.07	-0.540	1.1	0.006	-2.128	-0.48451	0.524	-0.082
0.1	-0.375	1.1	0.006	-2.148	-0.48451	0.524	-0.041
0.2	-0.497	1.1	-0.004	-2.080	-0.48451	0.524	0.0
0.3	-0.707	1.1	-0.017	-2.028	-0.48451	0.524	0.0
0.4	-0.948	1.1	-0.028	-1.990	-0.48451	0.524	0.0
0.5	-1.238	1.1	-0.040	-1.945	-0.48451	0.524	0.0
0.75	-1.858	1.1	-0.050	-1.865	-0.48451	0.524	0.0
1	-2.355	1.1	-0.055	-1.800	-0.48451	0.524	0.0
1.5	-3.057	1.1	-0.065	-1.725	-0.48451	0.524	0.0
2	-3.595	1.1	-0.070	-1.670	-0.48451	0.524	0.0
3	-4.350	1.1	-0.080	-1.610	-0.48451	0.524	0.0
4	-4.880	1.1	-0.100	-1.570	-0.48451	0.524	0.0

Table 2.7 Dispersion Relationships for Horizontal Rock Motion (Sadigh et al., 1997)

Period	$\sigma_{ln(\gamma)}$
0	1.39-0.14M; 0.38 for M>7.21
0.07	1.40-0.14M; 0.39 for M>7.21
0.10	1.41-0.14M; 0.40 for M>7.21
0.20	1.43-0.14M; 0.42 for M>7.21
0.30	1.45-0.14M; 0.44 for M>7.21
0.40	1.48-0.14M; 0.47 for M>7.21
0.50	1.50-0.14M; 0.49 for M>7.21
0.75	1.52-0.14M; 0.51 for M>7.21
1.00	1.53-0.14M; 0.52 for M>7.21
>1.00	1.53-0.14M; 0.52 for M>7.21

Table 2.8 Coefficients for Deep Soil Sites (Sadigh et al., 1997)

Period	c_6 Strike-Slip	c_6 Reverse	c_7	Standard Error*
0	0.0	0.0	0.0	1.52-0.16M
0.075	0.4572	0.4572	0.005	1.54-0.16M
0.1	0.6395	0.6395	0.005	1.54-0.16M
0.2	0.9187	0.9187	-0.004	1.565-0.16M
0.3	0.9547	0.9547	-0.014	1.58-0.16M
0.4	0.9251	0.9005	-0.024	1.595-0.16M
0.5	0.8494	0.8285	-0.033	1.61-0.16M
0.75	0.7010	0.6802	-0.051	1.635-0.16M
1.0	0.5665	0.5075	-0.065	1.66-0.16M
1.5	0.3235	0.2215	-0.090	1.69-0.16M
2.0	0.1001	-0.0526	-0.108	1.7-0.16M
3.0	-0.2801	-0.4905	-0.139	1.71-0.16M
4.0	-0.6274	-0.8907	-0.160	1.71-0.16M

* Standard error for M>7 set equal to the value for M=7.

2.3.4.1.4 Ambraseys et al. (1996)

Ambraseys, et al. (1996) carried out a study in order to predict absolute spectral acceleration ordinates in Europe and the Middle East. The database used in this study consists of 422 triaxial records taken from 157 earthquakes in Europe and adjacent areas (including Turkey) with magnitudes ranging from 4.0 and 7.9. As the site to source distance, the closest distance to the projection of the fault rupture is used. Four different site classes are defined based on shear wave velocity averaged over the upper 30 m of the site, V_s : rock ($V_s > 750\text{m/s}$); stiff soil ($360\text{m/s} < V_s \leq 750\text{m/s}$); soft soil ($180\text{m/s} < V_s \leq 360\text{m/s}$); very soft soil ($V_s \leq 180\text{m/s}$).

Ambraseys et al. (1996) proposed the relationship given in Eq. (2.44) with the coefficients presented in Table 2.9.

$$\log(Y) = C_1' + C_2 M_s + C_4 \log \sqrt{d^2 + h_0^2} + C_A S_A + C_S S_S + \sigma P \quad (2.44)$$

In Eq. (2.44), Y is the ground motion parameter (PGA, SA) in g; M_s is surface magnitude; d is the shortest distance to the projection of fault rupture, in km; h_0 , C_1' , C_2 and C_4 are constants given in Table 2.9. σ is the standard deviation of $\log(y)$ and the constant P takes a value of 0 for mean values and 1 for 84-percentile values of $\log(Y)$. S_A and S_S account for the soil and soft soil types taking values given below:

Rock ($V_s > 750\text{m/s}$): $S_A=0$, $S_S=0$

Stiff soil ($360\text{m/s} < V_s \leq 750\text{m/s}$): $S_A=1$, $S_S=0$

Soft soil ($180\text{m/s} < V_s \leq 360\text{m/s}$): $S_A=0$, $S_S=1$

Very soft soil ($V_s \leq 180\text{m/s}$): $S_A=0$, $S_S=1$

Table 2.9 Coefficients of the Attenuation Relationship Proposed by Ambraseys et al. (1996)

Period(sec)	C_1'	C_2	h_0	C_4	C_A	C_S	σ
0.10	-0.84	0.219	4.5	-0.954	0.078	0.027	0.27
0.11	-0.86	0.221	4.5	-0.945	0.098	0.036	0.27
0.12	-0.87	0.231	4.7	-0.960	0.111	0.052	0.27
0.13	-0.87	0.238	5.3	-0.981	0.131	0.068	0.27
0.14	-0.94	0.244	4.9	-0.955	0.136	0.077	0.27
0.15	-0.98	0.247	4.7	-0.938	0.143	0.085	0.27
0.16	-1.05	0.252	4.4	-0.907	0.152	0.101	0.27
0.17	-1.08	0.258	4.3	-0.896	0.140	0.102	0.27
0.18	-1.13	0.268	4.0	-0.901	0.129	0.107	0.27
0.19	-1.19	0.278	3.9	-0.907	0.133	0.130	0.28
0.20	-1.21	0.284	4.2	-0.922	0.135	0.142	0.27
0.22	-1.28	0.295	4.1	-0.911	0.120	0.143	0.28
0.24	-1.37	0.308	3.9	-0.916	0.124	0.155	0.28
0.26	-1.40	0.318	4.3	-0.942	0.134	0.163	0.28
0.28	-1.46	0.326	4.4	-0.946	0.134	0.158	0.29
0.30	-1.55	0.338	4.2	-0.933	0.133	0.148	0.30
0.32	-1.63	0.349	4.2	-0.932	0.125	0.161	0.31
0.34	-1.65	0.351	4.4	-0.939	0.118	0.163	0.31
0.36	-1.69	0.354	4.5	-0.936	0.124	0.160	0.31
0.38	-1.82	0.364	3.9	-0.900	0.132	0.164	0.31
0.40	-1.94	0.377	3.6	-0.888	0.139	0.172	0.31
0.42	-1.99	0.384	3.7	-0.897	0.147	0.180	0.32
0.44	-2.05	0.393	3.9	-0.908	0.153	0.187	0.32
0.46	-2.11	0.401	3.7	-0.911	0.149	0.191	0.32
0.48	-2.17	0.410	3.5	-0.920	0.150	0.197	0.32
0.50	-2.25	0.420	3.3	-0.913	0.147	0.201	0.32
0.55	-2.38	0.434	3.1	-0.911	0.134	0.203	0.32
0.60	-2.49	0.438	2.5	-0.881	0.124	0.212	0.32
0.65	-2.58	0.451	2.8	-0.901	0.122	0.215	0.32
0.70	-2.67	0.463	3.1	-0.914	0.116	0.214	0.33
0.75	-2.75	0.477	3.5	-0.942	0.113	0.212	0.32
0.80	-2.86	0.485	3.7	-0.925	0.127	0.218	0.32
0.85	-2.93	0.492	3.9	-0.920	0.124	0.218	0.32
0.90	-3.03	0.502	4.0	-0.920	0.124	0.225	0.32
0.95	-3.10	0.503	4.0	-0.892	0.121	0.217	0.32
1.00	-3.17	0.508	4.3	-0.885	0.128	0.219	0.32
1.10	-3.30	0.513	4.0	-0.857	0.123	0.206	0.32
1.20	-3.38	0.513	3.6	-0.851	0.128	0.214	0.31
1.30	-3.43	0.514	3.6	-0.848	0.115	0.200	0.31
1.40	-3.52	0.522	3.4	-0.839	0.109	0.197	0.31
1.50	-3.61	0.524	3.0	-0.817	0.109	0.204	0.31
1.60	-3.68	0.520	2.5	-0.781	0.108	0.206	0.31
1.70	-3.74	0.517	2.5	-0.759	0.105	0.206	0.31
1.80	-3.79	0.514	2.4	-0.730	0.104	0.204	0.32
1.90	-3.80	0.508	2.8	-0.724	0.103	0.194	0.32
2.00	-3.79	0.503	3.2	-0.728	0.101	0.182	0.32

2.3.4.2 Attenuation Models Developed for Turkey

After two destructive earthquakes occurred in 1999 in Turkey, there has been an increase in the strong ground motion data. Therefore, researchers have been encouraged to develop local attenuation relationships for Turkey. In 2002, Gülkan and Kalkan (2002) compiled a database that contains 93 records from 47 horizontal components of 19 earthquakes that occurred between 1976 and 1999 in Turkey. They derived a set of empirical attenuation relationships to estimate free field horizontal components of peak ground acceleration and 5 percent damped pseudo acceleration response by using this database. In 2004, they updated this database and accordingly revised the relationship. Also, other researchers, Özbey et al. (2004) and Ulusay et al. (2004), developed attenuation models from the recorded ground motions in Turkey. In addition to these recent relationships, there are other attenuation relationships suggested by İnan et al. (1996), Aydan et al. (1996) and Aydan (2001) for Turkey. These relationships will be briefly explained in the following sections.

2.3.4.2.1 *İnan et al. (1996)*

İnan et al. (1996) developed the following equation for peak ground acceleration (PGA);

$$\log \text{PGA} = 0.65M - 0.9 \log R - 0.44 \quad (2.45)$$

where M is the earthquake magnitude and R is the distance to epicenter in kilometers. It should be noted that this relationship gives too conservative PGA values particularly in near source areas (Ulusay et al., 2004).

2.3.4.2.2 *Aydan et al. (1996) and Aydan (2001)*

The attenuation relationship developed by Aydan et al. (1996) is given in the following form:

$$a_{\max} = 2.8 \left(e^{0.9M_s} e^{-0.025R} - 1 \right) \quad (2.46)$$

where a_{\max} is the maximum ground acceleration; M_s and R are the surface wave magnitude and the hypocentral distance of a given earthquake, respectively.

Aydan (2001) modified the attenuation equation suggested by Aydan et al. (1996) as follows:

$$a_{\max} = 2.8 e^{-0.025R} \left(e^{0.9M_s} - 1 \right) \quad (2.47)$$

2.3.4.2.3 *Gülkan and Kalkan (2002), Kalkan and Gülkan (2004)*

Gülkan and Kalkan (2002) derived a set of empirical attenuation relationships to estimate free field horizontal components of peak ground acceleration and 5 percent damped pseudo acceleration response by using a strong ground motion database which contains 93 records from 47 horizontal components of 19 earthquakes that occurred between 1976 and 1999 in Turkey.

They used same definitions of predictory variables; i.e. earthquake size, site-to source distance and site condition parameter; and same general form of the ground motion estimation equation with Boore et al. (1997). Since actual shear wave velocities and detailed site description were not available for most of the stations, they divided site conditions in Turkey into three groups; soft soil, soil and rock; and they assigned shear wave velocities of 200, 400 and 700 m/s to these groups, respectively.

Gülkan and Kalkan (2002) applied nonlinear regression procedure to determine unknown coefficients in Eq. 2.39 and they are given in Table 2.10.

In 2004, they expanded and updated the database. This new database consists of 112 strong ground motion records of 57 earthquakes that occurred between 1976 and 2003. The coefficients estimated by Kalkan and Gülkan (2004) by using this updated database are given in Table 2.11.

Table 2.10 Coefficients of Attenuation Relationships Developed by Gülkan and Kalkan (2002)

Period (sec)	b_1	b_2	b_3	b_5	b_V	V_A	h	$\sigma_{\ln(Y)}$
0 (PGA)	-0.682	0.253	0.036	-0.562	-0.297	1381	4.48	0.562
0.10	-0.139	0.200	-0.003	-0.553	-0.167	1063	3.76	0.621
0.11	0.031	0.235	-0.007	-0.573	-0.181	1413	3.89	0.618
0.12	0.123	0.228	-0.031	-0.586	-0.208	1501	4.72	0.615
0.13	0.138	0.216	-0.007	-0.590	-0.237	1591	5.46	0.634
0.14	0.100	0.186	0.014	-0.585	-0.249	1833	4.98	0.635
0.15	0.090	0.210	-0.013	-0.549	-0.196	1810	2.77	0.620
0.16	-0.128	0.214	0.007	-0.519	-0.224	2193	1.32	0.627
0.17	-0.107	0.187	0.037	-0.535	-0.243	2433	1.67	0.621
0.18	0.045	0.168	0.043	-0.556	-0.256	2041	2.44	0.599
0.19	0.053	0.180	0.063	-0.570	-0.288	2086	2.97	0.601
0.20	0.127	0.192	0.065	-0.597	-0.303	2238	3.48	0.611
0.22	-0.081	0.214	0.006	-0.532	-0.319	2198	1.98	0.584
0.24	-0.167	0.265	-0.035	-0.531	-0.382	2198	2.55	0.569
0.26	-0.129	0.345	-0.039	-0.552	-0.395	2160	3.45	0.549
0.28	0.140	0.428	-0.096	-0.616	-0.369	2179	4.95	0.530
0.30	0.296	0.471	-0.140	-0.642	-0.346	2149	6.11	0.540
0.32	0.454	0.476	-0.168	-0.653	-0.290	2144	7.38	0.555
0.34	0.422	0.471	-0.152	-0.651	-0.300	2083	8.30	0.562
0.36	0.554	0.509	-0.114	-0.692	-0.287	2043	9.18	0.563
0.38	0.254	0.499	-0.105	-0.645	-0.341	2009	9.92	0.562
0.40	0.231	0.497	-0.105	-0.647	-0.333	1968	9.92	0.604
0.42	0.120	0.518	-0.135	-0.612	-0.313	1905	9.09	0.634
0.44	0.035	0.544	-0.142	-0.583	-0.286	1899	9.25	0.627
0.46	-0.077	0.580	-0.147	-0.563	-0.285	1863	8.98	0.642
0.48	-0.154	0.611	-0.154	-0.552	-0.293	1801	8.96	0.653
0.50	-0.078	0.638	-0.161	-0.565	-0.259	1768	9.06	0.679
0.55	-0.169	0.707	-0.179	-0.539	-0.216	1724	8.29	0.710
0.60	-0.387	0.698	-0.187	-0.506	-0.259	1629	8.24	0.707
0.65	-0.583	0.689	-0.159	-0.500	-0.304	1607	7.64	0.736
0.70	-0.681	0.698	-0.143	-0.517	-0.360	1530	7.76	0.743
0.75	-0.717	0.730	-0.143	-0.516	-0.331	1492	7.12	0.740
0.80	-0.763	0.757	-0.113	-0.525	-0.302	1491	6.98	0.742
0.85	-0.778	0.810	-0.123	-0.529	-0.283	1438	6.57	0.758
0.90	-0.837	0.856	-0.130	-0.512	-0.252	1446	7.25	0.754
0.95	-0.957	0.870	-0.127	-0.472	-0.163	1384	7.24	0.752
1.00	-1.112	0.904	-0.169	-0.443	-0.200	1391	6.63	0.756
1.10	-1.459	0.898	-0.147	-0.414	-0.252	1380	6.21	0.792
1.20	-1.437	0.962	-0.156	-0.463	-0.267	1415	7.17	0.802
1.30	-1.321	1.000	-0.147	-0.517	-0.219	1429	7.66	0.796
1.40	-1.212	1.000	-0.088	-0.584	-0.178	1454	9.10	0.790
1.50	-1.340	0.997	-0.055	-0.582	-0.165	1490	9.86	0.788
1.60	-1.353	0.999	-0.056	-0.590	-0.135	1513	9.94	0.787
1.70	-1.420	0.996	-0.052	-0.582	-0.097	1569	9.55	0.789
1.80	-1.465	0.995	-0.053	-0.581	-0.058	1653	9.35	0.827
1.90	-1.500	0.999	-0.051	-0.592	-0.047	1707	9.49	0.864
2.00	-1.452	1.020	-0.079	-0.612	-0.019	1787	9.78	0.895

Table 2.11 Coefficients of Attenuation Relationships Developed by Kalkan and Gülkan (2004)

Period (sec)	b1	b2	b3	b5	bv	VA	h	$\sigma_{ln(Y)}$
PGA	0.393	0.576	-0.107	-0.899	-0.200	1112	6.91	0.612
0.10	1.796	0.441	-0.087	-1.023	-0.054	1112	10.07	0.658
0.11	1.627	0.498	-0.086	-1.030	-0.051	1290	10.31	0.643
0.12	1.109	0.721	-0.233	-0.939	-0.215	1452	6.91	0.650
0.13	1.474	0.500	-0.127	-1.070	-0.300	1953	10.00	0.670
0.14	0.987	0.509	-0.114	-1.026	-0.500	1717	9.00	0.620
0.15	1.530	0.511	-0.127	-1.070	-0.300	1953	10.00	0.623
0.16	1.471	0.517	-0.125	-1.052	-0.298	1954	9.59	0.634
0.17	1.500	0.530	-0.115	-1.060	-0.297	1955	9.65	0.651
0.18	1.496	0.547	-0.115	-1.060	-0.301	1957	9.40	0.646
0.19	1.468	0.575	-0.108	-1.055	-0.302	1958	9.23	0.657
0.20	1.419	0.597	-0.097	-1.050	-0.303	1959	8.96	0.671
0.22	0.989	0.628	-0.118	-0.951	-0.301	1959	6.04	0.683
0.24	0.736	0.654	-0.113	-0.892	-0.302	1960	5.16	0.680
0.26	0.604	0.696	-0.109	-0.860	-0.305	1961	4.70	0.682
0.28	0.727	0.733	-0.127	-0.891	-0.303	1963	5.74	0.674
0.30	0.799	0.751	-0.148	-0.909	-0.297	1964	6.49	0.720
0.32	0.749	0.744	-0.161	-0.897	-0.300	1954	7.18	0.714
0.34	0.798	0.741	-0.154	-0.891	-0.266	1968	8.10	0.720
0.36	0.589	0.752	-0.143	-0.867	-0.300	2100	7.90	0.650
0.38	0.490	0.763	-0.138	-0.852	-0.300	2103	8.00	0.779
0.40	0.530	0.775	-0.147	-0.855	-0.264	2104	8.32	0.772
0.42	0.353	0.784	-0.150	-0.816	-0.267	2104	7.69	0.812
0.44	0.053	0.782	-0.132	-0.756	-0.268	2103	7.00	0.790
0.46	0.049	0.780	-0.157	-0.747	-0.290	2059	7.30	0.781
0.48	-0.170	0.796	-0.153	-0.704	-0.275	2060	6.32	0.789
0.50	-0.146	0.828	-0.161	-0.710	-0.274	2064	6.22	0.762
0.55	-0.306	0.866	-0.156	-0.702	-0.292	2071	5.81	0.808
0.60	-0.383	0.881	-0.179	-0.697	-0.303	2075	6.13	0.834
0.65	-0.491	0.896	-0.182	-0.696	-0.300	2100	5.80	0.845
0.70	-0.576	0.914	-0.190	-0.681	-0.301	2102	5.70	0.840
0.75	-0.648	0.933	-0.185	-0.676	-0.300	2104	5.90	0.828
0.80	-0.713	0.968	-0.183	-0.676	-0.301	2090	5.89	0.839
0.85	-0.567	0.986	-0.214	-0.695	-0.333	1432	6.27	0.825
0.90	-0.522	1.019	-0.225	-0.708	-0.313	1431	6.69	0.826
0.95	-0.610	1.050	-0.229	-0.697	-0.303	1431	6.89	0.841
1.00	-0.662	1.070	-0.250	-0.696	-0.305	1405	6.89	0.874
1.10	-1.330	1.089	-0.255	-0.684	-0.500	2103	7.00	0.851
1.20	-1.370	1.120	-0.267	-0.690	-0.498	2103	6.64	0.841
1.30	-1.474	1.155	-0.269	-0.696	-0.496	2103	6.00	0.856
1.40	-1.665	1.170	-0.258	-0.674	-0.500	2104	5.44	0.845
1.50	-1.790	1.183	-0.262	-0.665	-0.501	2104	5.57	0.840
1.60	-1.889	1.189	-0.265	-0.662	-0.503	2102	5.50	0.834
1.70	-1.968	1.200	-0.272	-0.664	-0.502	2101	5.30	0.828
1.80	-2.037	1.210	-0.284	-0.666	-0.505	2098	5.10	0.849
1.90	-1.970	1.210	-0.295	-0.675	-0.501	1713	5.00	0.855
2.00	-2.110	1.200	-0.300	-0.663	-0.499	1794	4.86	0.878

2.3.4.2.4 Özbey et al. (2004)

The study conducted by Özbey et al. (2004) resulted in empirical attenuation relationships for horizontal peak ground acceleration and 5 percent spectral acceleration. They used a database that contains 195 recordings from 17 earthquakes including Kocaeli and Düzce earthquakes in addition to their aftershocks and other events. Earthquake size was defined in terms of moment magnitude and the site to source distance was taken as the closest horizontal distance to the vertical projection of the rupture plane. Sites were divided into 4 classes according to their shear wave velocities. Site class definitions are shown in Table 2.12.

They used following empirical attenuation model:

$$\log(Y_{ij}) = a + b(M_i - 6) + c(M_i - 6)^2 + d \log \sqrt{R_{ij}^2 + h^2} + eG_1 + fG_2 \quad (2.48)$$

where;

Y_{ij} : geometric mean of the two horizontal components of the ground motion parameter in cm/s^2 from the j th recording of the i th event

M_i : moment magnitude of i th event

R_{ij} : closest horizontal distance to the vertical projection of the rupture from i th event to the location of j th recording.

The coefficients G_1 and G_2 take on values as follows;

$G_1=0$ and $G_2=0$ for site classes A and B

$G_1=1$ and $G_2=0$ for site class C

$G_1=0$ and $G_2=1$ for site class D.

Table 2.12 Site Class Definitions Used by Özbey et al. (2004)

Site Class	Shear Wave Velocity
A	>750 m/s
B	360-750 m/s
C	180-360 m/s
D	<180m/s

The coefficients a, b, c, d, e, f and h were estimated by using mixed effect model in which some of the attenuation model coefficients were modeled as random and others as fixed. These coefficients are given in Table 2.13.

2.3.4.2.5 *Ulusay et al. (2004)*

Ulusay et al. (2004) carried out a study in which a local attenuation relationship for peak ground acceleration (PGA) was developed by using 221 records from 122 earthquakes that occurred between 1976 and 2003 in Turkey. Moment magnitude was used to define earthquake size and epicentral distance was as site to source distance. Nonlinear regression method was applied to obtain an attenuation relationship for PGA.

They proposed the following relationship to predict PGA;

$$PGA = 2.18e^{0.0218(33.3M_w - R_e + 7.8427 S_A + 18.9282 S_B)} \quad (2.49)$$

where;

PGA: peak ground acceleration in gal

M_w : moment magnitude

R_e : distance to epicenter in km

The terms to include site conditions, S_A and S_B , take on following values;

$S_A=0$ and $S_B=0$ for rock sites

$S_A=1$ and $S_B=0$ for soil sites

$S_A=0$ and $S_B=1$ for soft soil sites.

Table 2.13 Attenuation Coefficients in the Equation Proposed by Özbey et al. (2004)

Period (sec)	a	b	c	d	h	e	f	$\sigma_{\log Y}$
PGA	3.287	0.503	-0.079	-1.1177	14.82	0.141	0.331	0.260
0.10	3.755	0.419	-0.052	-1.3361	17.22	0.173	0.255	0.274
0.15	3.922	0.463	-0.085	-1.3422	21.41	0.182	0.268	0.266
0.20	3.518	0.494	-0.094	-1.1162	14.87	0.113	0.285	0.243
0.25	3.270	0.517	-0.099	-0.9781	9.75	0.053	0.288	0.250
0.30	3.040	0.549	-0.095	-0.8762	6.54	0.062	0.320	0.262
0.35	2.951	0.579	-0.121	-0.8402	6.48	0.080	0.352	0.267
0.40	2.825	0.593	-0.112	-0.8089	6.48	0.102	0.394	0.281
0.45	2.690	0.605	-0.111	-0.7572	6.17	0.105	0.408	0.289
0.50	2.685	0.653	-0.171	-0.7302	5.58	0.051	0.385	0.293
0.55	2.581	0.685	-0.177	-0.6928	3.56	0.061	0.393	0.306
0.60	2.423	0.708	-0.177	-0.6291	3.41	0.059	0.399	0.302
0.65	2.325	0.724	-0.177	-0.6032	2.50	0.063	0.411	0.303
0.70	2.276	0.741	-0.174	-0.5932	2.12	0.055	0.407	0.300
0.75	2.247	0.750	-0.170	-0.5946	2.34	0.054	0.396	0.305
0.80	2.247	0.755	-0.166	-0.6075	3.22	0.070	0.392	0.307
0.85	2.243	0.774	-0.161	-0.6353	3.22	0.094	0.407	0.315
0.90	2.272	0.791	-0.172	-0.6630	4.21	0.102	0.416	0.324
0.95	2.246	0.807	-0.182	-0.6570	4.23	0.099	0.414	0.328
1.00	2.237	0.828	-0.207	-0.6543	4.14	0.100	0.413	0.331
1.10	2.227	0.855	-0.248	-0.6616	3.78	0.113	0.415	0.334
1.20	2.267	0.874	-0.267	-0.6910	4.49	0.103	0.397	0.330
1.30	2.353	0.901	-0.284	-0.7516	5.35	0.092	0.394	0.339
1.40	2.376	0.932	-0.296	-0.7752	6.90	0.070	0.375	0.349
1.50	2.445	0.943	-0.314	-0.8117	7.73	0.045	0.328	0.357
1.75	2.466	0.964	-0.331	-0.8671	7.85	0.038	0.298	0.364
2.00	2.490	0.973	-0.331	-0.9397	8.55	0.059	0.301	0.353
2.25	2.581	0.977	-0.326	-1.0345	11.21	0.070	0.299	0.347
2.75	2.559	0.980	-0.282	-1.1235	11.68	0.060	0.286	0.323
3.00	2.564	0.998	-0.282	-1.1473	12.04	0.044	0.273	0.324
3.50	2.549	1.011	-0.278	-1.1950	10.93	0.044	0.261	0.329
4.00	2.366	1.028	-0.244	-1.1710	10.72	0.025	0.253	0.324

2.3.5 Seismic Hazard Calculations

The probability of exceedance of a specified ground motion level is obtained by calculating the contribution of each seismic source independently and aggregating them based on the theorem of total probability. In order to construct a seismic hazard curve for a specific site, a set of ground motion values are selected and the annual frequency of the ground motion parameter, Y , exceeding each ground motion value, y , is calculated from the following expression:

$$\lambda(Y \geq y) = \sum_{\text{Sources } i} v_i \iint \dots \int \Pr(Y \geq y/X) f_{\tilde{X}}(\tilde{X}) d\tilde{X} \quad (2.50)$$

where; v_i is the annual rate of occurrence of earthquakes on seismic source i ; \tilde{X} is the vector of random variables that influence Y and $f_{\tilde{X}}(\tilde{X})$ is the joint probability density function of \tilde{X} . Generally, random variables in \tilde{X} are the magnitude, M , and distance, R . Assuming that these variables are independent, the annual frequency of exceedance, $\lambda(Y \geq y)$, can be written as;

$$\lambda(Y \geq y) = \sum_{\text{Sources } i} v_i \iint \Pr[Y \geq y/M, R] f_{M_i}(m) f_{R_i}(r) dm dr \quad (2.51)$$

where $f_{M_i}(m)$ and $f_{R_i}(r)$ are the probability density functions of magnitude and distance for source i , respectively.

It is too difficult to evaluate the integrals in Eq. (2.51) analytically. Therefore, in practice, earthquake magnitude distribution is discretized by dividing the possible range of magnitudes into small intervals. Then, center of each interval, denoted as M_j , is used in calculations. The possible locations of each earthquake magnitude, M_j , are also discretized by distance R_k . Therefore, a set of earthquake scenarios with magnitude, M_j , occurring at a distance of R_k from the site of interest are defined. For each scenario, the annual earthquake occurrence rate, $v(j,k)$, is calculated based on probability distributions of earthquake magnitude and ruptures. Then the annual frequency of exceedance, $\lambda(Y \geq y)$, is calculated from;

$$\lambda(Y \geq y) = \sum_{\text{Sources } i} \sum_{\text{Magnitudes } j} \sum_{\text{Dis tan ces } k} v(j, k) \Pr[Y \geq y/M_j, R_k] \quad (2.52)$$

Note that conditional probability; $P[Y \geq y/M_j, R_k]$; is computed by considering the uncertainty in the ground motion parameter predicted from the attenuation relationship as will be explained in Section 2.3.6.1.

2.3.6 Consideration of Uncertainties

PSHA accounts for uncertainties associated with randomness in various input parameters describing seismicity and modeling of ground motion attenuation. Uncertainties in PSHA are divided into two types: aleatory and epistemic. Aleatory uncertainty is the inherent variability due to unpredictable nature of future events. In other words, this is the uncertainty in the data used in the analysis and randomness related with prediction of a parameter from a specific model, assuming that the model is correct (Thenhaus and Campbell, 2003). On the other hand, epistemic or modeling uncertainty results from incomplete knowledge in the predictive models and variability in the interpretations of the data used to develop the models (Thenhaus and Campbell, 2003). This type of uncertainties can be reduced as more data are collected, more information acquired and more research completed. Some examples of uncertainties in PSHA are presented in Table 2.14. In PSHA, the aleatory uncertainties in the parameters are described by suitable probability distributions and are included directly into calculations by quantifying the appropriate statistical parameters (i.e., standard deviation, coefficient of variation). Epistemic uncertainty is considered by including alternative models and aggregating them through logic tree methodology.

Table 2.14 Examples of Uncertainties in Seismic Hazard Analysis (McGuire, 2004)

Aleatory Uncertainties

- Future earthquake locations
- Future earthquake source properties (e.g., magnitudes)
- Ground motion at a site given the median value of motion
- Details of the fault rupture process (e.g., direction of rupture)

Epistemic Uncertainties

- Geometry of seismotectonic and seismogenic zones
 - Distributions describing source parameters (e.g., rate, b value, maximum magnitude)
 - Median value of ground motion given the source properties
 - Limits on ground shaking
-

2.3.6.1 Uncertainty Due to Attenuation Equation

In both deterministic and probabilistic seismic hazard analysis approaches, the effect of a likely future earthquake in terms of desired ground motion parameter at a certain distance is estimated by using available ground motion estimation equations (attenuation relationships). These equations express ground motion as a function of earthquake magnitude, site-to-source distance, source mechanism and site conditions. They are generally derived from statistical analyses of recorded ground motion data. Figure 2.7 shows median values of Peak Ground Acceleration (PGA) at rock sites predicted by Kalkan and Gülkan (2004) attenuation relationship for Kocaeli, 1999 Earthquake as well as measured data. It can be seen from this figure that recorded PGA values may deviate from the value predicted by using the derived attenuation relationship. This uncertainty is treated in such a way that natural logarithm of ground motion parameter follows a normal distribution around the mean attenuation curve. In other words, uncertainty in the ground motion parameter at specified magnitude and distance levels is represented by a lognormal distribution. Therefore, the probability density function of natural logarithm of specified ground motion parameter, Y , is as follows:

$$f_Y(y) = \frac{1}{\sqrt{2\pi}\sigma_{\ln Y}} \exp\left[-\frac{1}{2}\left(\frac{\ln(y) - \overline{\ln Y(m,r)}}{\sigma_{\ln Y}}\right)^2\right] \quad (2.53)$$

where; y is the ground motion level of interest; $\overline{\ln Y(m,r)}$ is the mean value of natural logarithm of ground motion caused by an earthquake with magnitude, m , occurred at a distance, r , to the site and $\sigma_{\ln Y}$ is the standard deviation of $\ln Y$. Figure 2.8 (a) shows the visual description of Eq. (2.53).

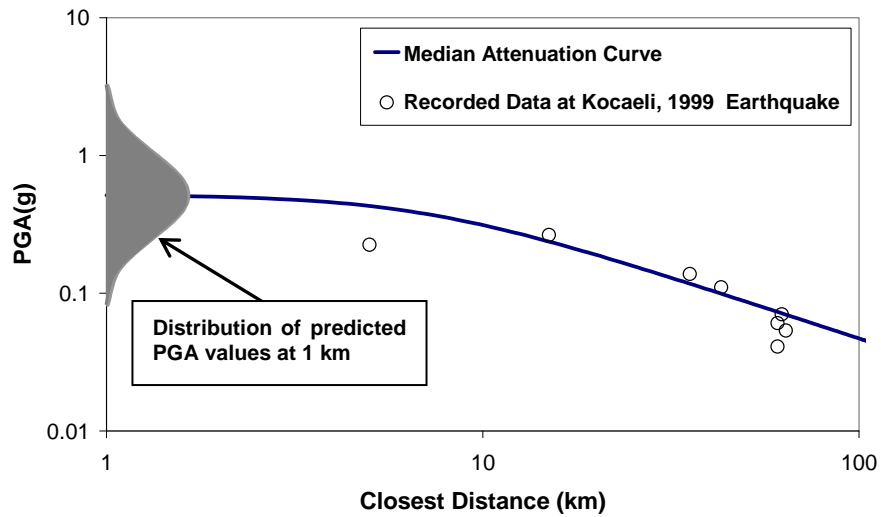


Figure 2.7 Median Peak Ground Acceleration (PGA) Curve Predicted for Kocaeli, 1999 Earthquake by Using Kalkan and Gülkan (2004) Attenuation Relationship at Rock Sites; Distribution of PGA Values at 1 km Distance and the Recorded Data

After the classical PSHA model was introduced, this uncertainty has been incorporated into the analysis directly. Therefore, the annual probability of ground motion parameter exceeding a specified level is determined not only by its median value but also by its standard deviation. In PSHA, for each earthquake scenario the probability of exceeding a specified ground motion level, y , is calculated by integrating Eq. (2.53) as shown by Eq. (2.54).

$$\Pr(Y > y) = \frac{1}{\sqrt{2\pi}\sigma_{\ln Y}} \int_{\ln y}^{\infty} \exp\left[-\frac{1}{2}\left(\frac{\ln(y) - \overline{\ln Y(m,r)}}{\sigma_{\ln Y}}\right)^2\right] d \ln y \quad (2.54)$$

For each ground motion level, the probability given in Eq. (2.54) is calculated and then it is plotted to obtain a hazard curve like the one shown in Figure 2.8 (b). This curve actually shows the complementary cumulative distribution function of a selected ground motion parameter. For an assumed earthquake scenario, annual rate of ground motion parameter exceeding a specified level, y , is calculated by multiplying the $\Pr(Y>y)$ with the annual rate of this scenario.

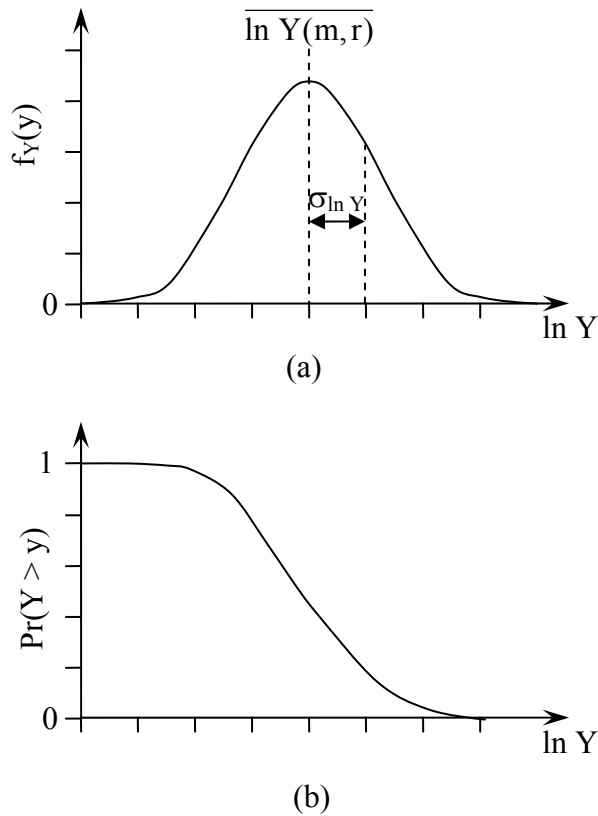


Figure 2.8 (a) Probability Density Function of Ground Motion Parameter, Y , for a Single Scenario, (b) Complementary Cumulative Distribution Function Describing the Probability of Ground Motion Parameter Exceeding the Level, Y , for a Single Scenario

Consider the site and fault discussed above and assume that this fault has provided only one scenario earthquake with magnitude equal to 7.5. This earthquake is assumed to rupture the entire fault. Firstly, classical PSHA model, in which uncertainty in the attenuation relationship is not taken into account, is applied to obtain the seismic hazard at the site. Since there is only one scenario earthquake, only one hazard value that is equal to the annual rate of this earthquake corresponding to median value of PGA is obtained. This median value is calculated by using the attenuation relationship of Kalkan and Gülkan (2004). Then uncertainty in the attenuation equation is introduced. Different values of uncertainty in $\ln(\text{PGA})$ are assumed and seismic hazard analyses are performed by using EZ-FRISK (Risk Engineering, 2005). In other words, $\sigma_{\ln \text{PGA}}$ is first taken as 0.612, that is the original value reported by Kalkan and Gülkan (2004), and then 1/3, 2/3, 4/3, 5/3 times of this value (i.e. the values of 0.204, 0.408, 0.612, 0.816 and 1.02) are considered in the subsequent analyses. Figures 2.9 and 2.10 show the probability density functions and seismic hazard curves corresponding to these cases.

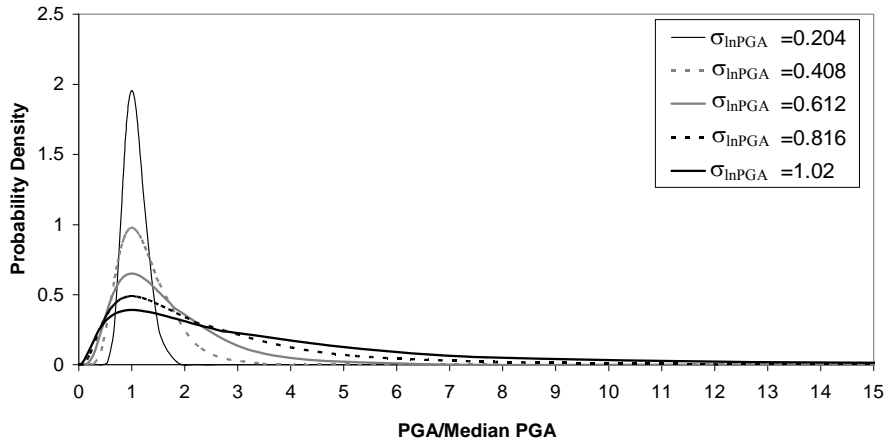


Figure 2.9 Probability Density Functions Corresponding to Different Values of $\sigma_{\ln(\text{PGA})}$

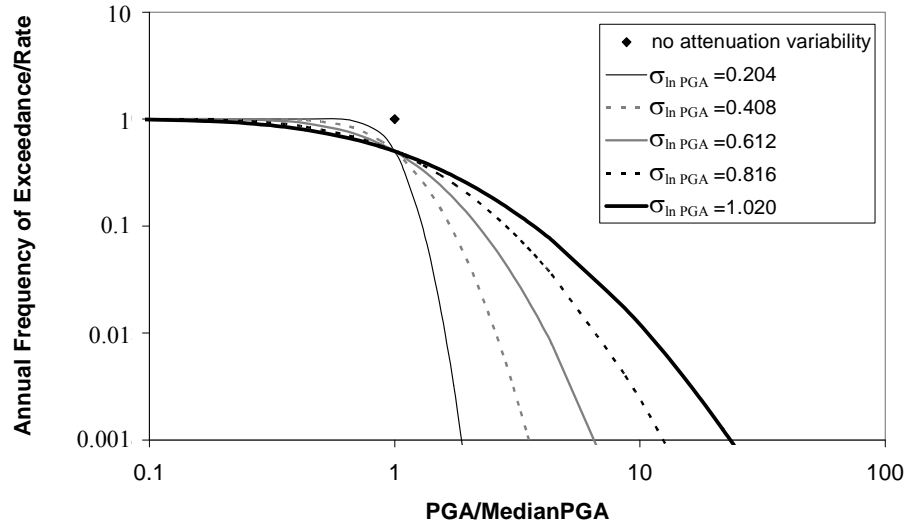


Figure 2.10 Hazard Curves Corresponding to Different Values of $\sigma_{\ln(\text{PGA})}$

Since the normal distribution has a nonzero probability over all ground-motion levels, there is a finite probability for ground motion parameter exceeding physically impossible higher values. Although these values have very low annual probabilities of exceedance or long return periods, they are considered for rare situations where seismic hazard analysis must consider such extreme cases. For very long return periods, the hazard estimates are mainly governed by the tail of the lognormal distribution. Therefore, this confusion is eliminated by truncating the distribution at some upper bound. Since the maximum ground motion that can be experienced at the site is controlled by many factors like magnitude, the upper bound is generally assumed to lie a certain number of standard deviations above the median value. Due to truncation of the distribution, the probability density function is normalized and becomes:

$$f_Y(y) = \begin{cases} \frac{1}{(1-K_\Phi)} \frac{1}{\sqrt{2\pi}\sigma_{\ln Y}} \exp\left[-\frac{1}{2}\left(\frac{\ln(y) - \ln Y(m,r)}{\sigma_{\ln Y}}\right)^2\right] & \text{for } y \leq y_{\text{trun}} \\ 0 & \text{for } y > y_{\text{trun}} \end{cases} \quad (2.55)$$

$$K_{\Phi} = \Phi * \left(\frac{\ln(y_{\text{trun}}) - \overline{\ln Y(m,r)}}{\sigma_{\ln Y}} \right) \quad (2.56)$$

where; y is ground motion level of interest; $\overline{\ln Y(m,r)}$ is the mean value of natural logarithm of ground motion caused by an earthquake with magnitude, m , occurred at a distance, r , to the site and $\sigma_{\ln Y}$ is its standard deviation; y_{trun} is the upper bound of ground motion, Φ^* is the normal (Gaussian) complementary cumulative distribution function.

In order to exhibit the influence of truncation of attenuation residuals on seismic hazard results, the example mentioned above is considered. But, this time, seismic hazard analyses are performed by truncating the probability density function on the attenuation relationship at different levels. In these analyses, upper bound for natural logarithm of PGA is assumed to lie 3, 2, 1, 0.8, 0.6, 0.4, 0.2 times $\sigma_{\ln \text{PGA}}$ above the mean value that is calculated by Kalkan and Gülkan (2004) attenuation relationship. $\sigma_{\ln \text{PGA}}$ is taken as 0.612. Analyses are carried out by using EZ-FRISK (Risk Engineering, 2005). Figures 2.11 and 2.12 show the probability density functions and seismic hazard curves obtained from these analyses. In these graphs, PGA values are normalized with respect to the median PGA value predicted by Kalkan and Gülkan (2004) attenuation relationship. Actually, median value deviates from this value due to truncations of distribution. Still the median value calculated from the attenuation equation is used in these graphs.

As explained in Section 2.3.4, different attenuation relationships are proposed in the literature. In order to examine the sensitivity of seismic hazard to the choice of attenuation relationship, seismic hazard analyses are carried out by using EZ-FRISK (Risk Engineering, 2005) for the site considered above by using the attenuation relationships proposed by Kalkan and Gülkan (2004), Boore et al. (1997), Abrahamson and Silva (1997) and Sadigh et al. (1997) for PGA at rock sites. For each relationship, the original value of the standard deviation in natural

logarithm of PGA as given by the authors is applied. Figure 2.13 shows the hazard curves obtained from these analyses.

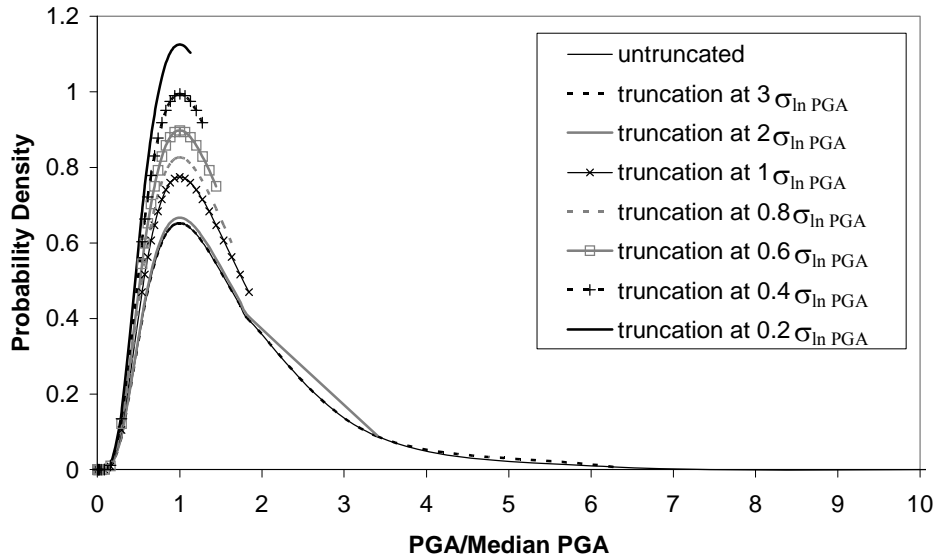


Figure 2.11 Probability Density Functions of PGA Truncated at Different Levels

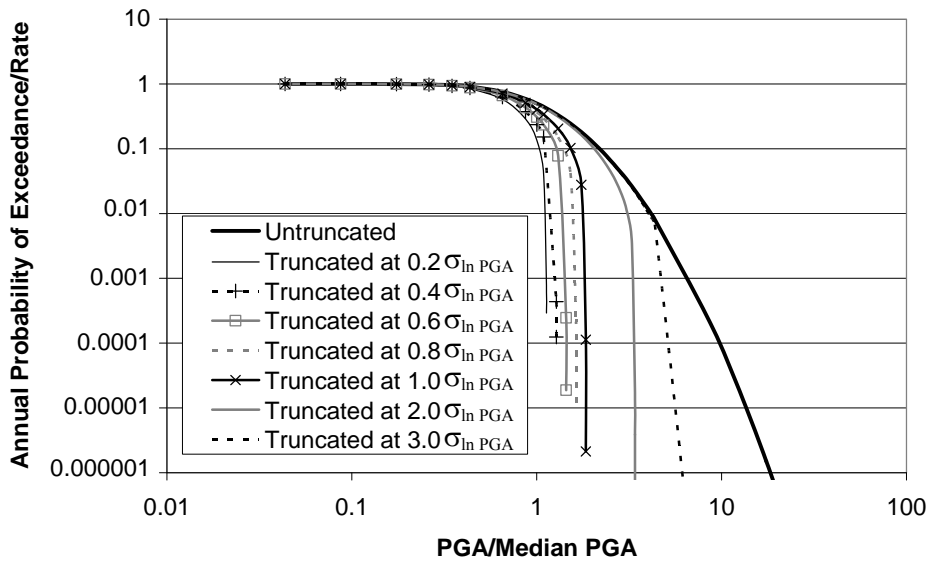


Figure 2.12 Hazard Curves Corresponding to Truncation of Attenuation Residuals at Different Levels

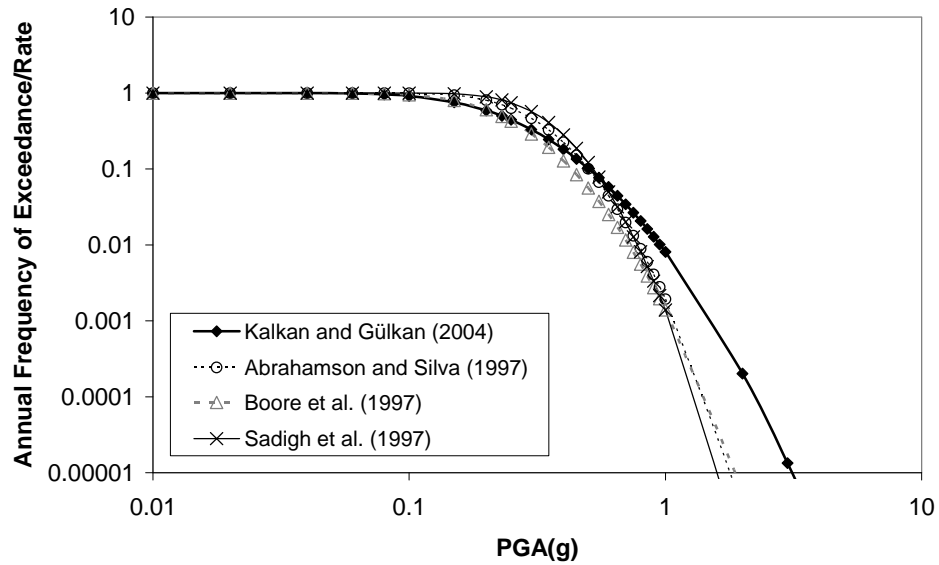


Figure 2.13 Hazard Curves Obtained by Using Different Attenuation Relationships

It can be observed from Figures 2.10 and 2.13 that seismic hazard results are sensitive to the choice of attenuation equation as well as to the variability around the mean prediction equation. Therefore, great care should be paid to determine the appropriate attenuation equation and the corresponding standard deviation of the selected ground motion parameter in seismic hazard analysis. Attenuation relationship should be selected based on the regional tectonic settings of the region considered. If there is not any reliable local attenuation relationship, equations developed for the regions with similar tectonic regime can be used. But, the analyst should check the consistency of these equations and their uncertainties by comparing them with available ground motion recorded from earthquakes that occurred at the region considered. In addition, truncation of attenuation residuals affects the ground motion values estimated especially for very low annual probabilities of exceedances or very long return periods. This is confirmed by the hazard curves presented in Figure 2.12. Therefore, the analyst who deals with such extreme cases should decide on the value of the upper bound of ground motion.

2.3.6.2 Uncertainty in the Spatial Distribution of Earthquakes

In PSHA, the uncertainty in future earthquake locations is compensated by delineating line (fault) or area sources.

In the earlier PSHA models, line sources are divided into infinitely small parts and each part is treated as a point source. Since then, many empirical ground motion estimation equations which use the shortest distance between the site of interest and a fault rupture as the distance measure have been developed. In order to use these relationships in PSHA, the future ruptures of the fault should be estimated. As explained in Section 2.3.1, there are three different models in literature; namely, fault-rupture, segmentation and cascading.

In fault-rupture model, estimated rupture length or area is used. In literature, there are many empirical relationships in which rupture length, RL, is correlated with earthquake magnitude. They are generally derived based on field observations after past earthquakes. Table 2.15 summarizes some of these relationships.

It can be seen from Table 2.15 that there is some degree of uncertainty (dispersion) in rupture length estimated by using the relationships given in the literature. This uncertainty is incorporated into PSHA computations by considering a set of rupture lengths for each earthquake magnitude. In other words, rupture of an earthquake with magnitude, m , is defined to have length, $\ell_i(m)$, given below (Bender and Perkins, 1987):

$$\text{Log}_{10}[\ell_i(m)] = a + bm + \eta(i)\sigma_\ell \quad (2.57)$$

where a and b are constants; σ_ℓ is the standard deviation of rupture length.

Table 2.15 Relationships between Magnitude and Rupture Length

Data	Fault Type	Equation	Dispersion $\sigma_{\log RL}$	Reference
World-wide	Strike-slip	$\text{Log RL} = -3.55+0.74M_w$	0.23	Wells and Coppersmith (1994)
World-wide	Strike-slip	$\text{Log RL} = -4.10+0.804M_s$	0.334	Bonilla et al. (1984)
World-wide	Reverse	$\text{Log RL} = -2.86+0.63M_w$	0.20	Wells and Coppersmith (1994)
World-wide	Reverse	$\text{Log RL} = -1.96+0.497M_s$	0.202	Bonilla et al. (1984)
World-wide	Normal	$\text{Log RL} = -2.01+0.50M_w$	0.21	Wells and Coppersmith (1994)
World-wide	All	$\text{Log RL} = -3.22+0.69M_w$	0.22	Wells and Coppersmith (1994)
World-wide	All	$\text{Log RL} = -2.77+0.619M_s$	0.286	Bonilla, et al. (1984)
Middle East	All	$\text{Log RL} = -4.09+0.82M_s$	-	Ambraseys and Jackson (1998)
Turkey	All	$RL = 0.0014525M_s e^{1.31M_s}$	-	Aydan (1997), Aydan et al. (2001)

The probability of observing the i^{th} rupture length is calculated from (Bender and Perkins, 1987):

$$p(i) = \frac{1}{\sqrt{2\pi}} \int_{f(i)}^{f(i+1)} \exp\left(-\frac{x^2}{2}\right) dx \quad (2.58)$$

In Eq. (2.58), $f(i)$ is selected in such a way that $\eta(i)$ is:

$$f(i) < \eta(i) \leq f(i+1)$$

$$f(1) = -\infty$$

$$f(n_r+1) = \infty$$

$$\sum_{i=1}^{n_r} p(i) = 1$$

where n_r is the number of possible rupture lengths considered per magnitude.

The rupture in a future earthquake can be located at anywhere along the fault. In EZ-FRISK (Risk Engineering, 2005), two parameters are used in the determination of possible rupture locations; namely, horizontal integration increment and vertical integration increment. The algorithm followed in EZ-FRISK (Risk Engineering, 2005) for the determination of rupture locations is as follows (Dobbs, 2008):

When considering the location of the first rupture, EZ-FRISK first calculates the rupture length. For a given rupture length, the first rupture is placed at 1/2 the rupture length from the start of the fault trace. The last rupture is placed at 1/2 the rupture length from the end of the fault. The number of increments in placing the rupture lengths is calculated by dividing the end position minus the start position by the horizontal integration increment. Then EZ-FRISK calculates the actual horizontal integration increment - this is actually an arc length increment. It proceeds to place the other ruptures at even intervals along the fault. A similar approach is used for the vertical placement.

In order to investigate the effect of rupture length uncertainty on seismic hazard results, consider the fault discussed in the previous section. It is now assumed that

this fault has produced an earthquake with magnitude 6.3. Sites having 1 km, 5 km and 10 km closest distances to fault are selected as shown in Figure 2.14. Site names begin with S and continue with closest distance to fault and then relative location of it from fault like a, b, c...etc. Seismic hazard analyses are performed by using the rupture length equation developed by Wells and Coppersmith (1994) for all fault types. The empirical ground motion prediction equation developed by Kalkan and Gülkan (2004) for peak ground acceleration at rock sites is selected to model the attenuation characteristics of ground motion. For the standard deviation of logarithm of rupture length, the value of 0.22 which is given by the Wells and Coppersmith (1994) is used. In EZ-FRISK (Risk Engineering, 2005), the uncertainty in rupture length is incorporated into seismic hazard analyses by defining the number of different discrete ruptures as an input parameter which is named as number of rupture lengths. Analyses are performed for the sites by assigning different values to this parameter, i.e. 2, 4, 8, 16 and 100. Also, additional analyses in which the uncertainty in rupture length is not taken into consideration are performed by using EZ-FRISK (Risk Engineering, 2005). The difference in seismic hazard results obtained by ignoring rupture length uncertainty and considering it by using different numbers of rupture lengths are given in figures presented in Appendix A.

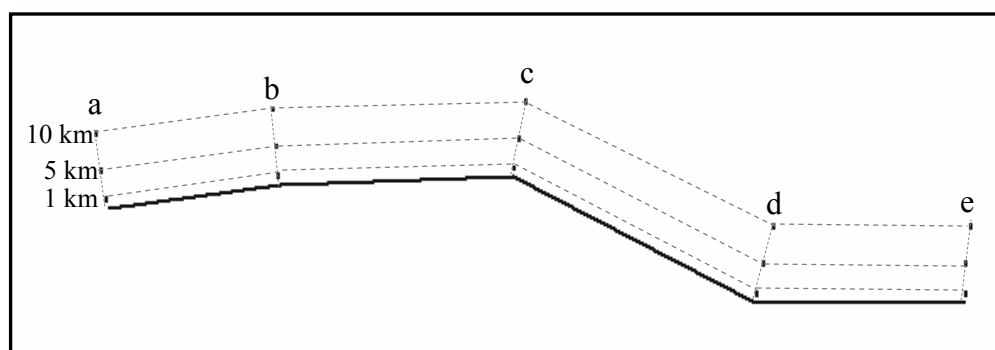


Figure 2.14 Locations of Fault and Sites Considered in the Analyses Performed to Investigate the Effect of Rupture Length Uncertainty on Seismic Hazard Results

It can be observed from the figures given in Appendix A that no significant difference is observed between the results obtained by considering and ignoring rupture length uncertainty at the sites located near the ends of the fault (e.g., Site1a, Site5a, Site10a, Site1e, Site5e, Site10e in Figure 2.14). On the other hand, higher difference is observed for the intermediate sites (e.g. 1c, 5c, 10c, 1d, 5d in Figure 2.14). The difference is small at low PGA values and it increases as much as 12 % at high PGA values. The closest distance to the fault also influences the results. The difference decreases as distance to the fault increases. In addition, increasing number of possible rupture lengths per magnitude does not change the results significantly.

Seismic hazard analyses are performed for Site 1c by assigning different values to standard deviation of logarithm of rupture length. In other words, $\sigma_{\log RL}$ is taken as 0.11, 0.22, 0.33 or 0.44. Figure 2.15 shows the differences between the hazard values obtained by taking $\sigma_{\log RL}$ as 0.11, 0.22, 0.33 and 0.44 and those obtained by ignoring rupture length uncertainty for the site. In this figure, PGA values are normalized with respect to median PGA value which is obtained from DSHA for magnitude of 6.3. It can be seen from this figure that there is significant difference between the hazard values estimated by using different values for $\sigma_{\log RL}$, the difference increases as the $\sigma_{\log RL}$ increases. Besides, the difference is small for lower PGA values whereas it increases as high as 48% for higher PGA values.

Different equations are proposed in literature in order to estimate the mean value of log (RL). Figure 2.16 shows the variations of rupture length as a function of earthquake magnitude for the relationships proposed by Wells and Coppersmith (1994), Bonilla, et al. (1984) and Ambraseys and Jackson (1998) for all fault types. It can be observed from this figure that for magnitudes greater than 6.5 there is no significant difference between the rupture lengths estimated from these equations. For magnitudes less than 6.5, the difference increases as magnitude decreases. In order to examine the sensitivity of seismic hazard results to the choice of rupture length estimation equation, consider the fault discussed above. But, this time, it is

assumed that this fault has produced only earthquakes with magnitude 5.0 in order to check the sensitivity of results to the rupture length corresponding to smaller magnitudes. Seismic hazard analyses are carried out for Site 1c by utilizing the equations developed by Wells and Coppersmith (1994), Bonilla et al. (1984) and Ambraseys and Jackson (1998) for all fault types. Standard deviation of logarithm of rupture length is taken as zero in the computations. Figure 2.17 shows the seismic hazard curves obtained for Site 1c. It can be seen from this figure that there is no significant difference among the seismic hazard results.

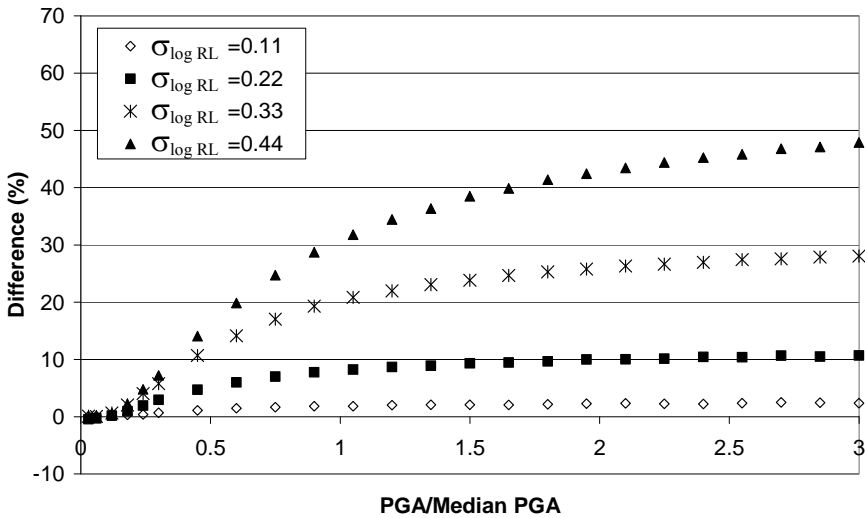


Figure 2.15 Differences in Seismic Hazard Values Obtained for Site 1c by Using Different Values of Standard Deviation for Logarithm of Rupture Length

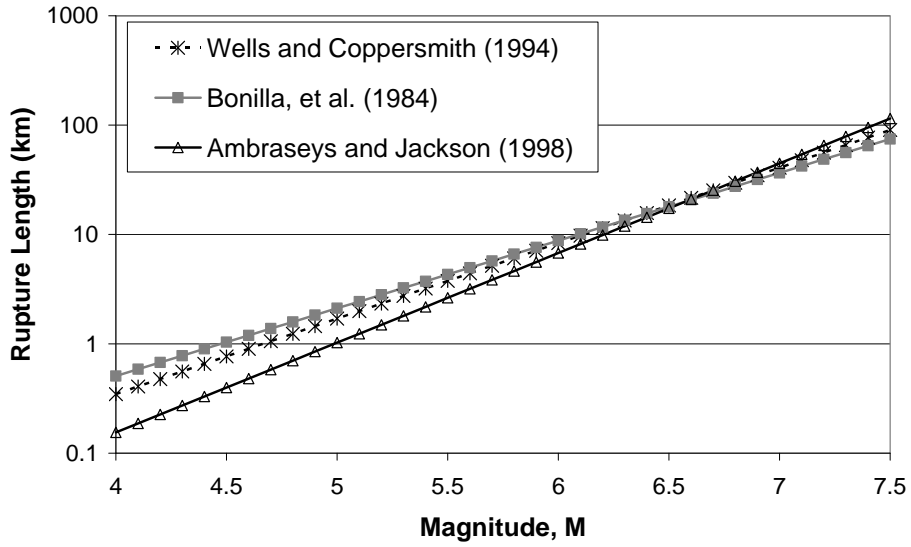


Figure 2.16 Variation of Rupture Length as a Function of Earthquake Magnitude According to the Relationships Proposed by Wells and Coppersmith (1994), Bonilla, et al. (1984) and Ambraseys and Jackson (1998)

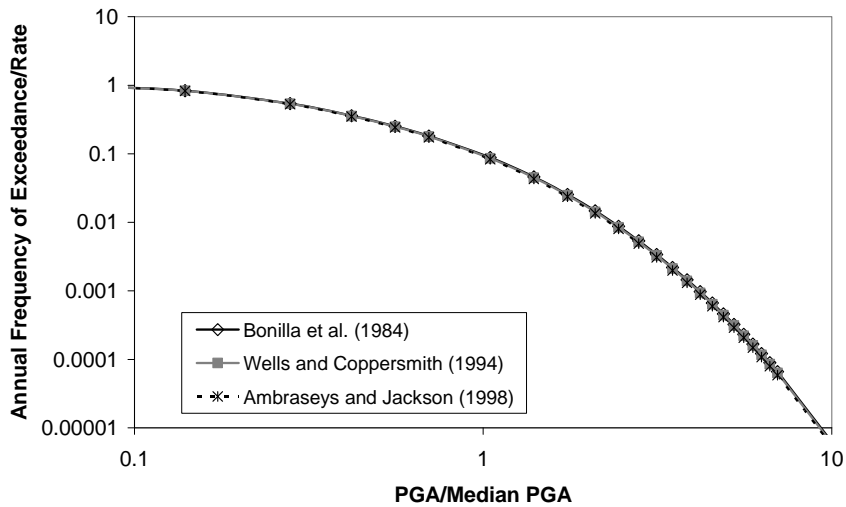


Figure 2.17 Seismic Hazard Curves Obtained for Site 1c by Using Different Rupture Length Estimation Equations for Magnitude 5 Earthquake

The fault used in the analyses explained above consists of four segments, namely, Darıca, Adalar, Yeşilköy and Kumburgaz segments (Yüçemen et al., 2006). Locations of these segments are shown in Figure 2.18 and their parameters are presented in Table 2.16. Seismic hazard analyses are performed by using fault segmentation concept for the three sites shown in Figure 2.18. In the analyses, lower bounds of the return intervals given in Table 2.16 are used to calculate activity rates of maximum magnitudes of the segments. In order to compare segmentation approach with the fault-rupture model, seismic hazard analyses are carried out by taking minimum and maximum earthquake magnitudes for the whole fault as 6.7 and 6.9, respectively. The total earthquake occurrence rate of segments is uniformly distributed over magnitudes between 6.7 and 6.9. Figure 2.19 shows seismic hazard curves obtained from these analyses for Site 1, Site 2 and Site 3.

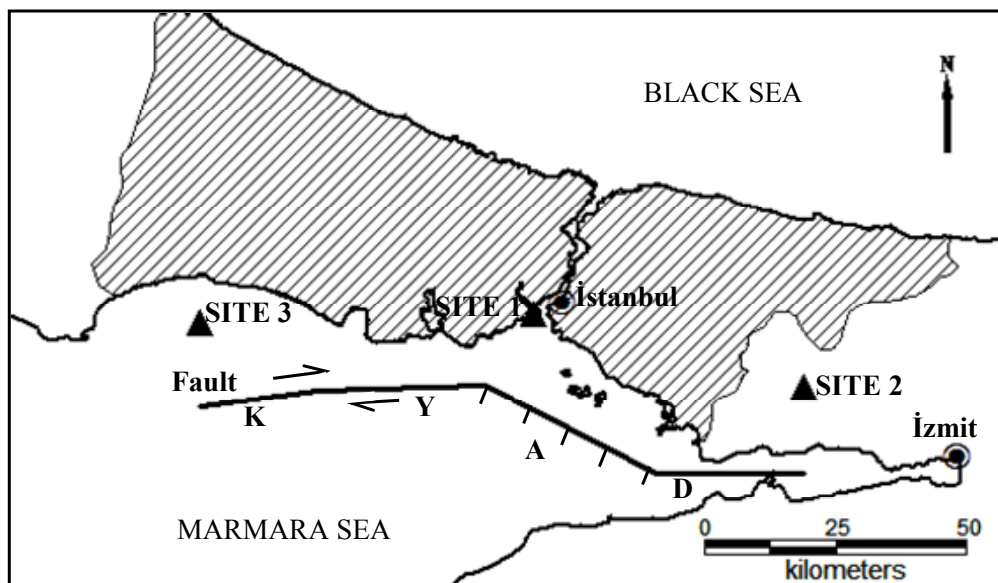


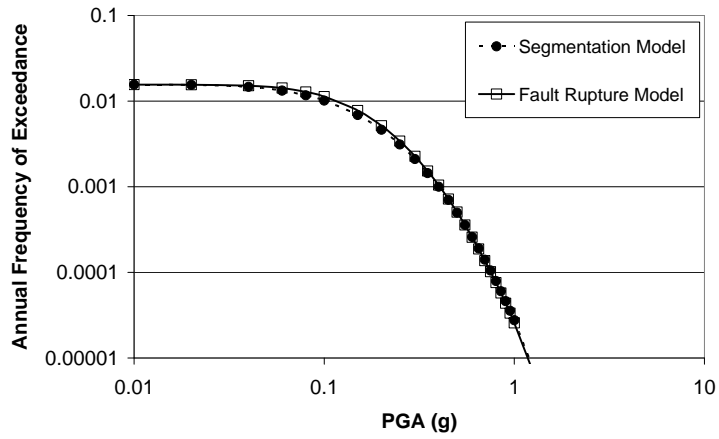
Figure 2.18 Locations of Darıca (D), Adalar (A), Yeşilköy (Y) and Kumburgaz (K) Segments (Yüçemen et al., 2006)

Table 2.16 Parameters of the Darıca, Adalar, Yeşilköy and Kumburgaz Segments

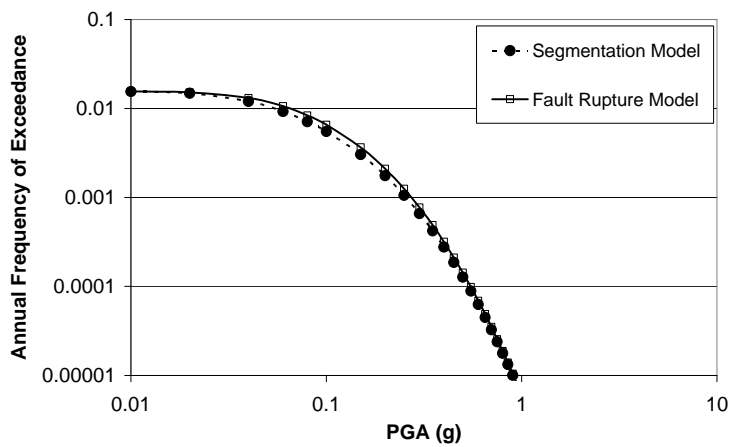
Segment Name	Type	Length (km)	Maximum Magnitude	Recurrence Interval* (RI) (in years)
Darıca	Strike Slip	28	6.8	$500 < RI \leq 1000$
Adalar	Normal	37	6.9	$200 < RI \leq 500$
Yeşilköy	Strike Slip	31	6.8	257 ± 23
Kumburgaz	Strike Slip	23	6.7	257 ± 23

* Recurrence intervals of the segments are taken from Yüçemen et al. (2006).

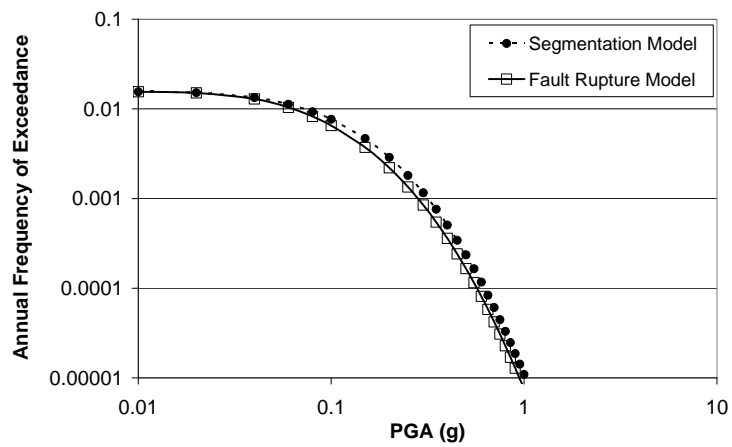
It can be observed from Figure 2.19 that segmentation and fault-rupture models may give different seismic hazard results depending on the earthquake occurrence rate of the segment nearest to the site as well as its maximum magnitude. Since earthquake magnitudes and their occurrence rates are distributed over the whole fault in the fault-rupture model, seismic hazard values predicted by using this model are higher at the sites which are located near the segment with low earthquake magnitude and earthquake occurrence rate. In this example, there is no significant difference between maximum magnitudes of the segments. Therefore, the difference may result from the earthquake occurrence rates of the segments. In Site 1 and Site 2, no significant difference is observed between the results obtained by using these two models. On the other hand, in Site 3 where Kumburgaz segment is the most critical source of seismic threat and its earthquake occurrence rate is high, segmentation model gives higher seismic hazard results compared with fault-rupture model. It should be noted that the difference between these two models is expected to increase as distance to fault decreases. As a result, the analyst should make detailed investigations to determine boundaries, maximum magnitudes and earthquake occurrence rates of the segments of a fault or fault system to apply the fault segmentation model in seismic hazard analysis.



(a) Site1



(b) Site2



(c) Site3

Figure 2.19 Seismic Hazard Curves Obtained by Considering Segmentation Concept and Fault-Rupture Model

For the segments explained above, the cascading methodology developed by Cramer et al. (2000) is also applied. In literature, this methodology is generally applied to rupture probabilities of segments calculated by using time dependent or renewal models. In order to compare the seismic hazard results obtained from the cascade model with those from the fault segmentation model, the probability of earthquake occurrences in 50 years is calculated for each segment based on the Poisson model. Table 2.17 shows the calculations carried out to obtain multi-segment and individual segment rupture probabilities by using the Eqs. (2.2) and (2.3) given in Section 2.3.1. The probabilities, P_{cj} , given in the final stage are converted to equivalent Poisson rates by using the equation given below;

$$v_{eq} = -\frac{\ln(1 - P_{cj})}{w} \quad (2.59)$$

Figure 2.20 shows seismic hazard curves obtained for the sites shown in Figure 2.18 by using the cascade and fault segmentation models.

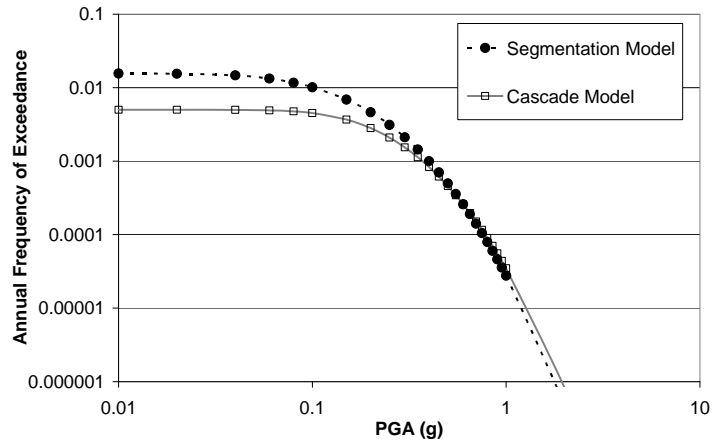
Compared with segmentation model, cascade model gives higher seismic hazard values for high PGA values whereas it resulted in lower values for low PGA values. This result is expected due to the reason that cascading of contiguous segments into longer ruptures results in an increase in maximum magnitude. Since cascade model is based on conservation of seismic moment rate, the total rate of earthquakes decreases as maximum magnitude of multi-segment rupture rises.

Sometimes, geographic conditions are the constraints to determine the exact locations of faults. This is the case for the segments discussed above because they extend beneath the Marmara Sea. Therefore, their locations are determined by bathymetry and reflection survey. In addition, there is an uncertainty in the locations of past earthquakes. Therefore, the epicenter of an earthquake generated by a fault may be located away from it due to prediction errors. In such a case, the narrow area sources can be used to compensate for these uncertainties.

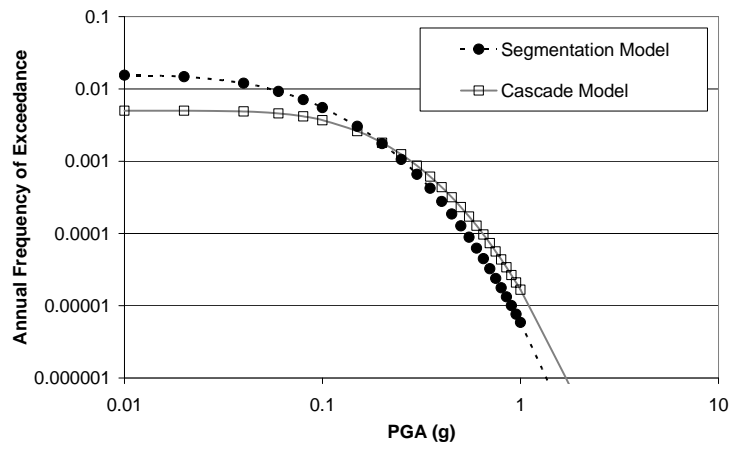
Table 2.17 Calculations of Multi-Segment and Individual Segment Probabilities According to the Cascade Methodology Defined by Cramer et al. (2000)

Cascade or Segment	Length (km)	M_{max}	P_i	$1-(1-P_i)/\prod(1-P_{c_j})$	P_{c_j}
1					
D+A+Y+K	119	7.5	-		0.095163
Darıca (D)	28	6.8	0.095163	$1-(1-0.095163)/(1-0.095163)^*$	0
Adalar (A)	37	6.9	0.221199	$1-(1-0.221199)/(1-0.095163)=$	0.139291
Yeşilköy (Y)	31	6.8	0.192389	$1-(1-0.192389)/(1-0.095163)=$	0.107451
Kumburgaz (K)	23	6.7	0.192389	$1-(1-0.192389)/(1-0.095163)=$	0.107451
2					
A+Y+K	91	7.4	-		0.107451
Adalar (A)	37	6.9	0.139291	$1-(1-0.139291)/(1-0.107451)=$	0.035673
Yeşilköy (Y)	31	6.8	0.107451	$1-(1-0.107451)/(1-0.107451)^*$	0
Kumburgaz (K)	23	6.7	0.107451	$1-(1-0.107451)/(1-0.107451)^*$	0
Final					
D+A+Y+K	119	7.5	-		0.095163
A+Y+K	91	7.4	-		0.107451
Darıca (D)	28	6.8	0.095163	$1-(1-0.095163)/(1-0.095163)^*$	0
Adalar (A)	37	6.9	0.221199	$1-(1-0.221199)/(1-0.095163)/(1-0.107451)=$	0.035673
Yeşilköy (Y)	31	6.8	0.192389	$1-(1-0.192389)/(1-0.095163)/(1-0.107451)=$	0
Kumburgaz (K)	23	6.7	0.192389	$1-(1-0.192389)/(1-0.095163)/(1-0.107451)=$	0

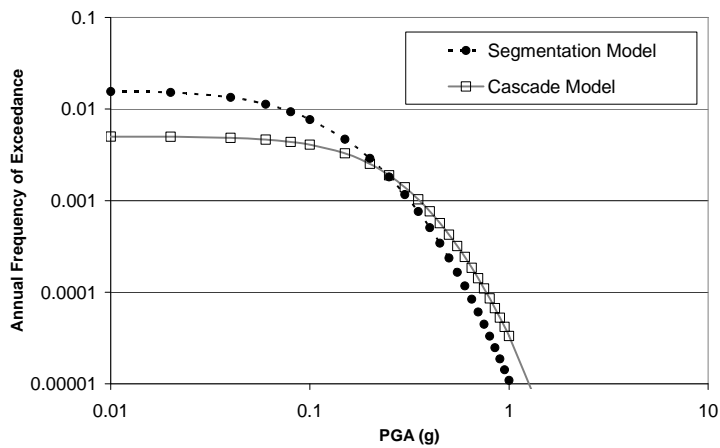
* Although P_{c_j} values for the segments with P_i values equal to cascade probability are equal to zero, Eq. (2.3) gives meaningless P_{c_j} values.



(a) Site 1



(b) Site 2



(c) Site 3

Figure 2.20 Seismic Hazard Curves Obtained for the Three Sites by Using Cascade and Fault Segmentation Models

In order to investigate the sensitivity of seismic hazard results to the selection of seismic source model, a narrow area source with 5 km width is defined instead of line (fault) source discussed above. Four sites are selected to perform seismic hazard analyses. Locations of sites and area source representing the fault which is considered in the analyses explained above are shown in Figure 2.21. Site 1 is placed within the area source and it has a closest distance of 1 km from the fault. Site 2 is situated at the boundary of area source (i.e. 2.5 km closest distance from the fault). Site 3 and Site 4 are at the outside of the area source with 10 km and 30 km closest distances to the fault, respectively. Figure 2.22 shows seismic hazard curves obtained by using area and line (fault) source models for these sites. It can be seen from Figure 2.22 that the analyses carried out by using area source model give lower seismic hazard values than those by the fault source model due to the fact that in area source model the occurrence rate of earthquakes is distributed over a wider region.

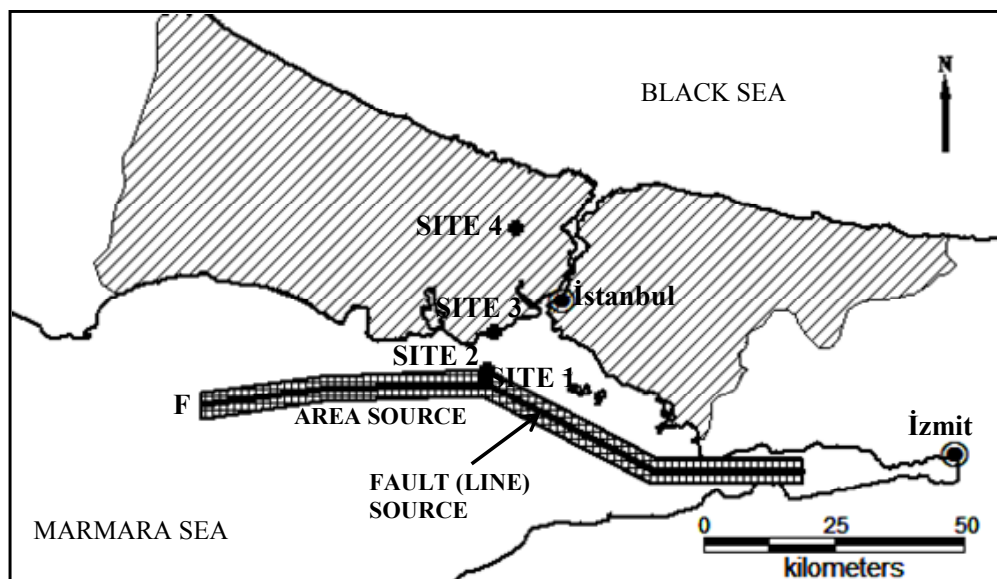
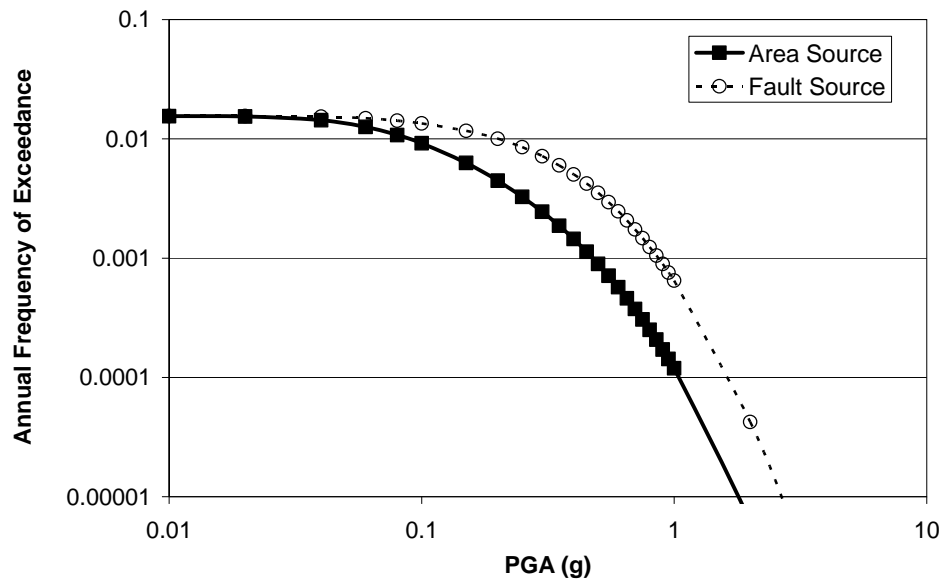
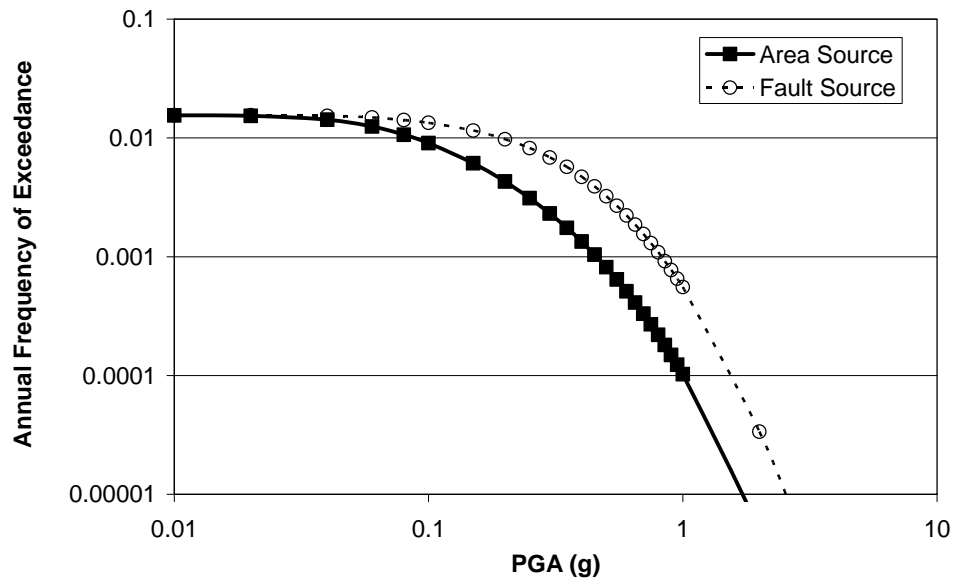


Figure 2.21 Locations of Sites, Line (Fault) Source and Area Source Representing the Fault

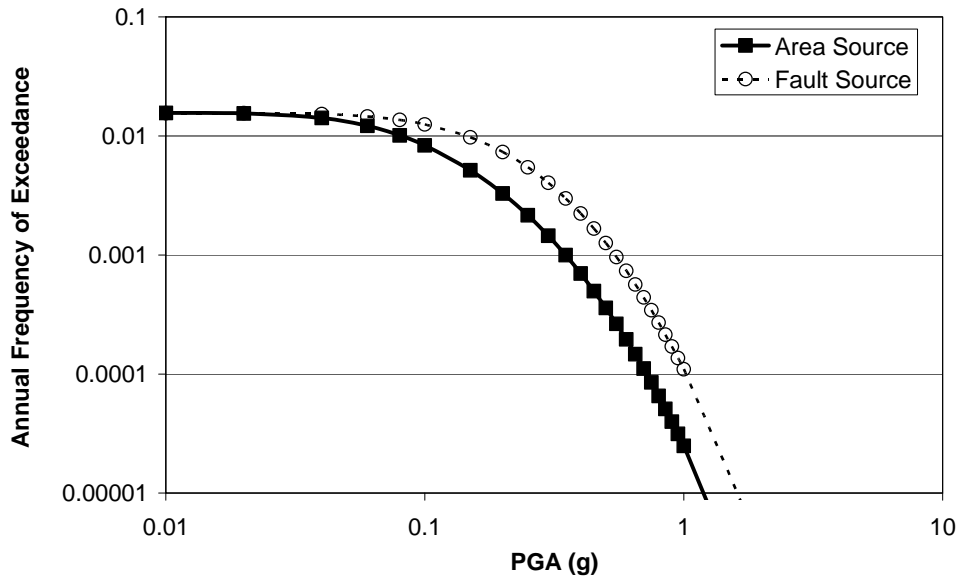


(a) Site 1

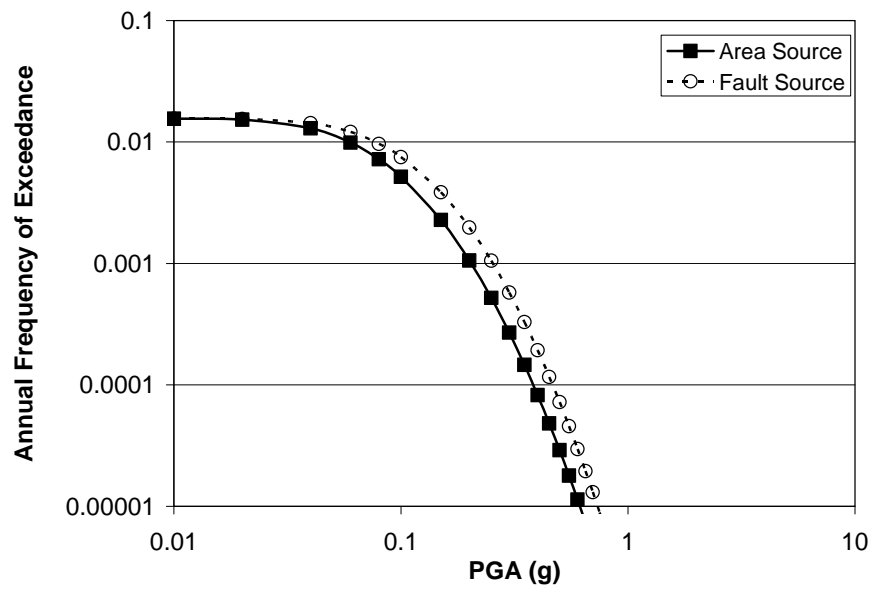


(b) Site 2

Figure 2.22 Seismic Hazard Curves Obtained by Using Area and Line (Fault) Source Models



(c) Site 3



(d) Site 4

Figure 2.22 (Continued) Seismic Hazard Curves Obtained by Using Area and Line (Fault) Source Models

It can be observed from the results of the analyses explained in this section that seismic hazard results are sensitive to source modeling (area or line). In literature, different methods; i.e. fault-rupture, segmentation and cascade models, are proposed for computation of seismic hazard from faults. In order to implement segmentation and cascade models, more detailed information (i.e., boundaries of segments, cascade scenarios, etc.) is required. Therefore, the analyst should select the source model depending on the level of available information. If the location of the fault has uncertainties, the area source model can be preferred instead of the line model. For faults whose segments are examined in detail, fault segmentation model can be used instead of the fault-rupture model. On the other hand, the rupture histories of the fault or other investigations are required to decide on the probable multi-segment rupture scenarios in the cascade model.

The delineation of area sources may involve uncertainty. One of the alternatives to include this uncertainty into the seismic hazard analysis is to assume randomness in the location of the boundaries of seismic sources (Bender, 1986; Yüçemen and Gülkan, 1994). According to this assumption, the introduction of the seismic source zone boundary uncertainty causes the seismicity concentrated around a seismic source to be dispersed over a wider region proportional to the standard deviation modeling this uncertainty. This causes a decrease in the intensity of seismic hazard in the neighbourhood of the seismic source, since the seismicity is distributed over a larger area. Based on a study conducted for Jordan, Yüçemen (1995) concluded that for sites under the threat of a number of seismic sources of either type (i.e. area or line), the incorporation of source location uncertainty influences the hazard estimate to a relatively smaller extent compared to other factors of uncertainty, such as the uncertainty involved in the attenuation model.

2.3.6.3 Uncertainty in the Magnitude Distribution

Uncertainty in the magnitude of a future earthquake that will occur in a seismic source is incorporated into PSHA by defining an appropriate magnitude recurrence relationship. The widely used models in seismic hazard studies are the truncated exponential distribution, characteristic earthquake model developed by Youngs and Coppersmith (1985) and maximum magnitude model.

Consider again the same fault and Site 1, Site 3 and Site 4 shown in Figure 2.21 and assume that the lower and upper bounds for the earthquake magnitudes are 4.5 and 7.5, respectively. The slope of the exponential magnitude distribution, $|\beta|$, is taken as 1.23 and the annual mean rate for earthquakes with $m \geq 4.5$, ν , is assumed as 0.2.

Seismic hazard analyses are performed by using truncated exponential distribution (TED) and characteristic earthquake model (CEM) developed by Youngs and Coppersmith (1985). In order to model the attenuation characteristics of ground motions, the empirical equation proposed by Kalkan and Gülkan (2004) for PGA at rock sites is used. A value of 0.612 is assigned to the standard deviation in natural logarithm of PGA. Figure 2.23 shows probability density functions corresponding to TED and CEM with varying Δm values, where Δm is the magnitude width between the lower bound of the characteristic earthquake magnitudes and the exponentially distributed magnitude whose probability density is assumed to be equal to probability densities of characteristic earthquakes and it is shown as a sketch in Figure 2.23.

Seismic hazard analyses are carried out also by using the maximum magnitude or purely characteristic earthquake model (PCEM). First, the rate associated with the characteristic earthquakes and which is uniformly distributed over the interval $(m_1, m_1 - 0.5)$ in the CEM with $\Delta m = 1.0$, is now lumped completely onto the maximum magnitude, m_1 , (PCEM) and the remaining rate is assigned to the range of the exponentially distributed magnitudes $(4.5 \leq m \leq 7.0)$. Then, a truncated Gaussian distribution (TGD) is used to consider uncertainty in the maximum magnitude. The

mean value of maximum magnitude, μ_m , is taken as 7.5 and its standard deviation, σ_m , as 0.28 as given by Wells and Coppersmith (1994) for the equation which relates magnitude with rupture length. The lower and upper limits of the distribution are assumed as $\mu_m - \sigma_m$ and $\mu_m + \sigma_m$ and the rate of characteristic earthquakes calculated by using CEM with $\Delta m = 1.0$ is distributed on the magnitudes between this range. To account for other earthquakes with smaller magnitudes, remaining rate is assigned to the range of the exponentially distributed magnitudes ($4.5 \leq m \leq 7.0$). Figure 2.24 shows probability density functions corresponding to these models.

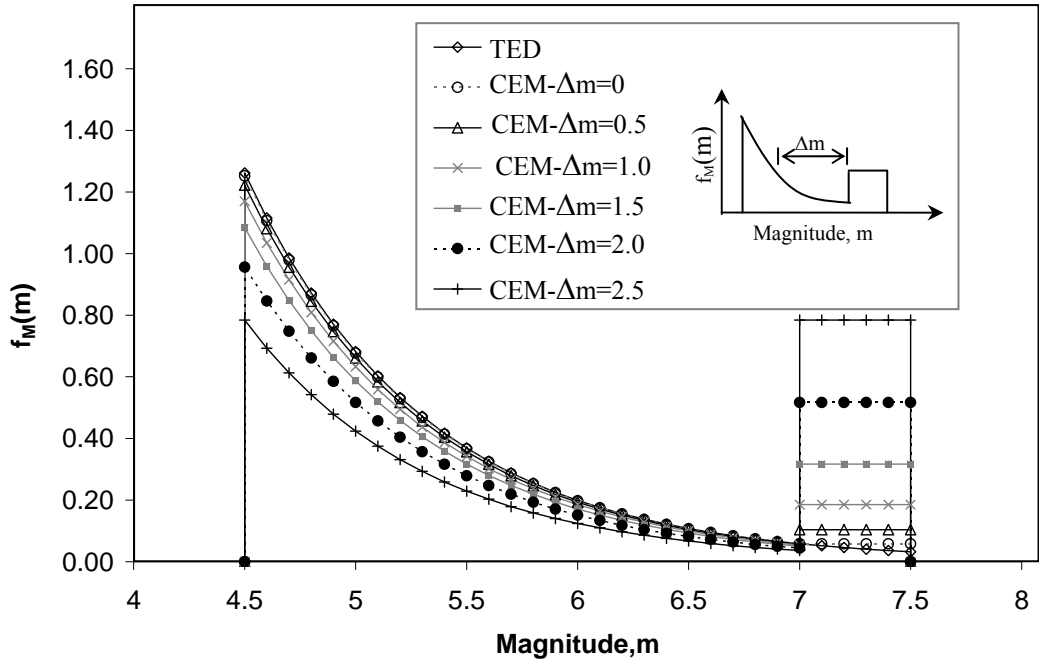


Figure 2.23 Probability Density Functions Corresponding to Truncated Exponential Distribution (TED) and Characteristic Earthquake Model (CEM) with Varying Δm values

Seismic hazard analyses are carried out by using EZ-FRISK (Risk Engineering, 2005). Figure 2.25 shows the seismic hazard curves for Site 4 estimated by using the magnitude distributions presented in Figures 2.23 and 2.24. Since general trends

of curves for Site 1 and Site 3 are the same with those obtained for Site 4, they are not presented here.

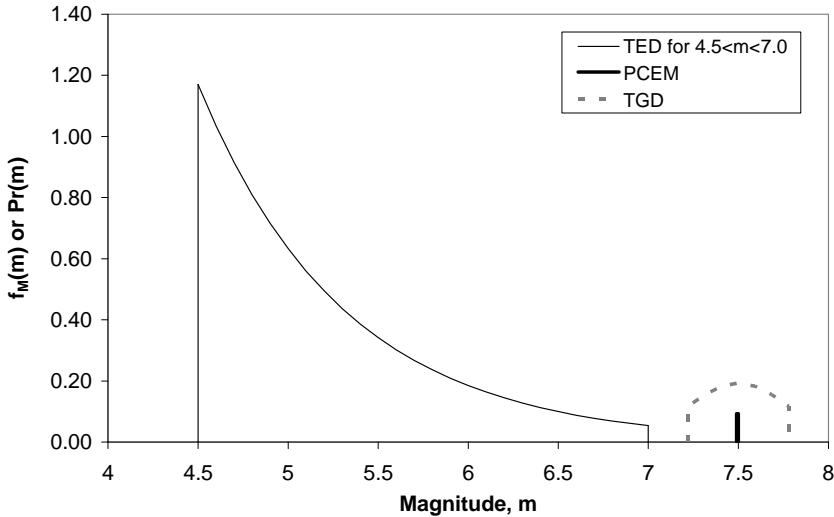


Figure 2.24 Probability Density Functions Corresponding to Purely Characteristic Earthquake Model (PCEM) and Truncated Gaussian Distribution (TGD) for Characteristic Magnitudes and Truncated Exponential Distribution (TED) for Smaller Magnitudes

The hazard curve obtained by using the truncated exponential magnitude distribution (TED in Figure 2.25) results in the lowest annual exceedance probabilities. On the other hand, the characteristic earthquake model (CEM) developed by Youngs and Coppersmith (1985) gives higher seismic hazard results compared to the TED. The difference increases especially for high levels of PGA values as Δm value increases. This is due to the fact that an increase in Δm value results in an increase in the rate of large magnitude earthquakes. Furthermore, there is no difference between the seismic hazard results obtained by using the two maximum magnitude models, PCEM and TGD, combined with exponential distribution for small magnitude earthquakes, TED. The hazard values obtained from these models are close to those obtained from CEM with $\Delta m=1.0$ for lower

PGA values whereas these models yield almost same results with CEM with $\Delta m=1.5$ for higher PGA values.

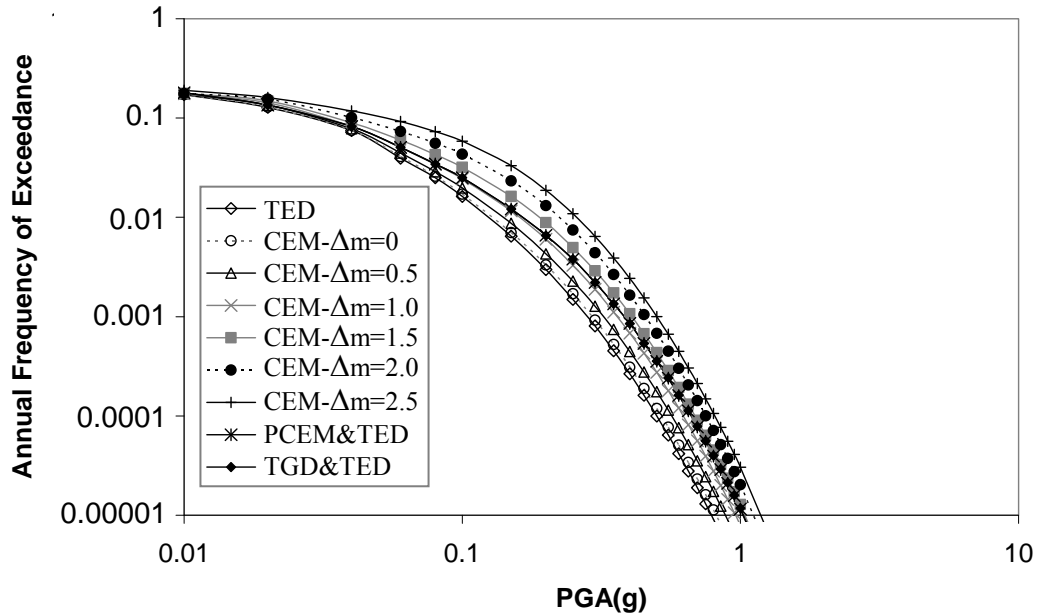


Figure 2.25 Seismic Hazard Curves for Site 4 Corresponding to: Truncated Exponential Distributions for $4.5 < m < 7.5$ (TED); Characteristic Earthquake Model (CEM) with Varying Δm values; Purely Characteristic Earthquake Model Combined with Exponential Distribution for Smaller Magnitudes ($4.5 \leq m \leq 7.0$) (PCEM&TED); Truncated Gaussian Distribution for Characteristic Magnitudes ($7.22 \leq m \leq 7.78$) Combined with Exponential Distribution for Smaller magnitudes ($4.5 \leq m \leq 7.0$) (TGD&TED)

2.3.6.4 Uncertainty in the Temporal Distribution of Earthquakes

In PSHA, two stochastic models, namely Poisson and renewal, are generally applied to predict probability of future earthquake occurrences. Seismic hazard analyses presented in the previous section are all based on the Poisson model. In this section, additional analyses are performed by using the renewal model in order to investigate the sensitivity of seismic hazard results to the choice of earthquake occurrence models in time domain.

Consider the fault described in the previous section. In the renewal model, probability distribution of inter-event times of characteristic earthquakes and time elapsed since the last event are used to predict probabilities of the occurrence of future earthquakes. Based on the characteristic earthquake rate obtained from the characteristic earthquake model with $\Delta m=1.0$, mean inter-event time of the earthquakes on this fault is estimated as 54 years. In order to determine the date of the last characteristic earthquake, the recent study of Parsons (2004) in which the ruptures resulted from historical earthquakes have been estimated as shown in Figure 2.26 is used. It can be observed from Figure 2.26 that after 1509 M~7.4 earthquake that is estimated to rupture the whole length of the fault, May 1766 M~7.2 earthquake ruptured a large part of it. Therefore, it can be assumed that May 1766 event released almost all of the energy accumulated and it is the last characteristic earthquake occurred on this fault. Thus, time elapsed since this event is 241 years.

Brownian Passage Time (BPT) and lognormal (LN) distributions are selected as the probability distribution functions for the inter-event times. Aperiodicity used in BPT distribution is assumed to be 0.5, which appears to be the most likely value according to the study conducted by Ellsworth et al. (1999). Since coefficient of variation equals to aperiodicity, it is also assumed to be 0.5. Figures 2.27 and 2.28 show probability density and hazard functions obtained for the BPT and LN distributions, respectively. As observed from these figures there is no significant difference between the functions derived from these two distributions.

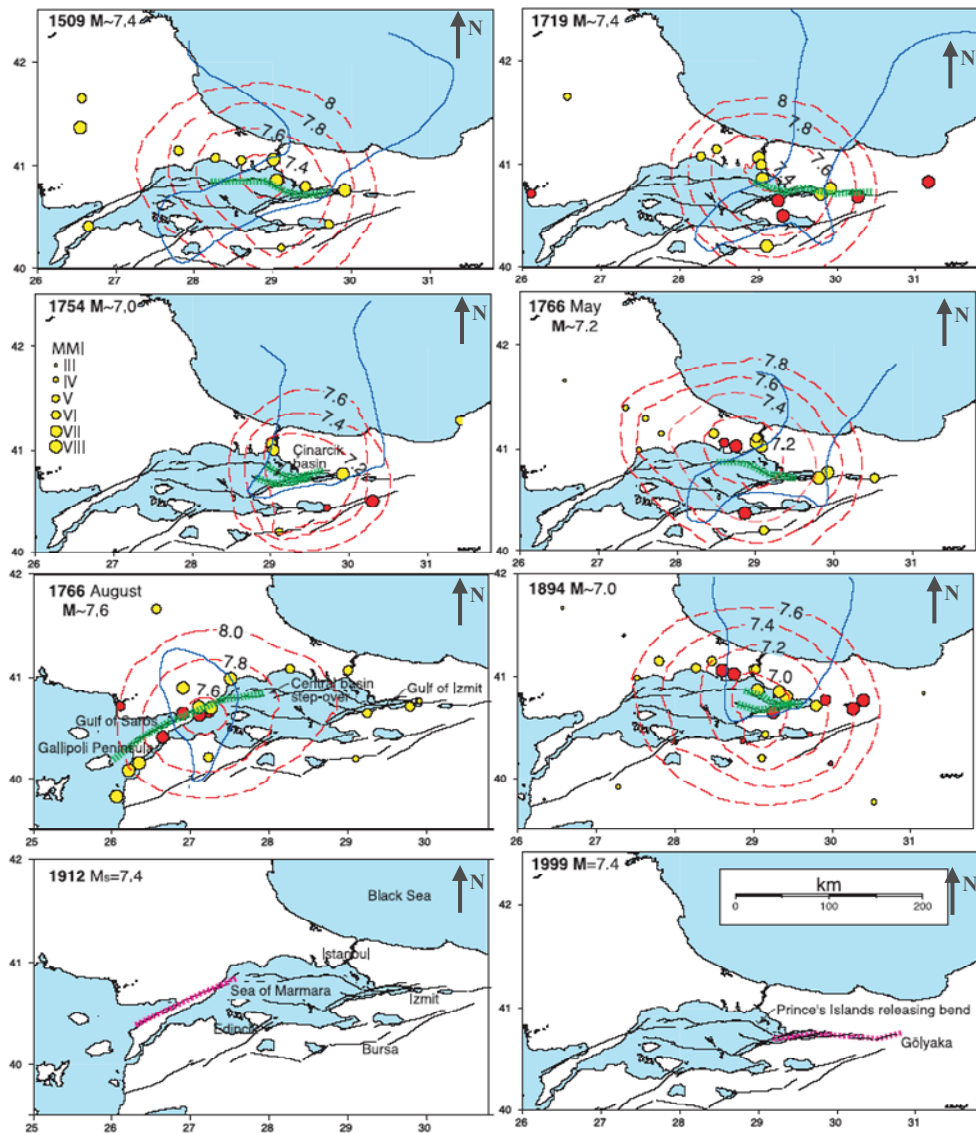


Figure 2.26 Estimated Ruptures (Thick Dashed Green Lines), Modified Mercalli Intensity (MMI) Values (Yellow Dots), Sites of Damage Potentially Enhanced by Soft Sediments (Red Dots), Moment Magnitude M Needed to Satisfy the Observations for a Given Location (Red Dashed Contours) for Large Earthquakes Occurred between A.D. 1500 and 2000 (After Parsons, 2004).

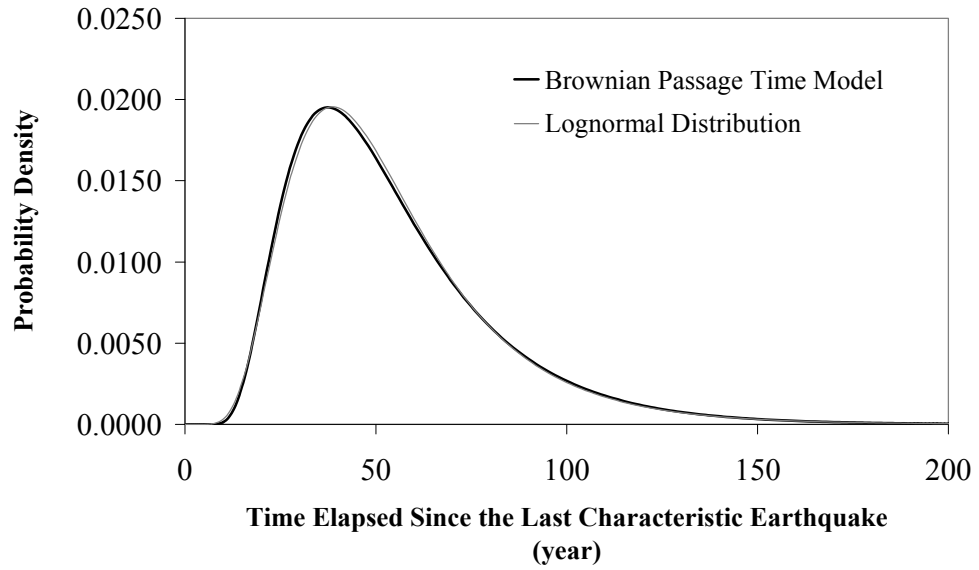


Figure 2.27 Probability Density Functions Corresponding to the BPT and LN Distributions Based on the Mean Inter-Event Time of $\mu_T = 54$ years and $\alpha = \text{cov} = 0.5$

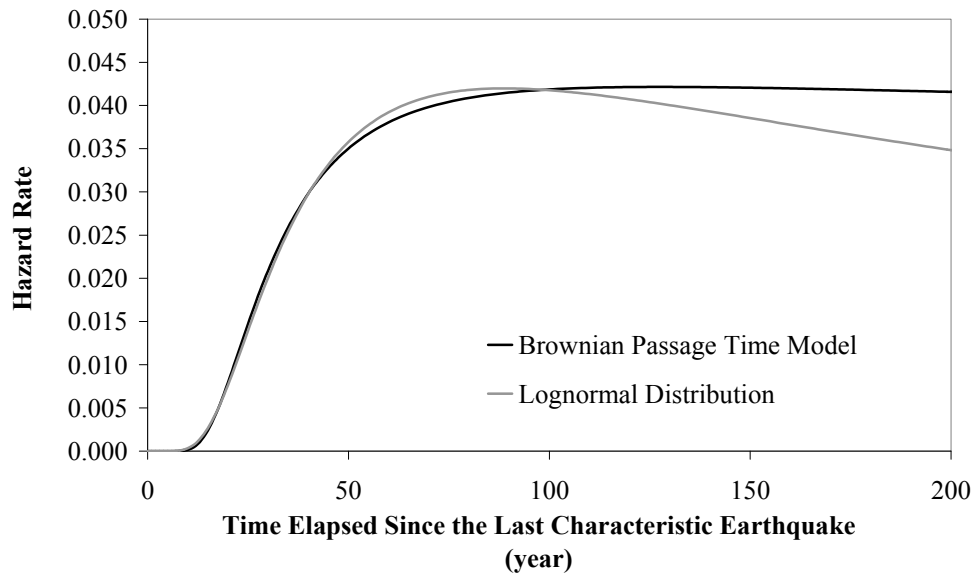
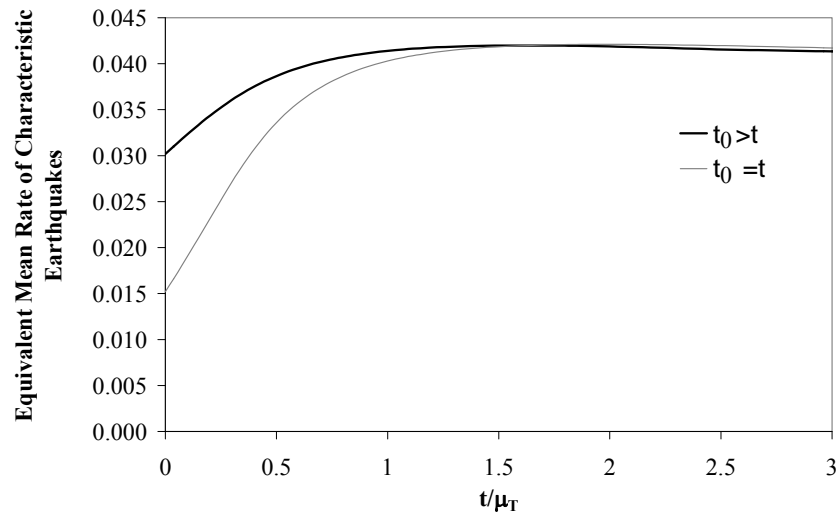


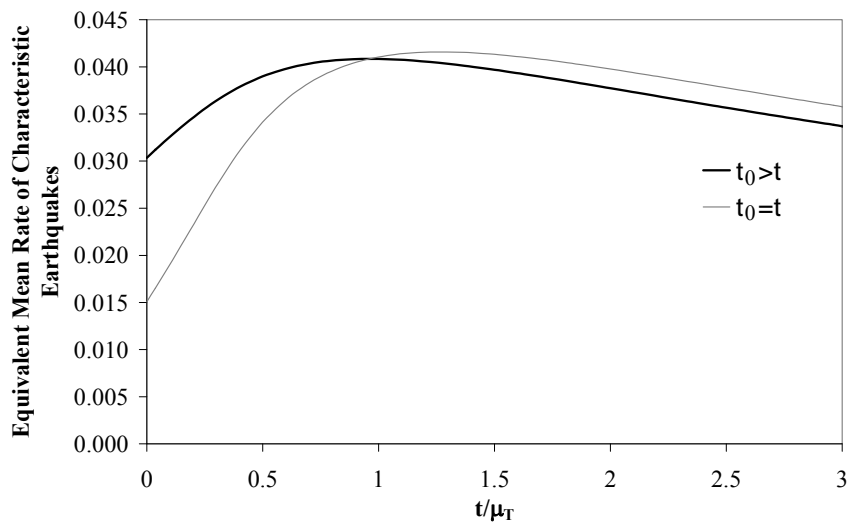
Figure 2.28 Hazard Functions Corresponding to the BPT and LN Distributions Based on the Mean Inter-Event Time of $\mu_T = 54$ years and $\alpha = \text{cov} = 0.5$

In the renewal hybrid model, the mean rate of characteristic earthquakes depends on probability distribution function of inter-event times as well as the time elapsed since the last characteristic earthquake, “ t_0 ”, and the next time interval, “ w ”. Besides, depending on the information available for t_0 , either Eq. (2.20) (if t_0 is known) or Eq. (2.28) (if t_0 is unknown) will be combined with Eq. (2.25) to calculate the mean rate of characteristic earthquakes. In this study, “ w ” is assumed to be 50 years. Two cases are considered. In the first case t_0 is set equal to an arbitrary value of t years and in the second case it is assumed to be greater than t years. Mean rates of characteristic earthquakes are calculated for these two cases by using BPT and LN distributions and are shown in Figure 2.29 for t/μ_T values changing between 0 and 3. Again no significant difference is observed between the general trends of these two distributions. Accordingly the BPT distribution is adopted to describe the inter-event times of the characteristic earthquakes in the renewal model.

Together with the renewal model both characteristic (Youngs and Coppersmith, 1985) and pure characteristic (maximum magnitude) models are utilized as the magnitude-recurrence relationships. Mean rate of characteristic earthquakes is calculated for $t_0=241$ years. Note that there is no significant difference between mean rates of characteristic earthquakes for $t_0=241$ years and $t_0 \geq 241$ years. Mean rate of characteristic earthquakes is assumed either uniformly distributed over magnitudes between m_1 and $m_1 - 0.5$ (CEM) or assigned only to m_1 (PCEM). The rate of smaller magnitude earthquakes ($4.5 \leq m \leq 7.0$) is obtained by subtracting the equivalent mean rate of characteristic earthquakes from the annual mean rate v for earthquakes with $m \geq 4.5$. Figure 2.30 shows seismic hazard curves obtained for Site 4 considered in the previous section from the renewal model combined with CEM and PCEM. In this figure, seismic hazard curves shown in Figure 2.25 for the CEM with $\Delta m=1.0$ and PCEM&TED are also presented in order to compare the results with those obtained from the Poisson model.



(a) BPT Distribution



(b) Lognormal Distribution

Figure 2.29 Variation of Equivalent Mean Rate of Characteristic Earthquakes Calculated Based on Eqs. (2.20) and (2.28) for the BPT and LN Distributions

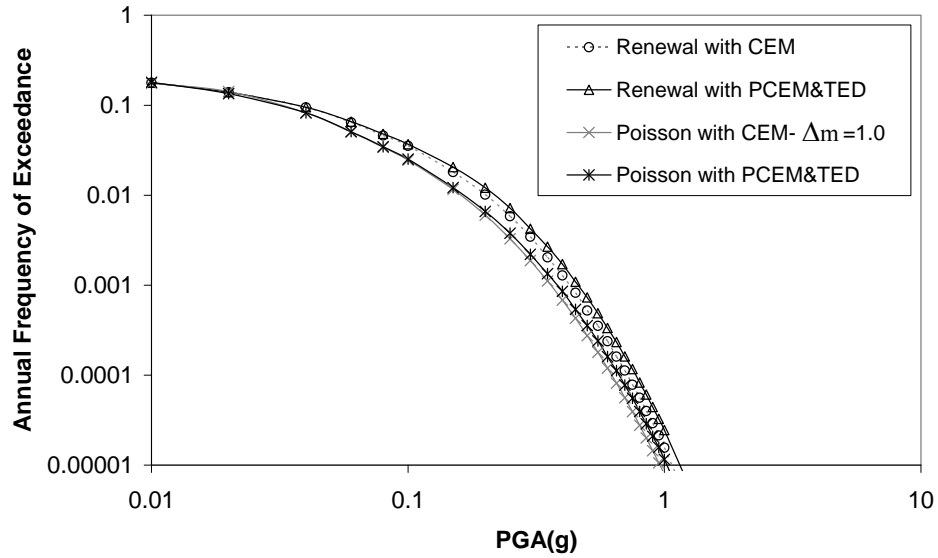


Figure 2.30 Seismic Hazard Curves for Site 4 Corresponding to the Combinations of Renewal Model with PCEM&TED and CEM; Poisson Model with PCEM and CEM with $\Delta m=1.0$

It can be observed from Figure 2.30 that renewal model gives consistently higher seismic hazard results compared to the Poisson assumption. In this example, compared with the mean inter-event time, a considerably long time (more than four times mean inter-event time) has passed after the last characteristic event. Thus, the rate of characteristic earthquake occurrence and consequently its probability increased in the renewal model. It can be seen from Figure 2.29 that immediately after the occurrence of the characteristic earthquake, this probability decreases. In such a case, the seismic hazard results are expected to be lower compared with those of the Poisson model. Therefore, the analyst should be careful in the determination of the values to be assigned to the parameters used in the renewal model. In this study, BPT model with aperiodicity of 0.5 is selected as inter-event time distribution. It can be observed from Figure 2.29 (a) that the rates calculated for the cases in which t_0 is known or unknown are almost the same when t_0 is greater than 1.5 times of the mean inter-event time, μ_T . Therefore, in this case study, there is no need to spend an extra effort in the evaluation of t_0 value if it is expected

to be greater than 1.5 times of the μ_T value. In addition, the same trend is observed for the Poisson model with respect to the recurrence models: i.e. the PCEM&TED giving higher seismic hazard values compared to those of CEM.

2.3.6.5 Uncertainties in Earthquake Catalogs

Earthquake catalogs are the most important sources of information used in seismic hazard analysis since they describe the spatial and temporal distribution of past earthquakes in the interested region. Unfortunately, certain degree of uncertainty results from the earthquake catalogs. Generally, earthquake magnitudes are reported in different magnitude scales in these catalogs and it is desirable to convert them into a common one. The other problem is that earthquake catalogs are generally incomplete for small magnitude earthquakes occurred in the ancient times due to inadequate instrumentation spread or scatter of relatively small population before the period of complete recording (Deniz, 2006).

The incompleteness of earthquake catalog creates biases in the database both in time and space. Accordingly, the resulting recurrence relationships may not represent the true long term rates. In other words, the annual rate of occurrences of smaller magnitude earthquakes and the absolute value of the slope of the recurrence relation are underestimated from the incomplete databases. For this reason, it is necessary to determine the time period over which the data in a given magnitude interval is completely reported. After the determination of complete time interval, the annual rate of earthquake occurrences having that magnitude range is computed by considering only that time interval.

2.3.7 Logic Tree Methodology

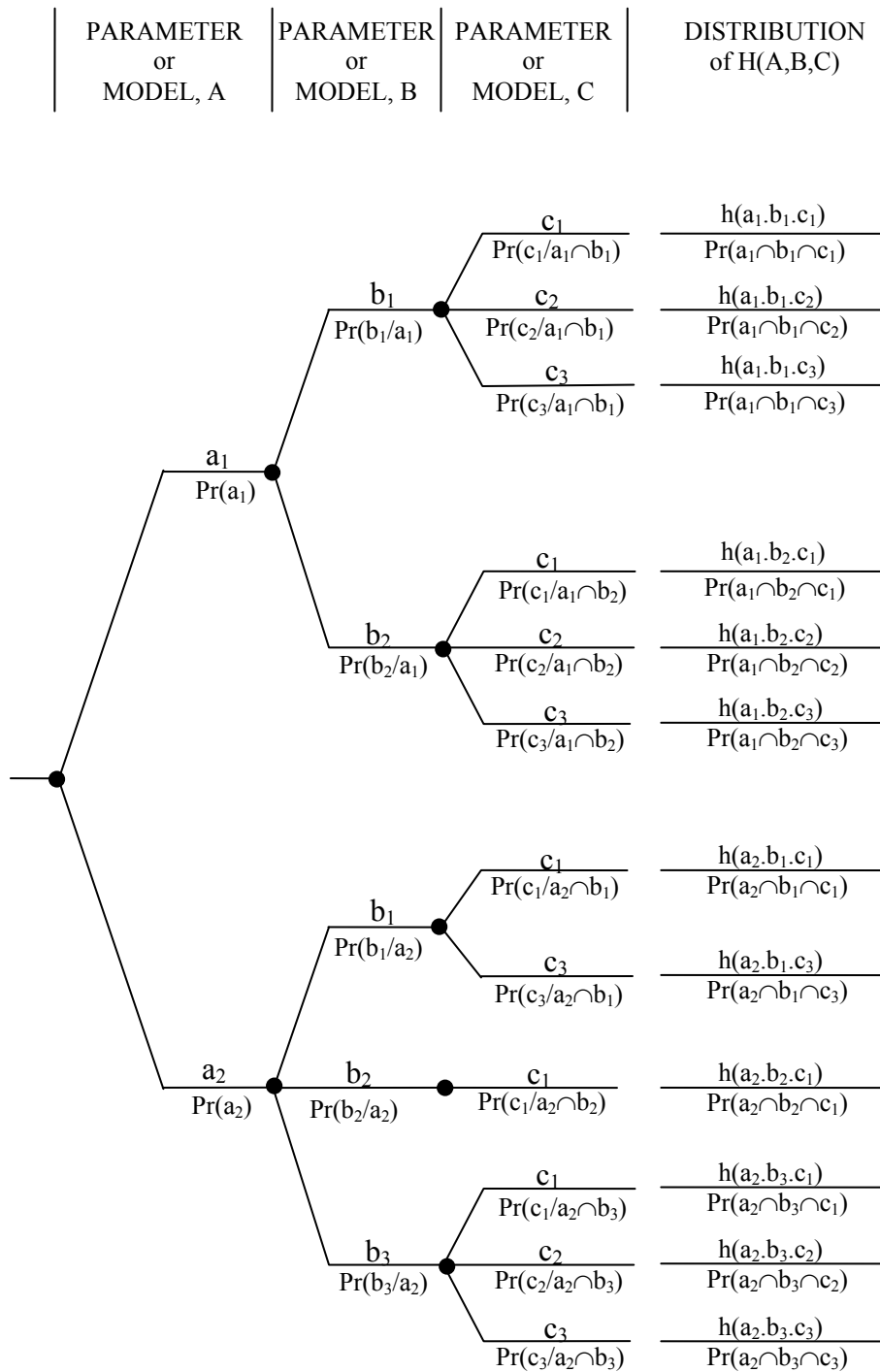
As explained in the previous section, different seismic hazard curves can be obtained by using different models and input parameters. The simple and systematic way to aggregate the epistemic uncertainties is to utilize the logic tree method.

A general logic tree model (Risk Engineering, 2006) is shown in Figure 2.31. A logic tree consists of nodes and branches. Each node represents a model, an input parameter, or an assumption that is uncertain. Branches extending from each node are discrete alternatives for that model, input parameter, or assumption. The nodes should be ordered in such a way that independent nodes are placed to the left while dependent ones are located to the right. The end branches of the logic tree represent mutually exclusive and collectively exhaustive states of all uncertain parameters, models and assumptions. Seismic hazard analysis is carried out for each end branch. For each seismic hazard curve, a subjective weight (discrete probability) which is equal to the product of weights on the branches leading to its corresponding end branch is assigned. Seismic hazard results are aggregated by using the theorem of total probability, which can be expressed through the following relationship (Yücemem, 1982):

$$P(Y > y) = \sum_{i=1}^n P(Y > y/G_i) w_i \quad (2.60)$$

where, G_i = combination of uncertain parameters, models or assumptions at the i th end branch; $w_i = P(G_i)$, subjective joint probability assigned to the i th end branch reflecting its likelihood to be “true” compared to the others; n = number of end branches. It is to be noted that the sum of w_i 's will be equal to unity. The seismic hazard obtained in this way is generally called as the Bayesian estimate.

The use of logic trees in probabilistic seismic hazard analysis often involves a large number of branches that reflect the uncertainty in the selection of different models and input parameters assigned to each model. It requires a long computation time due to several branches that might sometimes be unnecessary due to their little or no influence on the results. Therefore the sensitivity analysis is useful to discriminate which parameters contribute the most to the seismic hazard and its uncertainty, and can be used as a preliminary step for the construction of logic trees focusing efforts on the parameters found to be most sensitive (Barani et al., 2007).



Note that $\Pr(a_i \cap b_j \cap c_k) = \Pr(c_k/a_i \cap b_j) \cdot \Pr(b_j/a_i) \cdot \Pr(a_i)$

Figure 2.31 A General Logic Tree (After Risk Engineering, 2006)

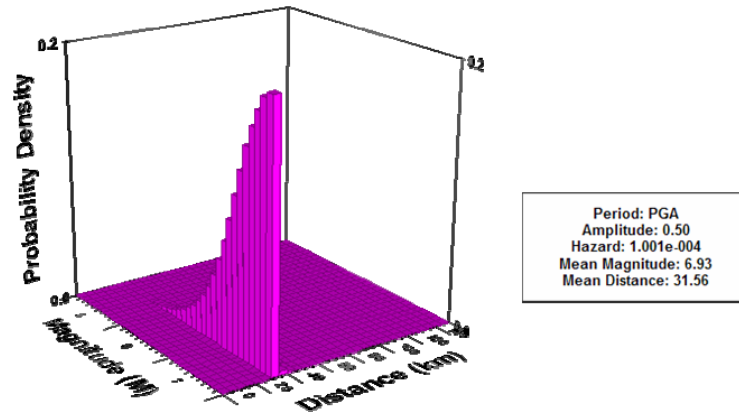
The other important point in logic tree methodology is the relative weight assigned to each branch of the logic tree. Final result depends on the subjective probabilities assigned to different alternatives as well as the alternatives taking place in the logic tree. Therefore, extreme care should be paid to the process of assigning these probabilities. Sabetta et al. (2005) carried out an investigation on sensitivity of probabilistic seismic hazard analyses results to ground motion relations and logic tree weights. The results obtained from their study showed that when four or more ground motion prediction relationships are included, the relative weights assigned to these relationships do not significantly influence the hazard unless strongly biased towards one or two relations. They stated that the choice of appropriate relationships to be included in the analysis has a greater impact than the weights assigned to these relationships.

2.3.8 Deaggregation of Seismic Hazard

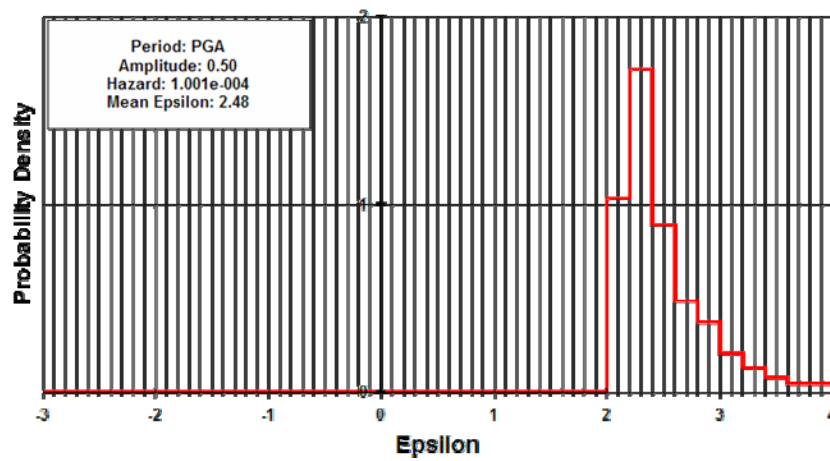
The probabilistic seismic hazard results can be disaggregated to determine the contribution of the magnitudes, distances and epsilon values to the calculated exceedance probabilities. The epsilon is the number of standard deviations that the ground motion value deviates from the median ground motion value for an event defined by the mean magnitude and distance. In other words, it is equal to $(y - \bar{y}) / \sigma_y$, where y is the logarithm of ground motion value to be deaggregated, \bar{y} and σ_y are the mean value and standard deviation of the logarithm of ground motion, respectively. The procedure that examines the spatial, magnitude and epsilon dependence of hazard results is called disaggregation or deaggregation.

In this procedure, the magnitude, distance and epsilon values are divided into bins. In order to calculate the relative contribution of each bin to the total exceedance probability of a specified ground motion value, the exceedance probability due to each bin is calculated and divided by the total exceedance probability of all bins. Results of this process can be presented as histograms that show the percent contributions of earthquakes, that can cause ground motions equal to or greater than

the specified one, to total hazard as a function of magnitude, distance and epsilon. From these plots, the analyst can observe which magnitude, distance and epsilon contribute the most of the seismic hazard and decide on where to spent more efforts for improved models and or gather additional information. Also, the deaggregation of PSHA is very useful in identifying the earthquake scenario that generates the largest ground motion at the interested site in DSHA. Figure 2.32 shows examples of deaggregation graphs obtained from a seismic hazard analysis carried out by using EZ-FRISK (Risk Engineering, 2005). From this figure, it is observed that for PGA value equal to 0.5g, maximum contribution to seismic hazard comes from the large magnitude earthquakes ($M \cong 7.5$) with distances of about 30 km to the site.



(a) Magnitude-Distance Deaggregation



(b) Epsilon (ϵ) Deaggregation

Figure 2.32 Examples of Deaggregation Graphs Obtained from a Seismic Hazard Analysis Carried Out by Using EZ-FRISK (Risk Engineering, 2005)

CHAPTER 3

CASE STUDY FOR A COUNTRY: SEISMIC HAZARD MAPPING FOR JORDAN

3.1 INTRODUCTION

In the previous chapter, the basic inputs of the probabilistic seismic hazard analysis model are explained in detail and the treatment of the related uncertainties is discussed. The sensitivity of results to the various inputs are examined by considering a line source (fault) and sites of varying distances to this fault.

As mentioned earlier, in developing seismic hazard maps or updating the existing ones, it is necessary to take into consideration the seismic hazard nucleating from faults. This requires the assessment of the main parameters of the faults. However, this process requires time and it is quite expensive if it is carried out for large regions like a country. This fact is observed in the study conducted for the development of the current earthquake zoning map of Turkey, where all seismic sources were defined as area sources.

In this chapter, a case study will be carried out to illustrate how seismic hazard analysis should be carried out for the seismic hazard assessment of the regions for which the data is not adequate to apply the more complex models, such as, cascading, segmentation and renewal. In certain cases, the locations of faults on the earth surface may not be well defined to use line source modeling. In such a case, the simplest models based on area sources and exponential magnitude distribution can be used in the assessment of seismic hazard. In cases where the exact locations of faults are defined, line source model combined with exponential magnitude distribution or characteristic earthquake model can be applied in seismic hazard

assessment studies. Besides, purely characteristic earthquake or maximum magnitude models can be used for faults and the remaining seismicity is to be considered in seismic hazard calculations by defining a background area source with uniform seismicity or by applying spatially smoothed seismicity model. In the case study presented in this chapter, Jordan is selected as the country to examine sensitivity of seismic hazard results to seismic source modeling and various assumptions with respect to magnitude distribution.

Most parts of Jordan, especially the regions along the Dead Sea-Jordan rift valley, are subject to significant seismic threat. Since the major cities and industry are located in earthquake prone regions, it is quite important to quantify the future seismic hazard in these regions and design and construct the engineering structures consistent with the resulting seismic hazard.

3.2 PREVIOUS PROBABILISTIC SEISMIC HAZARD ASSESSMENT STUDIES FOR JORDAN

The earlier probabilistic seismic hazard studies in the region are very limited in number and they date back to the development of seismic hazard maps for Palestine (Ben-Menahem, 1981; Shapira, 1981). Later, a number of studies were conducted for the prediction of seismic hazard in Jordan. Yücemem (1992) conducted a very comprehensive study for the assessment of the seismic hazard in Jordan and its vicinity by using probabilistic and statistical methods. Seven seismic sources, which include line sources for the well defined faults and area sources for others, were delineated in this study. The results were presented in the form of seismic hazard maps displaying iso-acceleration and iso-intensity contours corresponding to different return periods. In that study, the major problems were the identification of seismic source zones, delineation of faults, assessment of the fault parameters and the nonavailability of attenuation relationships derived based on local data.

In a later study conducted by Yücemem (1995), the problems associated with the location of seismic source zones were addressed in full and a model was described

to quantify and incorporate explicitly the errors made in the demarcation of the source zone boundaries. The basic concept introduced in that model was the assumption of random source zone boundaries instead of deterministic ones. To demonstrate the application of the proposed model, seismic hazard was computed at three different cities in Jordan. The sensitivity of results to the location uncertainty was examined and a comparison against the previous results was also made.

In the last decade a number of studies (Al-Tarazi, 1992; Batayneh, 1994; Husein Malkawi et al., 1995; Fahmi et al., 1996) were conducted for the development of seismic hazard maps for Jordan and its vicinity. The probabilistic methodology and the computational algorithms were not different than the ones utilized by Yüçemen (1992; 1995), however, these studies enjoyed the benefit of having more information and expert opinion for the delineation of seismic sources. Accordingly, more reliable seismic source models and seismicity parameters were used in these studies.

Jiménez (2004) carried out a comprehensive study for seismic hazard mapping of Jordan. This study was based on up-to-date information for seismic sources and seismicity of the region. 18 seismic sources were delineated in the region. They were modeled as area sources even where faults were well defined based on geological and seismological investigations in order to evaluate the inherent uncertainty in hypocenter determination of earthquakes. Narrow area sources were defined for Dead Sea Transform System while wider sources were used for the areas having more distributed seismicity. The attenuation relationships proposed by Ambraseys et al. (1996) for rock sites and for peak ground acceleration (PGA) and spectral accelerations (SA) for 0.1 sec, 0.2 sec, 0.3 sec, 0.5 sec, 1.0 sec and 2.0 sec were used in seismic hazard computations. Contour maps were presented to display predicted PGA and SA values at 10% probability of exceedance in 50 years.

Al-Tarazi and Sandvol (2007) recently conducted a study for seismic hazard evaluation along the Jordan-Dead Sea Transform. Three models were used to produce probabilistic seismic hazard maps for the region. Model I and Model II

were based on spatially smoothed earthquakes with magnitudes greater than 3.0 for the time period 1900 to 2003 and magnitude range between 5.0 and 7.0 for the time period 2100 B.C and A.D. 2003, respectively. No seismic source zones have been used in these two models. In Model III, contribution of the large events with magnitude equal to or greater than 7.0 to the seismic hazard is calculated by assigning them to major faults as characteristic events having a narrow magnitude range. Three different attenuation relationships proposed by Boore et al. (1997), Sadigh et al. (1997) and Campbell (1997) for peak ground acceleration at firm rock sites have been used in calculations and the results were combined by giving equal weights (0.333) to each one of these relationships. The results obtained from Model I, Model II and Model III were combined to form a single probabilistic seismic hazard map. For this purpose, the weights of 0.5 and 0.5 were given to Model I and Model II, respectively. The probabilities of exceedances obtained from Model III were added to weighted mean of the probabilities of exceedances from Model I and Model II. The maps showing the peak ground acceleration with 10 % probability of exceedance in 50 years were produced for Model I, Model II and Model III as well as for the combination of them.

3.3 ASSESSMENT OF SEISMIC HAZARD FOR JORDAN

3.3.1 Seismic Database and Seismic Sources

Two major steps of PSHA are the delineation of seismic sources and the assessment of the earthquake occurrence characteristics for each seismic source. Therefore, the past earthquake catalogs and tectonic structure of the region of interest must be studied to determine the locations and magnitude-recurrence relationships of seismic sources that generate the future seismic activity.

3.3.1.1 Seismic Database

In order to carry out a seismic hazard analysis for Jordan, the seismicity and tectonics of the rectangular region bounded by 27-36° N latitudes and 30.4-40° E

longitudes is studied. For this region, two earthquake catalogs which are presented in Jiménez (2004) are used. First earthquake catalog includes the earthquakes that occurred between the years 0 and 1989. In this study, the historical events that occurred between the years 0 and 1899 are not taken into consideration due to the incompleteness in smaller magnitudes. However, it is believed that it can be used to delineate seismic sources and to determine their maximum magnitudes. The magnitudes of the events between the years 1900 and 1989 are given in local magnitude (M_L) scale. The earthquake magnitudes in body wave magnitude (M_b) scale for the events with $M_L \geq 4.0$ as well as those in surface wave magnitude (M_s) scale for some events are also presented. The second earthquake catalog includes the events that occurred between the years 1990 and 1998. The magnitudes of these events are given in local magnitude scale. Therefore, the whole earthquake catalog contains events between the years 1900 and 1998.

Peak ground acceleration (PGA) and spectral acceleration (SA) at 0.2 and 1.0 seconds are selected as the basic parameters for the seismic hazard evaluation. The attenuation equations proposed by Ambraseys et al. (1996) are used to estimate seismic hazard in terms of these parameters. Since no information is available about the site conditions all over Jordan, all computations are carried out for rock site condition. In the equations proposed by Ambraseys et al. (1996), the magnitude values should be in terms of surface wave magnitude scale, M_s . Therefore, the magnitudes of earthquakes in the catalog are converted from the local magnitude scale, M_L , to M_s by using the equation derived by Jiménez (2004) based on earthquake catalog compiled for the seismic hazard assessment of Jordan as given below:

$$M_s = 1.11M_L - 0.50 \quad (3.1)$$

Poisson model assumes independence between the earthquakes. Therefore, secondary events; i.e. foreshocks and aftershocks sequences, should be removed from the earthquake catalog. Various methods are proposed in literature to identify secondary events. The simple one is that the earthquakes that fall into space and

time windows of another larger magnitude earthquake are identified as secondary events. In this study, time and space windows proposed by Deniz (2006) and Deniz and Yüçemen (2005) for earthquakes with moment magnitudes equal or greater than 4.5; as given in Table 3.1, are used. As described by Deniz and Yüçemen (2005), the earthquakes that fall into the space and time windows defined for the magnitude level of a preceding earthquake with larger magnitude are classified as aftershocks of this event. If a larger magnitude earthquake that occurred later in time and space windows of a smaller magnitude earthquake, this event is classified as the foreshock of the larger magnitude earthquake.

Table 3.1 Space and Time Windows to Identify Secondary Events (After Deniz and Yüçemen, 2005)

Moment Magnitude (M_w)	Width of Space Window (km)	Width of Time Window (days)
4.5	35.5	42
5.0	44.5	83
5.5	52.5	155
6.0	63.0	290
6.5	79.4	510
7.0	100.0	790
7.5	125.9	1326
8.0	151.4	2471

In order to implement the space and time windows proposed by Deniz (2006) and Deniz and Yüçemen (2005), the magnitudes of earthquakes in the whole catalog should be converted to moment magnitude scale. This is achieved by using the equation derived by Deniz (2006) based on earthquakes recorded in Turkey for converting the magnitudes of earthquakes given in the local magnitude scale (M_L) to the moment magnitude scale (M_w) which is given as follows:

$$M_w = 1.57M_L - 2.66 \quad (3.2)$$

The minimum magnitude earthquake, m_0 , to be considered in seismic hazard analysis is set equal to 4.0 in surface wave magnitude scale (M_s). Therefore, earthquakes with moment magnitude less than 3.6, which corresponds to 3.93 in surface magnitude scale according to Eqs. (3.1) and (3.2), are removed from the earthquake catalog.

A computer program is coded in order to apply the secondary event identification procedure explained above. The earthquake catalog and time and space windows of earthquake magnitudes defined for earthquakes in the catalog are inputs for this program. For magnitudes that are not given in Table 3.1, the linear and log-linear interpolations are applied for duration and distance values, respectively. Since the distance and duration windows are given for moment magnitudes equal to or greater than 4.5, some extrapolations are made to define windows for magnitudes less than this value. Besides, the earthquakes with magnitudes greater than 6.0 are assumed to be main shocks although they may be identified as secondary events of another main shock. The resulting earthquake catalog includes 175 main shocks, which can be treated as independent events, are listed in Appendix B. The spatial distribution of earthquakes in the resulting catalog is shown in Figure 3.1.

3.3.1.2 Seismic Sources

The Dead Sea Transform Fault System (DSTFS) which extends in approximately south-north direction near the west boundary of Jordan produced very destructive earthquakes since pre-historical times (Ben-Menahem, 1979). The DSTFS was formed as a result of the breakup of the Arabian plate from the African plate (Barazangi, 1983). Deformation in this boundary is intense and complex with faults trending not only sub parallel to the transform but also oblique to it (Bender, 1974). The tectonic setting of Dead Sea transform fault system is shown in Figure 3.2.

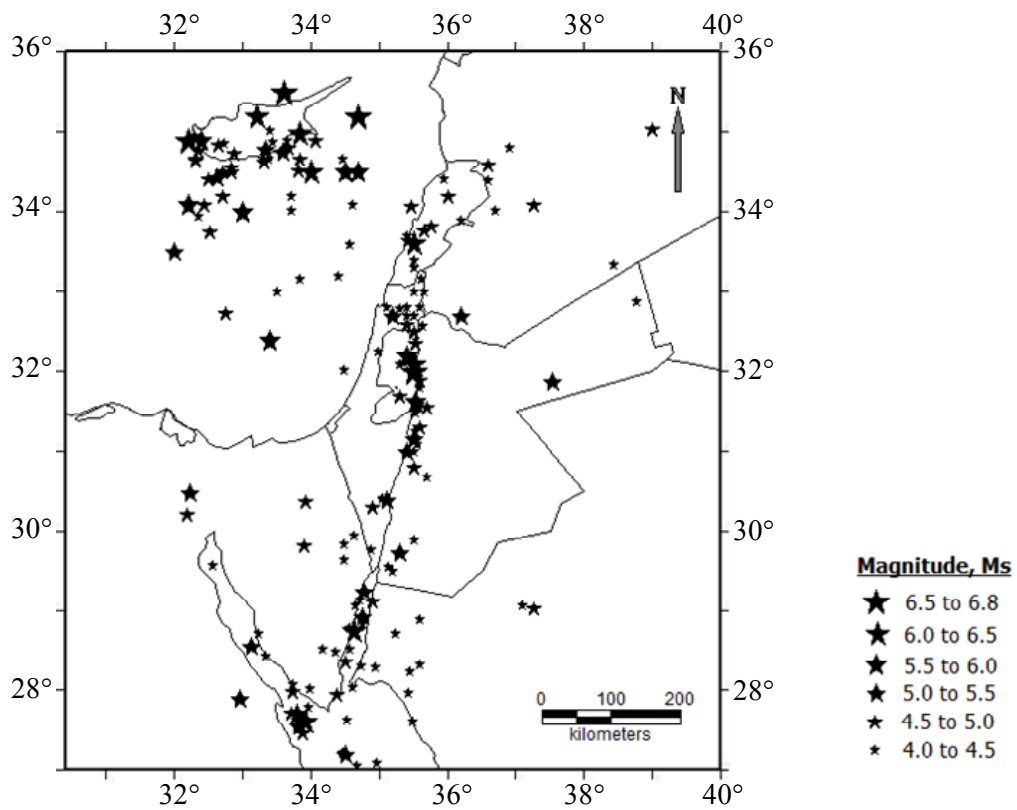


Figure 3.1 Map Showing the Spatial Distribution of Main Shocks in the Catalog Compiled for the Seismic Hazard Assessment of Jordan

The Dead Sea transform system extends from the Gulf of Aqaba in the south through Wadi Araba, Dead Sea Basin and continues in the north direction through Yammouneh and Ghab faults that intersects with the Arabia-Eurasia collision zone in southern Turkey (Al-Tarazi and Sandvol, 2007). This system has left-lateral en-echelon strike-slip faults that produced several deep pull-apart basins. The Dead Sea and Gulf of Aqaba are the larger ones among them (Ben-Avraham, 1985).

In this study, two different models, namely area and line, are used for the main seismic sources that affect Jordan. For the location of seismic sources, the information given in the report by Jiménez (2004) is used. The locations of area

sources and line sources are shown in Figure 3.3 and 3.4, respectively. Names and seismicity parameters of these sources will be explained in the following sections.

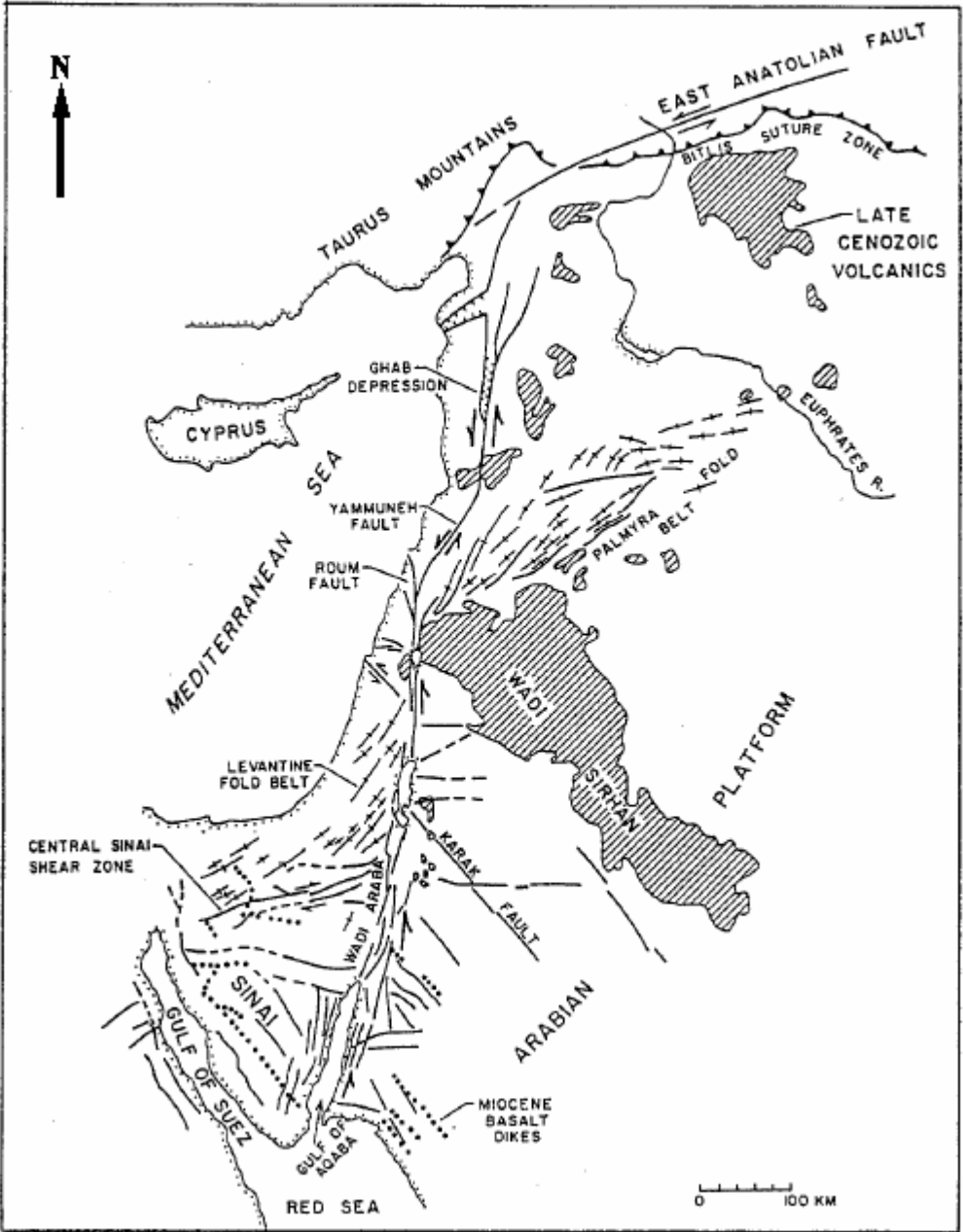


Figure 3.2 Tectonic Setting of Dead Sea Transform Fault System (After Barazangi, 1983)

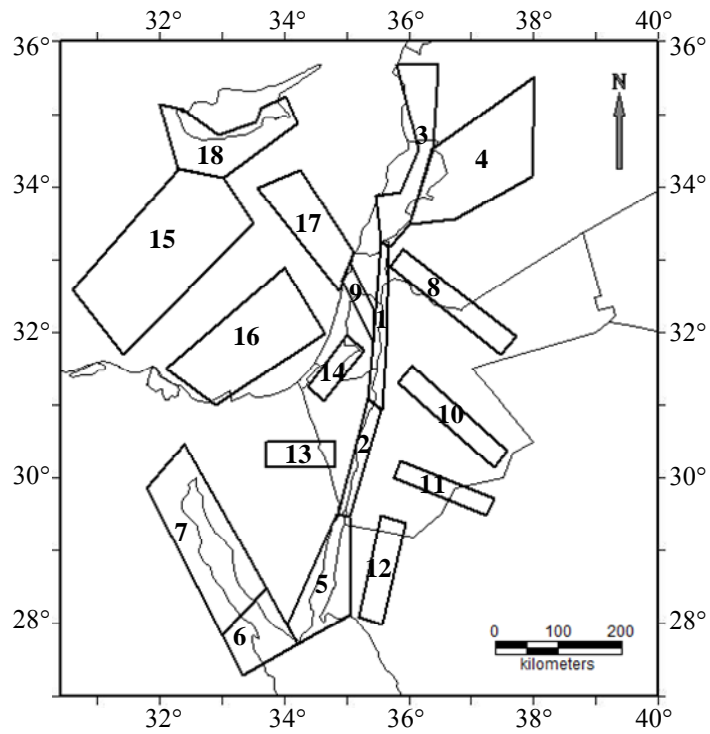


Figure 3.3 Locations of Area Sources Used in This Study (After Jiménez, 2004)

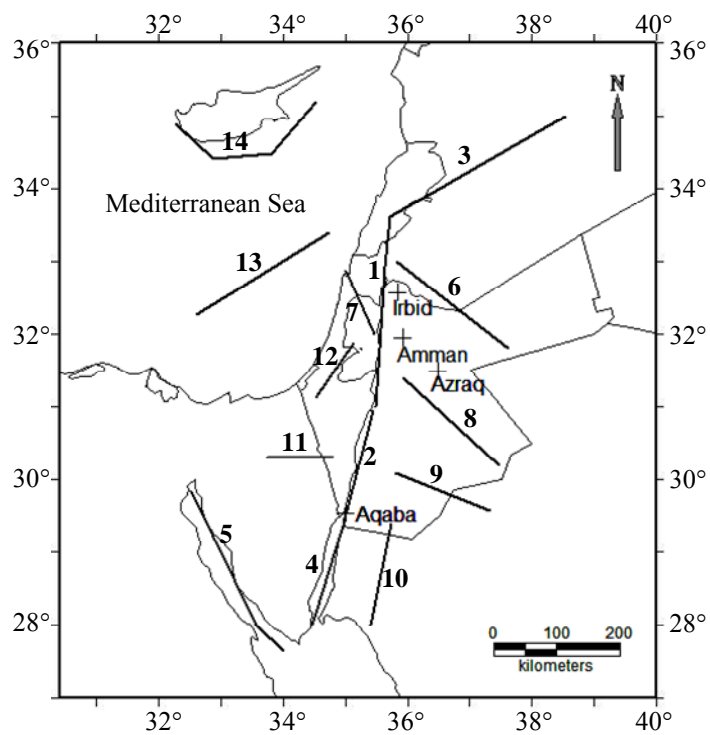


Figure 3.4 Locations of Line Sources Used in This Study (After Jiménez, 2004)

3.3.2 Alternative Models

Different seismic source models combined with different magnitude recurrence relationships are applied to calculate seismic hazard for Jordan. These models will be explained starting from the simplest to the more complex ones in the following sections.

3.3.2.1 Model 1

This is the simplest model compared with the others. The area sources shown in Figure 3.3 are used by assuming exponential magnitude distribution for all of them. The lower bound magnitude (m_0) is taken as 4.0 for all sources. The annual rate (ν) and slope of the exponential magnitude distribution (β) are assessed based on the information given in the report by Jiménez (2004) since this study appears to be the most comprehensive one and has compiled up-to-date information. However, a certain degree of cross checking has also been done by using some of the other references (Yüçemen, 1992; Al-Tarazi, 1992; Batayneh, 1994; Fahmi et al., 1996). The depths of seismic sources except those defined for Cyprus and Gulf of Suez are assumed to be 20 km based on the study of Al-Tarazi and Sandvol (2007). The depth for the Cyprus area source is taken as 40 km which is the average value of the depths of the earthquakes that are listed in the earthquake catalog which includes only the main shocks and fall into this source. Similarly, the depths of two seismic sources defined for Gulf of Suez, namely Gulf of Suez-North and Gulf of Suez-South, are taken as 25 km which is consistent with the study of Al-Tarazi and Sandvol (2007). In the earthquake catalog, there exist some events that cannot be associated with any one of the seismic sources identified in this model. These activities are treated as the background seismicity and its effect is smeared over the whole region. For the background seismic source, the parameter of the exponential magnitude distribution, β , is taken from the study of Yüçemen (1992). The seismicity parameters of the seismic sources in Model 1 are listed in Table 3.2.

Table 3.2 Parameters of Seismic Sources Considered in Model 1

Source No.*	Name of Source	m_1	ν (per year)	$ \beta $	Depth (km)
1	Dead Sea-Jordan River	7.5	0.33	1.73	20
2	Wadi-Araba	6.6	0.11	1.89	20
3	Yamune-Roum	8.0	1.47	2.12	20
4	Palmira	6.0	0.12	2.21	20
5	Gulf of Aqaba	6.5	1.51	1.96	20
6	Gulf of Suez-South	7.0	0.54	2.46	25
7	Gulf of Suez-North	7.0	0.19	1.84	25
8	Sirhan Faults	7.0	0.05	1.63	20
9	Farah Haifa	5.8	0.09	1.98	20
10	Wadi Karak	4.7	0.023	1.01	20
11	SE Maan	4.6	0.029	0.67	20
12	East Gulf of Aqaba	5.9	0.054	0.92	20
13	Central Sinai	4.0	0.01	0.69	20
14	North East Gaza	4.5	0.022	0.78	20
15	SE-Mediterranean 1	5.8	1.75	1.84	20
16	SE-Mediterranean 2	5.8	0.49	2.42	20
17	SE-Mediterranean 3	7.5	0.09	2.12	20
18	Cyprus	8.0	2.74	2.26	40
	Background	5.0	0.49	1.75	20

* These numbers correspond to the source numbers shown in Figure 3.3.

3.3.2.2 Model 2 and Model 3

In Model 2, all seismic sources, except SE-Mediterranean 1, SE-Mediterranean 2, SE-Mediterranean 3 and Cyprus, are modeled as line (fault) sources as shown in Figure 3.4. The lower bound magnitude (m_0) is taken as 4.0 for all sources. Similar to Model 1, a background area source is defined to take into account the seismic activity that cannot be related with any one of the seismic sources in this model. Exponential magnitude distribution is assumed for all sources.

In Model 3, same seismic sources and seismicity parameters are used. But, characteristic earthquake model proposed by Youngs and Coppersmith (1985) is

assumed for all line sources (faults) with $m_1 \geq 6.5$. The parameters of the seismic sources in Model 2 and Model 3 are listed in Table 3.3.

Table 3.3 Parameters of Seismic Sources Considered in Model 2 and Model 3

Source No.	Name of Source	Type of Source Model	Fault Type	m_1	ν (per year)	$ \beta $	Depth (km)
1	Dead Sea-Jordan River	Line	Strike-Slip	7.5	0.33	1.73	20
2	Wadi Araba	Line	Strike-Slip	6.6	0.11	1.89	20
3	Northern Faults	Line	Strike-Slip	8.0	1.59	2.13	20
4	Gulf of Aqaba	Line	Strike-Slip	6.5	1.51	1.96	20
5	Gulf of Suez	Line	Strike-Slip	7.0	0.73	2.30	25
6	Sirhan Faults	Line	Strike-Slip	7.0	0.05	1.63	20
7	Farah Haifa	Line	Strike-Slip	5.8	0.09	1.98	20
8	Wadi Karak	Line	Strike-Slip	4.7	0.023	1.01	20
9	SE Maan	Line	Strike-Slip	4.6	0.029	0.67	20
10	East Gulf of Aqaba	Line	Strike-Slip	5.9	0.054	0.92	20
11	Central Sinai	Line	Strike-Slip	4.0	0.01	0.69	20
12	North East Gaza	Line	Strike-Slip	4.5	0.022	0.78	20
15*	SE-Mediterranean 1	Area	-	5.8	1.75	1.84	20
16*	SE-Mediterranean 2	Area	-	5.8	0.49	2.42	20
17*	SE-Mediterranean 3	Area	-	7.5	0.09	2.12	20
18*	Cyprus	Area	-	8.0	2.74	2.26	40
	Background	Area	-	5.0	0.49	1.75	20

* These numbers correspond to the source numbers shown in Figure 3.3 while others correspond to the source numbers shown in Figure 3.4.

3.3.2.3 Model 4

All seismic sources are modeled as line (fault) sources as shown in Figure 3.4. Pure characteristic earthquake or maximum magnitude model is used for the sources with $m_1 \geq 6.5$. For the faults whose slip rates are available, the activity rate of the maximum magnitude, characteristic events are calculated by using the seismic moment balancing concept. This method is preferred due to the reason that the length of available earthquake catalog was not long enough to predict the frequency of characteristic earthquakes and paleoseismicity data was not available for the

faults considered. Seismic moment, first introduced by Aki (1966), describes size of an earthquake with static fault parameters as follows:

$$M_0 = \mu AD \quad (3.3)$$

where, M_0 is the seismic moment, μ is the rigidity or shear modulus of the crust (usually taken as 3.0×10^{11} dyne/cm²), A is the rupture area on the fault plane undergoing slip during the earthquake, and D is average displacement over the slip surface.

The seismic moment rate, M_0' , or the rate of seismic energy release can be calculated from the time derivative of Eq. (3.3) as follows:

$$M_0' = \mu AS \quad (3.4)$$

where M_0' is the seismic moment rate and S is the average slip-rate along the fault.

Seismic moment can be calculated from the moment magnitude, M_w , by using the following equation (Hanks and Kanamori, 1979):

$$M_w = 2/3 \log M_0 - 10.7 \quad (3.5)$$

or

$$M_0 = 10^{1.5M_w + 16.05} \quad (3.6)$$

The activity rate of earthquakes with magnitude, M_w , can be calculated from the combination of Eqs. (3.4) and (3.6) in the following form;

$$v_M = \frac{M_0'}{M_0} = \frac{\mu AS}{10^{1.5M_w + 16.05}} \quad (3.7)$$

Based on the study of Ambraseys (2006), average slip rate of 4.5 mm/year is assigned to the faults that constitutes the main Dead Sea fault system and extends in approximately south-north direction although it may be somewhat larger in the

north and smaller in the south. This value is also consistent with the slip rate distribution given by Mahmoud et al. (2005). For the Gulf of Suez and Cyprus faults, the slip-rate distribution of Mahmoud et al. (2005) is applied.

The seismic moment in the denominator of Eq. (3.7) is calculated from the moment magnitude scale. But, maximum magnitudes of the faults considered in this study are given in surface wave magnitude scale. Hanks and Kanamori (1979) stated that Eq. (3.5) is uniformly valid for $5.0 \leq M_s \leq 7.5$. Except Cyprus Fault, maximum magnitudes of the faults for which slip rates are available are in this range. In addition, Ambraseys (2001) proposed the following equation for Eastern Mediterranean and Middle East Region to calculate seismic moment from surface wave magnitude scale, M_s , greater than 6.0;

$$\log M_0 = 16.07 + 1.5M_s \quad (3.8)$$

The constants in Eq. (3.8) are approximately the same with those given by Hanks and Kanamori (1979). Therefore, the maximum magnitudes of the faults are not converted from surface wave magnitude scale to moment magnitude scale in order to calculate the activity rate of maximum magnitude earthquakes from Eq. (3.7).

For the rest of the faults with $m_1 \geq 6.5$, the activity rate of maximum magnitude events are taken as equal to the rate associated with characteristic earthquakes over the interval $(m_1, m_1-0.5)$ in characteristic earthquake model proposed by Youngs and Coppersmith (1985). For the faults with $m_1 < 6.5$, exponential magnitude distribution is used and the lower bound, m_0 , is set equal to 4.0. The parameters of the faults in Model 4 are listed in Table 3.4.

Table 3.4 Parameters of Seismic Sources Considered in Model 4

Source No.	Fault Name	Fault Type	Model Type	Slip-Rate (mm/yr)	v (per year)	m_0	m_1	$ \beta $	Average Depth (km)
1	Dead Sea -Jordan River	Strike-Slip	Pure Characteristic	4.5	0.00290	-	7.5	-	20
2	Wadi Araba	Strike-Slip	Pure Characteristic	4.5	0.04999	-	6.6	-	20
3	Northern Faults	Strike-Slip	Pure Characteristic	-	0.00828*	-	8.0	-	20
4	Gulf of Aqaba	Strike-Slip	Pure Characteristic	4.5	0.07403	-	6.5	-	20
5	Gulf of Suez	Strike-Slip	Pure Characteristic	1.9	0.01149	-	7.0	-	25
6	Sirhan Faults	Strike-Slip	Pure Characteristic	-	0.00334*	-	7.0	-	20
7	Farah Haifa	Strike-Slip	Exponential	-	0.090	4.0	5.8	1.98	20
8	Wadi Karak	Strike-Slip	Exponential	-	0.023	4.0	4.7	1.01	20
9	SE Maan	Strike-Slip	Exponential	-	0.029	4.0	4.6	0.67	20
10	East Gulf of Aqaba	Strike-Slip	Exponential	-	0.054	4.0	5.9	0.92	20
11	Central Sinai	Strike-Slip	Exponential	-	0.010	4.0	4.0	0.69	20
12	North East Gaza	Strike-Slip	Exponential	-	0.022	4.0	4.5	0.78	20
13	SE Mediterranean	Reverse	Pure Characteristic	-	0.00491*	-	7.4	-	20
14	Cyprus	Strike-Slip	Pure Characteristic	6.0	0.00171	-	8.0	-	40

* Rate is calculated from characteristic earthquake model proposed by Youngs and Coppersmith (1985)

The earthquakes that are not assigned to any one of the specific faults are assumed to be potential seismogenic sources and the contribution of these events to seismic hazard is calculated by using the spatially smoothed seismicity model of Frankel (1995). The earthquakes with magnitudes between 4.0 and 6.5 in the catalog including only main shocks are used in this model. Also, the earthquakes related with the faults having maximum magnitudes less than 6.5 are eliminated from the catalog. Figure 3.5 shows the distribution of earthquakes used in spatially smoothed seismicity model. The slope of the Gutenberg-Richter magnitude recurrence relationship, b , is computed as 0.71 based on this dataset. Figure 3.6 shows the magnitude-recurrence relationship derived as well as the data used.

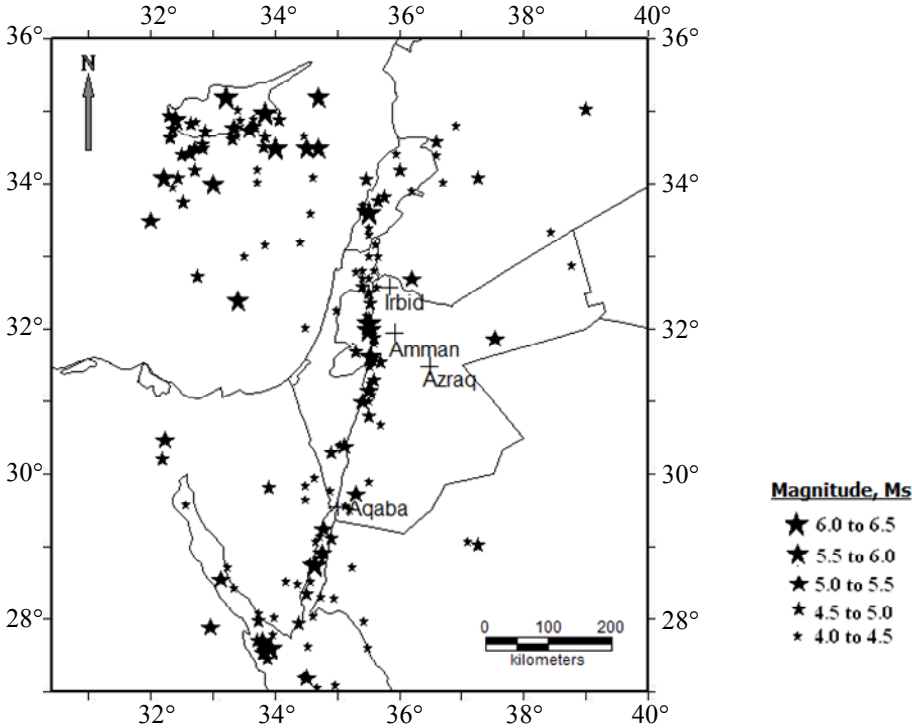


Figure 3.5 Map Showing the Distribution of Earthquakes Used in Spatially Smoothed Seismicity Model and Locations of the Cities for Which Seismic Hazard are Computed

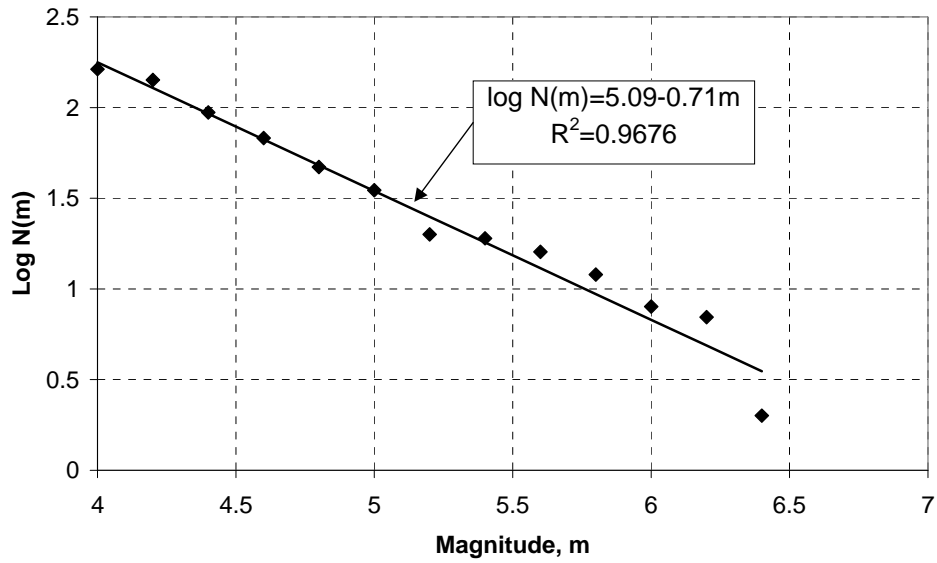


Figure 3.6 Magnitude-Recurrence Relationship Derived from the Data Used in Spatially Smoothed Seismicity Model

The region studied is divided into cells of a grid with spacing of $0.1^\circ \times 0.1^\circ$ in latitude and longitude. The number of earthquakes with magnitude equal to or greater than 4.0 are counted in each cell. Then, these cumulative values are converted to incremental values using the formula by Hermann (1977) and spatially smoothed over a grid of $0.1^\circ \times 0.1^\circ$ in latitude and longitude by using a Gaussian function having a correlation distance, c , of 50 km. The computations are carried out by using the computer program developed by USGS (Frankel et al., 1996) and modified by Kalkan (2007) in order to include additional attenuation relationships.

3.3.3 Seismic Hazard Computations

Seismic hazard analyses are carried out by using the models described in Section 3.3.2. EZ-FRISK (Risk Engineering, 2005) software is used to calculate seismic hazard nucleating from the main seismic sources (line and area sources) and background seismic source with uniformly distributed seismicity while the computer program developed by USGS (Frankel et al., 1996) is used to quantify the

seismic hazard based on the spatially smoothed seismicity model. For Model 4, the results of analyses obtained from these two computer programs are combined externally by summing annual exceedance probabilities corresponding to the same ground motion parameter (PGA or SA) level at each site and calculating the values corresponding to the selected return period. In order to achieve this, a computer program is coded.

Four sites which are located in Azraq, Amman, Irbid and Aqaba are selected. The sites corresponding to these cities are marked on Figure 3.4. Figures 3.7 through 3.10 show seismic hazard curves obtained for PGA at these sites according the four models explained in the previous section. It can be observed from these figures that modeling the faults as area sources coupled with exponential magnitude distribution (Model 1) resulted in the lowest annual exceedance probabilities for PGA values greater than 0.03g at all sites. On the other hand, modeling the faults, except Cyprus, SE-Mediterranean 1, SE-Mediterranean 2 and SE-Mediterranean 3, as line sources with exponential magnitude distribution (Model 2) gave higher seismic hazard results compared to Model 1 as expected, since the rates are distributed over the areas in Model 1 instead of those assigned along the fault lines in Model 2. The use of characteristic earthquake model proposed by Youngs and Coppersmith (1985) for major faults with magnitude, $m \geq 6.5$ (Model 3) resulted in higher seismic hazard results compared to the exponentially distributed magnitude assumption. This is due to the increased rate in large magnitude earthquakes consistent with the characteristic earthquake model. Compared with Model 3, modeling all faults as line sources and applying purely characteristic or maximum magnitude model for magnitude distribution of faults with magnitude, $m \geq 6.5$, combined with spatially smoothed seismicity model for earthquakes with $m < 6.5$ (Model 4) resulted in lower exceedance probabilities up to certain PGA levels. For the PGA values larger than these levels, the opposite trend is valid.

The contributions of the different seismic sources to the seismic hazard at these sites are evaluated for the peak ground acceleration (PGA) and shown in Figures 3.11 through 3.14.

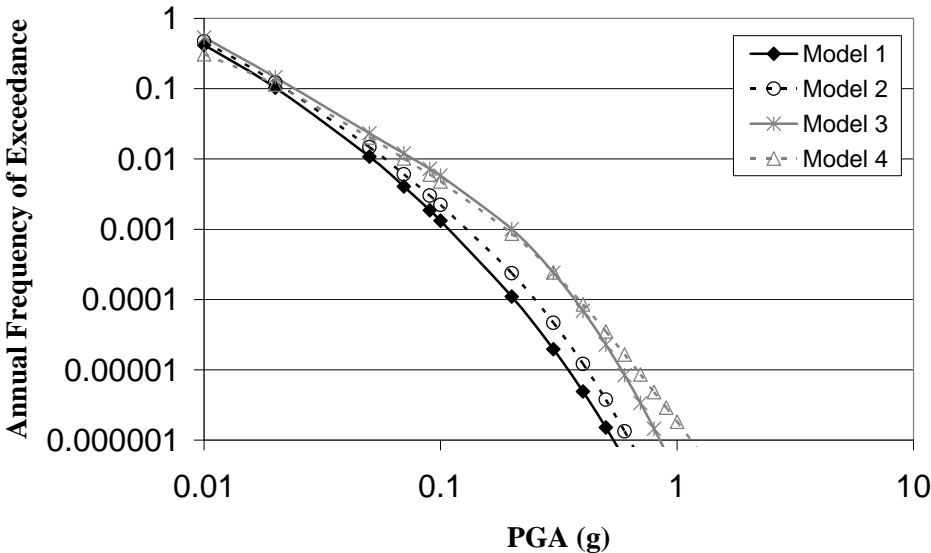


Figure 3.7 Seismic Hazard Curves Obtained for the Site Located in Amman

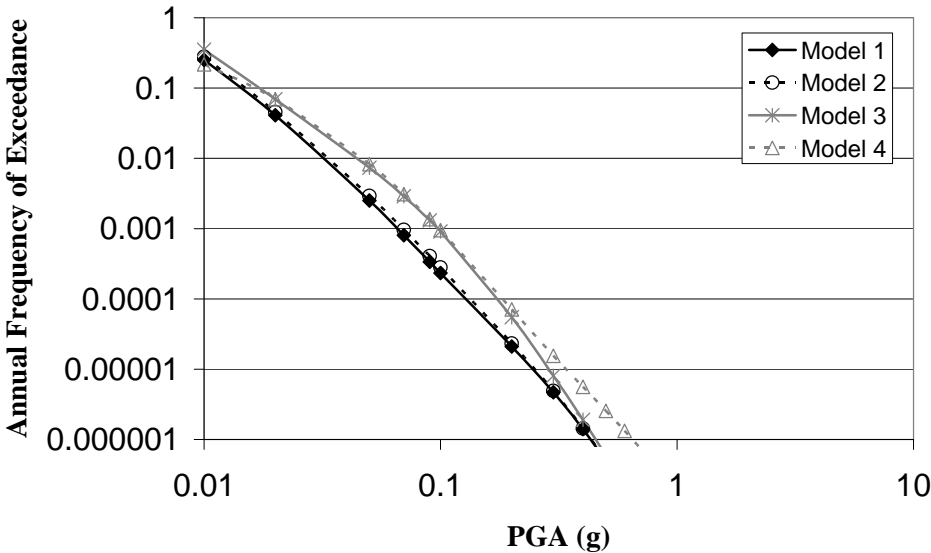


Figure 3.8 Seismic Hazard Curves Obtained for the Site Located in Azraq

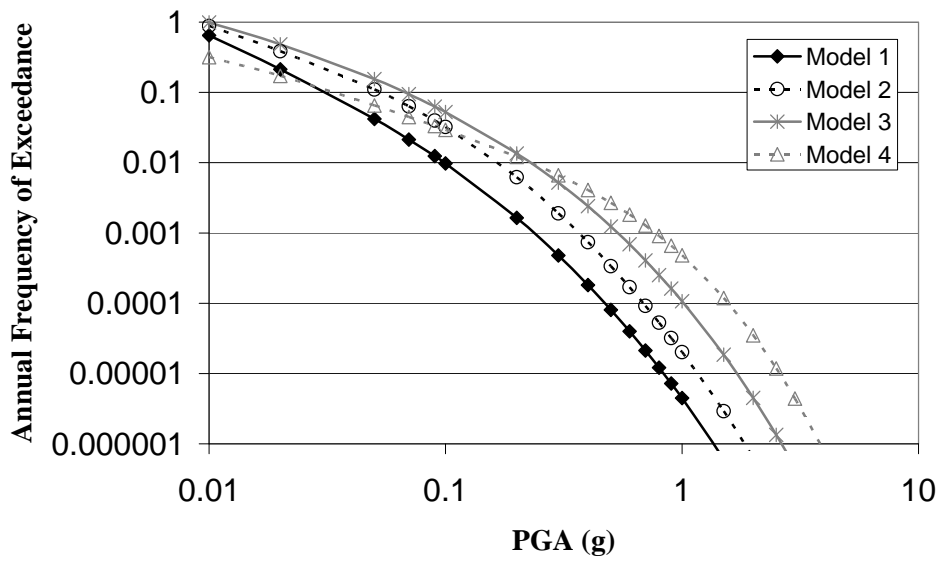


Figure 3.9 Seismic Hazard Curves Obtained for the Site Located in Aqaba

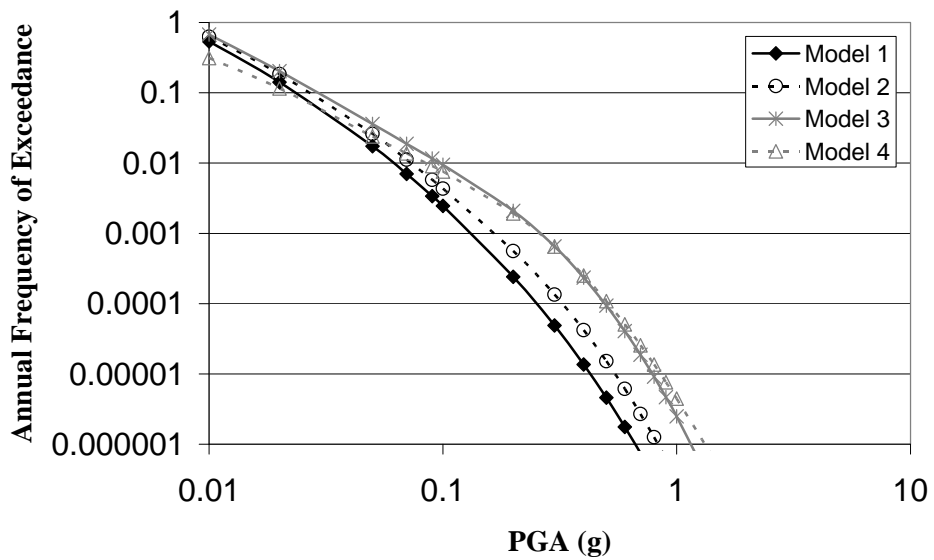
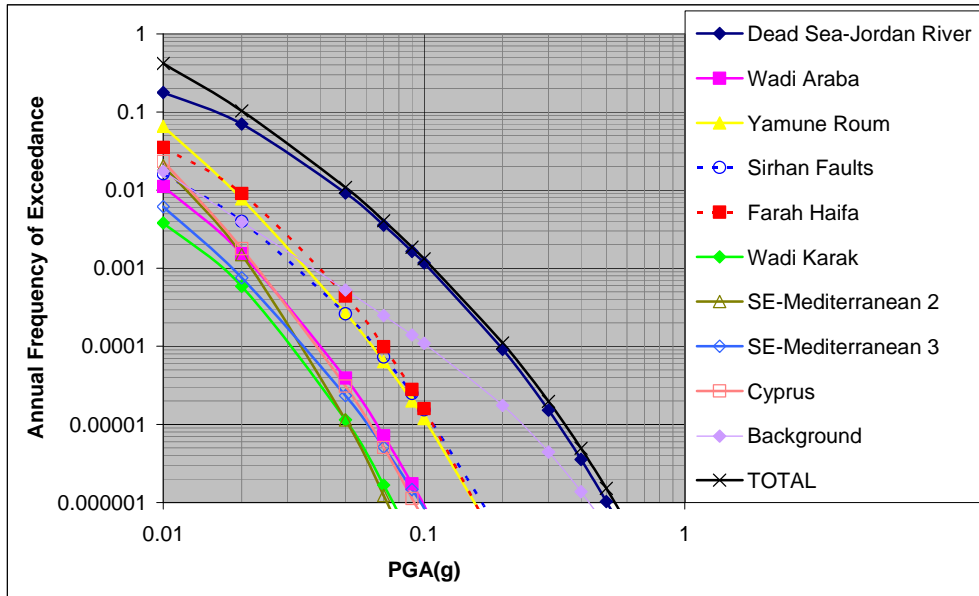
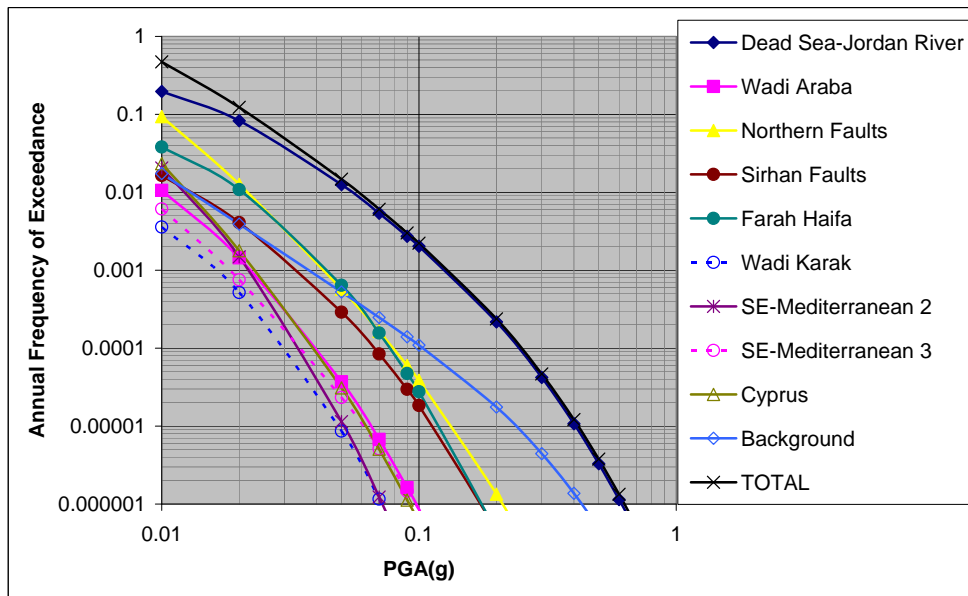


Figure 3.10 Seismic Hazard Curves Obtained for the Site Located in Irbid

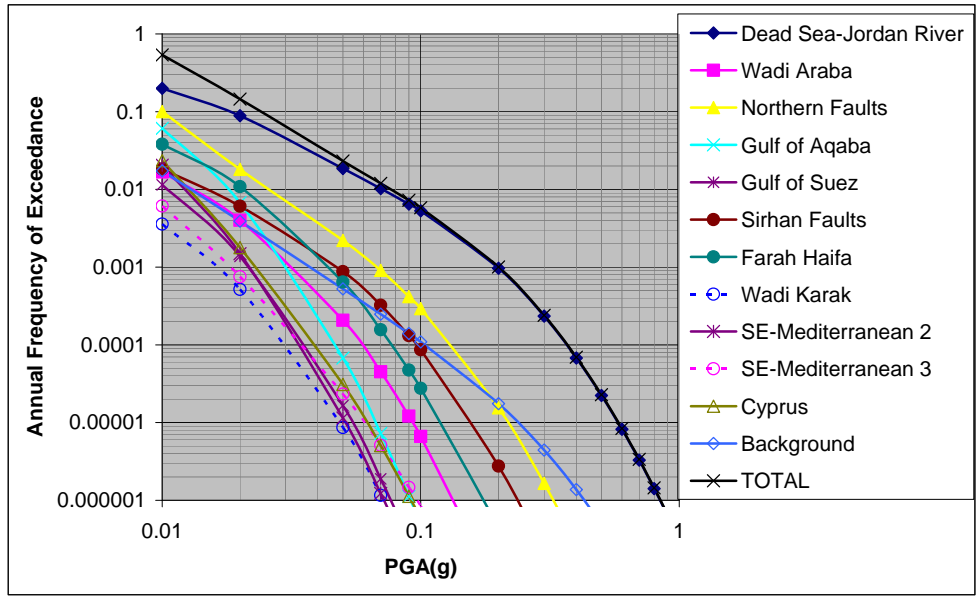


(a) Model 1

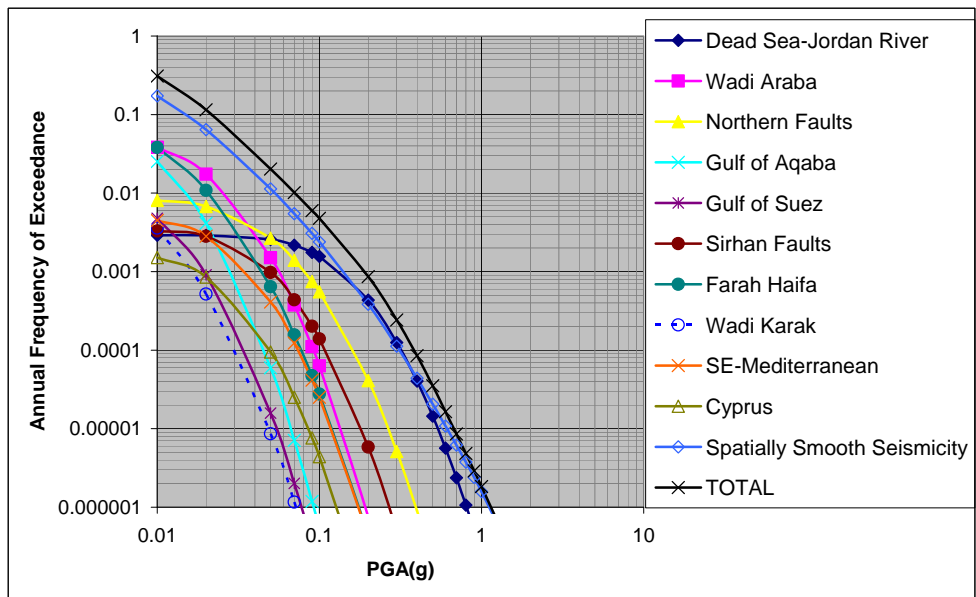


(b) Model 2

Figure 3.11 Contributions of the Different Seismic Sources to the Seismic Hazard at the Site Located in Amman

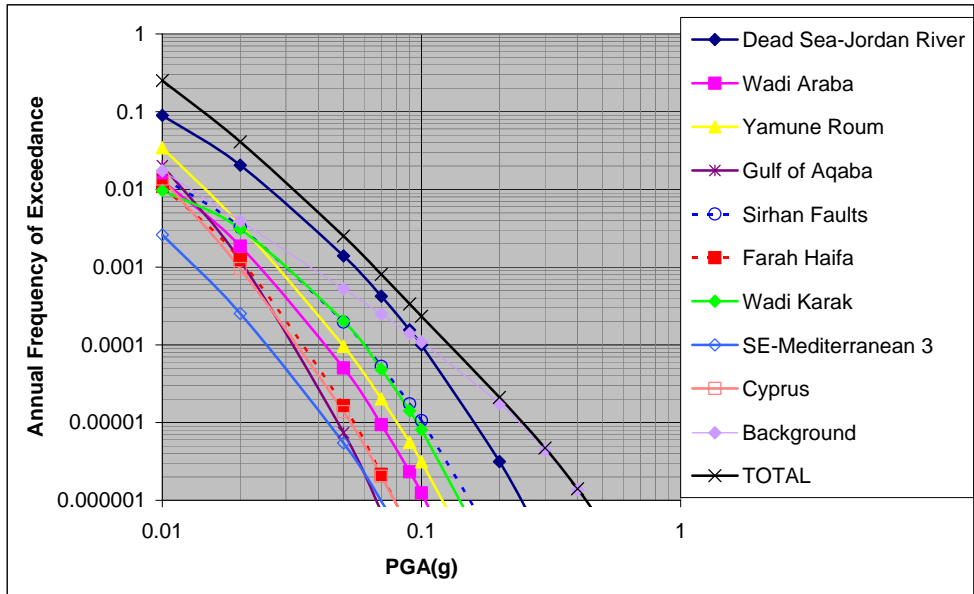


(c) Model 3

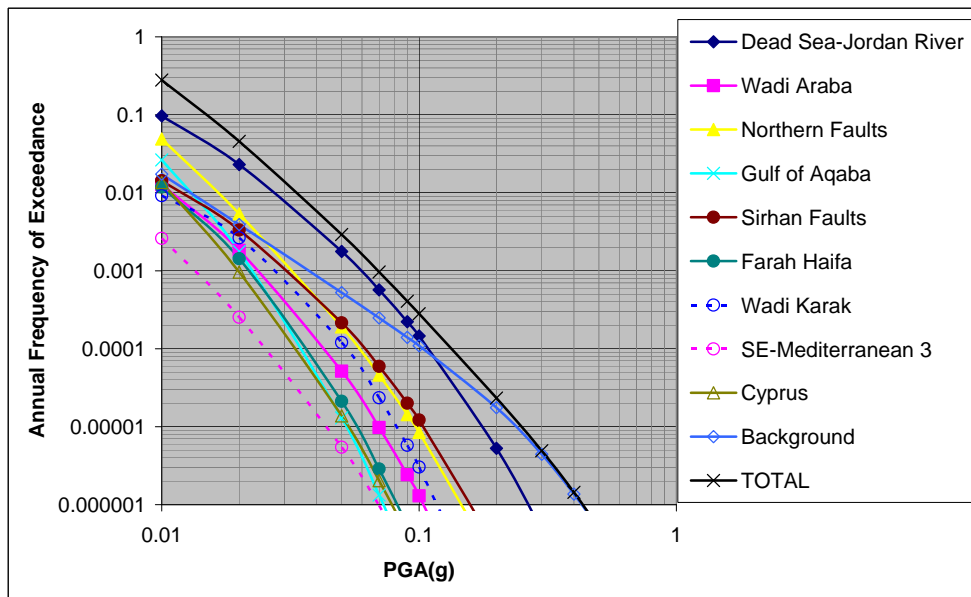


(d) Model 4

Figure 3.11(Continued) Contributions of the Different Seismic Sources to the Seismic Hazard at the Site Located in Amman

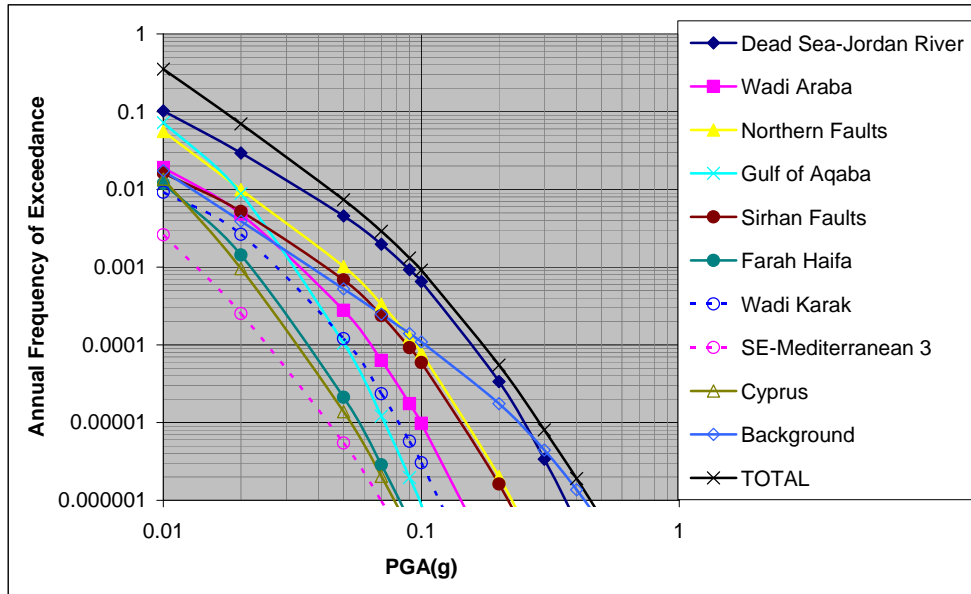


(a) Model 1

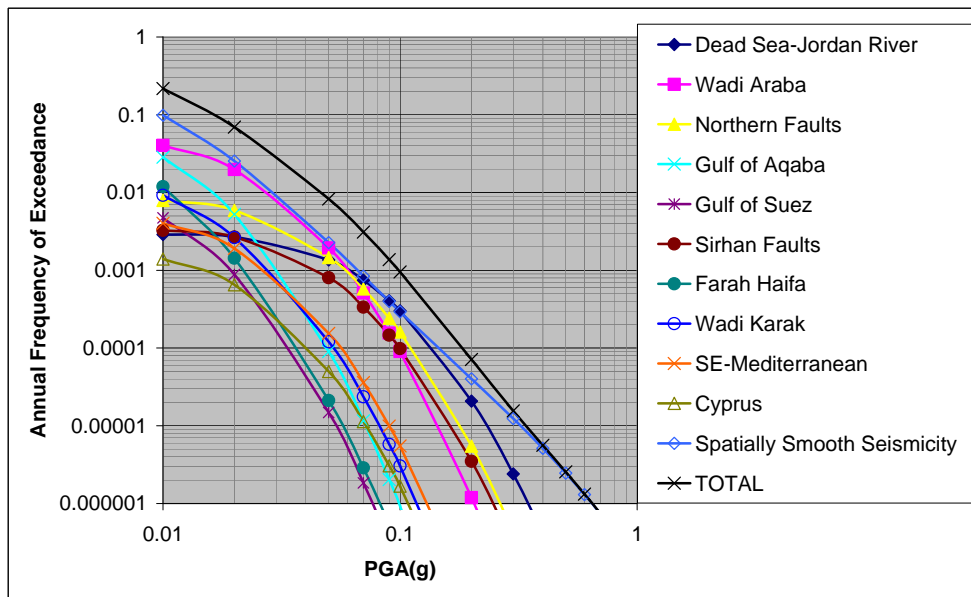


(b) Model 2

Figure 3.12 Contributions of the Different Seismic Sources to the Seismic Hazard at the Site Located in Azraq

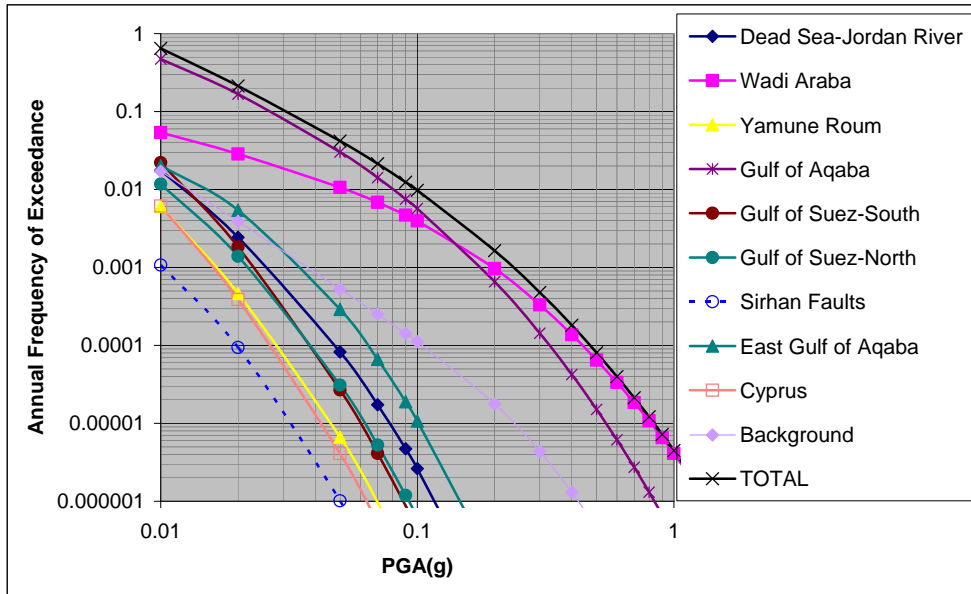


(c) Model 3

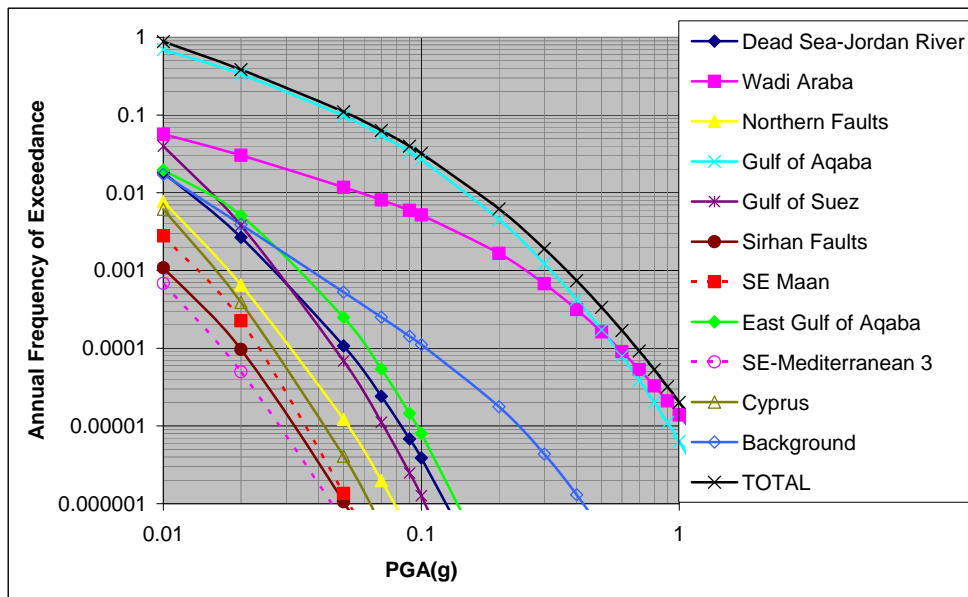


(d) Model 4

Figure 3.12(Continued) Contributions of the Different Seismic Sources to the Seismic Hazard at the Site Located in Azraq

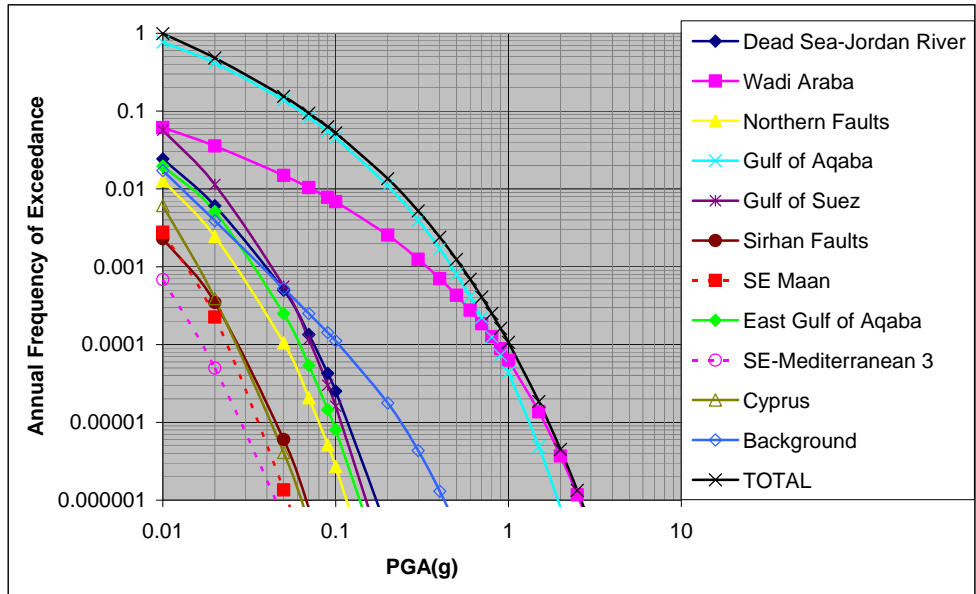


(a) Model 1

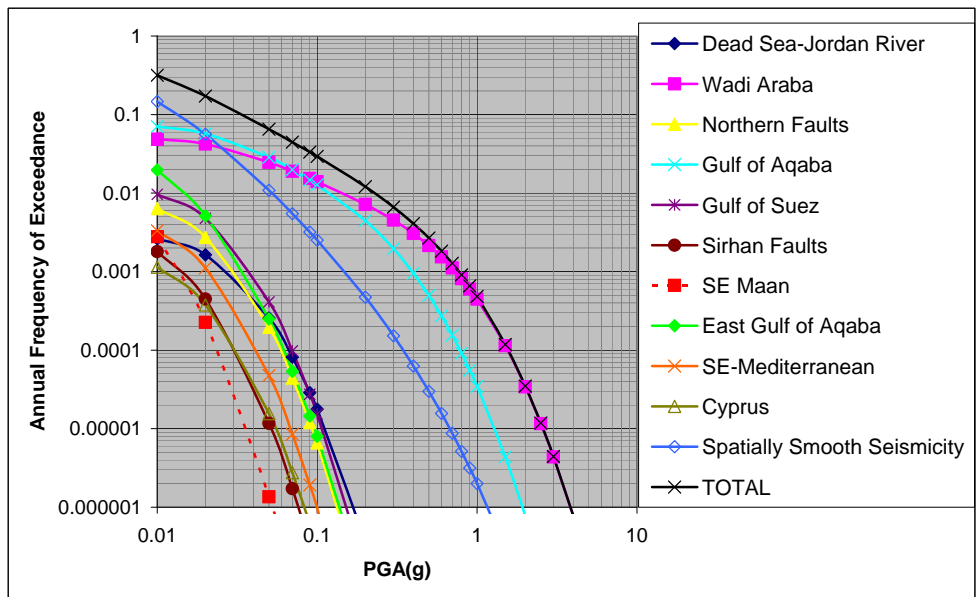


(b) Model 2

Figure 3.13 Contributions of the Different Seismic Sources to the Seismic Hazard at the Site Located in Aqaba

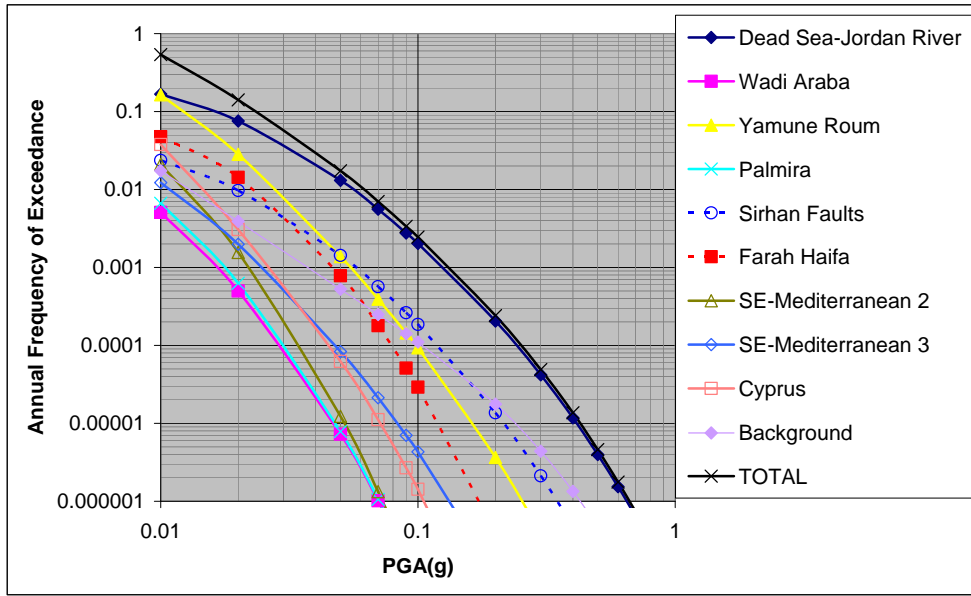


(c) Model 3

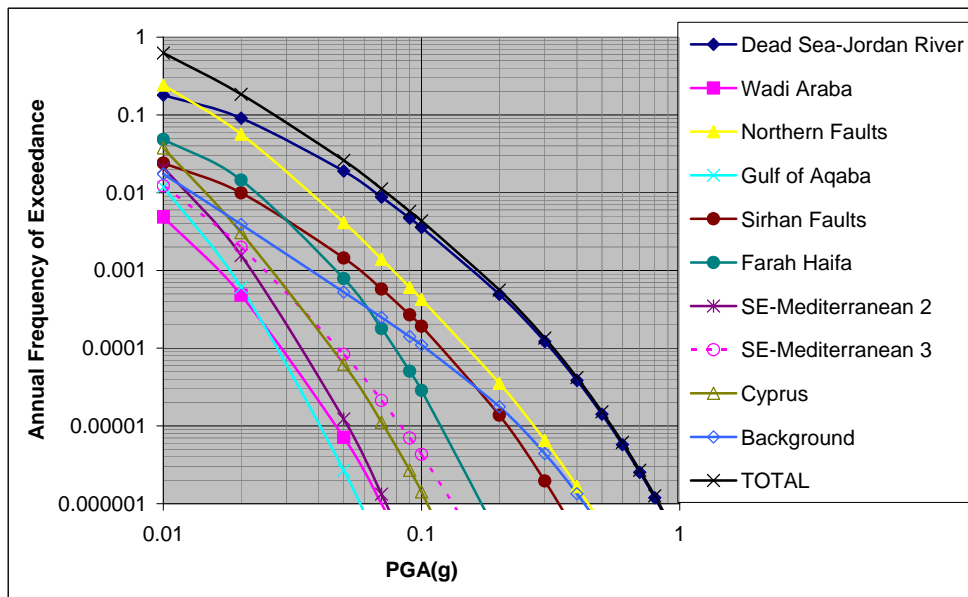


(d) Model 4

Figure 3.13(Continued) Contributions of the Different Seismic Sources to the Seismic Hazard at the Site Located in Aqaba

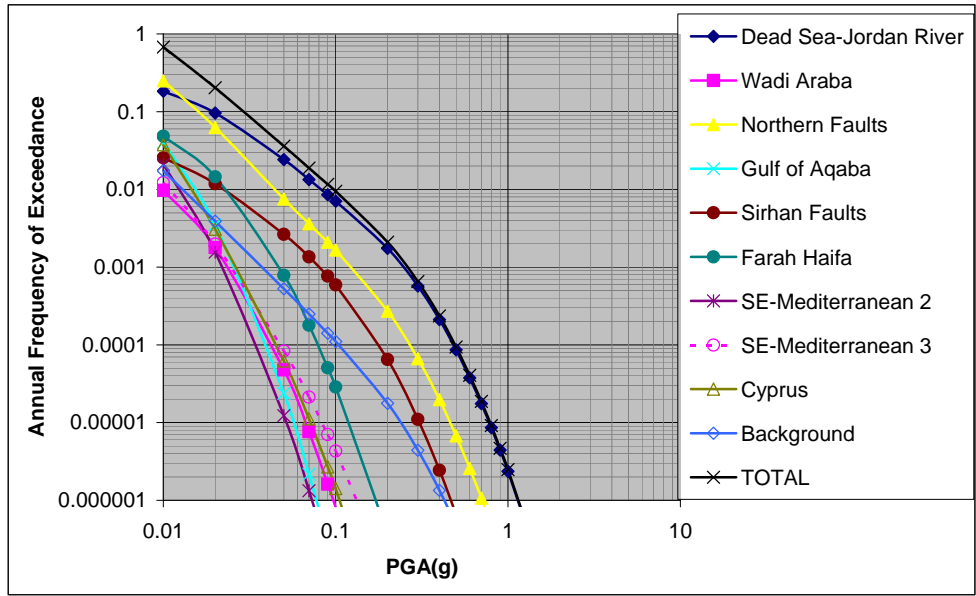


(a) Model 1

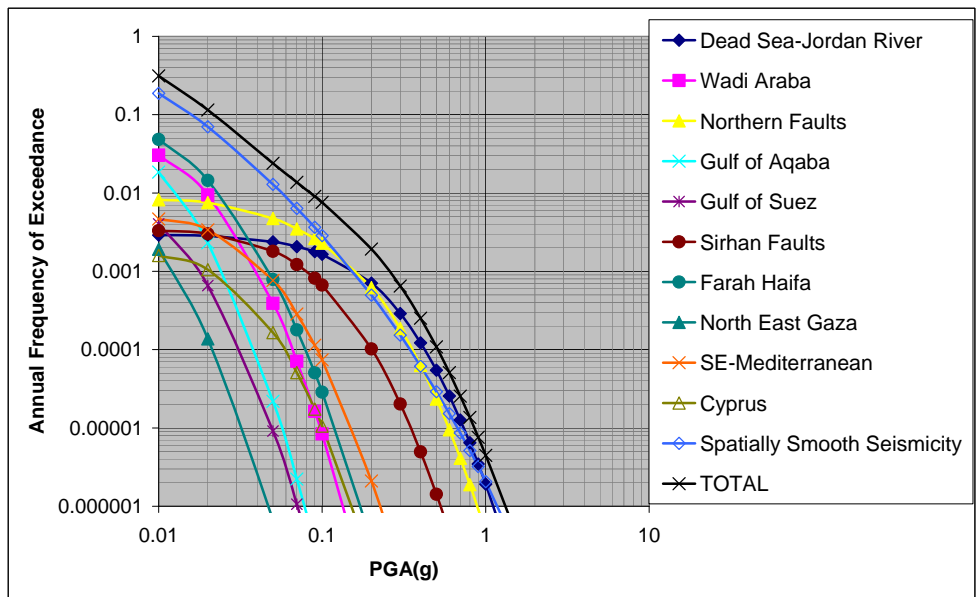


(b) Model 2

Figure 3.14 Contributions of the Different Seismic Sources to the Seismic Hazard at the Site Located in Irbid



(c) Model 3



(d) Model 4

Figure 3.14(Continued) Contributions of The Different Seismic Sources to the Seismic Hazard at the Site Located in Irbid

The highest contributing seismic source to the seismic hazards at the sites located in Amman and Irbid is the Dead Sea-Jordan River in Models 1, 2 and 3. For the site located in Amman, the background seismic activity modeled as spatially smoothed seismicity contributes most to the seismic hazard estimated from Model 4. For the site located in Irbid, background seismic activity for PGA values up to about 0.15g, and then the Dead Sea-Jordan River fault contribute most to the seismic hazard predicted by using Model 4. For the site located in Azraq, the highest contributing seismic source in Models 1, 2 and 3 is the Dead Sea-Jordan River for PGA values less than about 0.1g, 0.15g and 0.25g, respectively. At the same time, background is the most effective source to seismic hazard for larger PGA values. For the site located in Aqaba, Wadi Araba fault is the most effective source for PGA values greater than about 0.15g, 0.5g and 0.8g in Models 1, 2 and 3, respectively. For smaller PGA values, Gulf of Aqaba contributes most to the seismic hazard. For Model 4, background seismic activity modeled as spatially smoothed seismicity, Gulf of Aqaba and Wadi Araba are the main contributors to the seismic hazard at the site located in Aqaba.

PGA and SA ($T= 0.2$ sec and 1.0 sec) values corresponding to return periods of 475, 1000 and 2475 years are presented in Table 3.5 for the sites in Azraq, Amman, Irbid and Aqaba. These return periods correspond, respectively, to 10%, 5% and 2% probabilities of exceedance in 50 years. It is shown in Table 3.5 that for the sites located in Azraq, Model 1 and Model 2 give nearly same results. This is due to the reason that most of the seismic hazard in these models resulted from the Dead Sea-Jordan River source and compared with other sites, this site is located far away from this source. Therefore, modeling this source as line or area has a negligible effect on the results for the site in Azraq. For the sites located in Amman, Irbid and Aqaba, Model 2 gives higher seismic hazard values than Model 1. Among these cities, the difference is small for Amman, larger for Irbid and largest for Aqaba.

Table 3.5 PGA and SA (0.2 sec and 1.0 sec) Values Corresponding to Different Return Periods for the Four Sites According to Different Assumptions (in g)

Site	Model 1								
	PGA			SA(0.2 s)			SA(1.0 s)		
	475	1000	2475	475	1000	2475	475	1000	2475
Azraq	0.05	0.07	0.09	0.13	0.17	0.22	0.05	0.07	0.11
Amman	0.09	0.11	0.14	0.22	0.28	0.37	0.08	0.11	0.17
Irbid	0.10	0.13	0.17	0.27	0.34	0.45	0.10	0.13	0.20
Aqaba	0.18	0.24	0.32	0.43	0.56	0.75	0.10	0.13	0.19

Site	Model 2								
	PGA			SA(0.2 s)			SA(1.0 s)		
	475	1000	2475	475	1000	2475	475	1000	2475
Azraq	0.06	0.07	0.09	0.14	0.18	0.23	0.06	0.08	0.12
Amman	0.10	0.13	0.17	0.26	0.34	0.45	0.10	0.15	0.22
Irbid	0.13	0.16	0.22	0.33	0.43	0.58	0.13	0.18	0.28
Aqaba	0.29	0.37	0.47	0.69	0.87	1.13	0.16	0.22	0.32

Site	Model 3								
	PGA			SA(0.2 s)			SA(1.0 s)		
	475	1000	2475	475	1000	2475	475	1000	2475
Azraq	0.08	0.10	0.12	0.21	0.26	0.34	0.13	0.17	0.24
Amman	0.15	0.20	0.26	0.40	0.53	0.71	0.24	0.33	0.46
Irbid	0.20	0.26	0.34	0.52	0.70	0.94	0.31	0.44	0.63
Aqaba	0.42	0.53	0.70	1.02	1.30	1.72	0.35	0.47	0.65

Site	Model 4								
	PGA			SA(0.2 s)			SA(1.0 s)		
	475	1000	2475	475	1000	2475	475	1000	2475
Azraq	0.08	0.10	0.13	0.21	0.26	0.34	0.14	0.19	0.26
Amman	0.14	0.19	0.26	0.36	0.49	0.67	0.22	0.31	0.45
Irbid	0.19	0.26	0.35	0.50	0.68	0.93	0.33	0.48	0.71
Aqaba	0.56	0.77	1.05	1.32	1.80	2.48	0.52	0.73	1.03

Compared with Model 2, Model 3 gives slightly higher results for all sites. This is due to the reason that in Model 3, characteristic earthquake model is used for the faults with $m_1 \geq 6.5$. Compared with the exponential magnitude distribution adapted in Model 2, higher rates are assigned to characteristic earthquakes in Model 3.

Model 3 and Model 4 give nearly the same PGA and SA values for the sites in Azraq, Amman and Irbid. For Aqaba, PGA and SA values estimated from Model 4 are 1.3 to 1.6 times higher than those obtained from Model 3.

It should be mentioned that high PGA and SA values are obtained from Model 3 and Model 4 in Table 3.5 for Aqaba. The site selected for Aqaba is located almost on the top of Wadi Araba fault and very near to Gulf of Aqaba Fault (about 5 km to the fault). Therefore, the increase in the rates of maximum magnitude earthquakes of these faults in Model 3 and Model 4 resulted in such high seismic hazard values.

In addition to the analyses carried out for the four sites explained above, seismic hazard analyses are carried out to construct seismic hazard maps for Jordan in terms of PGA and SA at 0.2 sec and 1.0 sec for return periods of 475, 1000 and 2475 years. These return periods correspond to 10%, 5% and 2% probabilities of exceedance in 50 years. The rectangular region bounded by 27-36° N latitudes and 30.4-40° E longitudes is divided into grids with spacing of 0.1° x 0.1° in latitude and longitude. Seismic hazard computations are carried out at each grid point according to each one of the set of assumptions classified as Model 1, Model 2, Model 3 and Model 4, in order to display the spatial distributions of PGA and SA (T= 0.2 sec and 1.0 sec) values corresponding to 475, 1000 and 2475 years return periods. The maps constructed based on the results obtained for PGA are presented in Appendix C. It should be mentioned that only the values given within the boundaries of Jordan, drawn by thick black lines in these maps, are reliable. This is due to the fact that additional seismic sources that may contribute to the seismic hazard at the sites located outside of the boundaries of Jordan are not taken into consideration in seismic hazard calculations.

In Model 4, the contribution of background events to hazard is calculated by using the spatially smoothed seismicity model of Frankel (1995) instead of describing a background area source with uniform seismicity. However, to investigate the sensitivity of seismic hazard results to background events, seismic hazard analyses are also carried out by only using a background area source. The lower and upper

bounds of earthquake magnitudes are taken as 4.0 and 6.5. The slope of the exponential distribution, $|\beta|$, is calculated as 1.63 which corresponds to the b value (0.71) used for spatially smoothed seismicity model. The annual rate, ν , is calculated by dividing the number of earthquakes used in spatially smoothed seismicity model with the time length of the catalog. Figures 3.15 through 3.17 show the seismic hazard maps for PGA obtained by using the spatially smoothed seismicity model for return periods of 475, 1000, 2475 years, respectively.

In the case of spatially smoothed seismicity model, maximum PGA values (in g) range from 0 to 0.15, 0.21 and 0.31 for return periods of 475, 1000 and 2475 years, respectively. The larger values are observed at the regions where the epicenters of earthquakes cluster and these values decrease as the distance to these regions increases. In order to visualize this, the epicenters of the earthquakes used in spatially smoothed seismicity model are placed on the seismic hazard map obtained by using this model for PGA corresponding to the return period of 2475 years as shown in Figure 3.18. On the other hand, the maximum PGA values (in g) obtained from the analyses carried out by using the background seismic source model with uniform seismicity are 0.06, 0.08 and 0.12 for return periods of 475, 1000, and 2475 years, respectively. These values are fairly smaller than those obtained from the spatially smoothed seismicity model. Nearly uniform PGA values are observed in the maps constructed from the analyses carried out based on the background area source and these values change within narrow ranges. Therefore, background area source model with uniform seismicity gives higher PGA values than the spatially smoothed seismicity model at the sites located far away from the regions where the epicenters of earthquakes cluster. This can be observed from Figure 3.19 which shows the spatial variation of the difference in PGA values predicted from spatially smoothed seismicity model with respect to background seismic source with uniform seismicity for a return period of 2475 years as well as the epicenters of the earthquakes considered in spatially smoothed seismicity model. In order to construct the map in Figure 3.19, the difference between the PGA values obtained from these two models is calculated at each grid point in the rectangular region

bounded by 27-36° N latitudes and 30.4-40° E longitudes by using the following equation;

$$\text{Difference}(\%) = \left(\frac{\text{PGA}_s - \text{PGA}_b}{\text{PGA}_b} \right) \times 100 \quad (3.9)$$

where PGA_s and PGA_b denote the PGA values estimated from spatially smoothed seismicity model and background area source with uniform seismicity, respectively. The difference with negative sign (-) means that background area source with uniform seismicity gives higher PGA values than spatially smoothed seismicity model and that with positive sign (+) represents the opposite case.

The differences among Models 1, 2, 3 and 4, in terms of PGA, are calculated for the region within the boundaries of Jordan from the following equation;

$$\text{Difference}(\%) = \left(\frac{\text{PGA}_{\text{Model } j} - \text{PGA}_{\text{Model } i}}{\text{PGA}_{\text{Model } i}} \right) \times 100 \quad (3.10)$$

where $\text{PGA}_{\text{Model } i}$ and $\text{PGA}_{\text{Model } j}$ are PGA values obtained from Model i and Model j, respectively. The difference with positive sign (+) indicates that Model j gives higher PGA values than Model i and that with negative sign (-) represents the opposite case.

The spatial variation of these differences is shown in Figures 3.20 through 3.28.

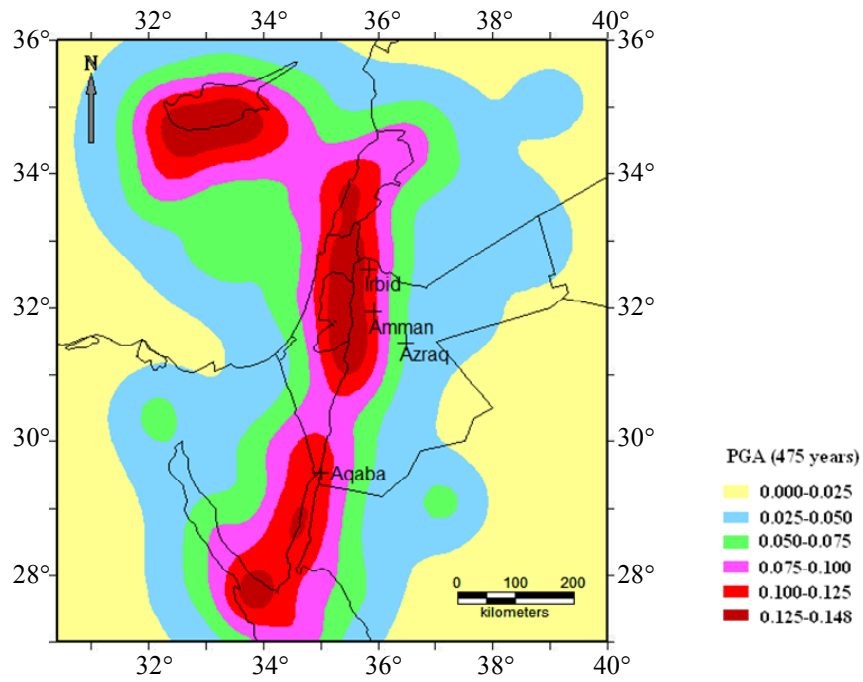


Figure 3.15 Seismic Hazard Map for PGA (in g) Obtained by Using Spatially Smoothed Seismicity Model for a Return Period of 475 Years

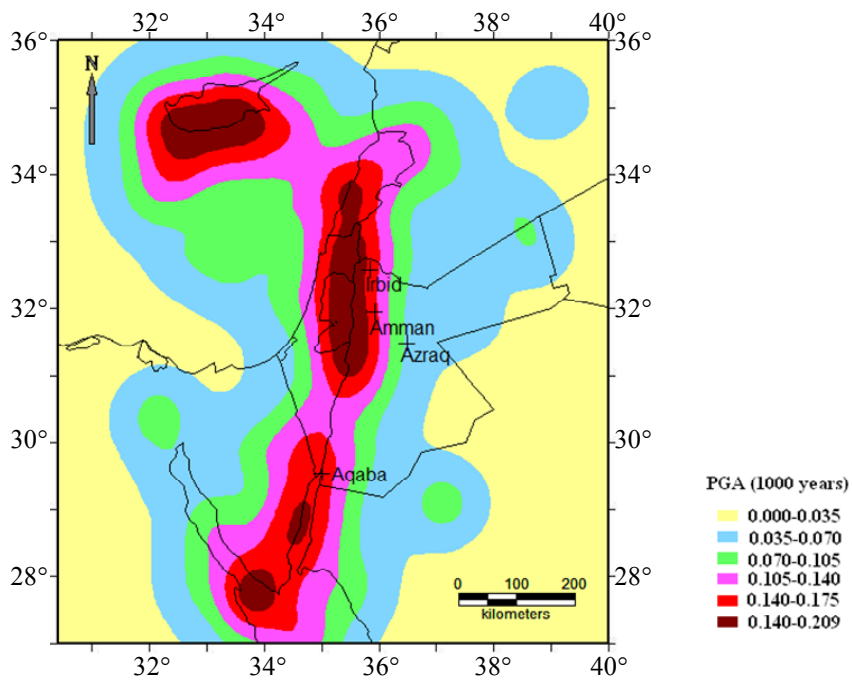


Figure 3.16 Seismic Hazard Map for PGA (in g) Obtained by Using Spatially Smoothed Seismicity Model for a Return Period of 1000 Years

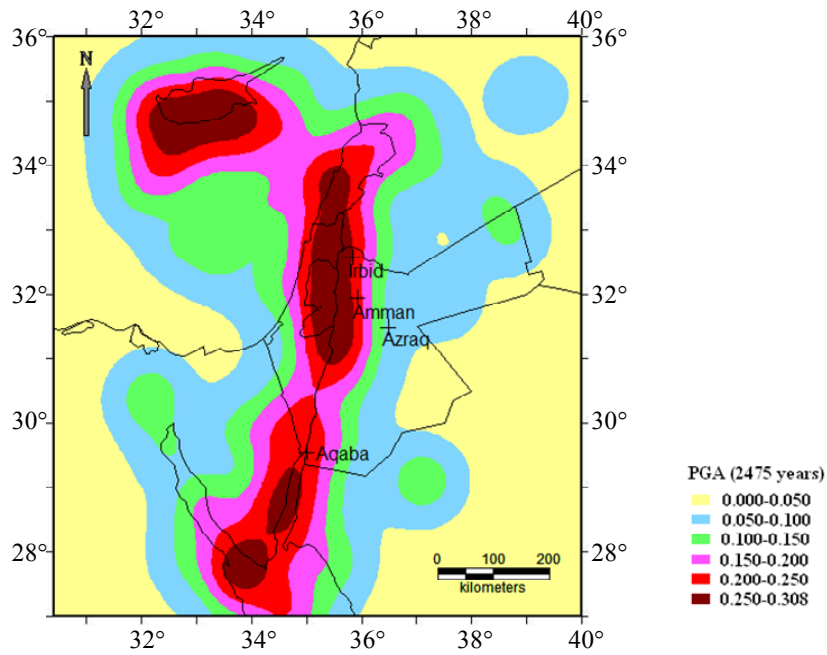


Figure 3.17 Seismic Hazard Map for PGA (in g) Obtained by Using Spatially Smoothed Seismicity Model for a Return Period of 2475 Years

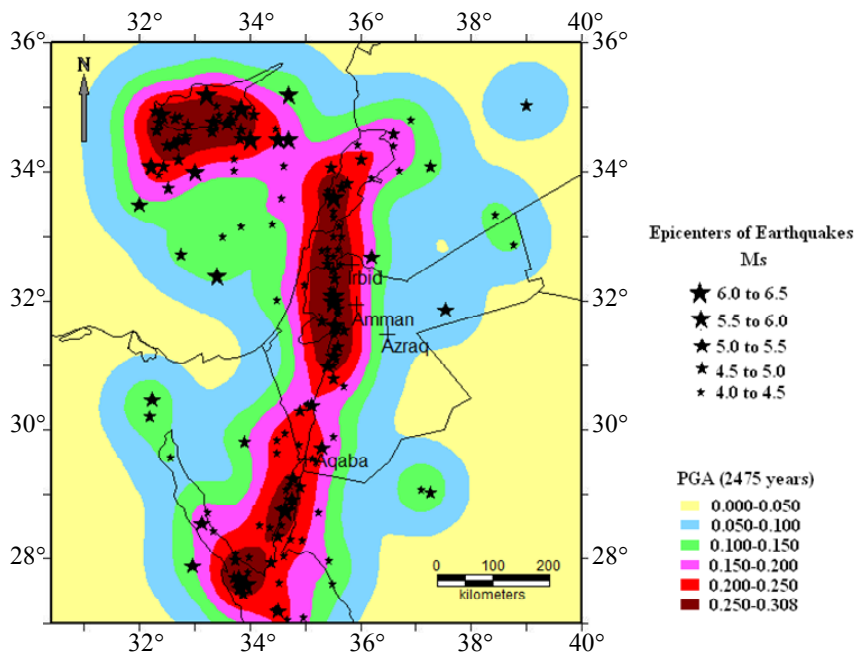


Figure 3.18 Seismic Hazard Map Showing the PGA Values (in g) Obtained by Using Spatially Smoothed Seismicity Model for a Return Period of 2475 Years and Epicenters of Earthquakes Considered in the Assessment of Seismic Hazard

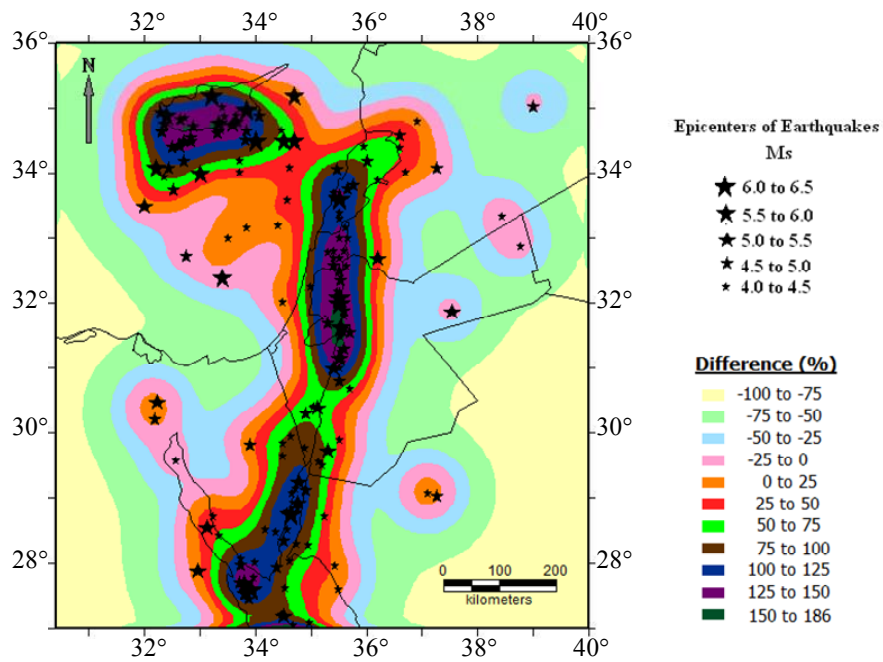


Figure 3.19 Map Showing the Spatial Variation of the Difference between PGA Values Obtained by Using Spatially Smoothed Seismicity Model and Background Seismic Source with Uniform Seismicity for a Return Period of 2475 Years and Epicenters of Earthquakes

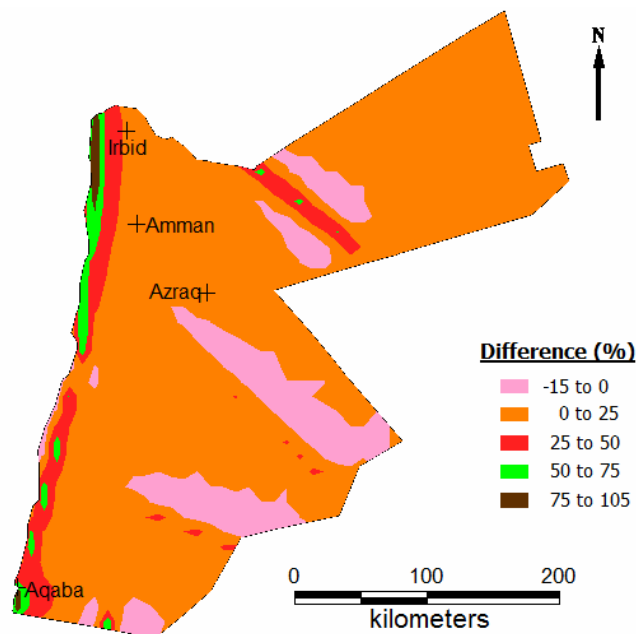


Figure 3.20 Map Showing the Spatial Variation of the Difference between the PGA Values Obtained from Model 2 and Model 1 for a Return Period of 475 Years

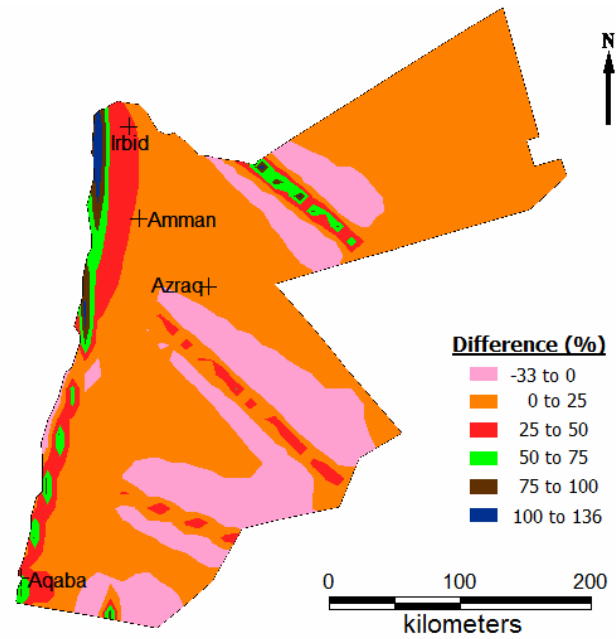


Figure 3.21 Map Showing the Spatial Variation of the Difference between the PGA Values Obtained from Model 2 and Model 1 for a Return Period of 2475 Years

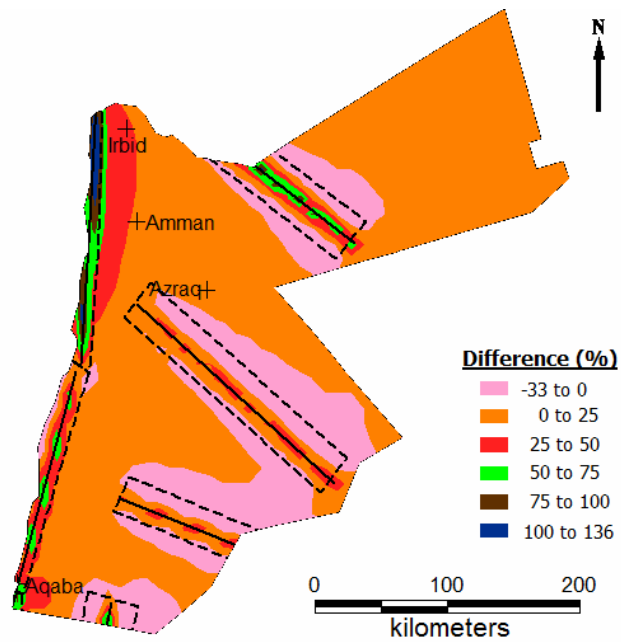


Figure 3.22 Map Showing the Spatial Variation of the Difference between the PGA Values Obtained from Model 2 and Model 1 for a Return Period of 2475 Years and Locations of Area Seismic Sources (Dashed Black Lines) and Line Sources (Black Lines)

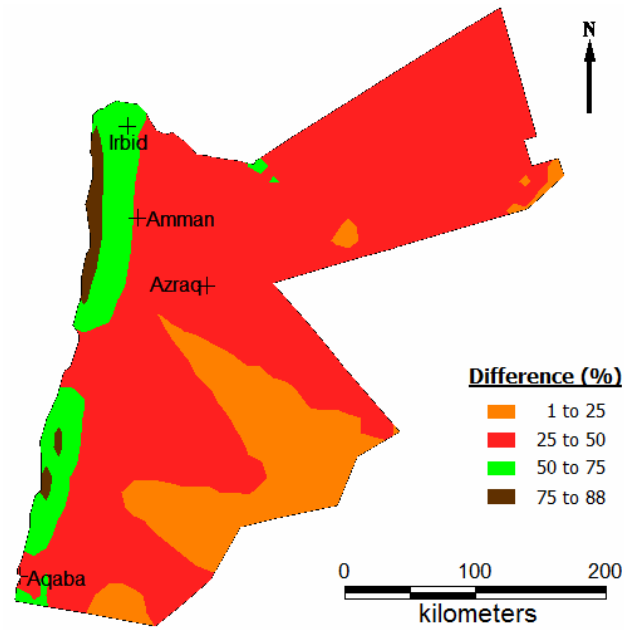


Figure 3.23 Map Showing the Spatial Variation of the Difference between the PGA Values Obtained from Model 3 and Model 2 for a Return Period of 475 Years

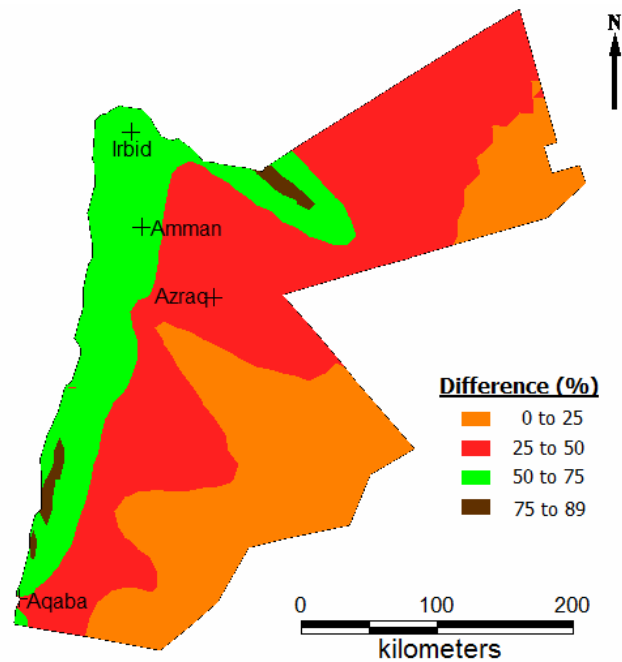


Figure 3.24 Map Showing the Spatial Variation of the Difference between the PGA Values Obtained from Model 3 and Model 2 for a Return Period of 2475 Years

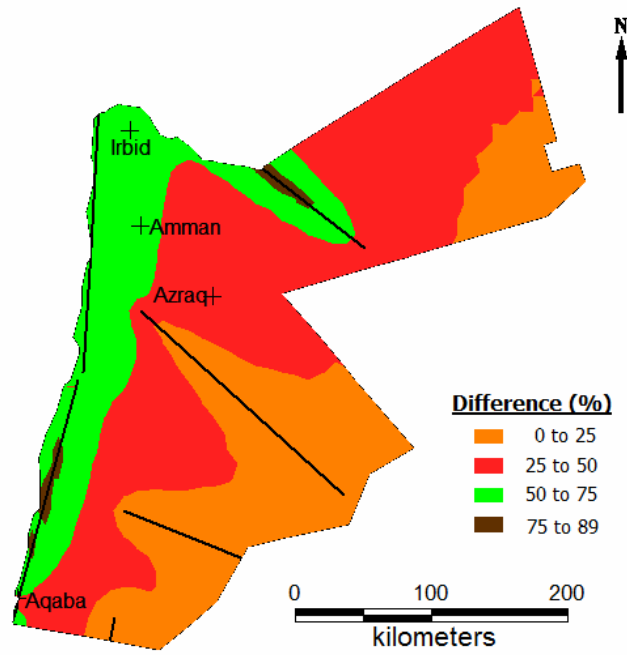


Figure 3.25 Map Showing the Spatial Variation of the Difference between the PGA Values Obtained from Model 3 and Model 2 for a Return Period of 2475 Years and Locations of Line Sources (Black Lines)

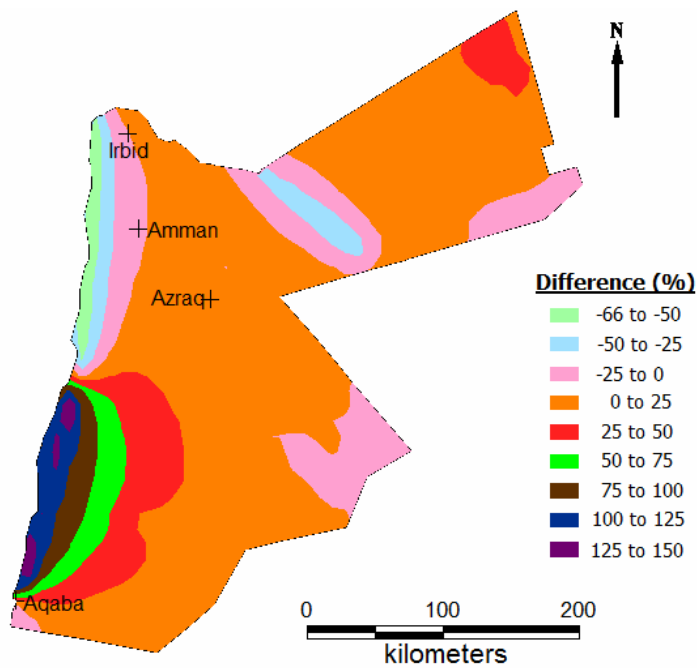


Figure 3.26 Map Showing the Spatial Variation of the Difference between the PGA Values Obtained from Model 4 and Model 3 for a Return Period of 475 Years

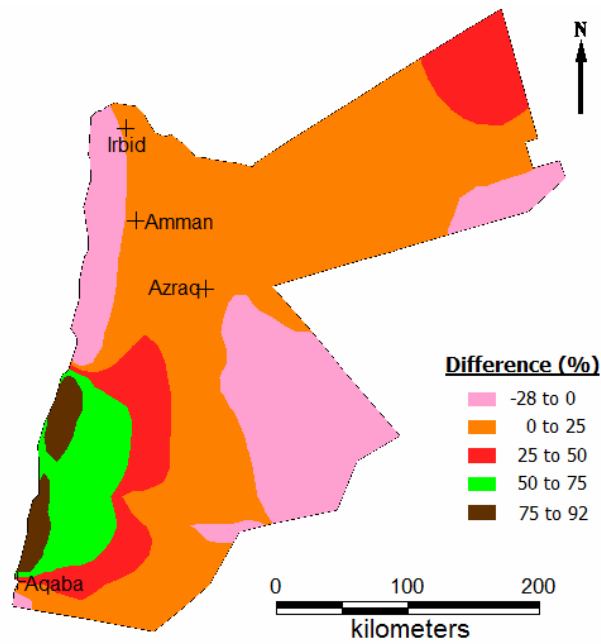


Figure 3.27 Map Showing the Spatial Variation of the Difference between the PGA Values Obtained from Model 4 and Model 3 for a Return Period of 2475 Years

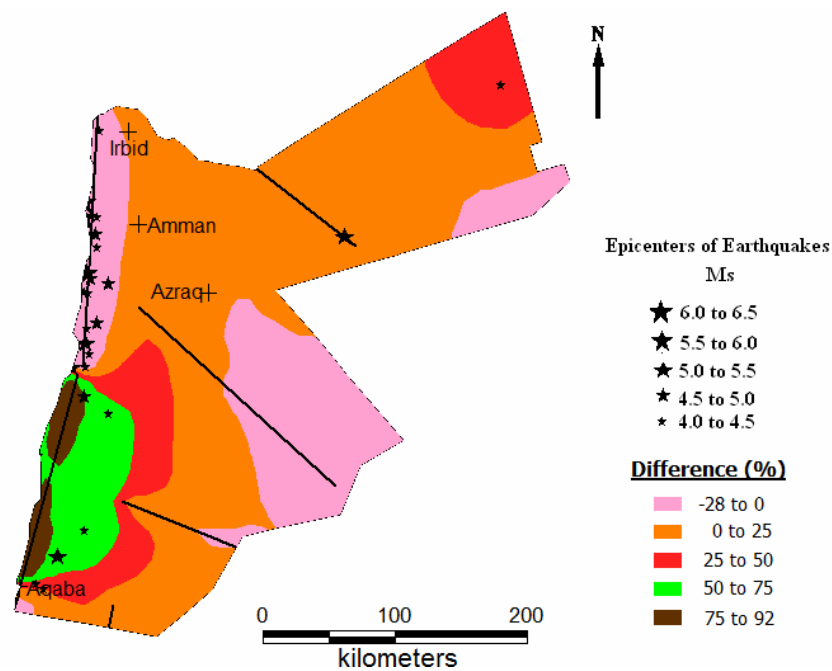


Figure 3.28 Map Showing the Spatial Variation of the Difference between the PGA Values Obtained from Model 4 and Model 3 for a Return Period of 2475 Years and Locations of Line Sources (Black Lines) and Epicenters of Earthquakes Considered in Spatially Smoothed Seismicity Model

Figures 3.20, 3.21 and 3.22 show the spatial variation of the difference in PGA values obtained from Model 2 with respect to Model 1 for return periods of 475 and 2475 years (i.e. $i=1, j=2$ in Eq. (3.10)). It can be observed from these figures that modeling seismic sources as line sources results in an increase in PGA values especially at the regions near to the western boundary of Jordan. The higher increases are concentrated at the regions along and near vicinity of line sources. On the other hand, compared with the line source model, modeling seismic sources having low annual activity rate (i.e. Sirhan, Wadi Karak, SE-Maan and East Gulf of Aqaba Faults) as area sources causes an increase in PGA values at the regions near the boundaries of area sources. Figures 3.23, 3.24 and 3.25 show the spatial variation of the difference in PGA values obtained from Model 3 with respect to Model 2 for return periods of 475 and 2475 years (i.e. $i=2, j=3$ in Eq. (3.10)). It can be seen from these figures that characteristic earthquake model proposed by Youngs and Coppersmith (1985) gives higher PGA values compared to those obtained from the truncated exponential magnitude distribution. In Model 3, characteristic earthquake model is used for seismic sources having maximum magnitude values equal to or greater than 6.5. Accordingly, the increases in PGA values are higher along Dead Sea-Jordan River, Wadi Araba, Gulf of Aqaba and Sirhan Faults. Figures 3.26, 3.27 and 3.28 show the spatial variation of the difference in PGA values obtained from Model 4 with respect to Model 3 for return periods of 475 and 2475 years (i.e. $i=3, j=4$ in Eq. (3.10)). In Model 4, maximum magnitude model is used for the faults with m_1 equal to or greater than 6.5 and their annual activity rates are calculated from their maximum magnitudes, annual slip rates and rupture areas. In addition, the contribution of earthquakes with magnitude between 4.0 and 6.5 to the seismic hazard is computed by applying spatially smoothed seismicity model. Model 4 gives lower PGA values around the Dead Sea Jordan River fault. In Model 4, this fault is assumed to generate only earthquakes with magnitude equal to 7.5. Since the earthquakes with magnitudes between 4.0 and 6.5 are used as background seismic activity, events that have magnitudes between 6.5 and 7.5 and considered in Model 3 for this fault are not included in Model 4. Also, compared to activity rates assigned to characteristic magnitudes (i.e. magnitude range between 7.0 and 7.5)

associated with this fault in Model 3, the rate calculated for its maximum magnitude earthquakes in Model 4 is lower. Similarly, Model 3 gives higher PGA values for a return period of 475 years around the Sirhan faults. Although the activity rates of characteristic events calculated from the characteristic earthquake model of Youngs and Coppersmith (1985) are lumped totally on maximum magnitude earthquakes, this region is far away from the area where the epicenter of earthquakes cluster. On the other hand, the PGA values computed from Model 4 are higher than Model 3 around the Wadi Araba fault. For this fault, the activity rate of maximum magnitude earthquakes is greater than the rate of the characteristic earthquakes (i.e. magnitude range between 6.1 and 6.6) computed according to characteristic earthquake model. The decrease in PGA values at the eastern boundaries of Jordan in Model 4 with respect to Model 3 is attributed to the use of the spatially smoothed seismicity model in Model 4.

3.3.4 “Best Estimate” Seismic Hazard Maps for Jordan

In the previous part, four different seismic hazard maps are obtained for each ground motion parameter, i.e. PGA and SA at 0.2 and 1.0sec, corresponding to each return period or probability of exceedance level. Different assumptions are made in the analyses carried out to derive these maps. The results of these analyses are aggregated through the use of the logic tree formulation as shown in Figure 3.29. This figure shows the assumptions made in modeling of main faults and models used for magnitude distribution as well as the weights assigned to each one of these assumptions. The logic tree terminates with 4 different branches which represent the models, named as Model 1, Model 2, Model 3 and Model 4 which are explained in Section 3.3.2. By multiplying the seismic hazard results computed for each model by the corresponding subjective probability, given in Figure 3.29, and adding these values, a weighted average seismic hazard curve, called as the “best estimate”, is constructed at each grid point. The seismic hazard maps constructed based on the “best estimate” seismic hazard curves are called as the “best estimate” seismic

hazard maps. Figures 3.30 through 3.38 show the “best estimate” seismic hazard maps derived in this study for Jordan.

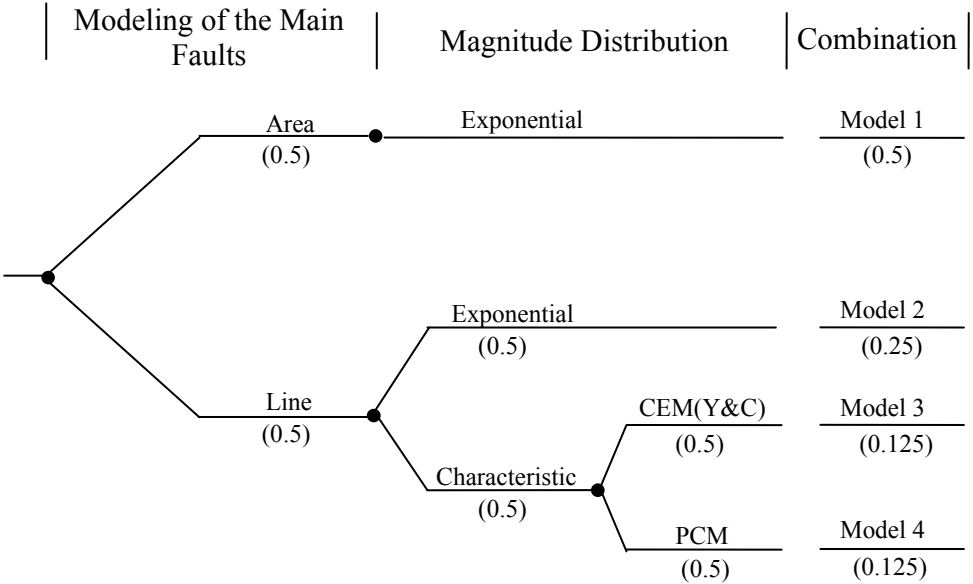


Figure 3.29 Logic Tree Formulation for the Combinations of Different Assumptions (The values given in the parentheses are the subjective probabilities assigned to the corresponding assumptions.)

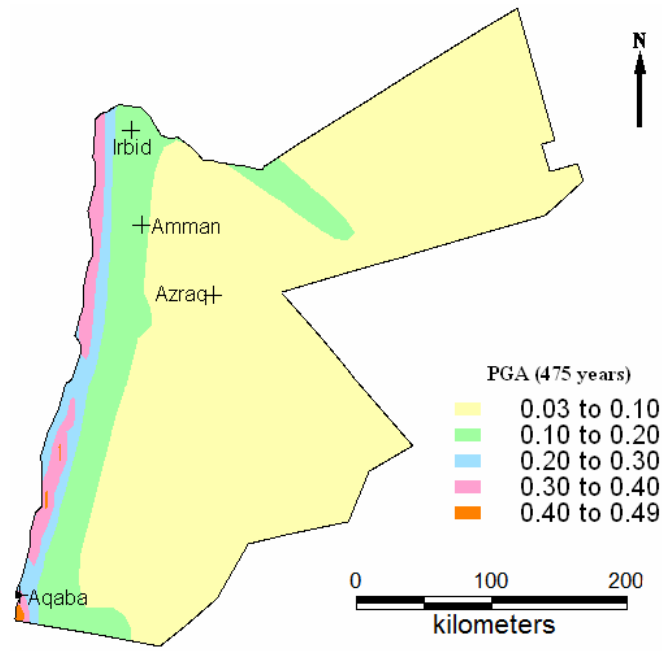


Figure 3.30 Best Estimate Seismic Hazard Map of Jordan for PGA (in g) Corresponding to 10% Probability of Exceedance in 50 Years (475 Years Return Period)

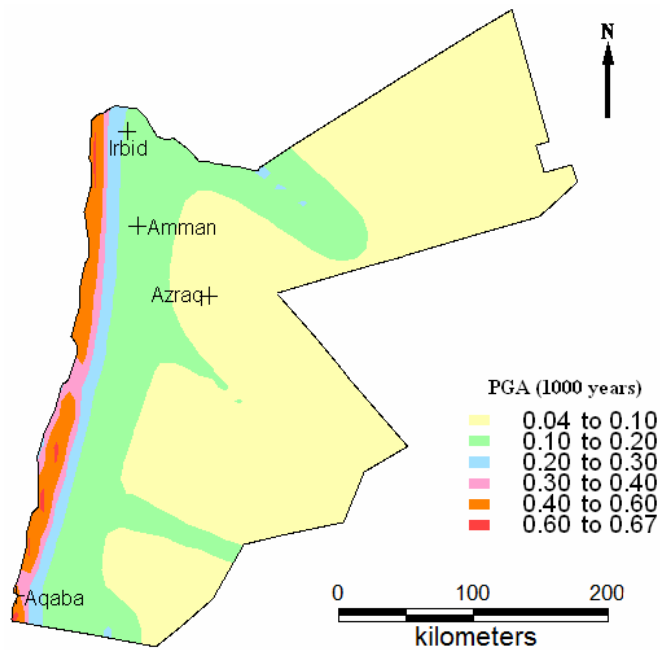


Figure 3.31 Best Estimate Seismic Hazard Map of Jordan for PGA (in g) Corresponding to 5% Probability of Exceedance in 50 Years (1000 Years Return Period)

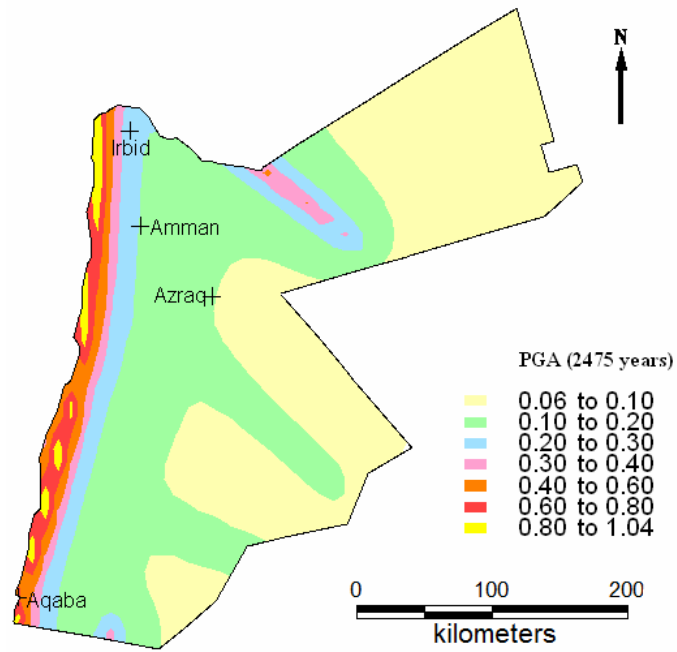


Figure 3.32 Best Estimate Seismic Hazard Map of Jordan for PGA (in g) Corresponding to 2% Probability of Exceedance in 50 Years (2475 Years Return Period)

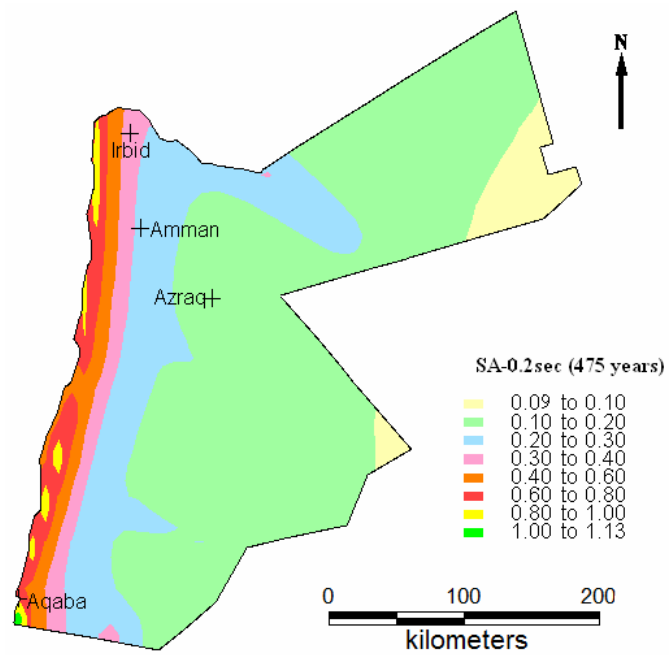


Figure 3.33 Best Estimate Seismic Hazard Map of Jordan for SA at 0.2 sec (in g) Corresponding to 10% Probability of Exceedance in 50 Years (475 Years Return Period)

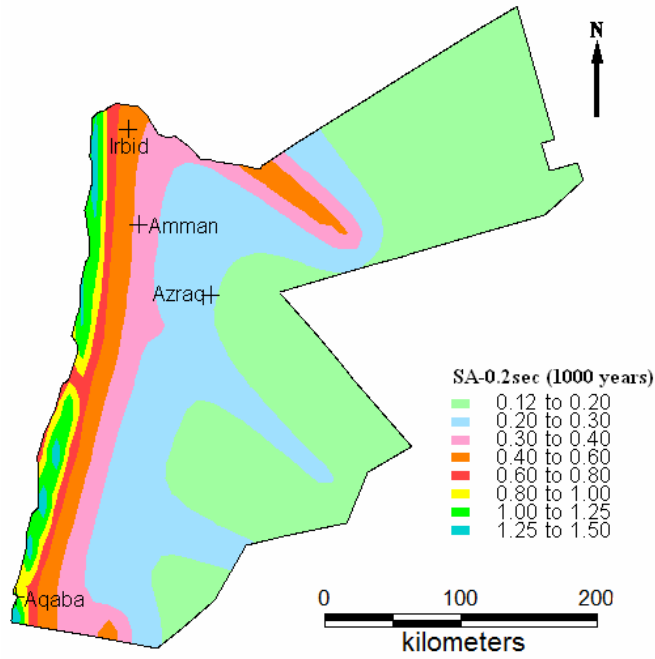


Figure 3.34 Best Estimate Seismic Hazard Map of Jordan for SA at 0.2 sec (in g) Corresponding to 5% Probability of Exceedance in 50 Years (1000 Years Return Period)

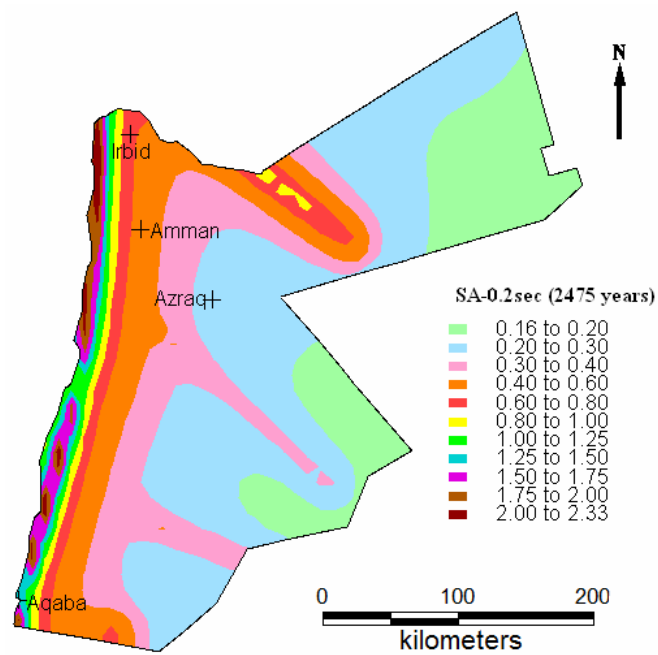


Figure 3.35 Best Estimate Seismic Hazard Map of Jordan for SA at 0.2 sec (in g) Corresponding to 2% Probability of Exceedance in 50 Years (2475 Years Return Period)

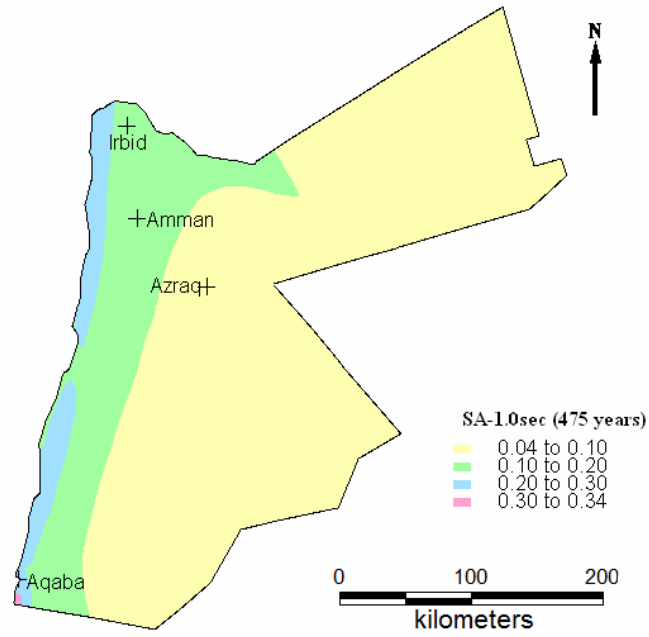


Figure 3.36 Best Estimate Seismic Hazard Map of Jordan for SA at 1.0 sec (in g) Corresponding to 10% Probability of Exceedance in 50 Years (475 Years Return Period)

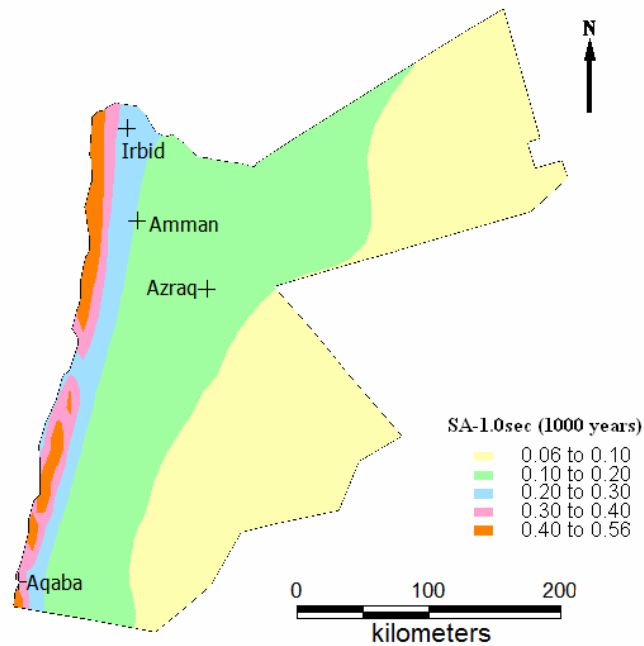


Figure 3.37 Best Estimate Seismic Hazard Map of Jordan for SA at 1.0 sec (in g) Corresponding to 5% Probability of Exceedance in 50 Years (1000 Years Return Period)

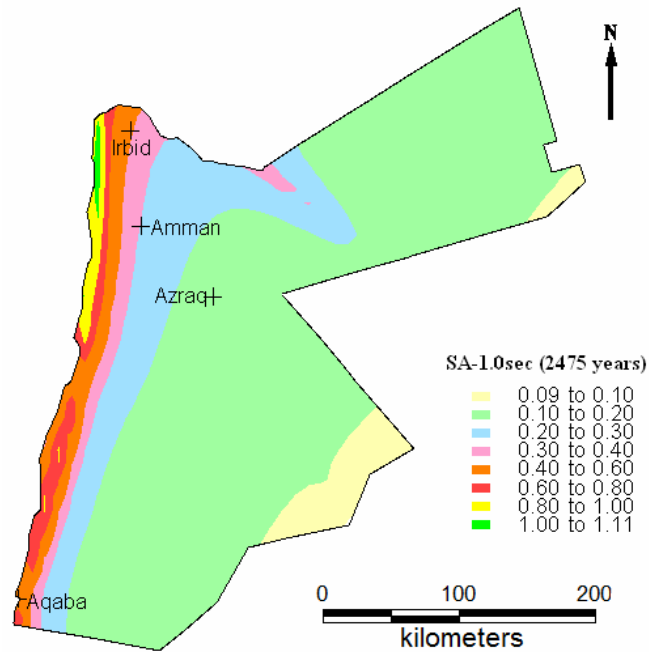


Figure 3.38 Best Estimate Seismic Hazard Map of Jordan for SA at 1.0 sec (in g) Corresponding to 2% Probability of Exceedance in 50 Years (2475 Years Return Period)

It can be observed from Figures 3.30 through 3.38 that high PGA and SA values concentrate at the west boundary of Jordan where the faults that form main Dead Sea Transform System are situated in this region. In order to visualize this, the faults located in Jordan are placed on the best estimate seismic hazard map for SA at 0.2 sec for a return period of 2475 years and it is shown in Figure 3.39. If such high values resulting from extreme closeness (less than 10 km) to the faults are excluded, maximum PGA values for Jordan are about 0.3g, 0.4g and 0.5g for return periods of 475, 1000 and 2475 years, respectively. If high values for SA are excluded in the same way, the maximum SA values at 0.2 sec are 0.8g, 1.0g, 1.4g and those at 1.0 sec are 0.3g, 0.4g and 0.7g for return periods of 475, 1000 and 2475 years, respectively.

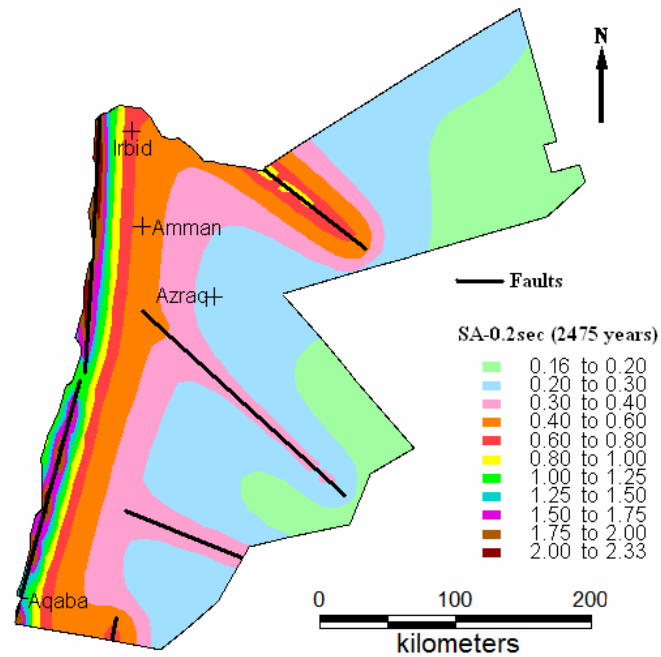


Figure 3.39 Best Estimate Seismic Hazard Map of Jordan for SA at 0.2sec (in g) Corresponding to 2% Probability of Exceedance in 50 Years (2475 Years Return Period) and Locations of Faults

Comparing the best estimate seismic hazard maps constructed in this study with the corresponding maps derived by Jiménez (2004), it is observed that higher values are obtained in this study. Jiménez (2004) applied area source modeling and exponential magnitude distribution. Therefore, this difference is due to the consideration of faults as line sources and the implementation of the characteristic earthquake and maximum magnitude models in this study.

Yüçemen (1992) derived a hazard map displaying the “Bayesian” estimate of seismic hazard for PGA corresponding to 475 years return period and Al-Tarazi and Sandvol (2007) obtained a seismic hazard map in terms of PGA with 10% probability of exceedance in 50 years. These maps are given with the map constructed in this study in Figure 3.40.

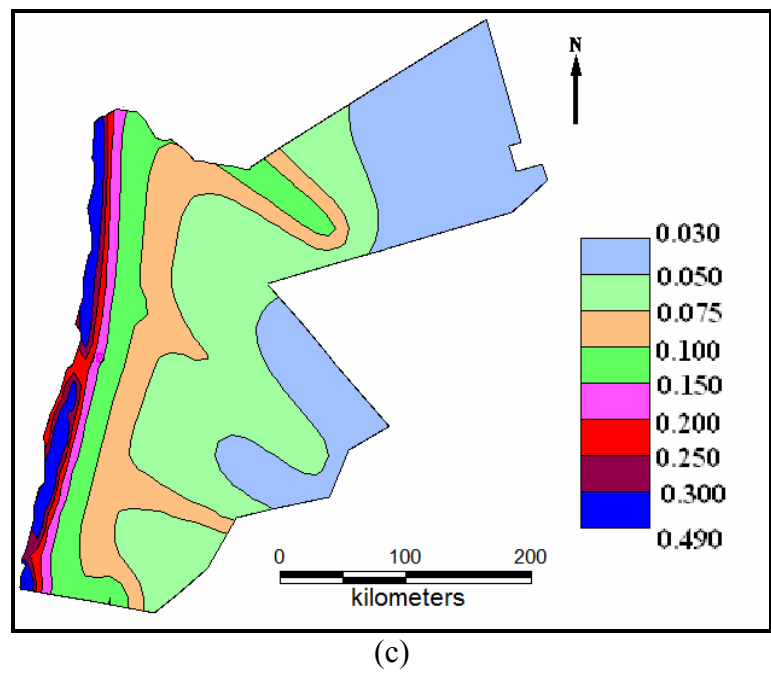
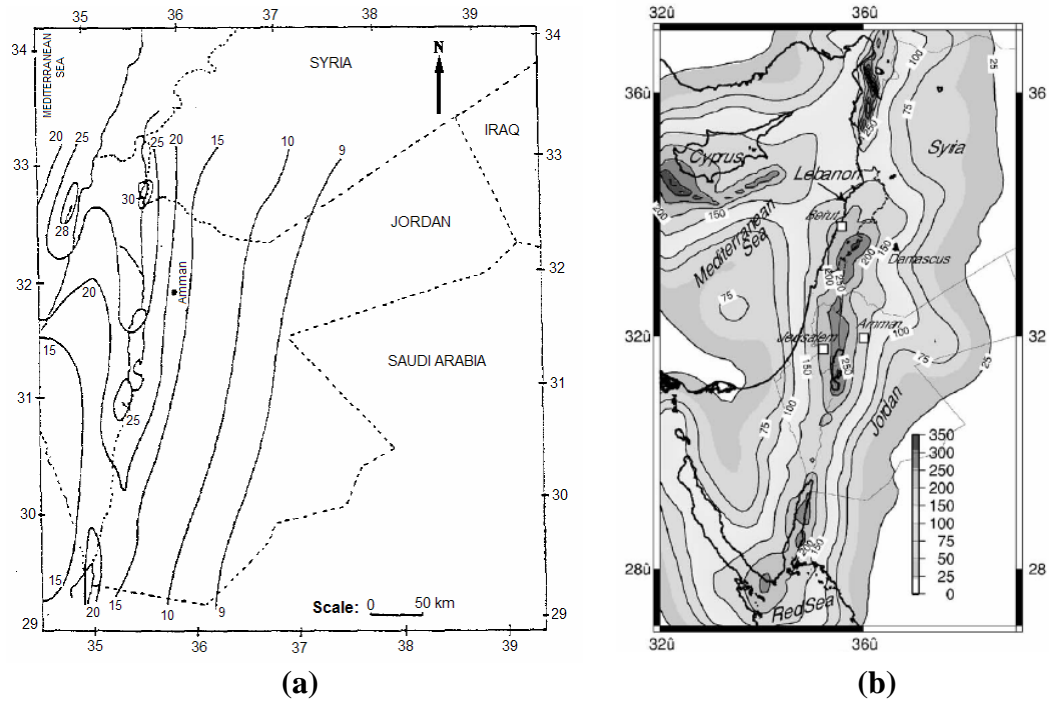


Figure 3.40 Seismic Hazard Maps Derived for PGA with 10% Probability of Exceedance in 50 Years by (a) Yüçemen (1992) (Values are given in terms of %g) (b) Al-Tarazi and Sandvol (2007) (Values are given in terms of cm/sec²) (c) This study (Values are given in terms of g)

Compared with the studies carried out by Yüçemen (1992) and Al-Tarazi and Sandvol (2007), the PGA values given in this most recent study are slightly higher. This difference can be attributed to the differences in seismic source modeling, seismicity parameters assigned to them and attenuation relationships used in computations as well as the use of more conservative models. It should be noted that Yüçemen (1992) used the attenuation equation proposed by Esteva and Villaverde (1973) for peak ground acceleration whereas Al-Tarazi and Sandvol (2007) used attenuation equations proposed by Boore et al. (1997), Sadigh et al. (1997) and Campbell (1997) for peak ground acceleration at firm rock sites.

CHAPTER 4

CASE STUDY FOR A REGION: SEISMIC HAZARD MAPPING FOR THE BURSA PROVINCE

4.1 INTRODUCTION

In the previous chapter, seismic hazard analysis is carried out for a large region where a country, namely Jordan, is taken into consideration. Since the main parameters of the faults were missing it was not possible to utilize the appropriate models to assess the seismic hazard associated with faults. In this chapter, seismic hazard analyses performed for a smaller region for which it was possible to collect more detailed tectonic data. It is to be noted that the area of Bursa province (about 11000 km²) is almost nine times smaller than the area of Jordan (about 90000 km²). The availability of the more detailed information on faults and fault segments enables the implementation of more complex physical and stochastic models, such as, segmentation and renewal in addition to the models applied in Chapter 3. This is actually the most up-to-date trend in the development of new generation of seismic hazard maps.

The Bursa province is selected as an example in order to illustrate the methodology to be followed for this type of problems. Bursa is one of the most populated cities in Turkey. Additionally, it is an important city for the industry in Turkey. Bursa is located within a transitional zone of the extensional and contractional active tectonic regimes (Yüçemen et al., 2006). Therefore, it is seismically a very active region. According to the current earthquake zoning map of Turkey, the portions of this city are located in 1st and 2nd degree earthquake zones. Recent investigations on the tectonics of the region and its near vicinity have resulted in better understanding of active faults and estimation of their parameters. In view of this recent

information, seismic hazard for the Bursa province will be examined by applying comprehensive source and earthquake occurrence models.

4.2 PREVIOUS PROBABILISTIC SEISMIC HAZARD ASSESSMENT STUDIES FOR BURSA

In literature, the studies focusing on the probabilistic estimation of seismic hazard for the city of Bursa are quite limited in number. Accordingly, the seismic hazard for this city is generally quantified based on current regulatory earthquake zoning map of Turkey. This map was prepared by using the peak ground acceleration (PGA) contour map that was constructed in the study of Gülkan et al. (1993) by using probabilistic seismic hazard analyses methodology for a return period of 475 years. The earthquake zones in this map were determined based on the estimated PGA values. The regions where PGA values are between 0.3g and 0.4g are classified as the 2nd degree earthquake zone and those where PGA values are greater than 0.4g are classified as the 1st degree earthquake zone.

Recently, Yüçemen et al. (2006) carried out a probabilistic case study for the assessment of seismic hazard of Bursa city center and its near vicinity. In this study, 41 fault segments were identified in the rectangular area bounded by 28°- 30° E longitudes and 39.75°- 40.75°N latitudes. Besides, five additional fault segments were also considered in the North Marmara Fault zone. All of these faults were modeled as line sources and they are assumed to produce only maximum magnitude, characteristic earthquakes according to either Poisson or renewal models. Therefore, maximum magnitude model was assumed as the magnitude distribution in the study. They used a background area source with a truncated exponential distribution in order to reflect the effects of earthquakes in the magnitude range of 4.5-6.0 and assumed to be not related with any of the faults identified. The seismicity parameters (i.e. ν and β) of the background area source are estimated based on the earthquake catalog provided by the Earthquake Research Department, General Directorate of Disaster Affairs. The epicentral distribution of earthquakes in this catalog lies between 27.8°- 30.2° E longitudes and 39°- 41° N

latitudes. An alternative catalog was prepared by removing the secondary events (i.e. fore- and after shocks) from this catalog. Also, incompleteness of these two catalogs for small magnitude earthquakes was examined. Different seismicity parameters were predicted from the combination of assumptions with respect to incompleteness and dependence of secondary events. The PGA and spectral accelerations (SA) at 0.2 sec and 1.0 sec were selected as ground motion parameters. The empirical ground motion prediction equations given by Boore et al. (1997) and Kalkan and Gülkan (2004) were used in their analyses. They performed probabilistic seismic hazard analyses for each one of the combination of assumptions and combined the results by the logic tree methodology. The results were presented in the form of seismic hazard maps which show the distribution of predicted PGA and SA values (T=0.2 sec and 1.0 sec) for return periods of 475 and 2475 years.

4.3 ASSESSMENT OF SEISMIC HAZARD FOR BURSA

4.3.1 Seismic Database and Seismic Sources

4.3.1.1 Seismic Database

Earthquake catalogs are the most important sources of information used in seismic hazard analysis since they describe the spatial and temporal distribution of past earthquakes in the interested region. In order to assess seismic hazard for Bursa, two seismic databases, namely ERD (Earthquake Research Department) and ISC (International Seismological Centre), provided in the website of the Earthquake Research Department in General Directorate of Disaster Affairs (ERD-GDDA, 2007) for the rectangular region between 26.0° - 31.8° E longitudes and 38.8° - 42.0° N latitudes are used. The ISC catalog contains the earthquakes that occurred between years 1900 and 2002 while ERD catalog includes events occurred after 1991. In this study, the information given in ISC catalog is used for events occurred until the end of year 2001 and since then the information given in ERD catalog is taken into consideration. The earthquake catalog prepared in this way contains the

earthquakes that occurred in the region considered between 1901 and 2006. The magnitudes of earthquakes in this catalog are given in different scales. They should be converted to a common scale. In this study, moment magnitude scale, M_w , is selected as the common magnitude scale.

Deniz (2006) developed the following conversion equations based on earthquakes recorded in Turkey by using orthogonal regression:

$$M_w = 2.25 \times M_b - 6.14 \quad (4.1)$$

$$M_w = 1.27 \times M_d - 1.12 \quad (4.2)$$

$$M_w = 1.57 \times M_L - 2.66 \quad (4.3)$$

$$M_w = 0.54 \times M_S + 2.81 \quad (4.4)$$

where, M_b : body wave magnitude, M_d : duration magnitude, M_L : local magnitude and M_S : surface wave magnitude scales.

Ulusay et al. (2004), on the other hand, proposed the following conversion equations derived by performing a simple linear regression analysis on the earthquakes recorded in Turkey;

$$M_w = 1.2413 \times M_b - 0.8994 \quad (4.5)$$

$$M_w = 0.9495 \times M_d + 0.4181 \quad (4.6)$$

$$M_w = 0.7768 \times M_L + 1.5921 \quad (4.7)$$

$$M_w = 0.6798 \times M_S + 2.0402 \quad (4.8)$$

The slope of the conversion equation estimated based on orthogonal regression is greater than that obtained from the standard least squares regression. Accordingly, moment magnitude values obtained from the conversion equations based on the orthogonal regression will be larger compared to those based on the standard least squares regression for large magnitude values. The opposite trend is valid for the

small magnitudes. Since the contribution of small magnitude earthquakes to seismic hazard is considerably less than that of the large magnitude earthquakes, the use of orthogonal regression based conversion equations will yield conservative seismic hazard values. Except for M_s scale, compared with the conversion equations developed by Ulusay et al. (2004), those proposed by Deniz (2006) underestimate small magnitude earthquakes and overestimate large magnitude earthquakes.

In this study, the conversion equations developed by Deniz (2006) are applied to achieve transformation of different magnitude scales to the M_w scale. In the catalog, there are some earthquakes with magnitude values given in more than one magnitude scale. For these earthquakes, the given magnitudes in different scales are converted to the M_w magnitude scale and their average value, $M_{w-(ave)}$, is taken as the “best estimate” M_w value. The earthquakes with magnitudes, M_w , less than 4.5 are eliminated from the catalog. The resulting earthquake catalog includes 343 events and is given in Appendix D.

Secondary events should be removed from the earthquake catalog in order to fulfill the underlying independence assumption of the Poisson distribution. This is achieved by the method described in the previous chapter (see Section 3.3.1.1). It should be noted that the earthquakes with magnitude equal to or greater than 6.0 are assumed to be main shocks although they may be aftershock or foreshock of other events. The resulting earthquake catalog includes 178 main shocks as given in Appendix E.

Both earthquake catalogs are assumed to be complete for earthquakes with magnitude greater than 5.0. However, the completeness is assumed to be valid since 1966 and 1967 for earthquakes with magnitudes between 4.5 and 5.0 in the catalogs that include whole earthquakes and only main shocks, respectively.

Peak ground acceleration (PGA) and spectral accelerations (SA) at 0.2sec and 1.0 sec periods are selected as the basic parameters for the seismic hazard evaluation. Taking into consideration the study conducted by Yüçemen et al. (2006), the

attenuation relationships proposed by Boore et al. (1997) and Kalkan and Gülkan (2004) are used to estimate seismic hazard in terms of this parameters. Since no information is available about the site conditions all over Bursa, all seismic hazard computations are carried out assuming for rock site condition.

4.3.1.2 Seismic Sources

Bursa is under the seismic threat caused by several normal and strike-slip faults and fault segments located in and near vicinity of Bursa. In the past, very destructive historical earthquakes occurred in Bursa. These are: 28th February 1855 and 11th April 1855 earthquakes with intensities of IX and X, respectively (Coburn and Kuran, 1985; Ambraseys and Jackson, 2000) and 6th October 1964 Manyas earthquake with Ms 7.0 (Erentöz and Kurtman, 1964) which caused the collapse or heavy damage of buildings and many deaths.

In addition to the faults in Bursa, this city can be affected by the seismic activity occurring in its vicinity. The North Anatolian Fault System (NAFS) is passing though north of the city. Based on the renewal model, the probability of occurrence of earthquakes with magnitude equal to or greater than 7.0 in the part of the NAFS cutting across the floor of Marmara Sea was computed as 44±18 percent in the next 30 years (Parsons, 2004). Considering the fact that the 1970 Gediz earthquake with magnitude 7.0 occurred at 250 km away from the Bursa caused heavy damage to factories in the city (Yüccemen et al., 2006), it is expected that an earthquake in the Marmara Sea will also result in major damages to the structures located in Bursa. Therefore, in addition to faults in and near vicinity of Bursa, main fault zones where any seismic activity may affect the city are taken into consideration.

In this study, the faults within 26.0° - 31.8° E longitudes and 38.8° - 42.0° N and their seismicity parameters are gathered from different sources available in the literature. For the fault segments located between 28° - 30° E longitudes and 39.75° - 40.75° N latitudes, a comprehensive field investigation was carried out by Prof. Koçyiğit

(Yüçemen et al., 2006). He identified forty one active fault segments in this region and provided the information on type, average strike, average dip amount, length, vertical and horizontal displacements, degree of activity, return period and the maximum magnitude values, m_1 (in M_w), for them. In addition, same type of information for the fault segments of the two fault zones located outside of this region; namely, Northern Marmara Fault Zone which is a part of the NAFS in the Marmara Sea and Simav Fault Zone, was also presented. For the fault segments in the 30° - 31° longitudes and 39.68° - 39.92° latitudes, the study carried out by Koçyiğit (2005) for the delineation of active faults and assessment of the relevant parameters of Eskişehir area is used. These segments are modeled based on the recommendations of Koçyiğit (2006). The locations of fault segments in the part of NAFS located east of İzmit Gulf are determined from Emre and Awata (2003), Awata et al. (2003) and Şaroğlu et al. (1992) and Koçyiğit (2007). The remaining main fault zones presented in Şaroğlu et al. (1992) are modeled as line sources. While modeling these faults, Koçyiğit (2007) was consulted. In this study, all of these faults and fault segments are examined in terms of the 91 segments as shown in Figure 4.1. The distributions of earthquakes in the catalogs including all earthquakes and only main shocks as well as the fault segments are shown in Figures 4.2 and 4.3, respectively.

4.3.2 Methodology

The seismic hazard in the region is assessed by combining the contributions of: (i) earthquakes with magnitudes, M , between 4.5 and 6.0 that are not assigned to any fault or fault segment and termed as “background seismic activity”, (ii) earthquakes with magnitudes equal to or greater than 6.0 that may emanate from faults or fault segments by rupturing the whole or a large portion of their lengths and release the energy accumulated on them. The computation of seismic hazard due to these two components will be explained in the following sections.

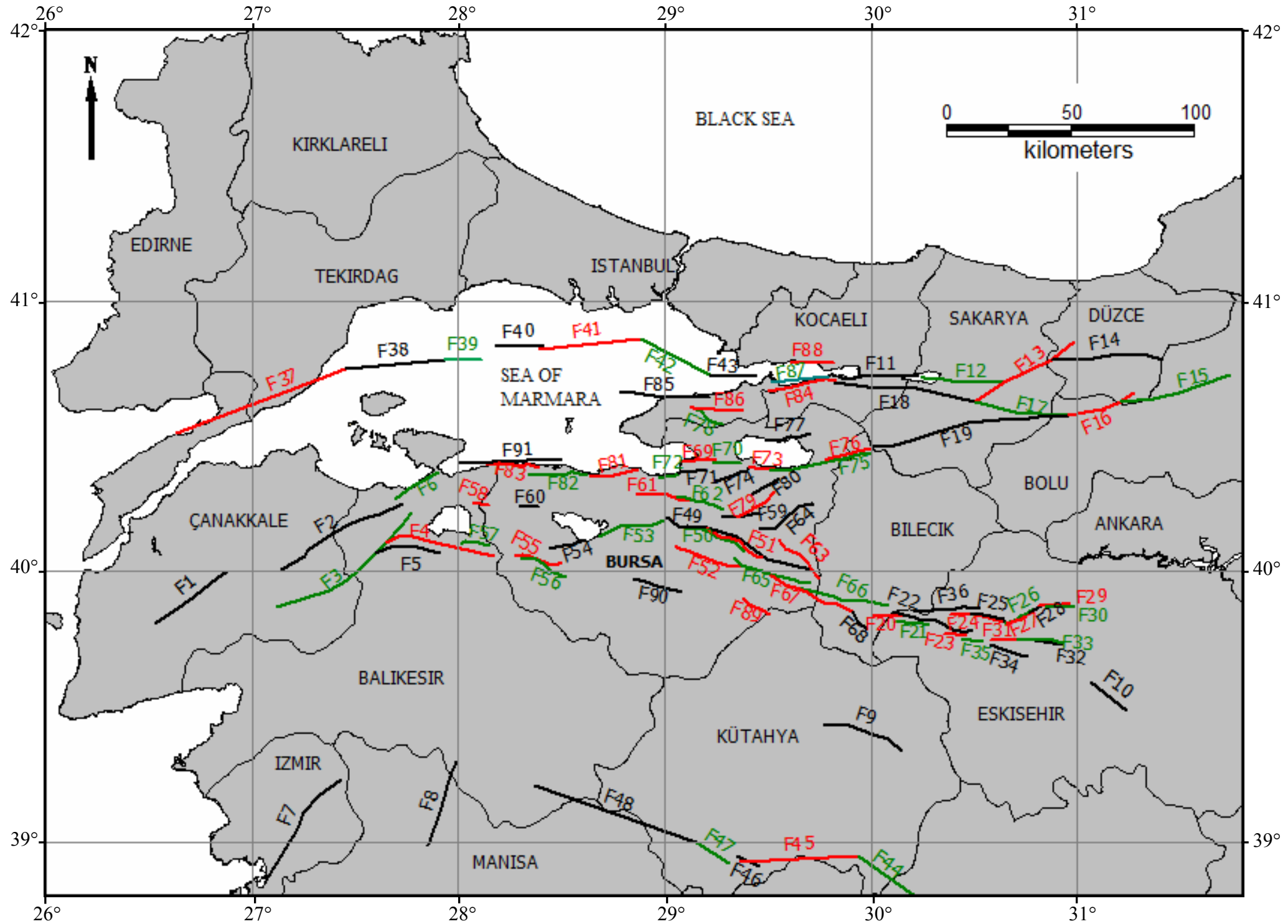


Figure 4.1 Map Showing the Locations of Faults (Thick Lines in Various Colors) Considered in This Study (Yüçemen et al., 2006; Koçyiğit, 2005; Koçyiğit, 2006; Emre and Awata (2003), Awata et al., 2003; Şaroğlu et al., 1992; Koçyiğit, 2007)

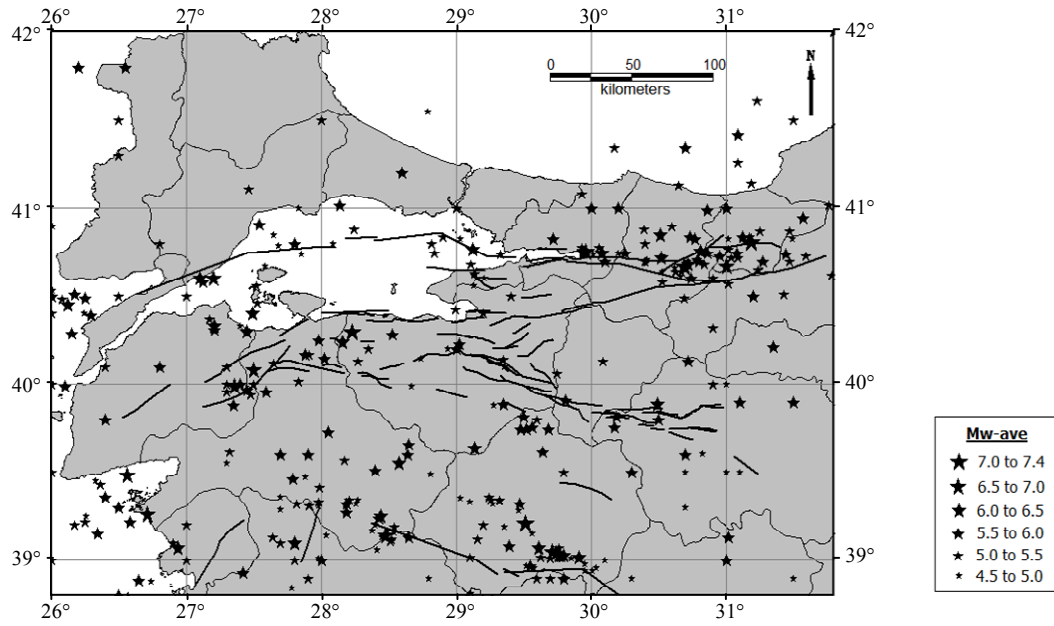


Figure 4.2 Map Showing the Faults (Thick Black Lines) and the Spatial Distribution of All Earthquakes

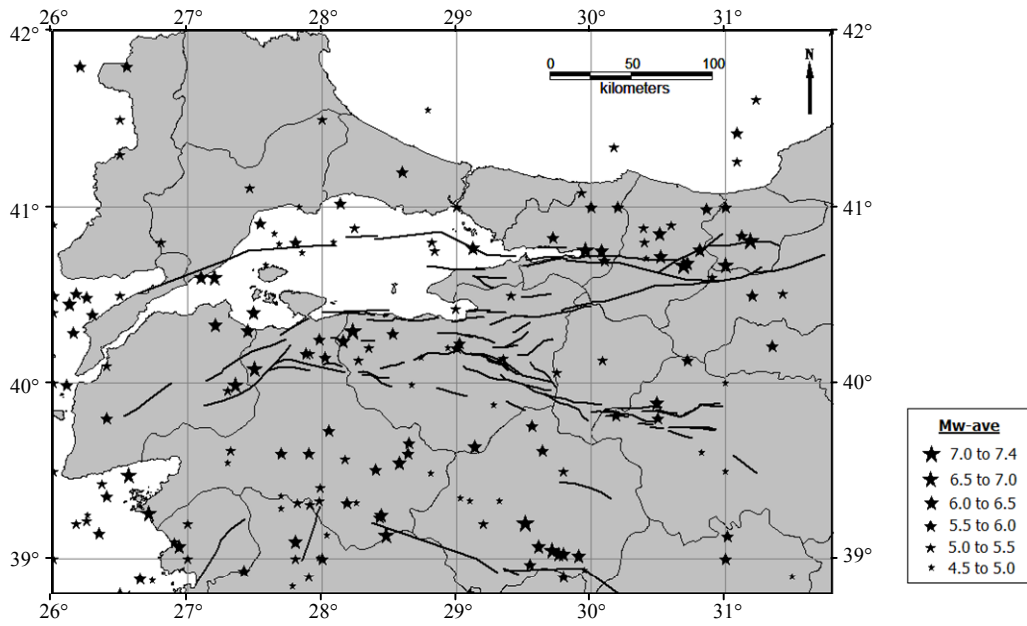


Figure 4.3 Map Showing the Faults (Thick Black Lines) and the Spatial Distribution of Main Shocks

4.3.2.1 Seismic Hazard Resulting From Background Seismic Activity

In order to quantify the seismic hazard due to background seismic activity, the information given for earthquakes within the range of $4.5 \leq M \leq 6.0$ in the two earthquake catalogs that include whole events and only main shocks are used. As explained in Section 4.3.1.1, the catalogs including the whole earthquakes and only the main shocks are assumed to be complete for events with $M \geq 5.0$ and for those with $4.5 \leq M < 5.0$ since 1966 and 1967, respectively. For background seismic activity, four different values are computed for the slope of Gutenberg Richter magnitude recurrence relationships, $|b|$, $\beta = b \times \ln 10$ and for the annual activity rate, v , by considering the alternative assumptions on completeness and elimination of secondary events as outlined in Table 4.1. In the cases where the catalog data are corrected for completeness, the range of magnitudes between 4.5 and 6.0 are divided into bins. Then, the number of earthquakes having magnitude between the bounds of each magnitude bin are counted and divided by the period where the data is complete to calculate the corresponding artificially completed annual activity rates, v_i . Afterwards, the v and $|b|$ values are calculated based on the v_i values.

Table 4.1 b , β and v Values Computed According to Alternative Assumptions for the Background Seismic Activity

Catalog Type	Correction for Incompleteness	$ b $	β	v
All Earthquakes	No	0.99	2.285	2.972
	Yes	1.08	2.491	4.213
Only Main Shocks	No	0.81	1.869	1.415
	Yes	0.88	2.037	1.944

Contribution of background events to seismic hazard is calculated by using two different models; spatially smoothed seismicity model of Frankel (1995) and background area source with uniform seismicity. Seismic hazard computations for background area source with uniform seismicity are carried out by using EZ-FRISK

(Risk Engineering, 2005). On the other hand, in the calculation of the contribution of background seismic activity based on the spatially smoothed seismicity model of Frankel (1995), the computer programs developed at USGS (Frankel et al., 1996) and later modified by Kalkan (2007) in order to include additional attenuation relationships are utilized. Analyses are carried out by using combinations of different assumptions with respect to incompleteness of earthquake catalogs and dependence of events in them (i.e., inclusion of secondary events or not). In the analyses carried out by using background source, an area source bounded by 26.0°-31.8° E longitudes and 38.8°-42.0° N latitudes is defined. For this source, truncated exponential magnitude distribution with different β and ν values presented in Table 4.1 is used in the analyses. The lower and upper bounds of this distribution are assigned as 4.5 and 6.0, respectively. Six different seismic hazard analyses are carried out by using spatially smoothed seismicity model of Frankel (1995) based on the same combinations of assumptions. The correlation distance for smoothing is assumed to be 50 km in all cases. In the analyses in which the completeness in the catalogs are not taken into consideration, the earthquakes with $4.5 \leq M \leq 6.0$ in the two earthquake catalogs that includes whole events and only main shocks are used. In order to adjust for incompleteness, seismic hazard analyses are carried out by using earthquakes with $5.0 \leq M \leq 6.0$ occurred since 1901; and those with $4.5 \leq M \leq 6.0$ since 1966 and 1967 in the catalogs including all events and only main shocks, respectively. Then, the results of analyses based on the same catalog are combined by giving equal weights to each one of the assumptions. Figure 4.4 describes schematically the different combinations considered and the methodology followed in these analyses.

First, seismic hazard analyses are performed to obtain the hazard curves for a selected site (40.24° N, 29.08° E) which approximately corresponds to the city center of Bursa. Figure 4.5 shows the seismic hazard curves obtained by using attenuation relationships proposed by Kalkan and Gülkan (2004) and Boore et al. (1997) for peak ground acceleration (PGA) at rock sites (shear wave velocity, V_s , is assumed to be equal to 700 m/s). From the comparison of seismic hazard curves

given in Figure 4.5 (i) with those in Figure 4.5 (ii), it can be observed that the influence of utilizing the attenuation models proposed by Kalkan and Gülkan (2004) and Boore et al. (1997) is insignificant at small PGA values but it becomes apparent at larger PGA values.

In order to illustrate the spatial sensitivity of seismic hazard results to the seismicity models and different assumptions, seismic hazard analyses are carried out at all grid points with a spacing of $0.02^\circ \times 0.02^\circ$ in latitude and longitude in the region bounded by 26.0° - 31.8° E longitudes and 38.8° - 42.0° N latitudes and seismic hazard maps for PGA corresponding to return periods of 475, 1000 and 2475 years are constructed. In the analyses, equal weights are given to both attenuation relationships. Figure 4.6 through Figure 4.11 show seismic hazard maps obtained by using spatially smoothed seismicity model.

As explained in Chapter 3, almost a uniform seismic hazard distribution is obtained for the selected ground motion parameter from the seismic hazard analyses carried out by using a background area source with uniform seismicity. The maximum PGA values obtained from the analyses carried out by using the background area source with uniform seismicity are presented in Table 4.2 for return periods of 475, 1000, and 2475 years.

Table 4.2 Maximum PGA Values (in g) Obtained from Background Area Source with Uniform Seismicity

Catalog Type	Correction for Incompleteness	Return Period (Year)		
		475	1000	2475
All Earthquakes	No	0.18	0.22	0.29
	Yes	0.19	0.24	0.31
Only Main Shocks	No	0.14	0.19	0.24
	Yes	0.16	0.20	0.26

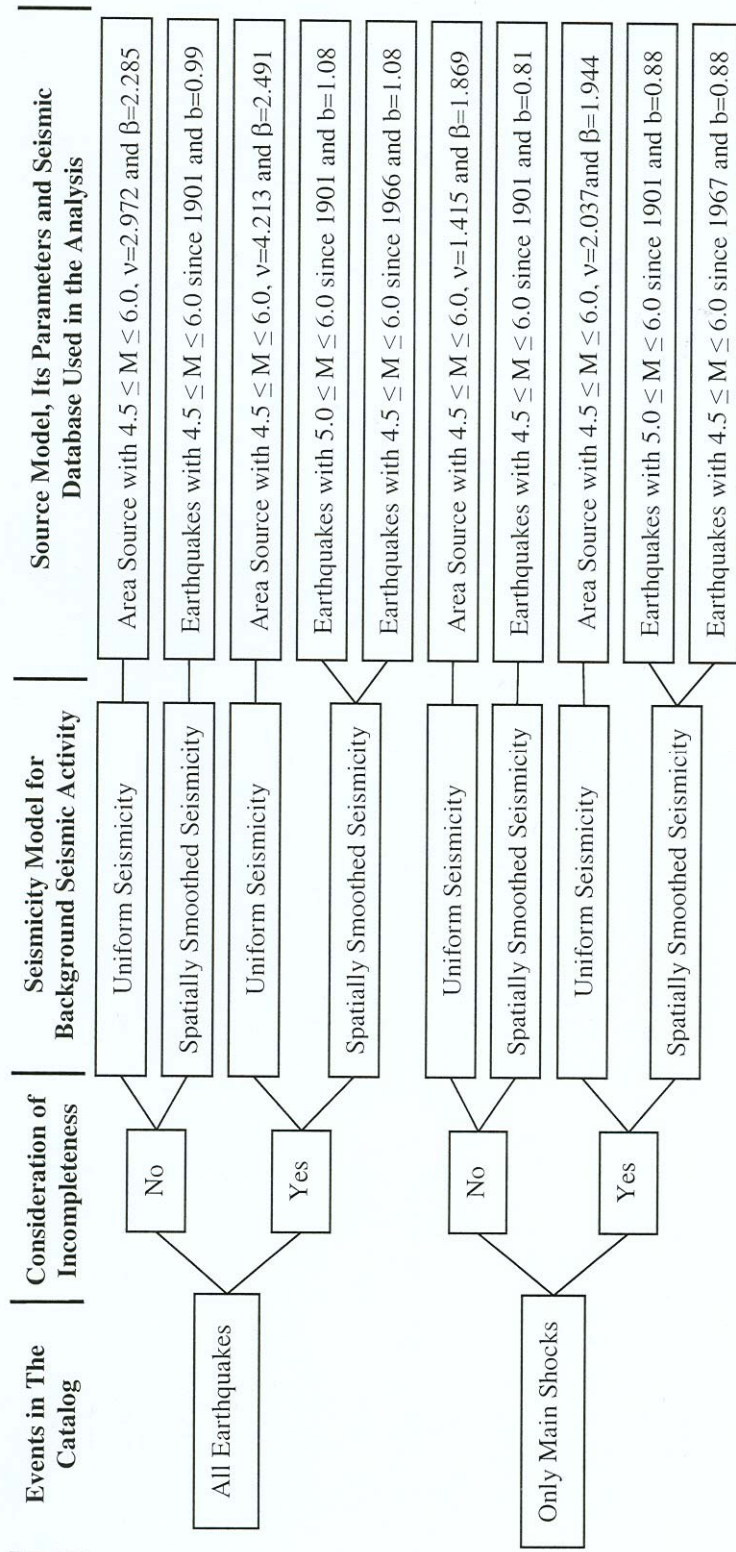
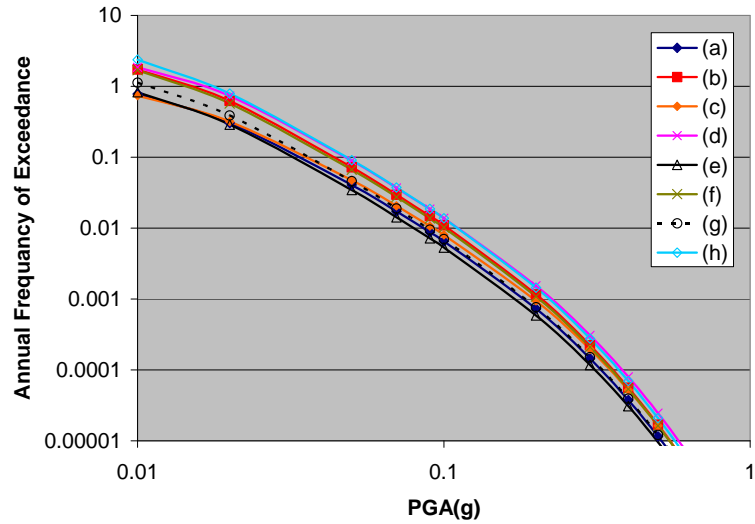
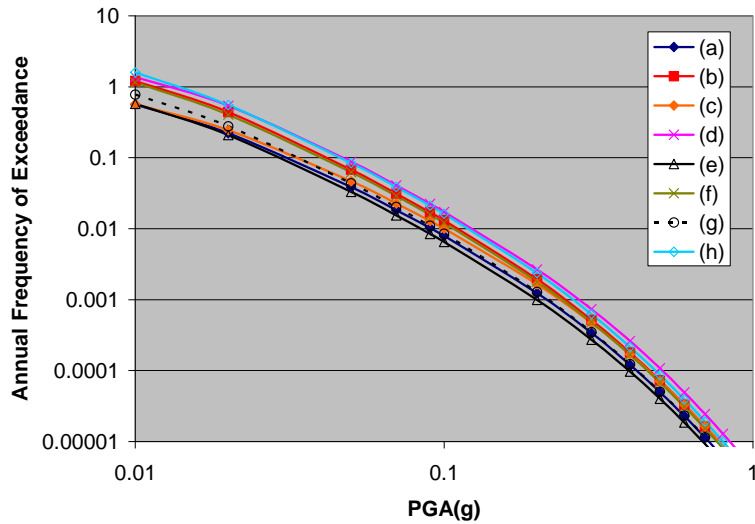


Figure 4.4 Schematic Description of the Procedure Utilized in the Assessment of Background Seismic Activity

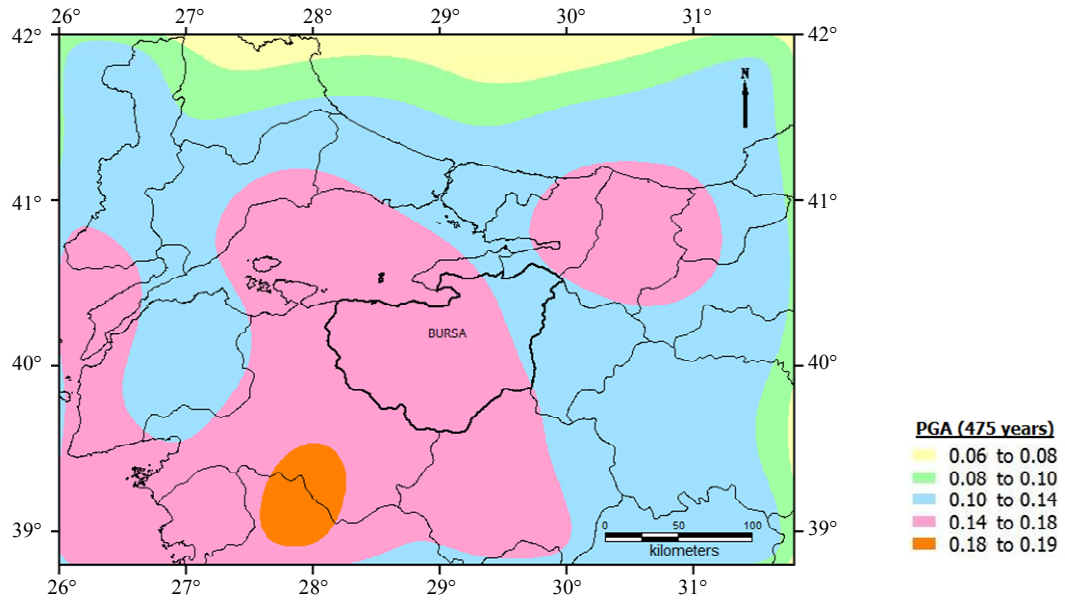


(i) Boore et al. (1997)

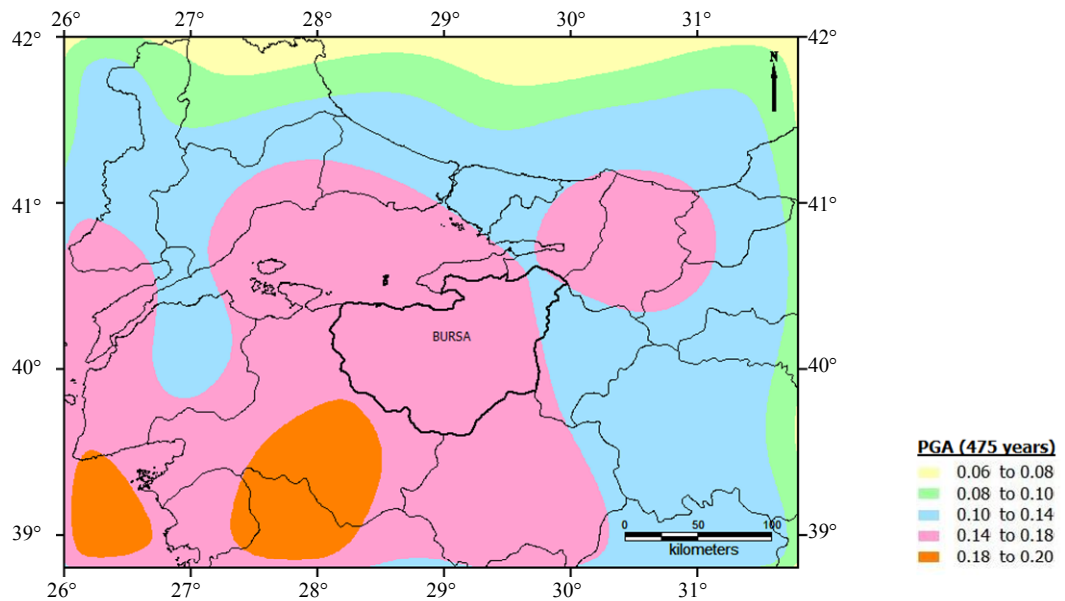


(ii) Kalkan and Gülkan (2004)

Figure 4.5 Seismic Hazard Curves Obtained by Using Spatially Smoothed Seismicity Model with; (a) Main Shocks in the Incomplete Database, (b) All Earthquakes in the Incomplete Database (c) Main Shocks and Adjusting for Incompleteness, (d) All Earthquakes and Adjusting for Incompleteness and by Using Uniform Seismicity with; (e) Main Shocks in the Incomplete Database, (f) All Earthquakes in the Incomplete Database, (g) Main Shocks and Adjusting for Incompleteness, (h) All Earthquakes and Adjusting for Incompleteness

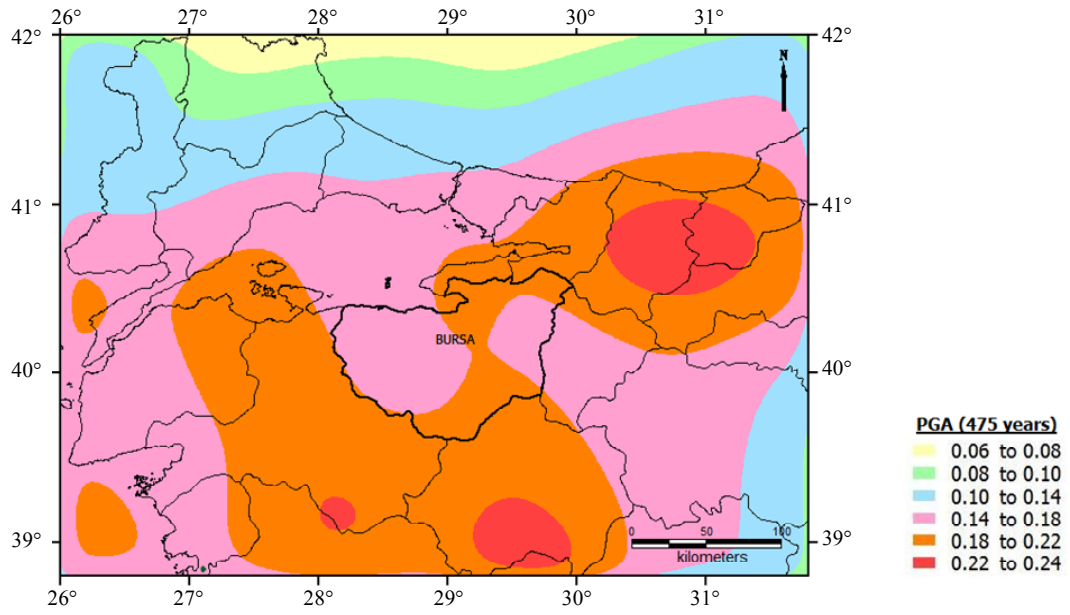


(a)

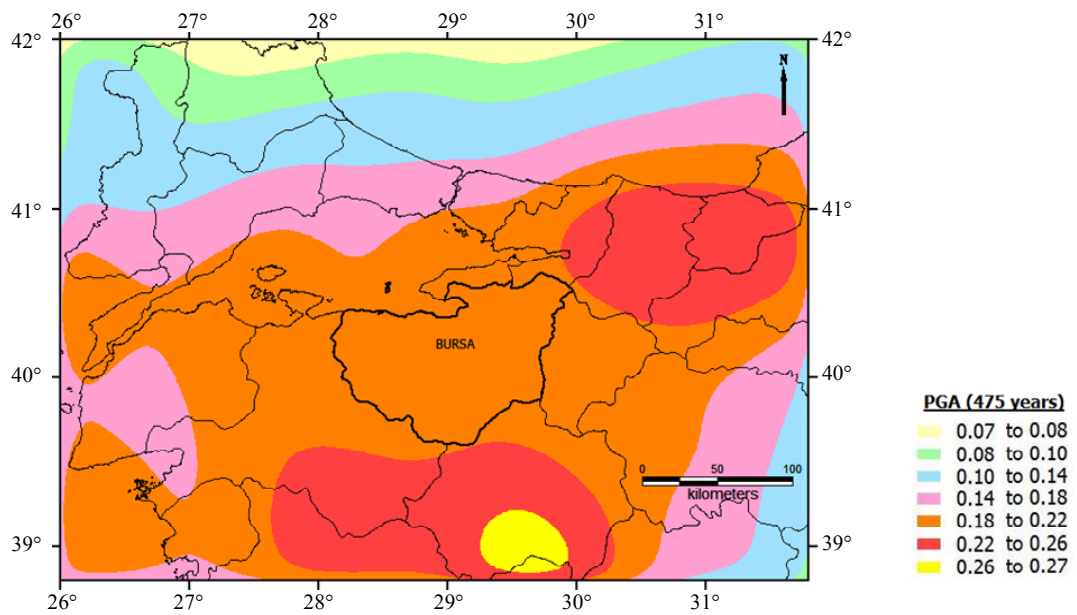


(b)

Figure 4.6 Seismic Hazard Maps for PGA (in g) Corresponding to the Return Period of 475 Years Obtained by Using Spatially Smoothed Seismicity Model with Main Shocks (a) Incomplete Database (b) Database Adjusted for Incompleteness



(a)



(b)

Figure 4.7 Seismic Hazard Maps for PGA (in g) Corresponding to the Return Period of 475 Years Obtained by Using Spatially Smoothed Seismicity Model with All Earthquakes (a) Incomplete Database (b) Database Adjusted for Incompleteness

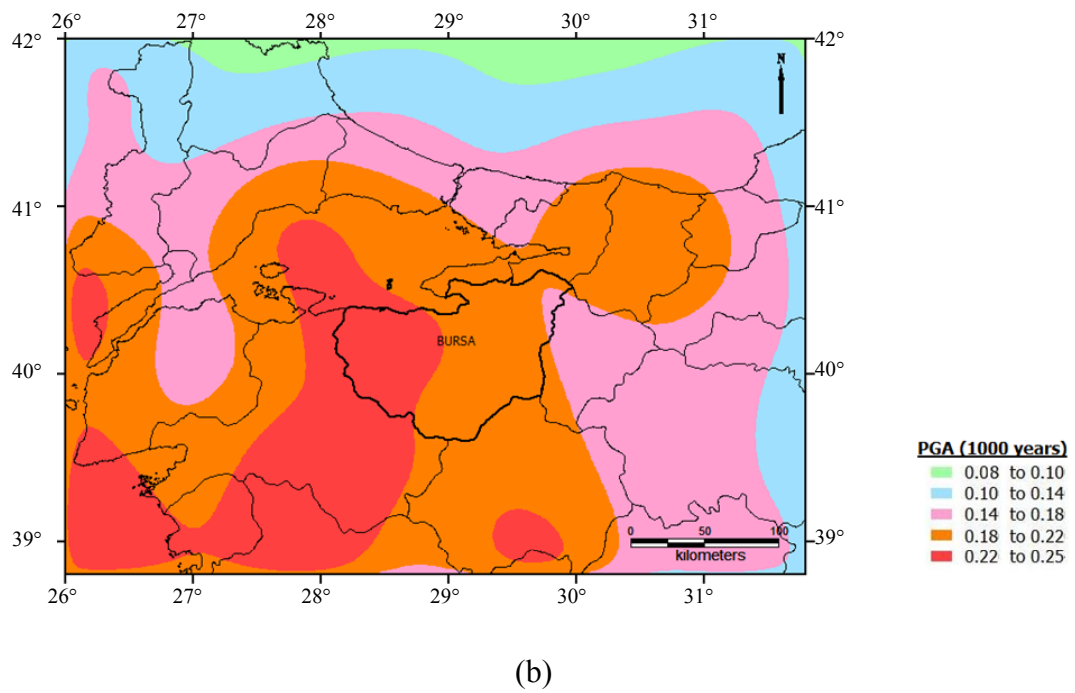
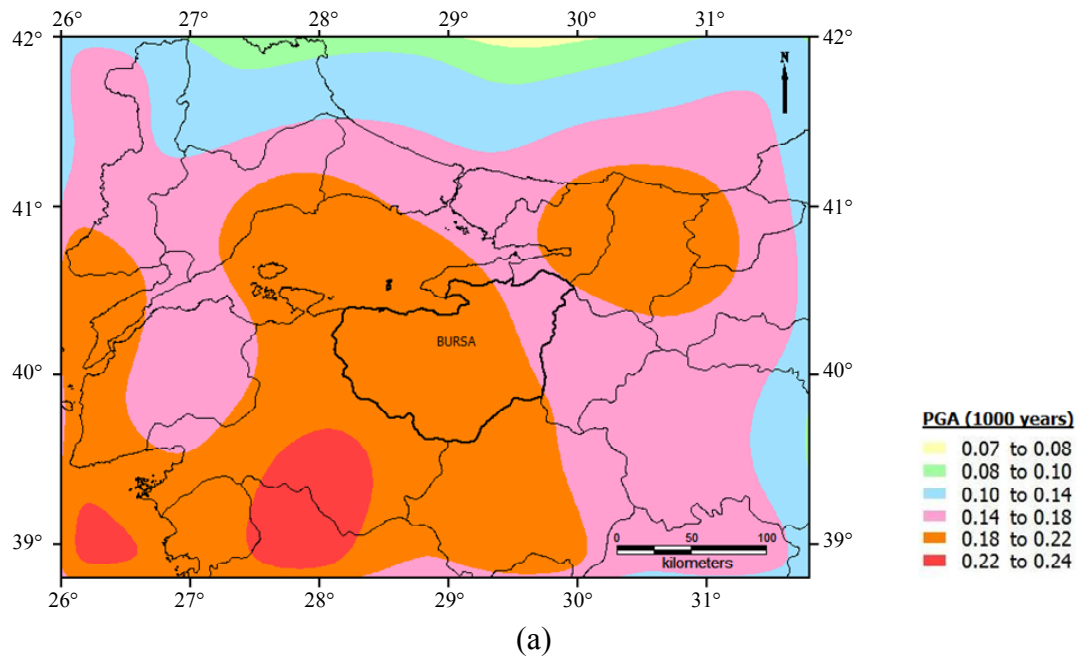
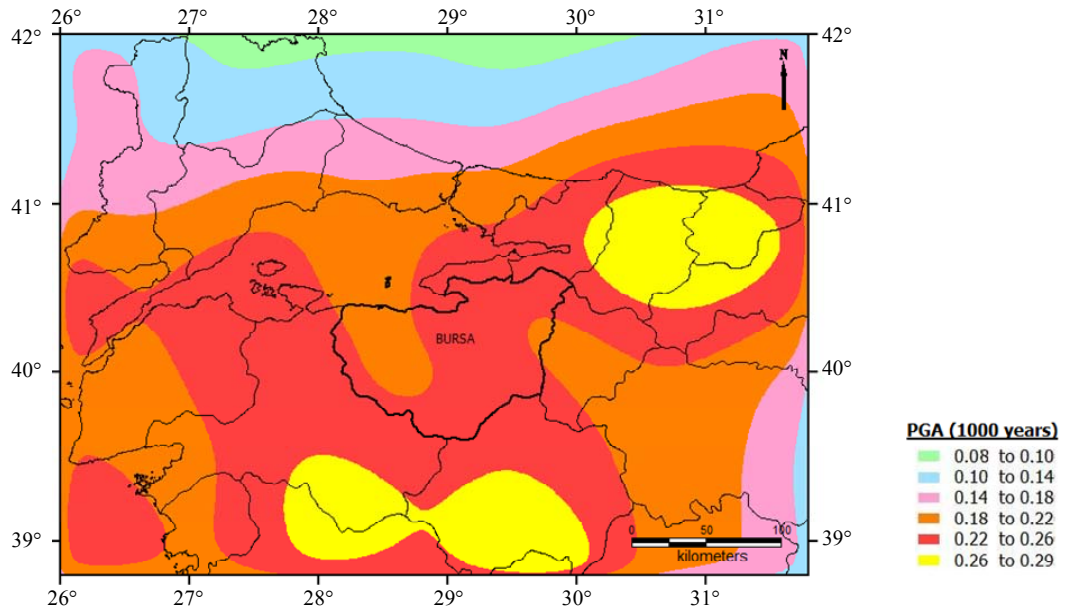
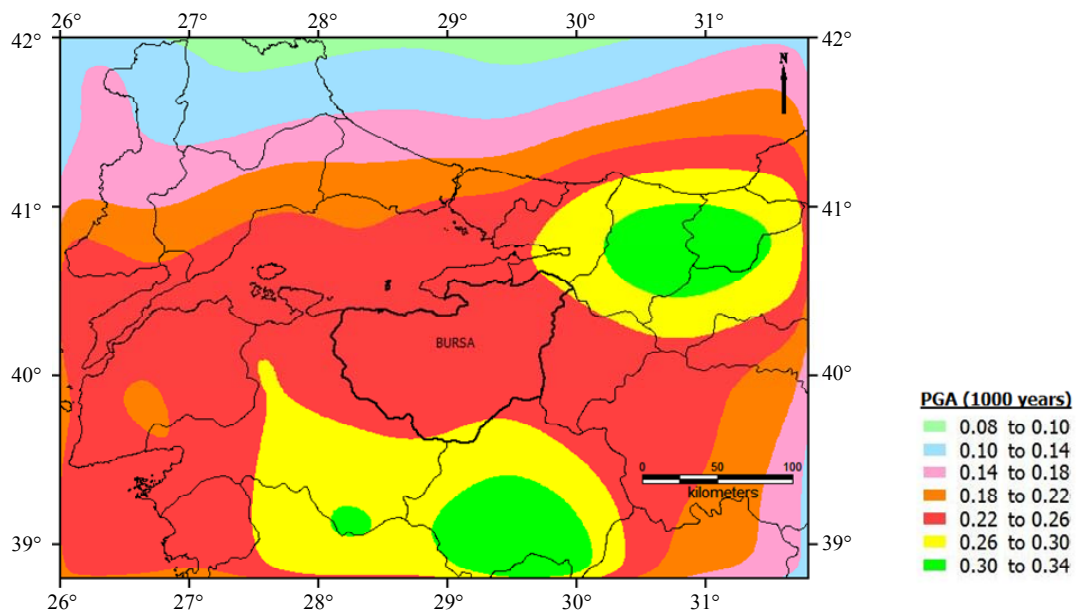


Figure 4.8 Seismic Hazard Maps for PGA (in g) Corresponding to the Return Period of 1000 years Obtained by Using Spatially Smoothed Seismicity Model with Main Shocks (a) Incomplete Database (b) Database Adjusted for Incompleteness



(a)



(b)

Figure 4.9 Seismic Hazard Maps for PGA (in g) Corresponding to the Return Period of 1000 years Obtained by Using Spatially Smoothed Seismicity Model with All Earthquakes (a) Incomplete Database (b) Database Adjusted for Incompleteness

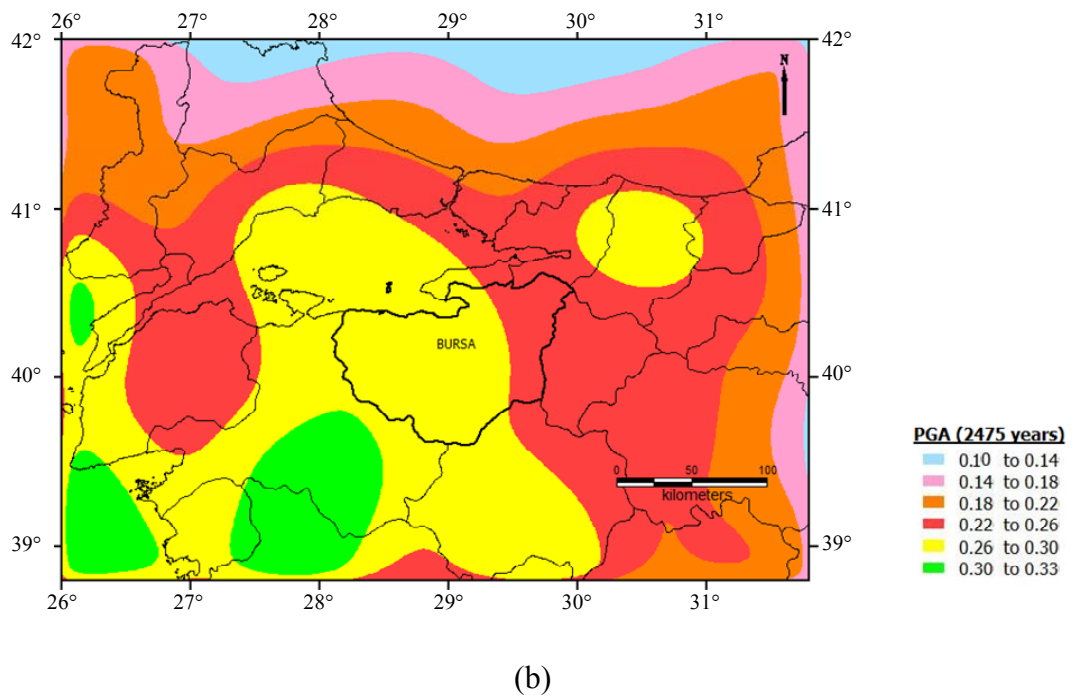
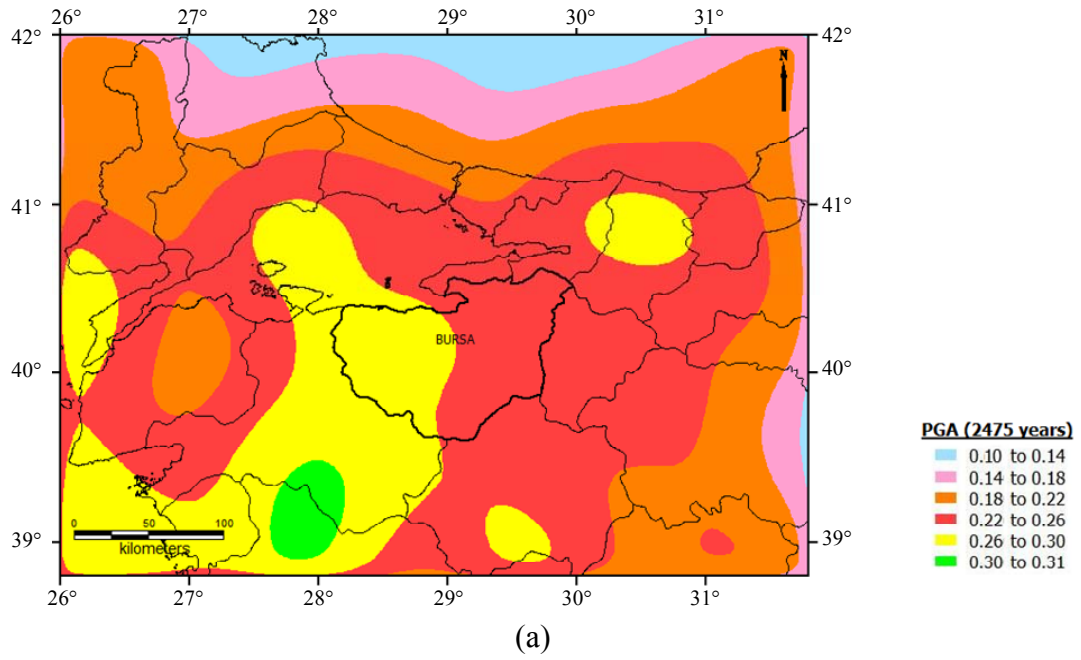
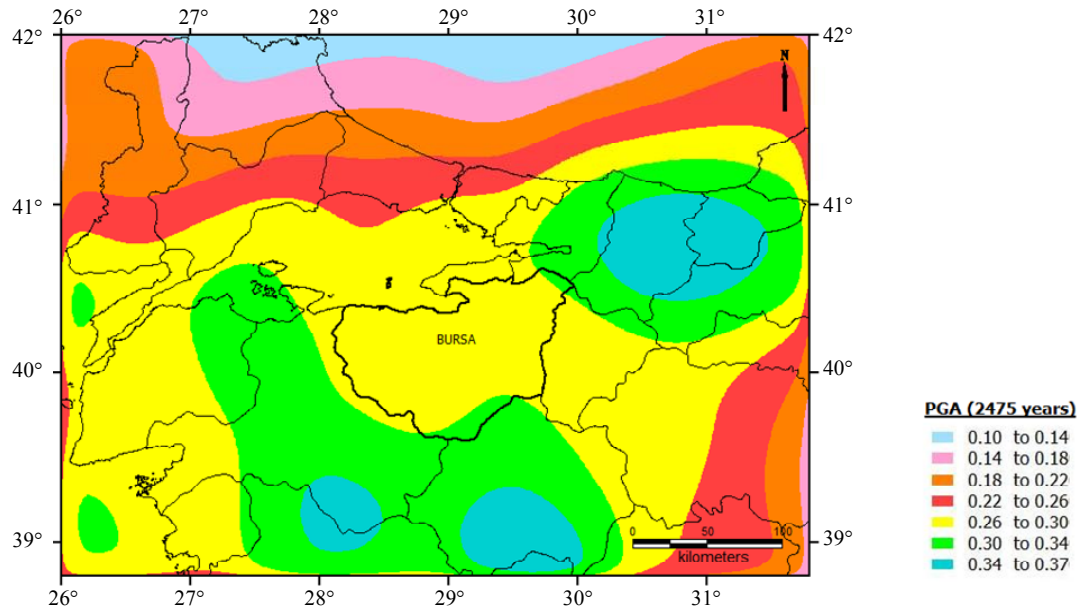
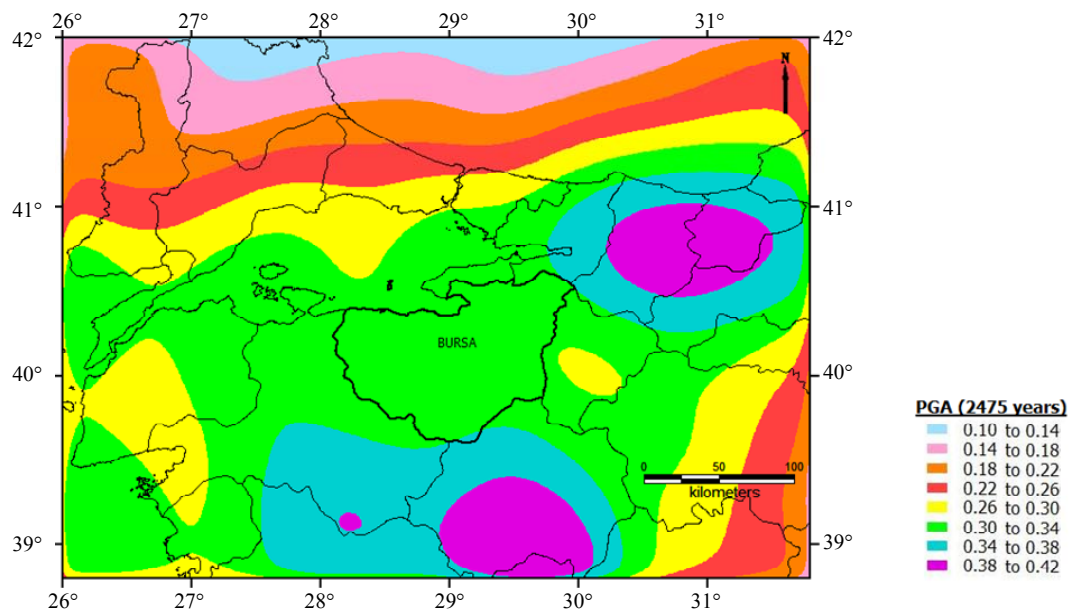


Figure 4.10 Seismic Hazard Maps for PGA (in g) Corresponding to the Return Period of 2475 years Obtained by Using Spatially Smoothed Seismicity Model with Main Shocks (a) Incomplete Database (b) Database Adjusted for Incompleteness



(a)



(b)

Figure 4.11 Seismic Hazard Maps for PGA (in g) Corresponding to the Return Period of 2475 years Obtained by Using Spatially Smoothed Seismicity Model with All Earthquakes (a) Incomplete Database (b) Database Adjusted for Incompleteness

It can be observed from Figures 4.6 through 4.11 and Table 4.2 that the analyses carried out by using only main shocks give smaller PGA values than those obtained by using all of the earthquakes in the database. The elimination of secondary events from the catalog resulted in smaller ν and β values. The decrease in ν values causes a reduction in the rate of seismic activity in the region as expected. Since $|\beta|$ represents the relative frequency of large magnitude earthquakes to the small magnitude ones, the decrease in $|\beta|$ values results in an increase in large magnitude earthquakes. Comparison of the ν and $|\beta|$ values given in Table 4.1 for the main shocks and all earthquakes, the ν values predicted from all earthquakes are almost 2 times greater than those obtained based on only main shocks. However, the $|\beta|$ values predicted by using all events are 1.2 times greater than those predicted by using only main shocks. Therefore, the rise in ν values results in an increase in PGA values predicted by using all earthquakes. Similarly, the PGA values predicted from the analyses by using ν and $|\beta|$ values predicted from the artificially completed earthquake catalogs are 1.1 and 1.4 times larger than those calculated from the incomplete catalogs, respectively. Therefore, larger PGA values are obtained from the analyses carried out by using artificially completed catalogs.

The maximum PGA values which is obtained from background area source with uniform seismicity and given in Table 4.2 are smaller than the maximum PGA values obtained from the spatially smoothed seismicity model. The difference between the PGA values obtained from these two models is calculated at each grid point in the region bounded by 26.0°- 31.8° E longitudes and 38.8°- 42.0° N latitudes by using the following equation;

$$\text{Difference(\%)} = \left(\frac{\text{PGA}_s - \text{PGA}_b}{\text{PGA}_b} \right) \times 100 \quad (4.9)$$

where PGA_s and PGA_b denote the PGA values estimated from spatially smoothed seismicity model and background area source with uniform seismicity, respectively. The difference with negative sign (-) means that the background area source with

uniform seismicity gives higher PGA values than the spatially smoothed seismicity model and the difference with positive sign represents the opposite case.

Figures 4.12 through 4.23 show the spatial variation of differences in PGA values obtained from the spatially smoothed seismicity model and the background area source with uniform seismicity according to different combinations of assumptions on earthquakes in the catalogs with respect to completeness and dependence. In these figures, it can be observed that spatially smoothed seismicity model gives higher PGA values than the background area source with uniform seismicity (i.e. positive difference values) especially at the regions where the epicenters of earthquakes become dense. On the other hand, negative differences (i.e. background area source gives higher PGA values than spatially smoothed seismicity model) are observed especially at the regions where the epicenters of earthquakes are scarce or no earthquakes occurred at the past. For the Bursa province in which the seismic hazard is under consideration for this study, positive differences is observed at southwestern part whereas negative one is seen at the northeastern part for the cases in which main shocks are used in the analyses. For the cases in which all earthquakes are considered, the positive differences are observed at the middle part of the Bursa province and extend through northeastern and southwestern parts. The maximum difference observed from all cases for Bursa province is less than 25%. This means that modeling background seismic activity with background area source model or spatially smoothed seismicity model has minor effect on the final results.

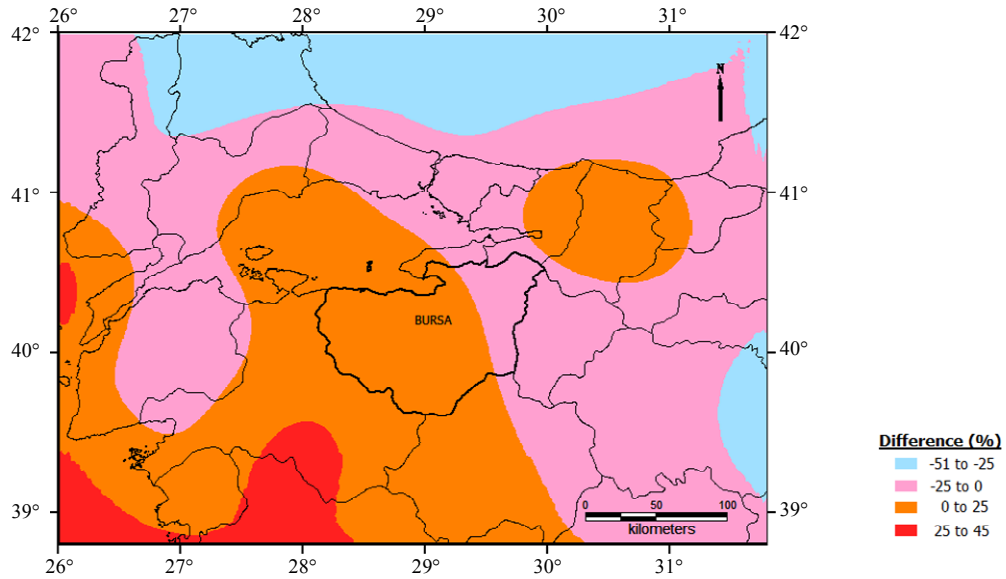


Figure 4.12 Map Showing the Spatial Variation of the Difference between the PGA Values Obtained from Spatially Smoothed Seismicity Model and Background Area Source with Main Shocks and Incomplete Database for a Return Period of 475 Years

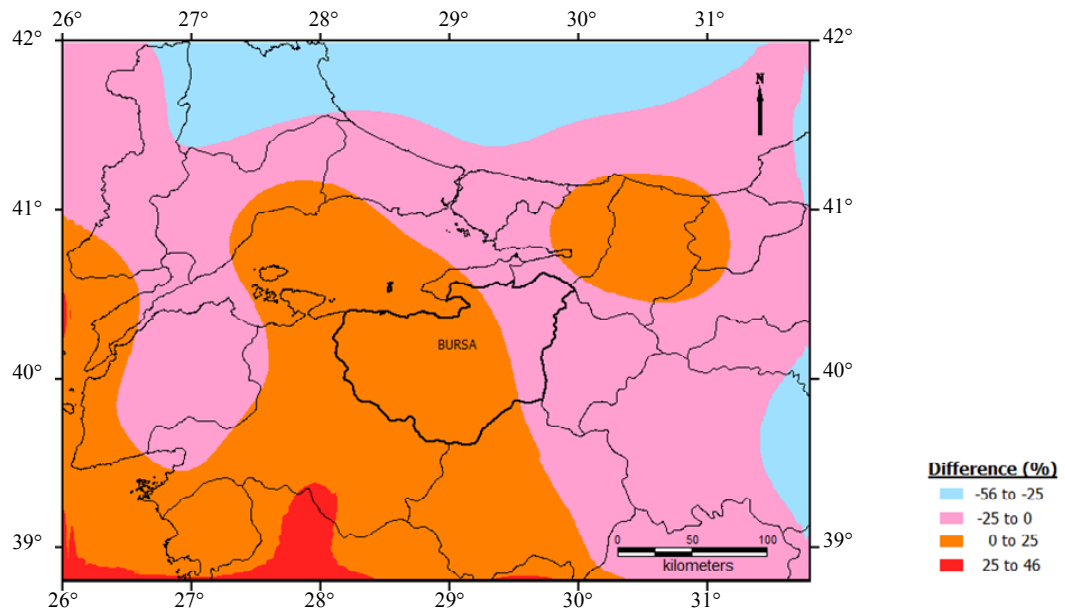


Figure 4.13 Map Showing the Spatial Variation of the Difference between the PGA Values Obtained from Spatially Smoothed Seismicity Model and Background Area Source with Main Shocks and Incomplete Database for a Return Period of 2475 Years

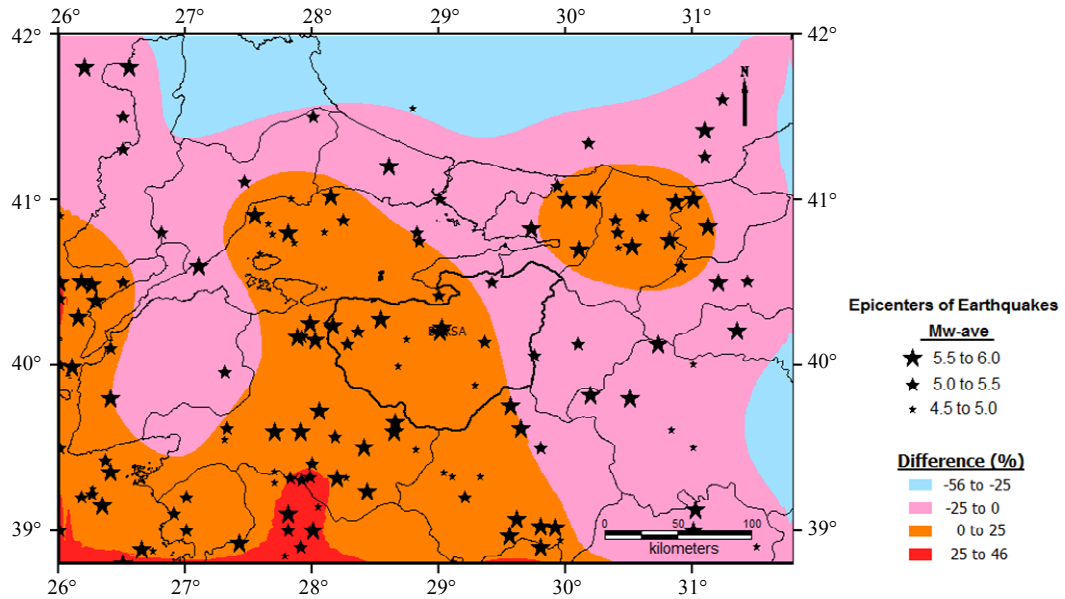


Figure 4.14 Map Showing the Spatial Variation of the Difference between the PGA Values Obtained from Spatially Smoothed Seismicity Model and Background Area Source with Main Shocks and Incomplete Database for a Return Period of 2475 Years and Epicenters of Earthquakes Considered in Spatially Smoothed Seismicity Model

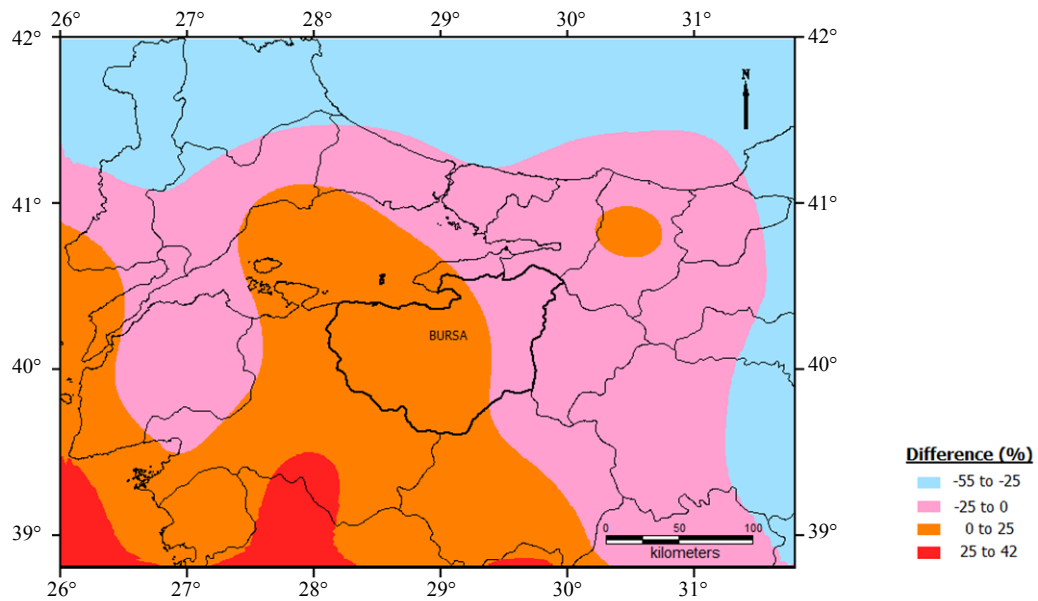


Figure 4.15 Map Showing the Spatial Variation of the Difference between the PGA Values Obtained from Spatially Smoothed Seismicity Model and Background Area Source with Main Shocks and Database Adjusted for Incompleteness for a Return Period of 475 Years

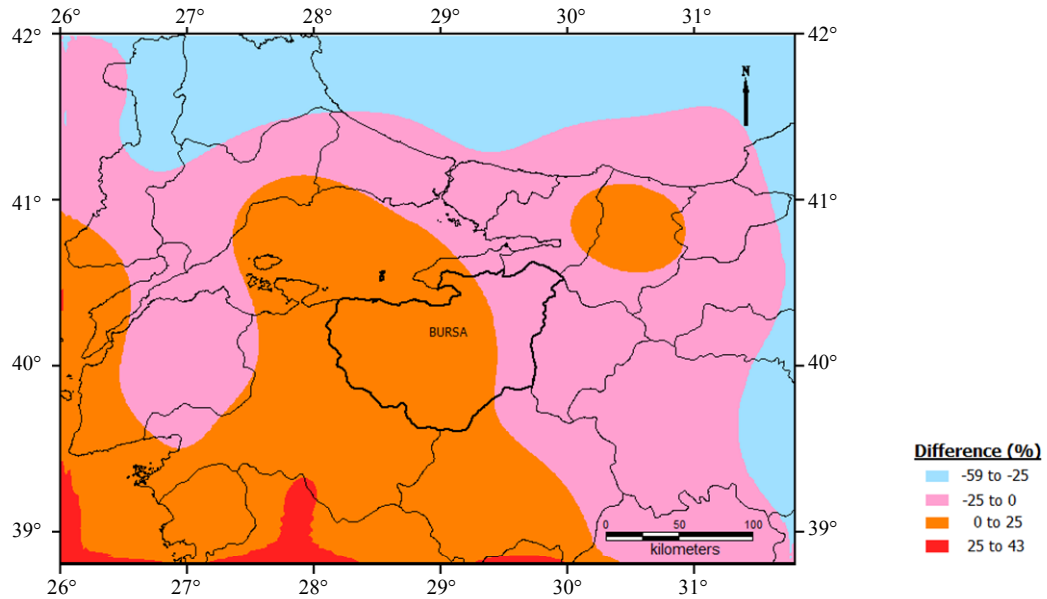


Figure 4.16 Map Showing the Spatial Variation of the Difference between the PGA Values Obtained from Spatially Smoothed Seismicity Model and Background Area Source with Main Shocks and Database Adjusted for Incompleteness for a Return Period of 2475 Years

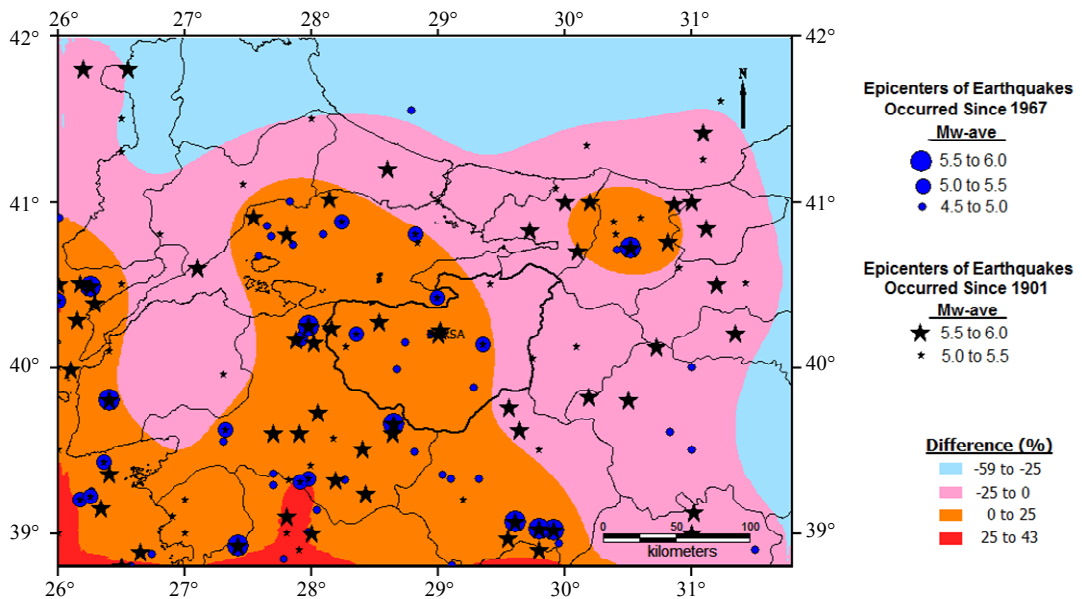


Figure 4.17 Map Showing the Spatial Variation of the Difference between the PGA Values Obtained from Spatially Smoothed Seismicity Model and Background Area Source with Main Shocks and Database Adjusted for Incompleteness for a Return Period of 2475 Years and Epicenters of Earthquakes Considered in Spatially Smoothed Seismicity Model

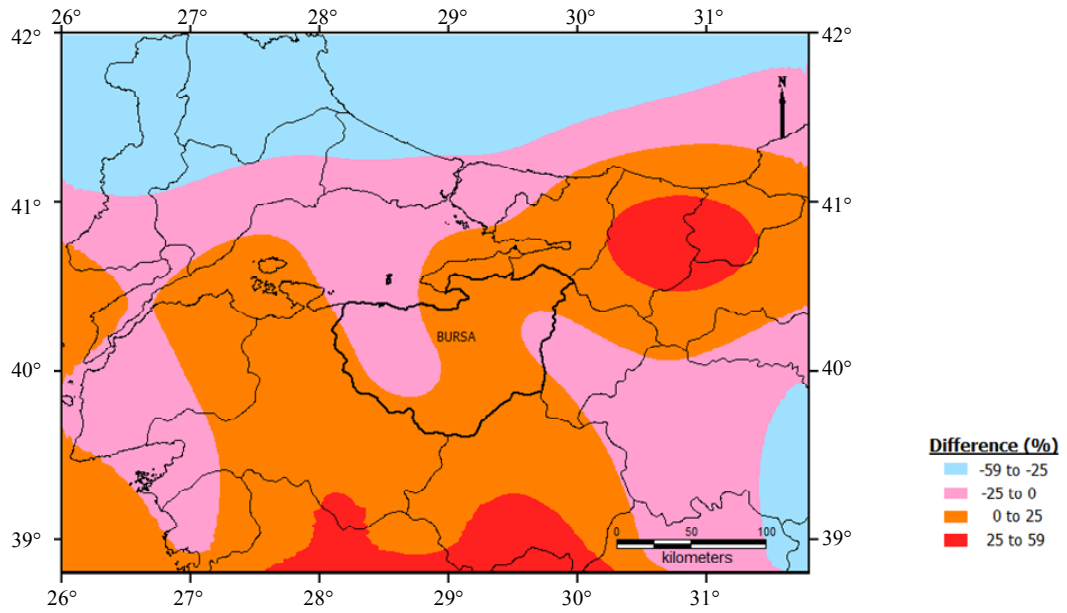


Figure 4.18 Map Showing the Spatial Variation of the Difference between the PGA Values Obtained from Spatially Smoothed Seismicity Model and Background Area Source with All Earthquakes and Incomplete Database for a Return Period of 475 Years

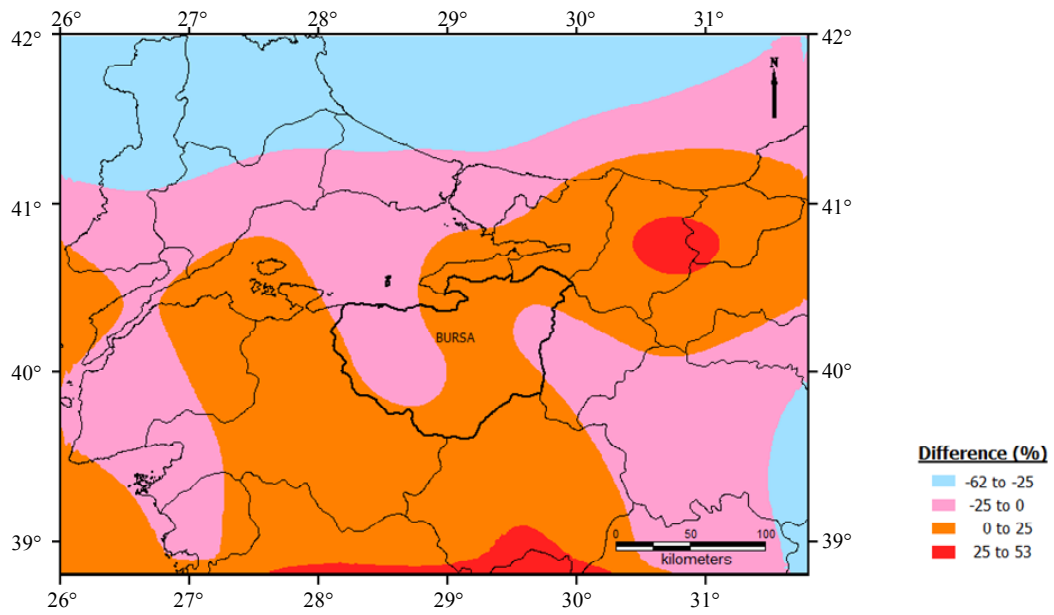


Figure 4.19 Map Showing the Spatial Variation of the Difference between the PGA Values Obtained from Spatially Smoothed Seismicity Model and Background Area Source with All Earthquakes and Incomplete Database for a Return Period of 2475 Years

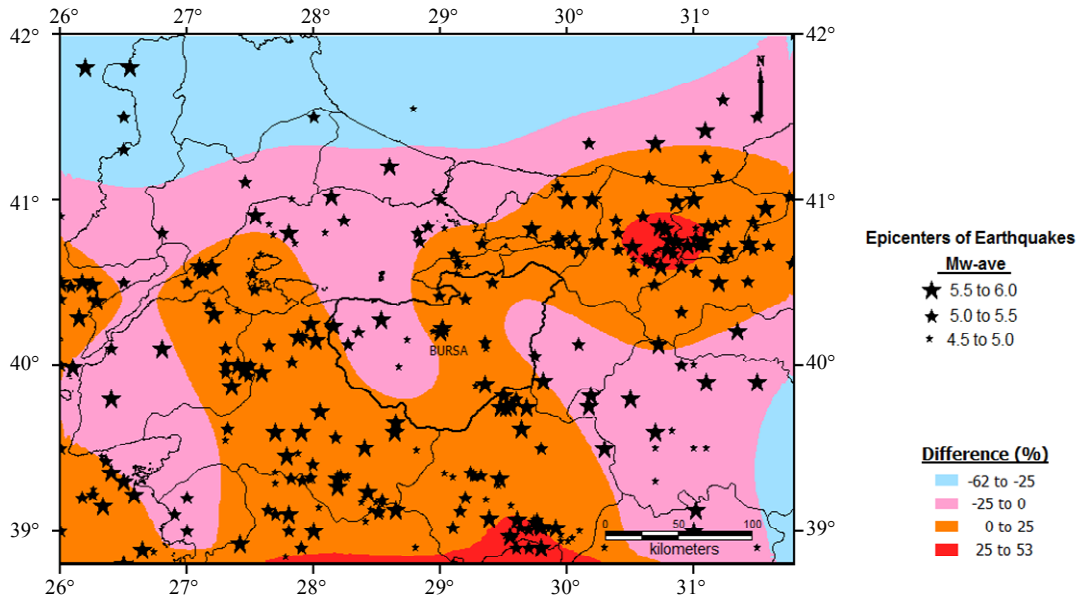


Figure 4.20 Map Showing the Spatial Variation of the Difference between the PGA Values Obtained from Spatially Smoothed Seismicity Model and Background Area Source with All Earthquakes and Incomplete Database for a Return Period of 2475 Years and Epicenters of Earthquakes Considered in Spatially Smoothed Seismicity Model

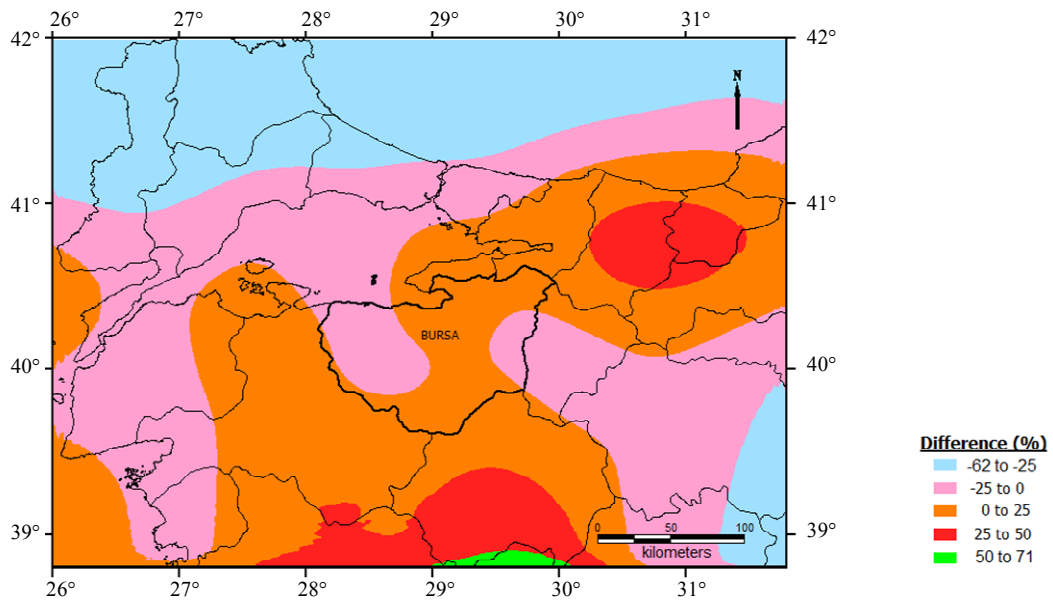


Figure 4.21 Map Showing the Spatial Variation of the Difference between the PGA Values Obtained from Spatially Smoothed Seismicity Model and Background Area Source with All Earthquakes and Database Adjusted for Incompleteness for a Return Period of 475 Years

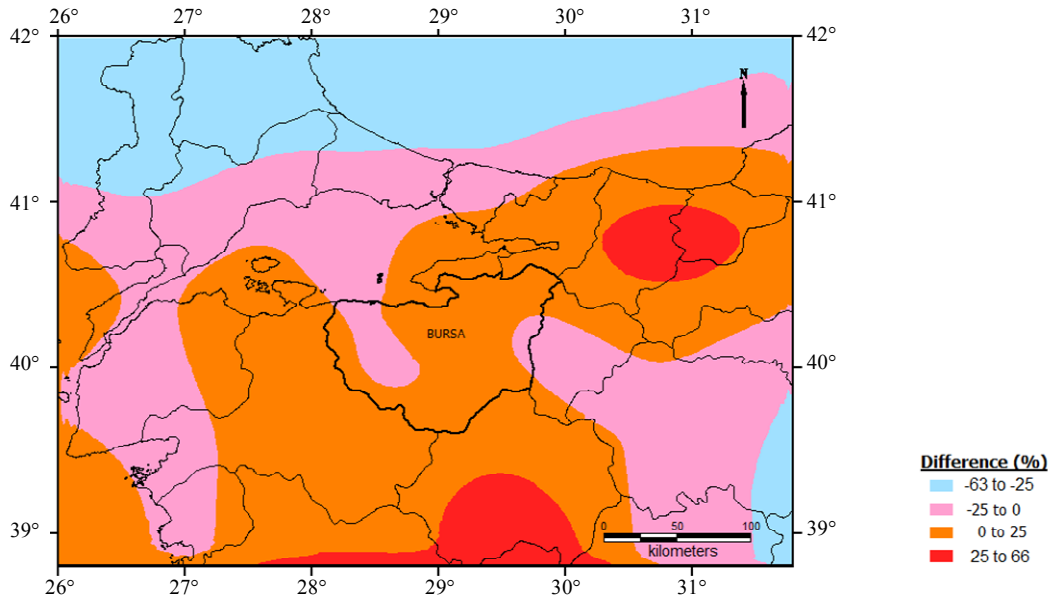


Figure 4.22 Map Showing the Spatial Variation of the Difference between the PGA Values Obtained from Spatially Smoothed Seismicity Model and Background Area Source with All Earthquakes and Database Adjusted for Incompleteness for a Return Period of 2475 Years

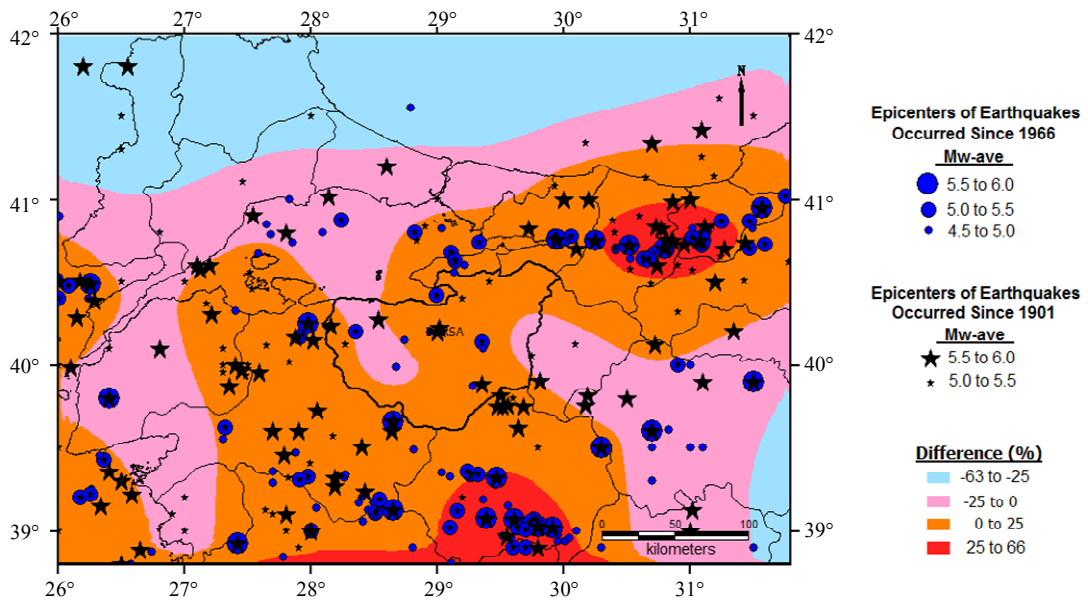


Figure 4.23 Map Showing the Spatial Variation of the Difference between the PGA Values Obtained from Spatially Smoothed Seismicity Model and Background Area Source with All Earthquakes and Database Adjusted for Incompleteness for a Return Period of 2475 Years and Epicenters of Earthquakes Considered in Spatially Smoothed Seismicity Model

4.3.2.2 Seismic Hazard Resulting From Faults

As explained above, the contributions of earthquakes with magnitude equal to or greater than 6.0 are calculated by attributing the related seismic activity to the faults and fault segments shown in Figure 4.1. It is assumed that energy along these faults and fault segments are released by characteristic events that rupture the whole or a large portion of the length of the fault. Consequently, the maximum magnitude earthquakes that the fault segments may generate and their return periods are the main parameters in these calculations.

For the fault segments that are delineated based on the study of Yüçemen et al. (2006), the maximum magnitude values and their return periods given in this reference are used. For those fault segments identified based on Koçyiğit (2005), only maximum magnitude values are given in his study. For the rest of the fault segments, their maximum magnitudes are assigned based on their lengths by using the equation proposed by Wells and Coppersmith (1994) which is given below:

$$M_w = 5.08 + 1.16 \log(\text{SRL}) \quad (4.10)$$

where; M is the earthquake magnitude, SRL is the surface rupture length. In this study, SRL is assumed to be equal to the fault length. However, the lengths of longest segments of faults; numbered as F2, F3, F7, F8 and F9 where F stands for fault, are used in the determination of their maximum magnitude earthquakes. For the return periods of the maximum magnitudes of all fault segments, except those given in Yüçemen et al. (2006), Koçyiğit (2007) is consulted. Table 4.3 shows the parameters of fault segments considered in this study.

In order to predict probabilities of future occurrences of maximum magnitude, characteristic earthquakes along these fault segments, both the memoryless Poisson and the time dependent renewal models are utilized. In the Poisson model, the annual rate of characteristic earthquakes for each segment is taken as the reciprocal of the lower bound of its return period given in Table 4.3. Therefore, conservative estimates of annual activity rates are used in the seismic hazard computations.

Table 4.3 Parameters of the Fault Segments Used in This Study (Koçyiğit, 2005; Yüçemen et al., 2006)

Segment No	Name of Fault	Type	Size of Peak Earthquake	Return Period (RP) (in years)	Year of Last Characteristic Earthquake
F1	Etili Fault	Strike-Slip	6.9	~ 250	-
F2	Sarıköy Fault	Strike-Slip	7.0	~ 250	1737
F3	Yenice-Gönen Fault	Strike-Slip	7.0	~ 250	1953
F4	Manyas Fault	Normal	7.0	500<RP≤1000	1964
F5	-	Normal	6.7	500<RP≤1000	-
F6	Edincik Fault	Strike-Slip	6.6	~ 250	-
F7	Zeytindağ Bergama Fault Zone	Normal	6.7	≥ 1000	-
F8	Akhisar Fault	Normal	6.6	≥ 1000	-
F9	Kütahya Fault	Oblique-Slip Normal	6.6	500<RP≤1000	-
F10	Kaymaz Fault	Normal	6.6	≥1000	-
F11	Tepetarla Fault	Strike-Slip	6.8	~ 250	1999
F12	Arifiye Fault	Strike-Slip	6.9	~ 250	1999
F13	Karadere Fault	Strike-Slip	7.0	~ 250	1999
F14	Düzce Fault	Strike-Slip	7.0	~ 250	1999
F15	-	Strike-Slip	7.0	~ 250	1944
F16	-	Strike-Slip	6.8	~ 250	1957
F17	-	Strike-Slip	6.9	~ 250	1967
F18	-	Strike-Slip	7.1	~ 250	-
F19	-	Strike-Slip	7.3	500<RP≤1000	-
F20	Kovalıca Fault	Oblique-Slip Normal	6.4	500<RP≤1000	-
F21	İnönü Fault	Oblique-Slip Normal	6.4	500<RP≤1000	-
F22	Hisarönü+Çukurhisar+Satılmışoğlu+Karagözler Faults	Normal	6.2	500<RP≤1000	-
F23	Yusuflar Fault	Oblique-Slip Normal	6	500<RP≤1000	-
F24	Keskin Fault	Normal	6.6	500<RP≤1000	-
F25	Kızılyar+Cumhuriyet Faults	Normal	6.4	500<RP≤1000	-
F26	Kızılcıören Fault	Oblique-Slip Normal	6.4	500<RP≤1000	-
F27	Gökdere Fault	Oblique-Slip Normal	6.1	500<RP≤1000	-
F28	Gündüzler Fault	Oblique-Slip Normal	6.1	500<RP≤1000	-
F29	Kozlubel Fault	Oblique-Slip Normal	6.3	500<RP≤1000	-
F30	Beyazaltın (Sepetçi) Fault	Oblique-Slip Normal	6.2	500<RP≤1000	-
F31	Sultandere Fault	Normal	6.3	500<RP≤1000	-
F32	Altıpatlar Fault	Normal	6.4	500<RP≤1000	-

Table 4.3 (Continued) Parameters of the Fault Segments Used in This Study
(Koçyiğit, 2005; Yüçemen et al., 2006)

Segment No	Name of Fault	Type	Size of Peak Earthquake	Return Period (RP) (in years)	Year of Last Characteristic Earthquake
F33	Karacaören Fault	Normal	6.5	500<RP≤1000	-
F34	Gülpınar Fault	Oblique-Slip Normal	6.3	≥ 1000	-
F35	Meşelik Fault	Oblique-Slip Normal	6.1	≥ 1000	-
F36	Esmekaya+Soğucak+ Karaözkuyu+Kavacık+ Eğriöz+Kozkaya Faults	Oblique-Slip Normal	6.7	500<RP≤1000	1956
F37	Uçmakdere+Ganos Fault	Strike-Slip	7.2	283	1912
F38	Kumbağı Fault	Strike-Slip	7	283	1912
F39	Central Fault	Strike-Slip	6.4	500<RP≤1000	1556
F40	Kumburgaz Fault	Strike-Slip	6.5	257±23	1766
F41	Yeşilköy Fault	Strike-Slip	7	257±23	1766
F42	Adalar Fault	Normal	6.9	200<RP≤500	1766
F43	Darıca Fault	Strike-Slip	6.5	500<RP≤1000	1894
F44	Ağaçlı Fault	Normal	6.8	≥ 1000	-
F45	Muratdağı Fault	Normal	7	≥ 1000	1970
F46	Erdoğmuş Fault	Normal	6.8	≥ 1000	1970
F47	Abide Fault	Normal	6.5	≥ 1000	-
F48	Simav Fault	Normal	7.2	≥ 1000	-
F49	Bursa Fault	Oblique-Slip Normal	7.2	≥ 1000	1855
F50	Sayfiye Fault	Oblique-Slip Normal	6.8	≥ 1000	-
F51	Alaçam Fault	Oblique-Slip Normal	6.7	500<RP≤1000	-
F52	Soğukpınar Fault	Oblique-Slip Normal	6.7	≥ 1000	-
F53	Çalı Fault	Oblique-Slip Normal	6.8	≥ 1000	1855
F54	Ayaz Fault	Oblique-Slip Normal	6.4	≥ 1000	1855
F55	M. Kemalpaşa Fault	Oblique-Slip Normal	6.5	≥ 1000	1964
F56	Derecik Fault	Oblique-Slip Normal	6.5	≥ 1000	1964
F57	Yeniköy Fault	Oblique-Slip Normal	6.2	≥ 1000	1964
F58	Çavuşköy Fault	Oblique-Slip Normal	6	≥ 1000	-
F59	Kestel Fault Set	Oblique-Slip Normal	6.4	≥ 1000	-
F60	Taşlık Fault	Oblique-Slip Normal	6	≥ 1000	-
F61	Demirtaş Fault	Oblique-Slip Normal	6.6	≥ 1000	-

Table 4.3 (Continued) Parameters of the Fault Segments Used in This Study
(Koçyiğit, 2005; Yüçemen et al., 2006)

Segment No	Name of Fault	Type	Size of Peak Earthquake	Return Period (RP) (in years)	Year of Last Characteristic Earthquake
F62	Karahıdır Fault	Oblique-Slip Normal	6.7	≥ 1000	-
F63	Eymir Fault	Oblique-Slip Normal	6.6	≥ 1000	-
F64	Boğazköy Fault	Oblique-Slip Normal	6.7	≥ 1000	-
F65	Eskiköy Fault	Oblique-Slip Normal	6.9	≥ 1000	-
F66	Kozpınar Fault	Oblique-Slip Normal	7	≥ 1000	-
F67	Erikli Fault	Oblique-Slip Normal	6.9	≥ 1000	-
F68	Dodurga Fault	Oblique-Slip Normal	6.2	≥ 1000	-
F69	Gemlik Fault	Strike-Slip	6.4	500<RP≤1000	-
F70	Gürle Fault	Strike-Slip	6.3	500<RP≤1000	-
F71	Gençali Fault	Strike-Slip	6.3	500<RP≤1000	-
F72	Altıntaş-Kurşunlu Fault	Strike-Slip	6.2	500<RP≤1000	-
F73	Narlıca Fault	Strike-Slip	6.2	500<RP≤1000	-
F74	Şükrüye Fault	Strike-Slip	6.5	500<RP≤1000	-
F75	Çamdibi Fault	Strike-Slip	7	≥ 1000	-
F76	Karadin Fault	Strike-Slip	6.5	500<RP≤1000	-
F77	Orhaniye Fault	Strike-Slip	6.5	500<RP≤1000	-
F78	Kurtköy-Gökçedere Fault	Oblique-Slip Normal	6.4	500<RP≤1000	-
F79	Koyunhisar Fault	Strike-Slip	6.5	500<RP≤1000	-
F80	Kavaklı Fault	Strike-Slip	6.3	500<RP≤1000	-
F81	Mudanya Fault	Strike-Slip	6.5	500<RP≤1000	-
F82	Boğazköy-Ekinli Fault	Strike-Slip	6.7	500<RP≤1000	-
F83	Kurşunlu Fault	Strike-Slip	6.6	500<RP≤1000	-
F84	Karamürsel Fault	Strike-Slip	6.7	250-300	1999
F85	Çınarcık Fault	Strike-Slip	6.9	≥ 400	-
F86	Laledere Fault	Strike-Slip	6.5	500<RP≤1000	-
F87	Gölcük Fault	Strike-Slip	6.7	210-280	1999
F88	Körfüz Fault	Strike-Slip	6.4	250-300	1999
F89	Ortaca Fault	Normal	6.3	≥ 1000	-
F90	Akçabük Fault	Normal	6.5	≥ 1000	-
F91	Bandırma Fault	Strike-Slip	7	≥ 1000	-

In the renewal model, the equivalent mean rate of characteristic earthquakes depends on probability distribution function of inter-event times as well as the time elapsed since the last characteristic earthquake and the next time interval considered. In this study, Brownian Passage Time (BPT) model is used as the probability distribution of inter-event times. For each fault segment, the following values are assigned to the parameters of the inter-event time distribution: (i) For the mean inter-event times, the lower bounds of the return periods given in Table 4.3 are used. (ii) Aperiodicity is assumed to be 0.5, which appears to be the most likely value according to the study conducted by Ellsworth et al. (1999). The time elapsed since the last characteristic earthquake, “ t_0 ”, is estimated based on the studies conducted by Yüçemen et al. (2006), Erdik et al. (2004), Emre and Awata (2003), Awata et al. (2003), Şaroğlu et al. (1992) and Koçyiğit (2007). For the segments for which the times elapsed since the last characteristic earthquakes are unknown, they are assumed to be 1000 years. The next time interval, “ w ”, to be considered in the seismic hazard analyses is taken as 50 years. For each segment, equivalent rate of characteristic earthquake is calculated from the following equation, the derivation of which is explained in Section 2.3.3:

$$v^C(w, t_0) = -\frac{1}{w} [\ln(|G(t_0 + w)|) - \ln(|G(t_0)|)] = -\frac{1}{w} \ln \left(\frac{\int_{t_0+w}^{\infty} f(t).dt}{\int_{t_0}^{\infty} f(t).dt} \right) \quad (4.11)$$

where; $v^C(w, t_0)$ is the equivalent mean rate of characteristic earthquakes; $f(t)$ and $G(t)$ are the probability density and complementary cumulative distribution functions of the inter-event times, respectively. The complementary cumulative distribution function $G(t)$ is estimated from the formulation given by Matthews et al. (2002) for the cumulative distribution function, $F(t)$, as shown in the following;

$$G(t) = 1 - F(t) \quad (4.12)$$

where

$$F(t) = P\{T \leq t\} = \Phi[u_1(t)] + e^{2/\alpha^2} \Phi[-u_2(t)] \quad (4.13)$$

$$u_1(t) = \alpha^{-1} \left[t^{1/2} \mu^{-1/2} - t^{-1/2} \mu^{1/2} \right] \quad (4.14)$$

$$u_2(t) = \alpha^{-1} \left[t^{1/2} \mu^{-1/2} + t^{-1/2} \mu^{1/2} \right] \quad (4.15)$$

Here; α is the aperiodicity and μ is the mean inter-event time.

Firstly, seismic hazard analyses are carried out by using only fault segments which are producing earthquakes in the time domain according to the Poisson and renewal models to obtain seismic hazard curves for a selected site (40.24° N, 29.08° E) corresponding to the city center of Bursa. Figure 4.24 shows the seismic hazard curves obtained by using attenuation relationships proposed by Kalkan and Gülkan (2004) and Boore et al. (1997) for PGA at rock sites. Contributions of different faults to seismic hazard are shown in Figure 4.25. In this figure, the curves show the seismic hazard values obtained as the average of the two attenuation relationships mentioned above.

It can be observed from Figure 4.24 that the analyses carried out by using the renewal model (curves (c) and (d)) give higher seismic hazard values than those obtained from the Poisson model (curves (a) and (b)) for the selected site. The same trend with background seismic activity is observed for the influence of the attenuation relationships proposed by Kalkan and Gülkan (2004) and Boore et al. (1997). In other words, the difference between the seismic hazard curves obtained by using these two attenuation relationships is insignificant at small PGA values but it increases at larger PGA values. It is shown in Figure 4.25 that the most contributing source to seismic hazard at small PGA values is the Adalar Fault in both of the Poisson and renewal models. At PGA values larger than 0.1g, Demirtaş, Karahıdır and Bursa Faults are the highest contributing sources to seismic hazard results obtained by using the Poisson model. In the renewal model, the effect of Bursa fault on seismic hazard results decreases. Since it is assumed that this fault ruptured and released energy in the earthquake occurred in 1855, the probability of

future earthquakes sourced from this fault and consequently the annual activity rate are reduced according to the renewal model.

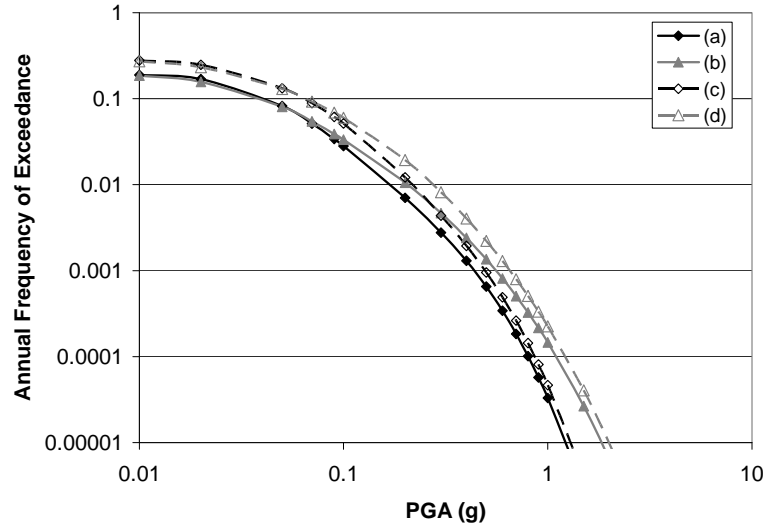
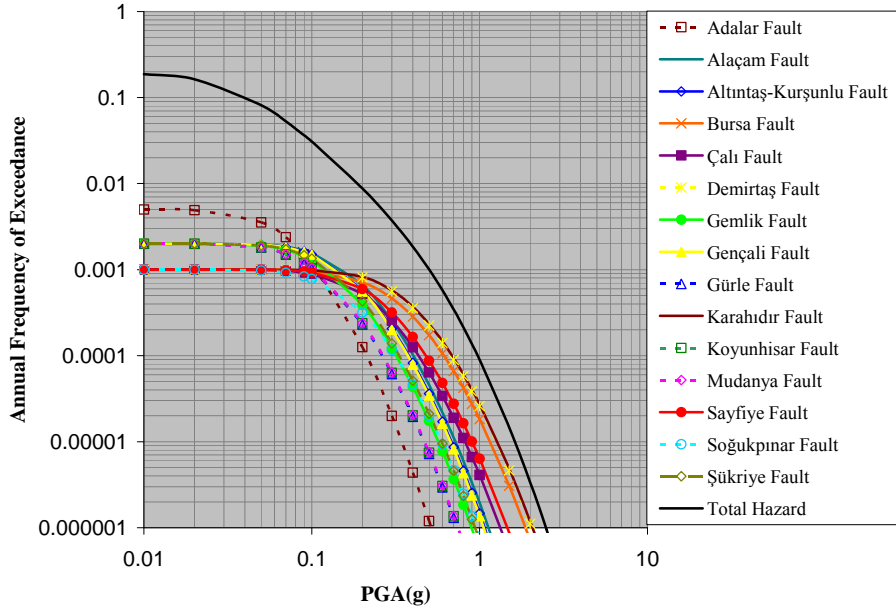
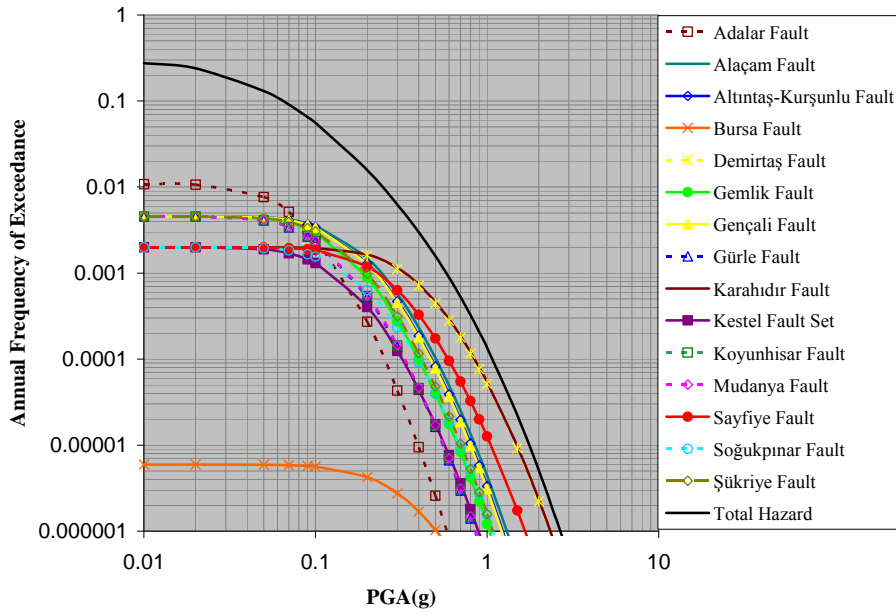


Figure 4.24 Seismic Hazard Curves Obtained by Using Fault Segments: with Poisson Model and Attenuation Relationships proposed by (a) Boore et al. (1997); (b) Kalkan and Gülkan (2004); and with Renewal Model and Attenuation Relationships proposed by (c) Boore et al. (1997); (d) Kalkan and Gülkan (2004)

In order to investigate the influence of Poisson and renewal models on the variation of seismic hazard results in space, seismic hazard analyses are carried out by considering only the contribution of all faults and fault segments in Figure 4.1 at all grid points with a spacing of $0.02^{\circ} \times 0.02^{\circ}$ in latitude and longitude in the region bounded by 26.0° - 31.8° E longitudes and 38.8° - 42.0° N latitudes. Then, seismic hazard maps are constructed for PGA corresponding to return periods of 475, 1000 and 2475 years. In the analyses, equal weights are given to both attenuation relationships. Figures 4.26 through 4.28 show seismic hazard maps obtained in this way based on the Poisson and renewal models.



(a)



(b)

Figure 4.25 Contributions of Different Faults to Seismic Hazard under the Assumption of (a) Poisson Model and (b) Renewal Model

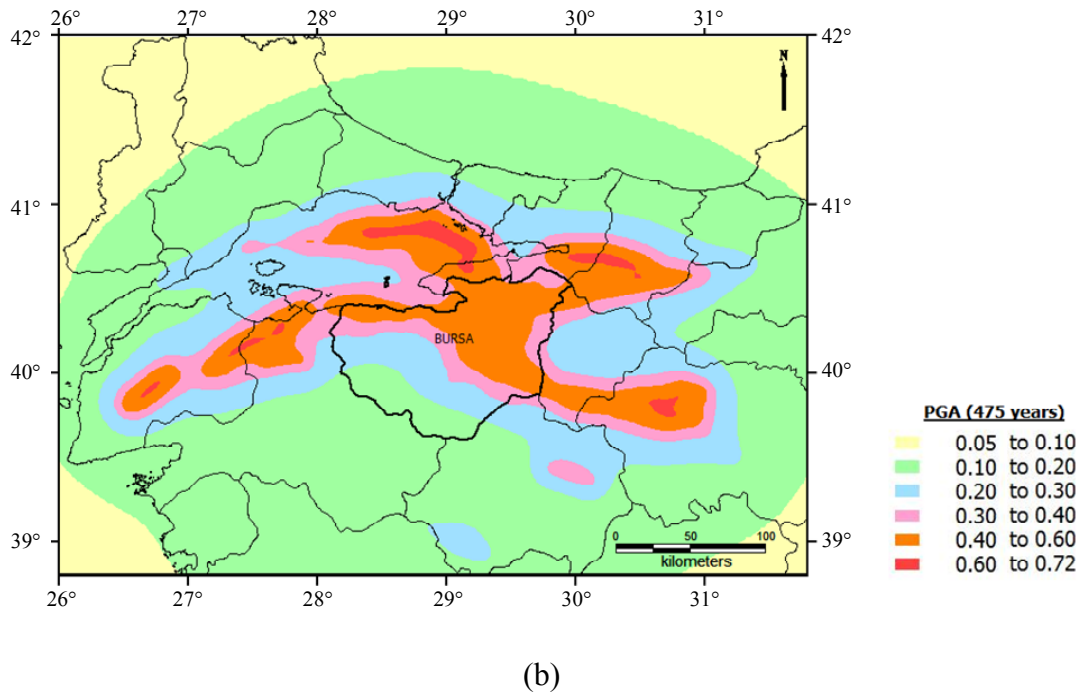
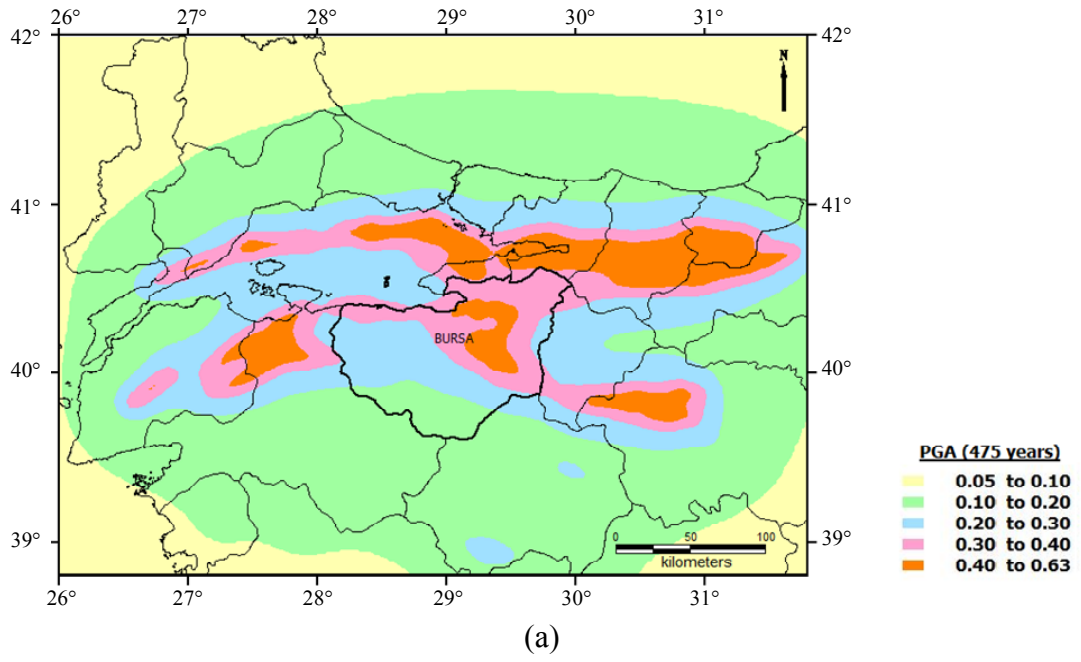


Figure 4.26 Seismic Hazard Map Obtained for PGA (in g) Corresponding to the Return Period of 475 Years (10% Probability of Exceedance in 50 Years) by Considering Only Faults with (a) Poisson Model, (b) Renewal Model

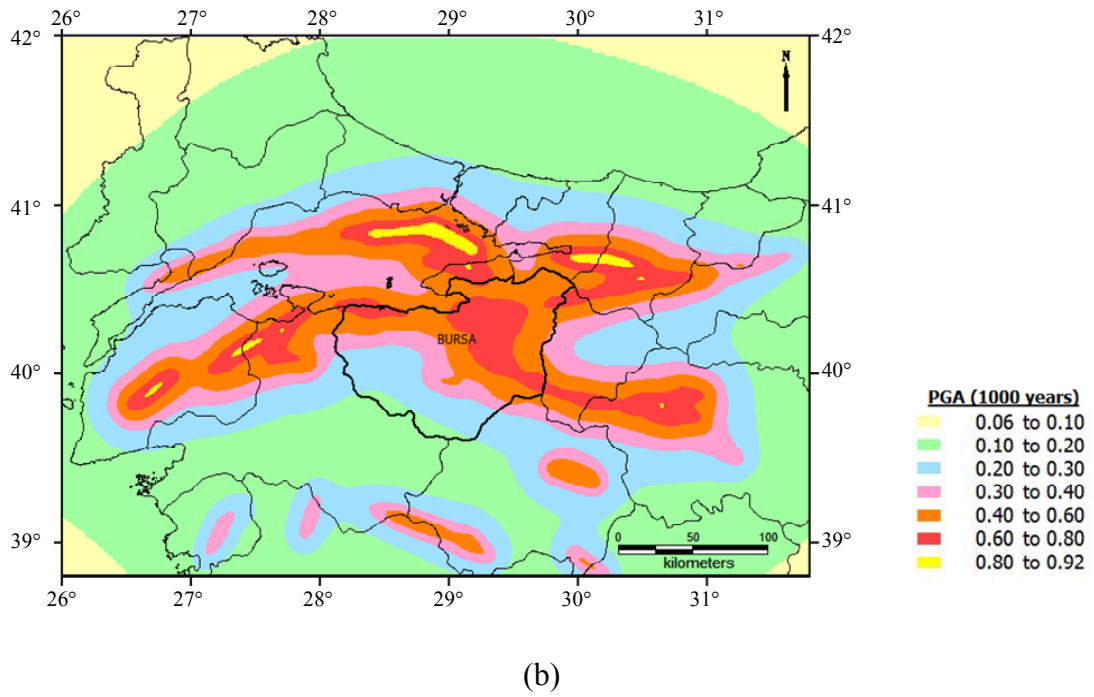
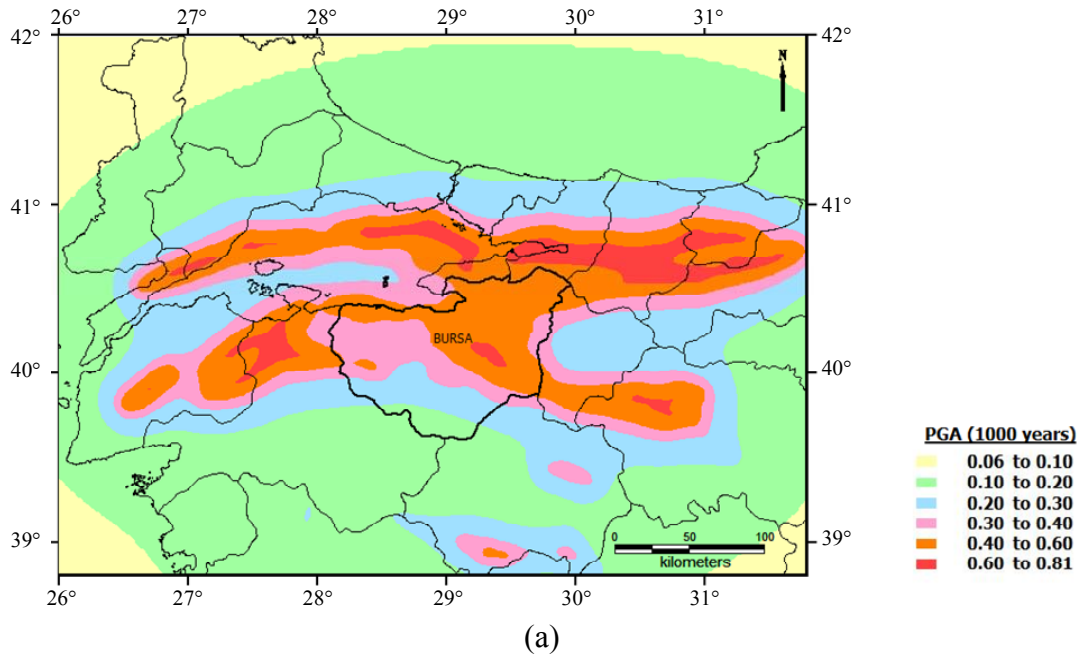
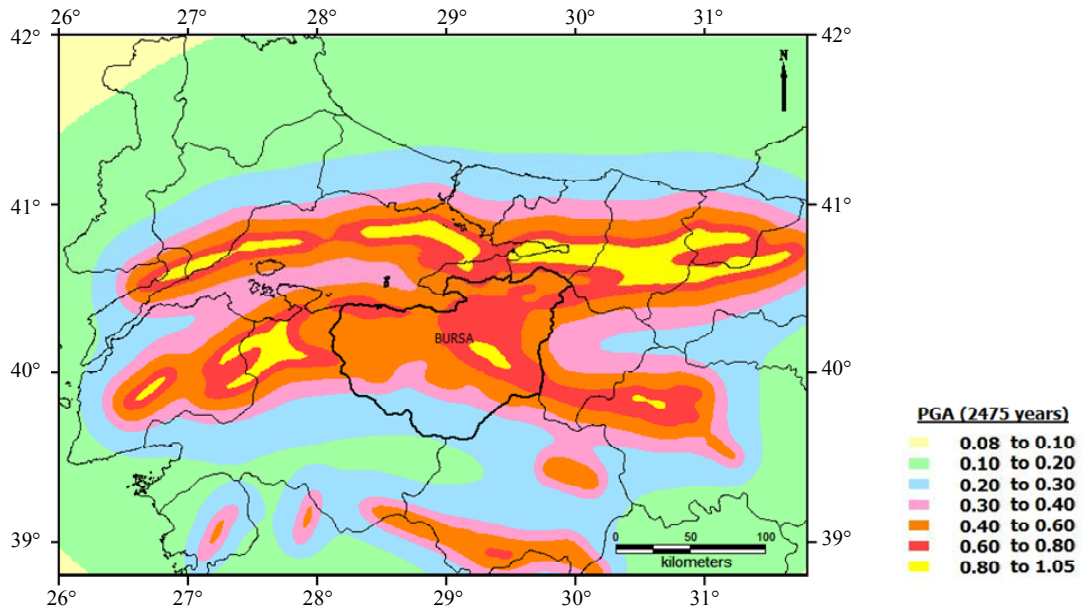
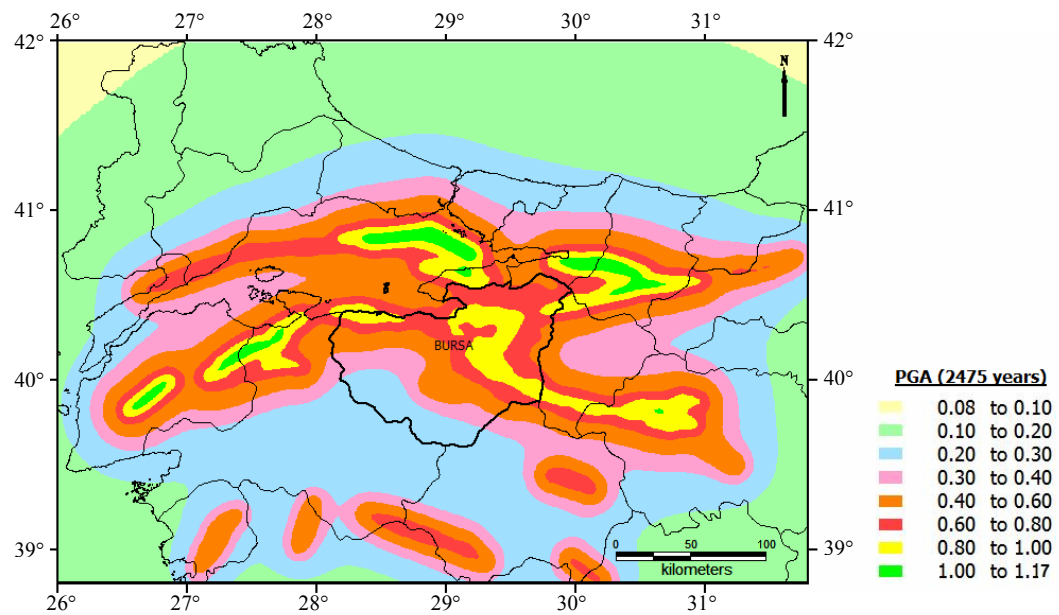


Figure 4.27 Seismic Hazard Map Obtained for PGA (in g) Corresponding to the Return Period of 1000 Years (5% Probability of Exceedance in 50 Years) by Considering Only Faults with (a) Poisson Model, (b) Renewal Model



(a)



(b)

Figure 4.28 Seismic Hazard Map Obtained for PGA (in g) Corresponding to a Return Period of 2475 Years (2% Probability of Exceedance in 50 Years) by Considering Only Faults with (a) Poisson Model, (b) Renewal Model

In order to visualize the spatial variation of differences between the PGA values obtained from Poisson and renewal models, the difference is calculated at each grid point in the region bounded by 26.0°- 31.8° E longitudes and 38.8°- 42.0° N latitudes by using the following equation;

$$\text{Difference}(\%) = \left(\frac{\text{PGA}_r - \text{PGA}_p}{\text{PGA}_p} \right) \times 100 \quad (4.16)$$

where PGA_r and PGA_p denote the PGA values estimated from renewal and Poisson models, respectively. The difference with negative sign (-) means that Poisson model gives higher PGA values than renewal model and that with positive sign represents the opposite case.

Figures 4.29 through 4.31 show the spatial variation of differences in PGA values obtained from renewal and Poisson models. It can be observed from these maps that the renewal model gives more than 25% higher PGA values than the Poisson model, especially at the regions where the faults have not produced characteristic earthquakes for a long period of time or date of the last characteristic earthquake is unknown (e.g. regions around F1, F7, F8, F9, F10, F48, namely Etili, Edincik, Akhisar, Kütahya, Kaymaz, Simav faults). On the other hand, the PGA values predicted by the renewal model are more than 25% lower than those of the Poisson model at the regions where the faults have ruptured and produced large magnitude, characteristic earthquakes short time before compared with their mean inter-event times (e.g. regions in the near vicinity of F13, F14, F55, F56, F57, F84, F87, F88, namely Karadere, Düzce, M.Kemalpaşa, Derecik, Yeniköy, Karamürsel, Gölcük, Körfez faults). It can be observed from Figures 4.29 and 4.30 that for Bursa province, the absolute values of the maximum positive and negative differences between the results obtained from the renewal and Poisson models are less than 55% and 65%, respectively.

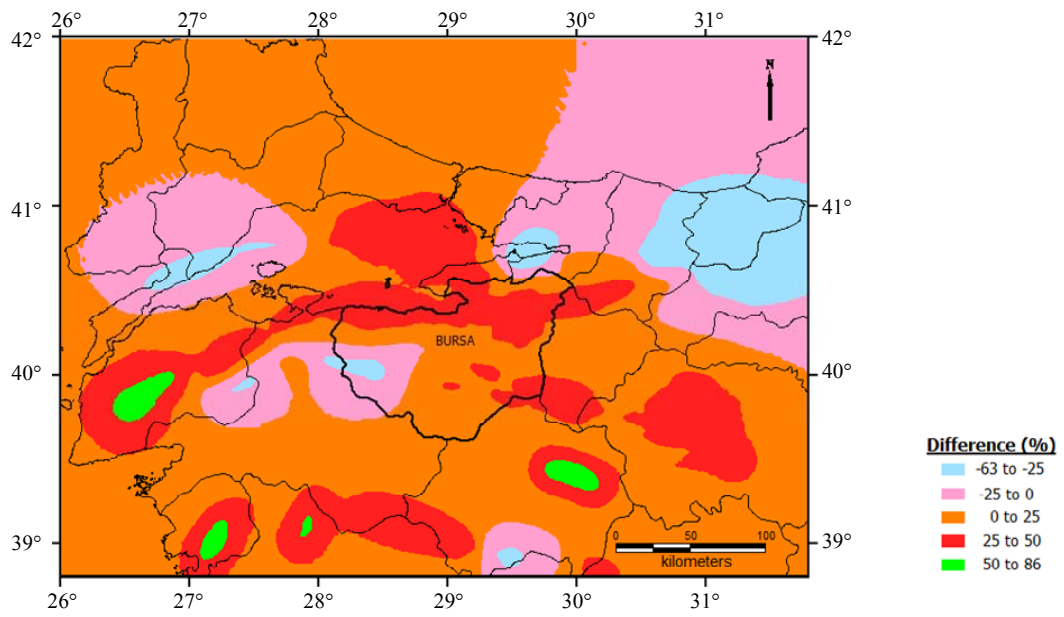


Figure 4.29 Map Showing the Spatial Variation of the Difference between the PGA Values Obtained from Renewal and Poisson Models for a Return Period of 475 Years

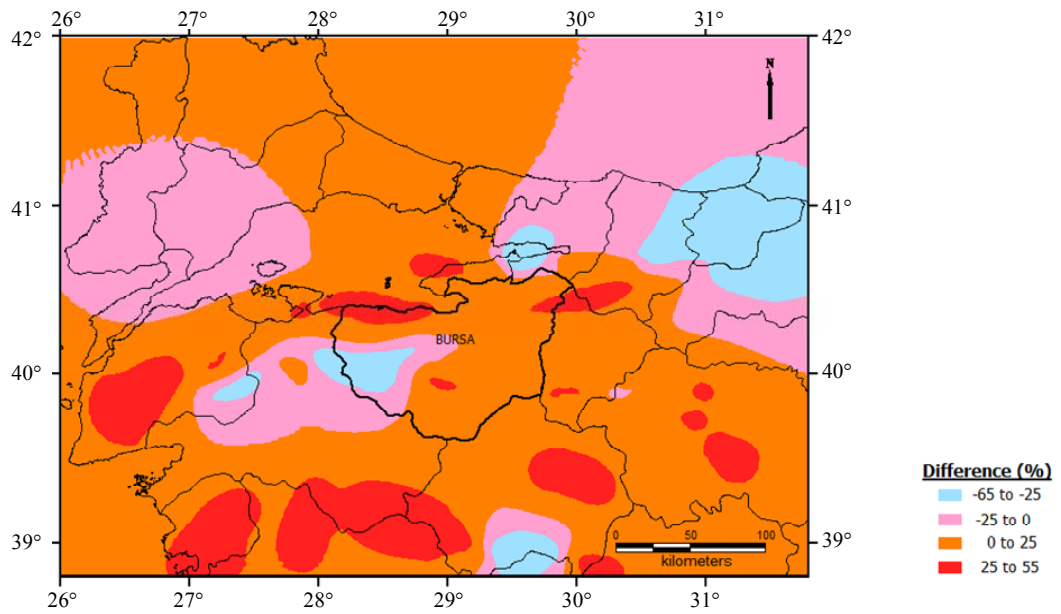


Figure 4.30 Map Showing the Spatial Variation of the Difference between the PGA Values Obtained from Renewal and Poisson Models for a Return Period of 2475 Years

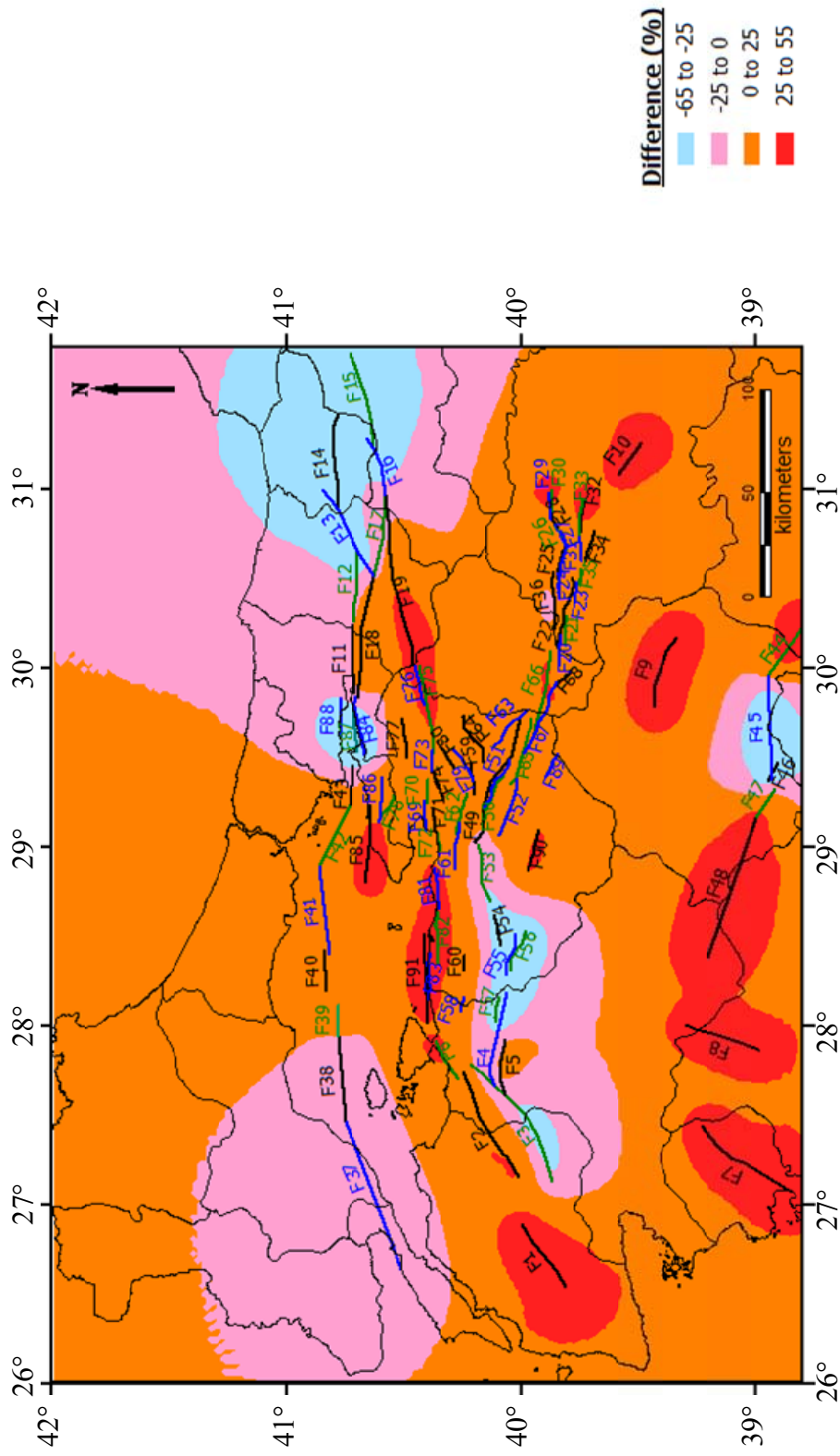


Figure 4.31 Map Showing the Spatial Variation of the Difference between the PGA Values Obtained from Renewal and Poisson Models for a Return Period of 2475 Years and Faults (Thick Black, Dark Blue, Dark Green Lines)

4.3.3 “Best Estimate” of Seismic Hazard for the Bursa Province

In the previous sections, different assumptions were made in the analyses carried out to calculate the contributions of background seismic activity and fault segments to seismic hazard. The results of these analyses are now aggregated through the use of the logic tree formulation by assigning subjective probabilities to the different assumptions and/or alternatives as displayed in Table 4.4. “Best estimate” seismic hazard curve as well as the contribution of different sources (i.e. background seismic activity and faults) to the seismic hazard for the site (40.24° N, 29.08° E) at the center of the city of Bursa are shown in Figure 4.32. It can be seen from this figure that contribution of background seismic activity to seismic hazard is significant at lower PGA values (i.e. less than 0.03g) that are generally of no interest from structural engineering point of view. For PGA values larger than 0.1g, faults contribute most of the seismic hazard at this site.

Table 4.4 Subjective Probabilities Assigned to Different Assumptions

Source	Alternatives	Subjective Probabilities
Background Seismic Activity	Uniform Seismicity	0.5
	Spatially Smoothed Seismicity	0.5
	The Whole Seismic Database	0.4
	Only Main Shocks	0.6
	Incomplete Seismic Database Artificially Completed Seismic Database	0.3 0.7
Faults	Poisson Model	0.3
	Renewal Model	0.7
Attenuation Relationship	Kalkan and Gülkan (2004)	0.5
	Boore et al. (1997)	0.5

Similarly, the results of seismic hazard analyses carried out at each grid point are aggregated to construct the “best estimate” seismic hazard maps for PGA and SA at 0.2 sec and 1.0 sec periods. Figures 4.33 through 4.41 show “best estimate” seismic

hazard maps for the Bursa province for PGA and SA (T=0.2 sec and 1.0 sec) corresponding to the return periods of 475, 1000 and 2475 years (10%, 2% and 5% probability of exceedances in 50 years, respectively).

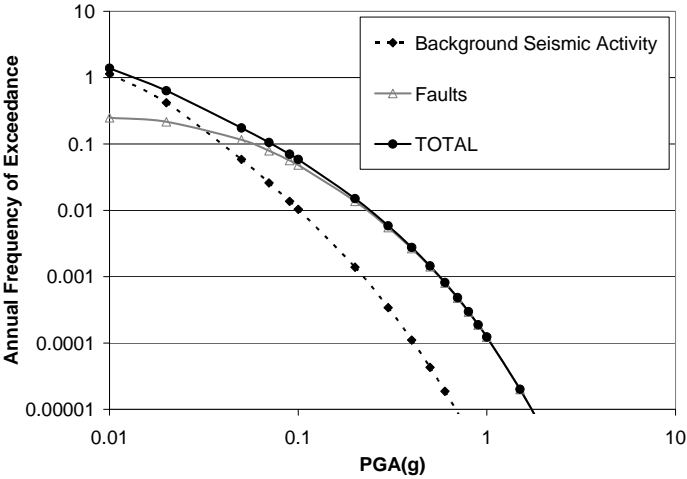


Figure 4.32 Seismic Hazard Curves Resulting from Background Seismic Activity and Faults and the “Best estimate” Seismic Hazard Curve for the Site (40.24° N, 29.08° E) at the City Center of Bursa

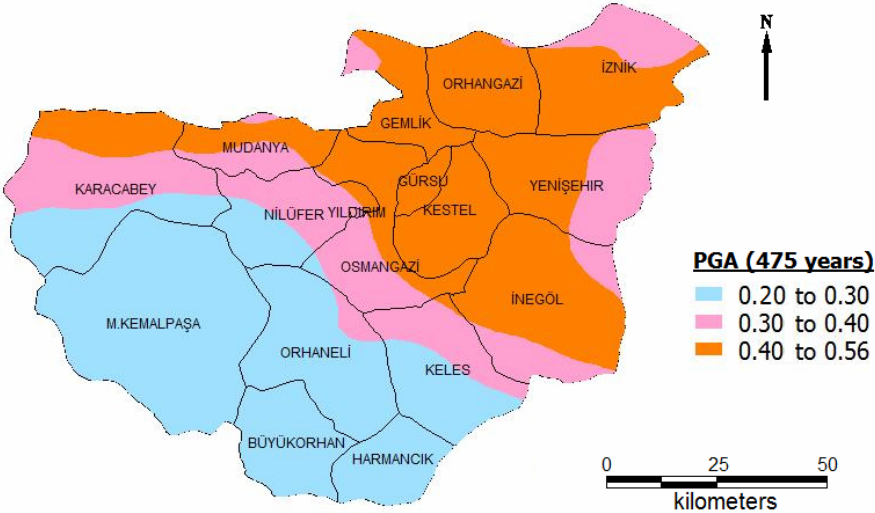


Figure 4.33 Best Estimate Seismic Hazard Map of Bursa Province for PGA (in g) Corresponding to the Return Period of 475 Years (10% Probability of Exceedance in 50 Years)

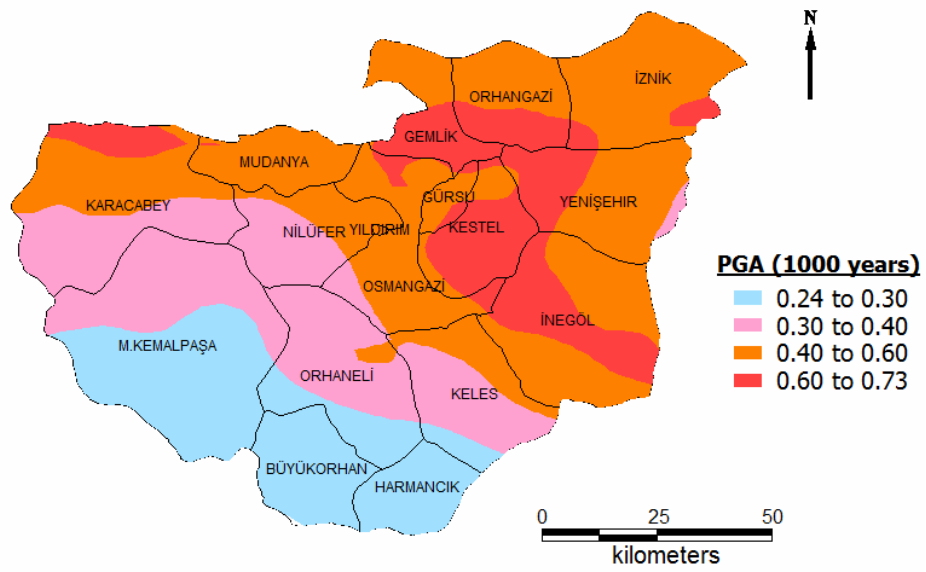


Figure 4.34 Best Estimate Seismic Hazard Map of Bursa Province for PGA (in g) Corresponding to the Return Period of 1000 Years (5% Probability of Exceedance in 50 Years)

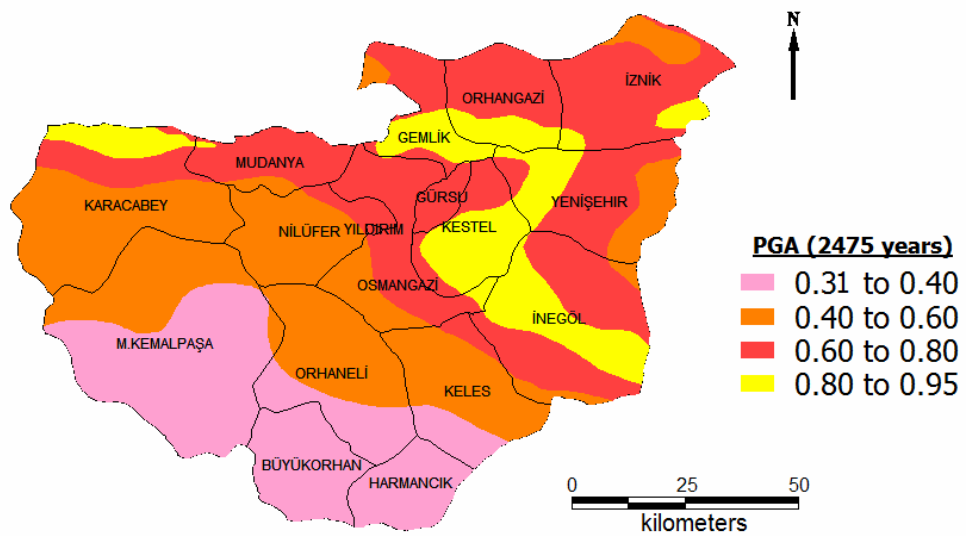


Figure 4.35 Best Estimate Seismic Hazard Map of Bursa Province for PGA (in g) Corresponding to the Return Period of 2475 Years (2% Probability of Exceedance in 50 Years)

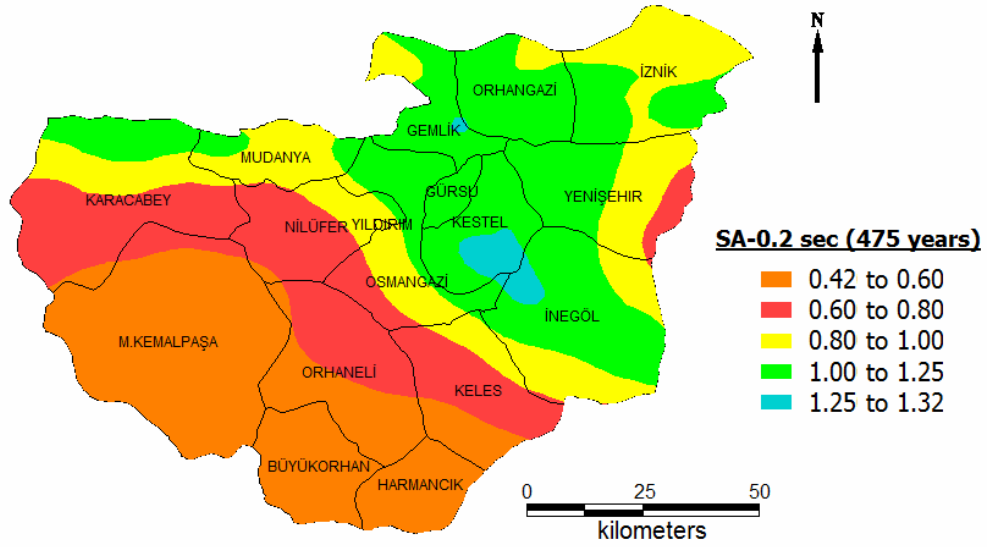


Figure 4.36 Best Estimate Seismic Hazard Map of Bursa Province for SA at 0.2 sec (in g) Corresponding to the Return Period of 475 Years (10% Probability of Exceedance in 50 Years)

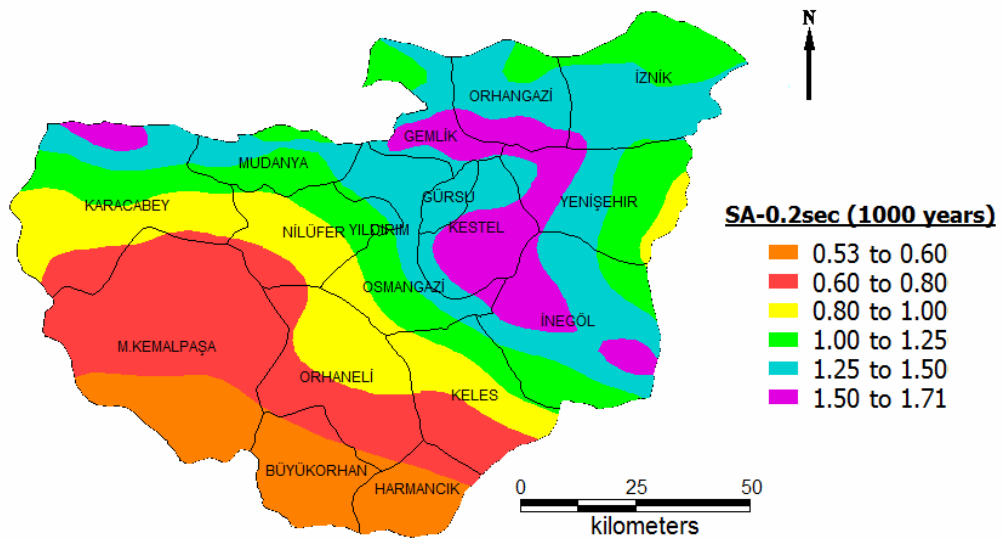


Figure 4.37 Best Estimate Seismic Hazard Map of Bursa Province for SA at 0.2 sec (in g) Corresponding to the Return Period of 1000 Years (5% Probability of Exceedance in 50 Years)

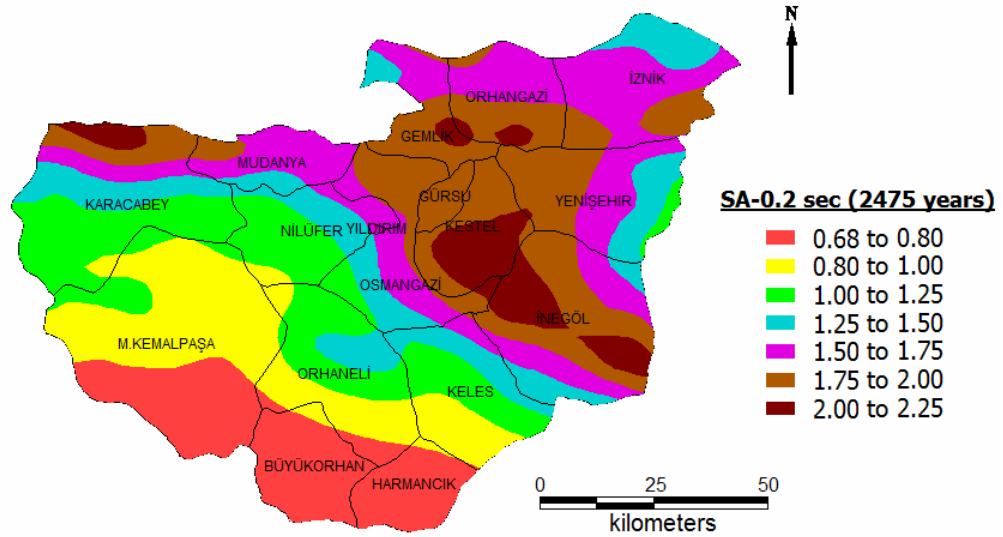


Figure 4.38 Best Estimate Seismic Hazard Map of Bursa Province for SA at 0.2 sec (in g) Corresponding to the Return Period of 2475 Years (2% Probability of Exceedance in 50 Years)

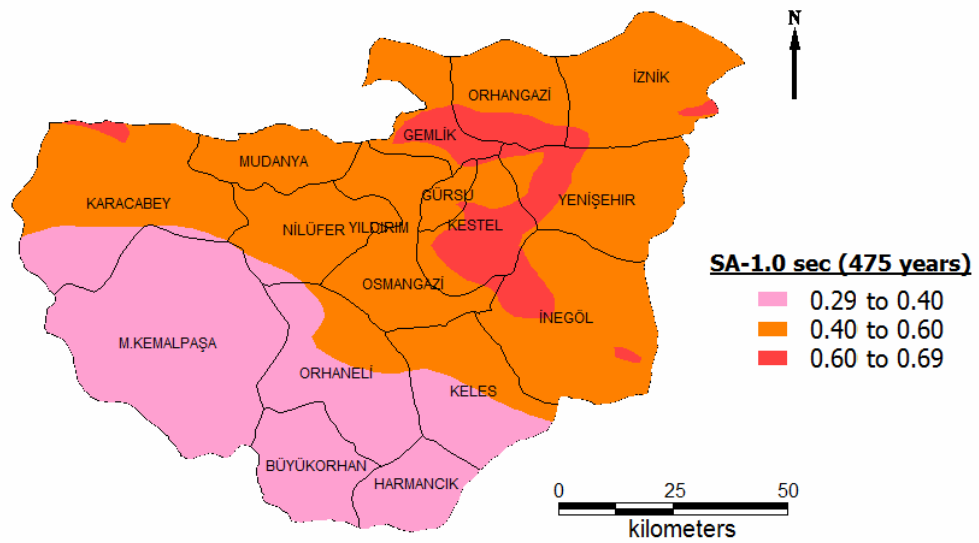


Figure 4.39 Best Estimate Seismic Hazard Map of Bursa Province for SA at 1.0 sec (in g) Corresponding to the Return Period of 475 Years (10% Probability of Exceedance in 50 Years)

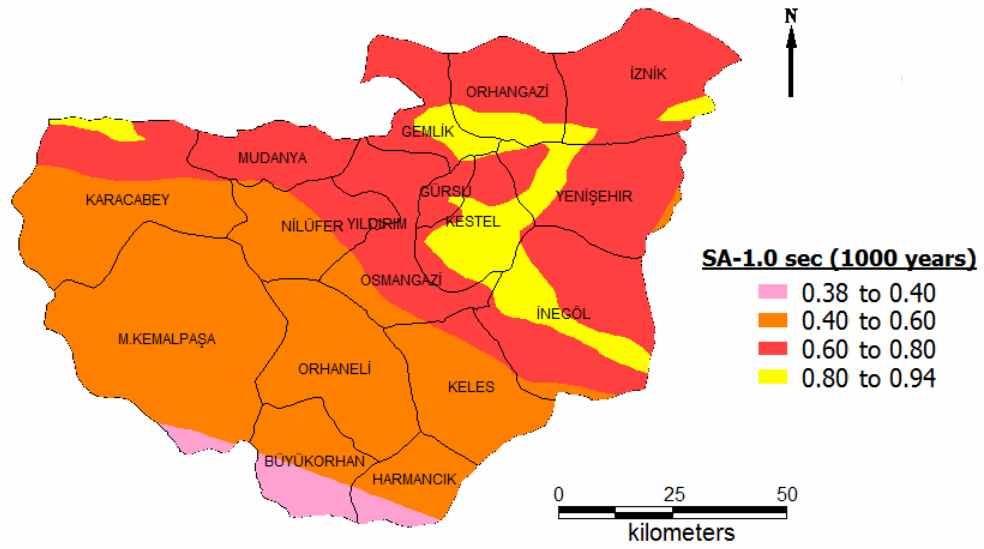


Figure 4.40 Best Estimate Seismic Hazard Map of Bursa Province for SA at 1.0 sec (in g) Corresponding to the Return Period of 1000 Years (5% Probability of Exceedance in 50 Years)

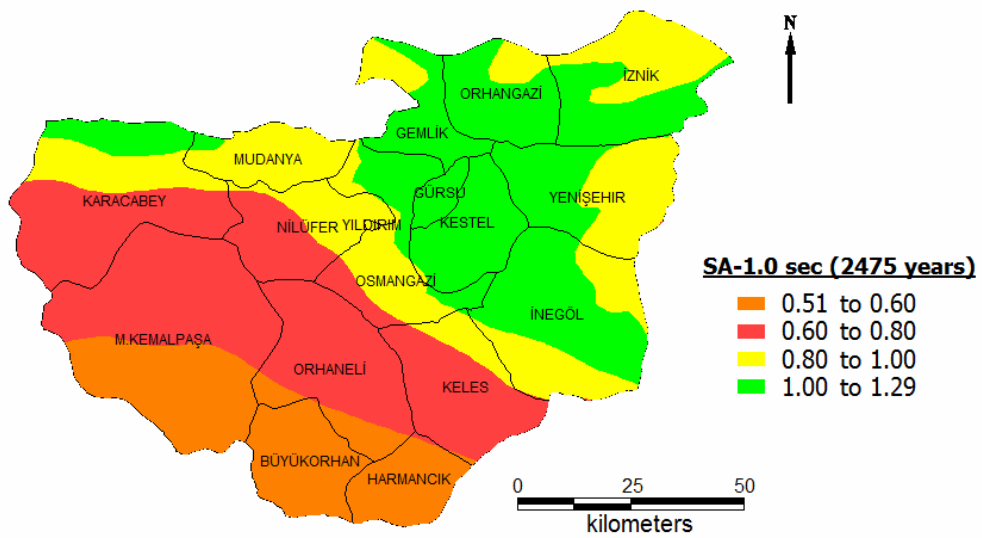


Figure 4.41 Best Estimate Seismic Hazard Map of Bursa Province for SA at 1.0 sec (in g) Corresponding to the Return Period of 2475 Years (2% Probability of Exceedance in 50 Years)

Figure 4.42 shows the seismic hazard map in terms of PGA values corresponding to a 475 years return period constructed by Yüçemen et al. (2006) for Bursa city center and its near vicinity. For the purpose of comparison of this map with the corresponding best estimate seismic hazard map constructed in this study, the Bursa province is cropped out and redrawn as given in Figure 4.43 (a). Since the minimum and maximum PGA value estimated by Yüçemen et al. (2006) for the Bursa province are 0.2 and 0.62, the legend that shows the range of PGA values is modified. Figure 4.43 (b) shows the best estimate seismic hazard map obtained in this study for the Bursa province. It should be noted that the legend displayed in Figure 4.43 (b) is different from the one given in Figure 4.33, because it is modified to enable a direct comparison of results obtained in this study with those obtained by Yüçemen et al. (2006). Comparison of the seismic hazard map shown in Figure 4.43 (a) with that given in Figure 4.43 (b) shows that the PGA values predicted in this study are very close to those obtained in the study of Yüçemen et al. (2006). Smaller PGA values at the regions between Kestel and İnegöl towns are predicted in this study than those given by Yüçemen et al. (2006). This difference could be due to the fact that in this study Bursa fault is assumed to be ruptured during the 1855 earthquake. Therefore, the probability of occurrence of future characteristic earthquakes produced by this fault is decreased according to the renewal model. Additionally, Yüçemen et al. (2006) predicted higher PGA values at the region in M.Kemalpaşa Town. This may be explained by the assumption made in this study that M.Kemalpaşa and Derecik faults ruptured during the 1964 earthquake. Figure 4.43 (c) shows the current regulatory earthquake zoning map for Bursa. In this map, the PGA values are predicted to be larger than 0.4g are displayed as 1st degree and those between 0.3g and 0.4g are as 2nd degree earthquake zone. Compared to the seismic hazard map obtained in this study, a different pattern is observed for the distribution of PGA values in this map. This difference may be due to differences in the seismic source models, earthquake occurrence models and the attenuation relationships used in these studies. Current regulatory earthquake zoning map was prepared based on the study conducted by Gülkan et al. (1993). They used area sources to model the seismic activities related to the main fault zones. The northern

part of Bursa is located in the area source used for the description of the seismic activity in and near vicinity of Marmara and North Aegean. Therefore, this source has the most significant influence on the spatial distribution of PGA values in the Bursa province.

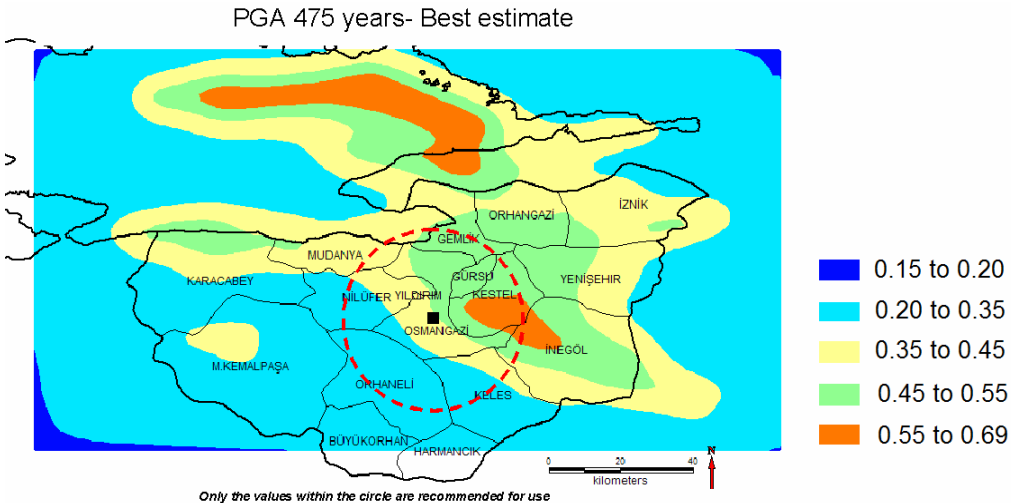
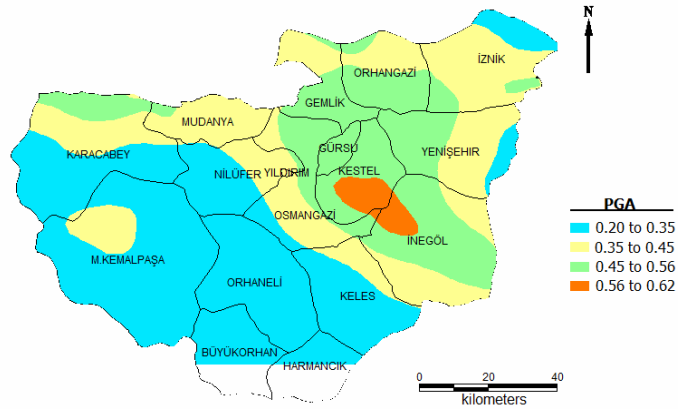
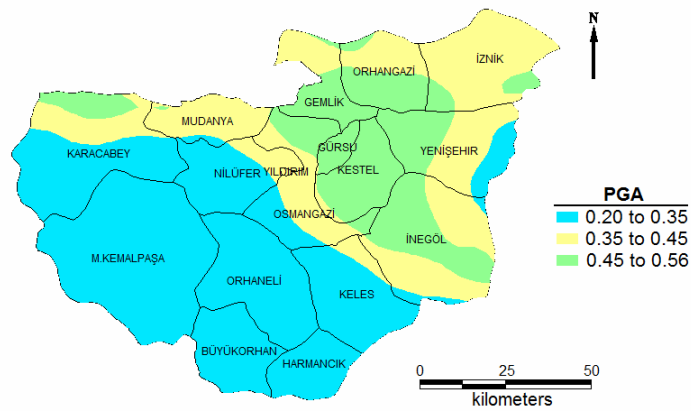


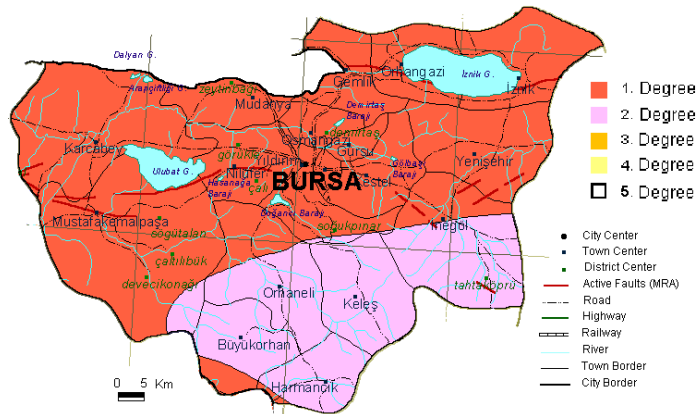
Figure 4.42 Seismic Hazard Map Obtained by Yüçemen et al. (2006) for PGA Corresponding to the Return Period of 475 Years (10% Probability of Exceedance in 50 Years)



(a)



(b)



(c)

Figure 4.43 Seismic Hazard Maps for Bursa Province for PGA Corresponding to the Return Period of 475 Years (10% Probability of Exceedance in 50 Years) Constructed from the Results of (a) the Study Conducted by Yüçemen et al. (2006) (Values are given in terms of g), (b) This Study (Values are given in terms of g); (c) Current Regulatory Earthquake Zoning Map for Bursa (Özmen et al., 1997)

CHAPTER 5

SUMMARY AND CONCLUSIONS

5.1 SUMMARY

In this study, the sensitivity of seismic hazard results to the different models used with respect to seismic source description, magnitude distribution, earthquake occurrence in time and the type of attenuation relationship is investigated, taking also into consideration the uncertainties associated with these models.

First, the differences in deterministic and probabilistic seismic hazard analyses approaches are presented with an illustrative example where a site under the threat of a single fault is considered. Then, effects of uncertainties involved in the attenuation relationship and alternative assumptions on source modeling, magnitude distribution and earthquake occurrences in time to the probabilistic seismic hazard analysis results are investigated for a number of sites. The results were discussed and a number of recommendations are presented for those who will carry out probabilistic seismic hazard analysis.

Two case studies were carried out for a large (a country) and a smaller region (a province) based on real data in order to examine the influence of different assumptions and/or models to the probabilistic seismic hazard results. These two case studies also serve for the purpose of illustration of the actual implementation of the different models and assumptions for seismic source description (line or area), background seismic activity (background area source with uniform seismicity or spatially smoothed seismicity model), magnitude distribution (exponential, characteristic earthquake model proposed by Youngs and Coppersmith (1985) or maximum magnitude model) and earthquake occurrence in time (Poisson or

renewal). In this respect, the application of the logic tree method which is utilized to combine the results of alternative assumptions and compensate for the epistemic uncertainties is also demonstrated.

5.2 DISCUSSION OF RESULTS AND MAIN CONCLUSIONS

In this section, the results obtained from the case studies carried out in this study are briefly discussed and the main conclusions drawn based on these results are presented.

- The seismic hazard results obtained from both deterministic and probabilistic seismic hazard analyses methodologies are observed to be sensitive to the choice of the attenuation relationship (ground motion prediction equation) as well as the variability of ground motion around the mean prediction curve. This observation is consistent with other similar studies (e.g. Sabetta et al., 2005). In view of this observation, special attention should be paid to the choice of the attenuation relationships to be included in the logic tree method.
- The uncertainty in the ground motion parameter at a specified magnitude and distance levels is represented by a lognormal distribution. For very long return periods, the tail of this distribution governs the seismic hazard estimates. In order to eliminate estimation of physically impossible higher ground motion values in such extreme cases, the distribution should be truncated at some upper bounds. Truncation of attenuation residuals and the bound at which truncation is made affects the seismic hazard results at low annual probabilities of exceedance. This observation is consistent with other similar studies (e.g. Bommer et al., 2004).
- Fault-rupture, segmentation and cascade models are used for the spatial distribution of earthquakes along the line (fault) seismic sources. In the fault-rupture model, empirical equations are used to estimate the rupture

length for a specified magnitude. There is a certain degree of uncertainty in the rupture length estimated from these relationships. Inclusion of this uncertainty results in higher seismic hazard values for higher ground motion parameter levels at the sites located near the central portions of the fault considered in this study. The effect of rupture length uncertainty on seismic hazard results decreases as the closest distance to the fault increases. In addition, increase in standard deviation of the logarithm of rupture length results in higher exceedance probabilities at higher ground motion parameter levels at the site which is found to be most sensitive to the uncertainty in rupture length. Cascade model gives higher exceedance probabilities than segmentation model at higher ground motion parameter levels whereas segmentation model results in higher values at lower ground motion parameter levels.

- For the case that only large magnitude events are taken into consideration, modeling a fault as a narrow area source (say of 5 km width) results in lower seismic hazard values than fault (line) source representation of the faults at the sites near the center of the fault, as expected.
- Line (fault) source model with exponential magnitude distribution may give higher seismic hazard values than the area source model. Higher differences are concentrated at the regions along and near vicinity of line sources. On the other hand, modeling faults having low annual activity rates as area sources may cause an increase in seismic hazard values at the regions near the boundaries of area sources compared to line source representation of faults.
- Based on the same seismicity parameters (i.e., ν and β), use of characteristic earthquake model proposed by Youngs and Coppersmith (1985) yields higher seismic hazard results than the classical truncated exponential distribution for the line (fault) source model. Additionally, lumping the rates

uniformly distributed over characteristic magnitudes in the characteristic earthquake model totally to the maximum magnitude together with exponentially distributed magnitudes for smaller magnitude earthquakes, gives higher seismic hazard results, as expected.

- In the renewal model, the date of the last characteristic earthquake occurred on the faults are used to compute the probability or equivalent mean rate of occurrence of characteristic earthquakes. For the case that no information is available on this date, different equations are proposed by Wu et al. (1995) to compute the mean rate of characteristic earthquakes. For the Brownian Passage Time model, with aperiodicity value of 0.5, the mean rates of characteristic earthquakes calculated by the equations proposed for which date of last characteristic earthquake is known and unknown are observed to approach each other, for the time period which is some multiples of mean inter-event time. In cases where the date of last characteristic earthquake is unknown, the analyst could calculate the rates of characteristic earthquake from these two equations. When there is no significant difference between these two values, it is not necessary to spend extra effort to make detailed investigations for evaluating the date of last characteristic earthquake.
- For background seismic activity, the use of spatially smoothed seismicity model or the alternative background area source with uniform seismicity affects the results. For the case studies carried out for Jordan and Bursa, it is observed that spatially smoothed seismicity model gives higher seismic hazard values at the regions where the epicenters of earthquakes cluster. On the other hand, nearly a spatially uniform hazard distribution is obtained from the seismic hazard analyses carried out by using a background area source with uniform seismicity. Therefore, background area source model with uniform seismicity is expected to give higher seismic hazard values compared to the spatially smoothed seismicity model at the sites located far away from clustering regions of past earthquake epicenters; i.e. where the

epicenters of earthquakes are scarce or no earthquakes have occurred in the past. In both models, seismicity parameters are determined from the earthquake catalogs. In addition, the information given in the earthquake catalogs (year, location of epicenter, depth and magnitude) are one of the main inputs of the code developed for the computation of seismic hazard by using spatially smoothed seismicity model by Frankel et al. (1996). The analyses carried out for the background seismic activity by using both spatially smoothed seismicity model of Frankel (1995) and a background area source with uniform seismicity with different combinations of assumptions on earthquakes in the catalog with respect to completeness and dependence yield different seismic hazard values. Therefore, the validity of the results obtained for background seismic activity depends on the reliability of the earthquake catalog compiled, the method used to identify main shocks and completeness of the catalog with respect to small magnitude earthquakes.

- The use of the maximum magnitude model for faults combined with spatially smoothed seismicity model for background seismic activity and characteristic earthquake model proposed by Youngs and Coppersmith (1985) may yield different seismic hazard results depending on the spatial distribution of past earthquakes and the activity rates assigned to the maximum magnitude. In cases where the period of available earthquake catalog is not long enough to predict the frequency of maximum magnitude earthquake and paleoseismicity data is not available, the activity rates of the maximum magnitude earthquakes can be calculated by using the maximum magnitudes, rupture areas and slip rates based on seismic moment balancing concept. Characteristic earthquake model proposed by Youngs and Coppersmith (1985) may give higher seismic hazard results in regions where the activity rates of maximum magnitude earthquakes of faults are lower than the rates assigned to characteristic events in the characteristic earthquake model and also a gap exists between the upper bound magnitude

of background seismic activity and the maximum magnitude earthquake of faults.

- Considering the stochastic characteristics of the memoryless Poisson model and the time-dependent renewal model, it is expected that seismic hazard results will differ if temporal data for the past seismic activity is taken into consideration. The main factors that create this difference are the time passed from the last characteristic earthquake and the inter-event time distribution of the characteristic earthquakes. For the case study carried out for Bursa province, it is observed that the renewal model gives higher seismic hazard values than the Poisson model at the regions where the faults have not produced characteristic earthquakes for a long period of time with respect to their mean-inter-event times. On the other hand, the seismic hazard values predicted by the Poisson model are greater than those of the renewal model at the regions where the faults have ruptured and produced large magnitude, characteristic earthquakes short time before, compared with their mean inter-event times.
- The results obtained by using different assumptions and models can be combined by employing the logic tree method in order to incorporate the effects of epistemic uncertainties into the probabilistic seismic hazard estimates. Since the final result depends on the subjective probabilities assigned to different alternatives as well as the alternatives taking place in the logic tree, extreme care should be paid to the process of assigning these probabilities and selection of the appropriate alternatives. In this respect expert opinion plays an important role.
- The current trend in probabilistic seismic hazard analysis is to give priority to the assessment of hazard stemming from the faults. This requires the appropriate modelling of faults as well as using the proper parameters. The case studies carried out in this study show that the modeling of faults by area sources may underestimate seismic hazard especially in the near vicinity of

faults. Besides, appropriate magnitude distribution and earthquake occurrence models consistent with characteristics of faults should be used, since the results are dependent on these assumptions. These observations justify the importance of basing the seismic hazard studies on faults with properly assessed parameters. The assessment of the fault parameters requires time and money especially for large regions like a country. Accordingly, in cases of time and money limitations hazard studies can be carried out on a region and/or province scale, giving priority to high risk areas.

5.3 RECOMMENDATIONS FOR FUTURE STUDIES

In order to improve the results obtained in this dissertation, following recommendations should be taken into consideration in future studies and research:

- In seismic hazard analysis, regional attenuation relationships (ground motion estimation equations) derived based on the regional tectonic settings of the region considered should be used. The derivation of a regional attenuation relationship depends on the availability of ground motion data recorded from the past earthquakes occurred in the region. Therefore, attempts should be made to increase the number of stations and derive local attenuation relationships based on the data recorded at the stations located in the region considered.
- Earthquake waves propagate with different characteristics in the directions parallel and perpendicular to fault rupture. Therefore, the direction of fault rupture can affect the ground motion. The effect of rupture directivity can be incorporated into seismic hazard analysis through modifications of the attenuation relationships. In this study, this effect is not considered in seismic hazard estimations. The sensitivity of seismic hazard results to this effect can be investigated in future studies.

- Earthquake catalogs are one of the main components of probabilistic seismic hazard analysis. They should be completed with respect to smaller magnitude earthquakes as well as distinction should be made with respect to main shocks and secondary events (i.e. fore- and after shocks). Unfortunately, all events, including fore- and after shocks are reported in these catalogs, without identifying their categories (main shocks or secondary events). In this study, the procedure described by Deniz (2006) is applied to identify the main shocks. The results obtained for the case studies carried out in this study can be validated and improved by using more reliable and complete earthquake catalogs and different main shock identification methods.
- While utilizing the spatially smoothed seismicity model of Frankel (1995) in the calculation of background seismic activity, the spatial correlation distance is assumed as 50 km in the case studies. This value should be compared with the epicentral uncertainty associated in the location of the past earthquakes that occurred in the region considered for Bursa and Jordan, separately.
- In the case study carried out for the seismic hazard assessment of Jordan, the activity rates of maximum magnitude earthquakes of faults were calculated from the geometry of the faults (length and width), their slip rates and maximum magnitudes. In order to improve the results, investigations should be carried out to obtain these parameters for each segment separately. In addition, Poisson model is used to predict the probability of future earthquake occurrences. This model can be replaced by the renewal model, if data on the recurrence intervals and other parameters used in the renewal model can be obtained, especially for the main active faults, like Dead Sea-Jordan River.

- In the case study carried out for the seismic hazard assessment of Bursa province, the maximum magnitude of faults are generally estimated from their lengths based on empirical relationships. Therefore, different segmentation models results in different maximum magnitude values. The results obtained from alternative segmentation models can be combined by using the logic tree method.
- In the two case studies, the weights given to alternative models and/or assumptions in the calculation of “best estimate” seismic hazard values are all subjective. Different weights could be based on the opinion of experts who have familiarity with the seismicity and tectonic structure of the region considered.
- In this study, sensitivity of seismic hazard results to the statistical procedure used to assess the values of the seismicity parameters of the seismic sources is not investigated. Regression analysis is applied in the determination of the slope of the Gutenberg-Richter magnitude recurrence relationship. Other statistical techniques, such as the maximum likelihood method, can be applied to assess the values of the seismicity parameters in future studies.
- The cascade model can be applied for the estimation of seismic hazard for Bursa if detailed information is obtained for identifying the possible multi-segment rupture of the faults considered in the study.
- In this study, local site conditions are not taken into consideration and all ground motion parameters are predicted assuming rock site conditions. The site condition should be considered in future studies.

REFERENCES

Abrahamson N. A. and Silva W. J. (1997). Empirical Response Spectral Attenuation Relations for Shallow Crustal Earthquakes, *Seismological Research Letters*, Vol. 68, No. 1, pp. 94-127.

Aki K. (1966). Generation and Propagation of G-waves from the Niigata Earthquake of June 16,1964, *Bull. Earthq. Res. Inst.*, Vol. 44, pp. 23-88.

Algermissen S. T., Perkins D. M., Isherwood W., Gordon D., Reagor B.G. and Howard C. (1976). Seismic Risk Evaluation of the Balkan Region, *Proceedings of the Seminar on Seismic Zoning Maps*, Vol. 2, Skopje, Yugoslavia, pp. 172-240.

Al-Tarazi E. (1992). *Investigation and Assessment of Seismic Hazard in Jordan and Its Vicinity*, Unpublished Ph.D. Thesis, Ruhr University, Bochum, Germany, 194 pp.

Al-Tarazi E. and Sandvol E. (2007). Alternative Models of Seismic Hazard Evaluation along the Jordan–Dead Sea Transform, *Earthquake Spectra*, Vol. 23, No. 1, pp. 1-19.

Ambraseys N. N. (2001). Reassessment of Earthquakes, 1900-1999, in the Eastern Mediterranean and the Middle East, *Geophysical Journal International*, Vol. 145, pp. 471-485.

Ambraseys N. N. (2006). Comparison of Frequency of Occurrence of Earthquakes with Slip Rates from Long-Term Seismicity Data: the Cases of Gulf of Corinth, Sea of Marmara and Dead Sea Fault Zone, *Geophysical Journal International*, Vol. 165, pp. 516-526.

Ambraseys N. N. and Jackson J. A. (1998). Faulting Associated with Historical and Recent Earthquakes in the Eastern Mediterranean Region, *Geophysical Journal International*, pp. 390-406.

Ambraseys N. N. and Jackson J. A. (2000). Seismicity of the Sea of Marmara (Turkey) since 1500, *Geophysical Journal International*, Vol. 141, F1-F6.

Ambraseys N. N., Simpson K. A. and Bommer J. J. (1996). Prediction of Horizontal Response Spectra in Europe, *Earthquake Engineering and Structural Dynamics*, Vol. 25, pp. 371- 400.

Awata Y., Yoshioka T., Emre Ö., Duman T. Y., Doğan A., Tsukuda E., Okamura M., Matsuoka H., Kuşçu İ. (2003). Outline of the Surface Rupture of 1999 İzmit Earthquake, *Surface Rupture Associated with the August 17, 1999 İzmit Earthquake*, Special Publication Series 1, General Directorate of Mineral Research and Exploration, Ankara, pp. 41-50.

Aydan Ö. (1997). *The Seismic Characteristics and the Occurrence Pattern of Turkish Earthquakes*, Turkish Earthquake Foundation, Report No. TDV/TR 97-007, 41 pp.

Aydan Ö. (2001). Comparison of Suitability of Submerged Tunnel and Shield Tunnel for Subsea Passage of Bosphorus, (in Turkish), *Geological Engineering Journal of Turkey*, Vol. 25, No. 1, pp. 1-17.

Aydan Ö., Sezaki M., Yazar R. (1996). The Seismic Characteristics of Turkish Earthquakes, *Eleventh World Conference on Earthquake Engineering*, Acapulco, Mexico, CD, paper no. 1025.

Aydan Ö., Kumsar H. and Ulusay R. (2001). How to Infer the Possible Mechanism and Characteristics of Earthquakes from the Striations and Ground Surface Traces of Existing Faults, *Seismic Fault Induced Failures*, pp. 161-170.

Barani S., Spallarossa D., Bazzurro P., Eva C. (2007). Sensitivity Analysis of Seismic Hazard for Western Liguria (North Western Italy): A First Attempt towards the Understanding and Quantification of Hazard Uncertainty, *Tectonophysics*, Vol. 435, pp. 13-35.

Barazangi M. (1983). A Summary of the Seismotectonic of the Arab Region, *Assessment and Mitigation of Earthquake Risk in the Arab Region*, UNESCO, pp. 43-58.

Batayneh J. S. F. (1994). *Seismic Assessment and Evaluation of Earthquake Hazard in Major Cities in Jordan*, Unpublished M.S. Thesis, Jordan University of Science and Technology, Irbid, Jordan, 130 pp.

Ben-Avraham Z. (1985). Structural Framework of the Gulf of Elat (Aqaba), Northern Red Sea, *J.Geophys. Res.*, Vol. 90, pp. 703–726.

Bender F. (1974). *Geology of Jordan*, Gebrtider Borntraeger, Berlin.

Bender B. (1984). Seismic Hazard Estimation Using A Finite-Fault Rupture Model, *Bulletin of the Seismological Society of America*, Vol.74, No.5, pp.1899-1923.

Bender B. (1986). Modeling Source Zone Boundary in Seismic Hazard Analysis, *Bulletin of the Seismological Society of America.*, Vol. 76, No. 2, pp. 329-341.

Bender B. and Perkins D. (1982). *SEISRISK II. A Computer Program for Seismic Hazard Estimation*, U.S. Geological Survey, Open File Report: 82-293.

Bender B. and Perkins D. (1987) *SEISRISK III: A Computer Program for Seismic Hazard Estimation*, U.S. Geological Survey Bulletin 1772.

Ben-Menahem A. (1979). Earthquake Catalogue for the Middle East (92 B.C-1980 A.D.), *Boll. Geofis. Teor. Appl.*, Vol. 21, No. 81, pp. 245-293.

Ben-Menahem A. (1981). A Seismicity Cycle of 1500 Years on the Dead Sea Rift, *Boll. Geofis. Teor. Appl.*, Vol. 22, No. 92, pp. 349-354.

Bonilla M. G., Mark R. K., Lienkaemper J. J. (1984). Statistical Relations Among Earthquake Magnitude, Surface Rupture Length, and Surface Fault Displacement, *Bulletin of the Seismological Society of America*, Vol.74, No.6, pp. 2379-2411.

Bommer J. J., Abrahamson N. A., Strasser F. O., Pecker A., Bard P.-Y., Bungum H., Cotton F., Fäh D., Sabetta F., Scherbaum F. and Studer J. (2004). The Challenge of Defining Upper Bounds on Earthquake Ground Motions, *Seismological Research Letters*, Vol. 75, No. 1, pp. 82-95.

Boore D. M., Joyner W. B. and Fumal T. E. (1997). Equations for Estimating Horizontal Response Spectra and Peak Acceleration from Western North American Earthquakes: A Summary of Recent Work, *Seismological Research Letters*, Vol. 68, No. 1, pp. 128-153.

Brillinger D. R. (1982). Some Bounds for Seismic Risk, *Bulletin of the Seismological Society of America*, Vol. 72, No. 4, pp. 1403-1410.

Campbell K. W. (1997). Empirical Near-Source Attenuation Relationships for Horizontal and Vertical Components of Peak Ground Acceleration, Peak Ground Velocity, and Pseudo Absolute Acceleration Response Spectra, *Seismological Research Letters*, Vol. 68, No. 1, pp. 154-179.

Chiang W-L., Guidi G. A., Mortgat C. P., Schoof C. C. and Shah H. C. (1984). *Computer Program for Seismic Hazard Analysis. A User Manual (Stanford Seismic Hazard Analysis-STASHA)*, Report No. 62, The J. A. Blume Earthquake Engineering Center, Stanford University.

Christian J. T., Borjeson R. W. and Tringale P. T. (1978). Probabilistic Evaluation of OBE for Nuclear Plant, *Journal of Geotechnical Engineering Division*, ASCE, Vol. 104, GT7.

Coburn A.W. and Kuran U. (1985). *Emergency Planning and Earthquake Damage Reduction for Bursa Province: A Preliminary Report on Seismic Risk*, (in Turkish), The Ministry of Public Works and Settlement, General Directorate of Disaster Affairs, Earthquake Research Department, Ankara, Turkey.

Cornell C. A. (1968). Engineering Seismic Risk Analysis, *Bulletin of the Seismological Society of America*, Vol. 58, No. 5, pp. 1583-1606.

Cornell C. A. (1971). *Probabilistic Analysis of Damage to Structures Under Seismic Load, Dynamic Waves in Civil Engineering*, J. Wiley and Sons, N.Y.

Cornell C. A. and Merz H. A. (1974). *A Seismic Risk Analysis of Boston*, M.I.T., Department of Civil Engineering, Research Report, R 74-2.

Cramer C.H., Petersen M. D., Cao T., Topozada T. R., Reichle M. (2000). A Time-Dependent Probabilistic Seismic-Hazard Model for California, *Bulletin of the Seismological Society of America*, Vol.90, No.1, pp.1-21.

Deniz A. (2006). *Estimation of Earthquake Insurance Premium Rates for Turkey*, M.Sc. Thesis, Department of Civil Engineering, METU.

Deniz A. and Yucemen M. S. (2005). Assessment of Seismic Hazard for the Antalya Region Using Stochastic Methods, (in Turkish), *Proceedings, Congress on the Civil Engineering Problems of the Antalya Region*, pp. 540-551.

Dobbs R. (2008). Personal communication, e-mail correspondence, Risk Engineering Inc., Colorado.

Ellsworth W. L., Matthews M. V., Nadeau R. M., Nishenko S. P., Reasenber P. A. and Simpson R. W. (1999). *A Physically-Based Earthquake Recurrence Model for Estimation of Long-Term Earthquake Probabilities*. U.S. Geological Survey, Open-File Report: 99-522.

Emre O. and Awata Y. (2003). Neotectonic Characteristics of the North Anatolian Fault System in the Eastern Marmara, *Surface Rupture Associated with the August 17, 1999 İzmit Earthquake*, Special Publication Series 1, General Directorate of Mineral Research and Exploration, Ankara, pp.31-39.

ERD-GDDA (2007). Internet page of the Earthquake Research Department, General Directorate of Disaster Affairs, Turkish Republic, The Ministry of Public Works and Settlement, <http://sismo.deprem.gov.tr>, last accessed date: 20 December 2007.

Erdik M., Demircioğlu M., Sesetyan K., Durukal E. and Siyahi B. (2004). Earthquake Hazard in Marmara Region, Turkey, *Soil Dynamics and Earthquake Engineering*, Vol. 24, pp. 605-631.

Erentöz, C. and Kurtman, F. (1964). Report on 1964 Manyas Earthquake, *Bulletin of the Mineral Research and Exploration Institute of Turkey*, No. 63, pp.1-5.

Esteva L. (1970). Seismic Risk and Seismic Design Decisions, in *Seismic Design for Nuclear Power Plants*, Ed. Hansen, R. J., MIT Press, Cambridge, Mass.

Esteva L. and Villaverde R. (1973). Seismic Risk, Design Spectra and Structural Reliability, *Proc. 5th World Conference on Earthquake Engineering*, Rome, Italy.

Fahmi K. J., Husein Malkawi I. and Al-Zoubi O. Y. (1996). Seismic Engineering Ground Motion Maps for Jordan Employing Local Attenuation Relations, *Environmental and Engineering Geosciences*, Vol. II, No. 1, pp. 23-33.

Frankel A. (1995). Mapping Seismic Hazard in the Central and Eastern United States, *Seismological Research Letters*, Vol. 66, No.4, pp. 8-21.

Frankel A., Mueller C., Barnhard T., Perkins D., Leyendecker E., Dickman N., Hanson S. and Hopper M. G. (1996). *National Seismic-Hazard Maps: Documentation*, U.S. Geological Survey, Open-File Report: 96-532.

Gupta I.D (2002). The State of the Art in Seismic Hazard Analysis, *ISSET Journal of Earthquake Technology*, Vol. 39, No. 4, pp.311-346.

Gülkan P. and Gürpınar A. (1977). *Northwestern Anatolian Earthquake Risk* , (in Turkish), METU, Earthquake Engineering Research Center, Report No 77-05, Ankara.

Gülkan P. and Kalkan E. (2002). Attenuation Modeling of Recent Earthquakes in Turkey, *Journal of Seismology*, Vol. 6, pp. 397-409.

Gülkan P., Koçyiğit A., Yüçemen M. S., Doyuran V., Başöz N. (1993). *A Seismic Zones Map of Turkey Derived From Recent Data*, (in Turkish), METU, Earthquake Engineering Research Center, Report No. 93-01.

Gülkan P. and Yüçemen M. S. (1975). A Seismic Risk Study of İzmir, *Proc. Fifth European Conference on Earthquake Engineering*, Vol. 2, İstanbul.

Gülkan P. and Yüçemen M. S. (1976). *Assessment of Seismic Risk for Akkuyu*, Applied Research Report No. 76-04-03-37, METU, Ankara.

Hanks T. C. and Kanamori H. (1979). A Moment Magnitude Scale, *Journal of Geophysical Research*, Vol. 84, pp. 2348-2350.

Hermann R.B. (1977). Recurrence Relations, *Earthquake Notes*, Vol. 48, pp.47-49.

Husein Malkawi I., Al-Homoud A. and Liang R.Y. (1995). Seismic Hazard Mapping of Jordan, *Quarterly J. of Engineering Geology & Hydrogeology*, Vol. 28, pp. 75-81.

İnan E., Çolakoğlu Z., Koç N., Bayülke N., Çoruh E. (1996). *Earthquake Catalogs with Acceleration Records from 1976 to 1996*, (in Turkish), General Directorate of Disaster Affairs, Earthquake Research Department, Ankara, Turkey, 98 pp.

Japan International Cooperation Agency (JICA) and Istanbul Metropolitan Municipality (IMM) (2002). *The Study on A Disaster Prevention/Mitigation Basic Plan in Istanbul including Seismic Microzonation in the Republic of Turkey*, Final Report, December.

Jiménez M. J. (2004). *Jordan Seismic Hazard Mapping*, Final Report, Institute of Earth Sciences, “Jaume Almera”.

Joyner W. B. and Boore D. M. (1981). Peak Horizontal Acceleration and Velocity from Strong-Motion Records Including Records from the 1979 Imperial Valley, California Earthquake, *Bulletin of the Seismological Society of America*, Vol. 71, No. 6, pp. 2011-2038.

Kalkan E. (2007). Personal communication, California Geological Survey, Sacramento.

Kalkan E. and Gülkan P. (2004). Site-Dependent Spectra Derived from Ground Motion Records in Turkey, *Earthquake Spectra*, Vol. 20, No. 4, pp. 1111-1138.

Kameda H. and Ozaki Y. (1979). A Renewal Process Model for Use in Seismic Risk Analysis, *Memoirs of the Faculty of Engineering*, Kyoto University, Vol. 41, pp. 11-35.

Kiremidjian A. S. and Shah H. C. (1975). *Seismic Hazard Mapping of California*, The John A. Blume Earthquake Engineering Center, Report No. 21, Department of Civil Engineering, Stanford University.

Koçyiğit A. (2005). *Active Fault Investigation in Pilot Municipalities and Their Neighbourhood: Eskişehir, Gemlik, Bandırma, Tekirdağ And Körfez*, Final Report, Project: MEER-A3 Microzonation and Hazard Vulnerability Studies For Disaster Mitigation in Pilot Municipalities, 17 pp.

Koçyiğit A. (2006). Personal communication, Department of Geological Engineering, METU, Ankara.

Koçyiğit A. (2007). Personal communication, Department of Geological Engineering, METU, Ankara.

Lomnitz C. (1969). An Earthquake Risk Map of Chili, *Proceeding Forth World Conference on Earthquake Engineering*, Chili.

Mahmoud S. , Reilinger R., McClusky S., Vernant P., Tealeb A. (2005). GPS Evidence for Northward Motion of the Sinai Block: Implications for E. Mediterranean Tectonics, *Earth and Planetary Science Letters*, Vol. 238, pp. 217–224

Matthews M. V., Ellsworth W. L. and Reasenberg P. A. (2002). A Brownian Model for Recurrent Earthquakes, *Bulletin of the Seismological Society of America*, Vol. 92, No. 6, pp. 2233-2250.

McGuire R. K. (1976). *Fortran Computer Program for Seismic Risk Analysis*, U.S. Geological Survey, Open-File Report No. 76-67, Denver, Colorado.

McGuire R. K. (1978). *FRISK: Computer Program for Seismic Risk Analysis Using Faults as Earthquake Sources*, U.S. Geological Survey, Open-File Report 78-1007.

McGuire R. K. (2004). *Seismic Hazard and Risk Analysis*, EERI, MNO-10, Oakland, CA.

Merz H. and Cornell C.A. (1973). Seismic Risk Analysis Based on a Quadratic Magnitude-Frequency Law, *Bulletin of the Seismological Society of America*, Vol. 63, No. 6, pp. 1999-2006.

Mortgat C. P. and Shah H. C. (1978). A Bayesian Model for Seismic Hazard Mapping-A Case for Algeria, *Proceeding of Sixth European Conference on Earthquake Engineering*, Vol. 1, Dubrovnik.

Nishenko S. P. and Buland R. (1987). Generic Recurrence Interval Distribution for Earthquake Forecasting, *Bulletin of the Seismological Society of America*, Vol. 77, pp. 1382-1399.

Ordaz M., Aguilar A. and Arboleda J. (2003). *CRISIS2003: Program for Computing Seismic Hazard*, Ver. 1.2.100.

Özbey C., Sarı A., Manuel L., Erdik M. and Fahjan Y. (2004). An Empirical Attenuation Relationship for Northwestern Turkey Ground Motion Using A Random Effects Approach, *Soil Dynamics and Earthquake Engineering*, Vol. 24, pp. 115-125.

Özmen B., Nurlu M. and Güler H. (1997). *Examination of Earthquake Zones by Geographic Information System*, (in Turkish), The Ministry of Public Works and Settlement, Ankara.

Parsons T. (2004). Recalculated Probability of $M \geq 7$ Earthquakes Beneath the Sea of Marmara, Turkey, *Journal of Geophysical Research*, Vol. 109.

Reid H. F. (1910). The Mechanics of the Earthquake, The California Earthquake of April 18, 1906, *Report of the State Investigation Commission*, Vol.2, Carnegie Institution of Washington, Washington, D.C., pp. 16-28.

Reiter L. (1990). *Earthquake Hazard Analysis: Issues and Insights*, New York, Columbia University Press.

Richter C. F. (1958). *Elementary Seismology*, W.H. Freeman and Company, San Francisco.

Risk Engineering Inc. (2005). *EZ-FRISK: 2005, User's Manual*, Version 7.12, Boulder, Colorado.

Risk Engineering Inc. (2006). *User's Manual for FRISK88M Software*, Version 2.124, Boulder, Colorado.

Sabetta F., Lucantoni A., Bungum H., Bommer J.J. (2005). Sensitivity of PSHA Results to Ground Motion Prediction Relations and Logic-Tree Weights, *Soil Dynamics and Earthquake Engineering*, Vol. 25, pp.317–329.

Sadigh K., Chang C.-Y., Egan J. A., Makdisi F. and Youngs R. R. (1997). Attenuation Relationships for Shallow Crustal Earthquakes Based on California Strong Motion Data, *Seismological Research Letters*, Vol. 68, No. 1, pp. 180-189.

Şaroğlu F., Emre Ö. and Kuşçu İ. (1992). *Active fault map of Turkey*, General Directorate of Mineral Research and Exploration, Turkey.

Schwartz D. P. and Coppersmith K. J. (1984). Fault Behavior and Characteristic Earthquakes: Examples from The Wasatch and San Andreas Fault Zones, *Journal of Geophysical Research*, Vol. 89, No. B7, pp. 5681-5698.

Shah H. C., Mortgat C. P. Kiremidjian A. and Zsutty T. C. (1975). *A Study of Seismic Risk for Nicaragua*, Part I, The John A. Blume Earthquake Engineering Centre, Stanford University.

Shapira, A. (1981). Assessment of the Potential Earthquake Risk in Israel and Adjacent Areas, *Israel J. of Earth Sciences*, Vol. 30, pp. 135-141.

Shlien S. and Toksöz M. N. (1970). Frequency-Magnitude Statistics of Earthquake Occurrence, *Earthquake Notes*, No. 41.

SSHAC Report (1997), *Recommendations for Probabilistic Seismic Hazard Analysis: Guidance on Uncertainty and Use of Experts*, NUREG/CR-6372, Vol. 1, Lawrence Livermore National Laboratory, Livermore, CA.

Thenhaus P. C. and Campbell K. W. (2003). Seismic Hazard Analysis, *Chapter 8, Earthquake Engineering Hand Book*, Wai-Fah Chen and Charles Schawthorn (editors), CRC Press.

Ulusay R., Tuncay E., Sönmez H. and Gökçeoğlu C. (2004). An Attenuation Relationship Based on Turkish Strong Motion Data and Iso-Acceleration Map of Turkey, *Engineering Geology*, Vol.74, pp. 265-291.

Vanmarcke E. H. and Cornell C. A. (1969). *Analysis of Uncertainty in Ground Motion and Structural Response Due to Earthquakes*, M.I.T., Department of Civil Engineering, Research Report, R 69-24.

Wells D. L. and Coppersmith K. J. (1994). New Empirical Relationships Among Magnitude, Rupture Length, Rupture Width, Rupture Area and Surface Displacement, *Bulletin of the Seismological Society of America*, Vol. 84, No. 4, pp. 974-1002.

Working Group on California Earthquake Probabilities (WGCEP) (1995). Seismic Hazards in Southern California: Probable Earthquakes, 1994 to 2024, *Bulletin of the Seismological Society of America*, Vol. 85, No. 2, pp. 379-439.

Working Group on California Earthquake Probabilities (WGCEP) (1999). *Earthquake Probabilities in the San Francisco Bay Region: 2000 to 2030-A Summary of Findings*, U.S. Geological Survey, Open-File Report 99-517.

Wu S.-C., Cornell C. A. and Winterstein S. R. (1995). A Hybrid Recurrence Model and Its Implication on Seismic Hazard Results, *Bulletin of the Seismological Society of America*, Vol. 85, No. 1, pp. 1-16.

Youngs R. R. and Coppersmith K. J. (1985). Implications of Fault Slip Rates and Earthquake Recurrence Models to Probabilistic Seismic Hazard Estimates, *Bulletin of the Seismological Society of America*, Vol. 75, No. 4, pp. 939-964.

Yücemem M. S. (1982), *Seismic Risk Analysis* , (in Turkish), Middle East Technical University, Ankara, 160 pp.

Yüçemen M.S. (1992). Seismic Hazard Maps for Jordan and Vicinity, *Natural Hazards*, Kluwer Academic Publishers, Vol. 6, No. 3, pp. 201-226.

Yüçemen M. S. (1995). Assessment of Seismic Hazard for Jordan Considering the Uncertainty in the Location of Seismic Sources, *Proc. International Conference on Earthquake Engineering*, Amman, Jordan, Vol. I, pp. 135-144.

Yüçemen M. S. and Gülkan P. (1994) Seismic Hazard Analysis with Randomly Located Sources, *Natural Hazards*, Vol. 9, Kluwer Academic Publishers, pp. 215-233.

Yüçemen M. S., Koçyiğit A., Yakut A., Gencoğlu S. (2006) *Guidelines for the Development of Seismic Hazard Maps*, Technical Report prepared for General Directorate of Disaster Affairs, Ankara, 78 pp.

APPENDIX A

GRAPHS SHOWING THE DIFFERENCE BETWEEN THE SEISMIC HAZARD RESULTS OBTAINED BY IGNORING AND CONSIDERING RUPTURE LENGTH UNCERTAINTY

In this appendix, the graphs which show the difference between the seismic hazard results obtained by ignoring rupture length uncertainty and considering it as a function of the number of rupture lengths are presented. In these graphs, the PGA values are normalized by median PGA value obtained from DSHA for magnitude 6.3 in order to reduce the effect of attenuation of PGA values with distance on results.

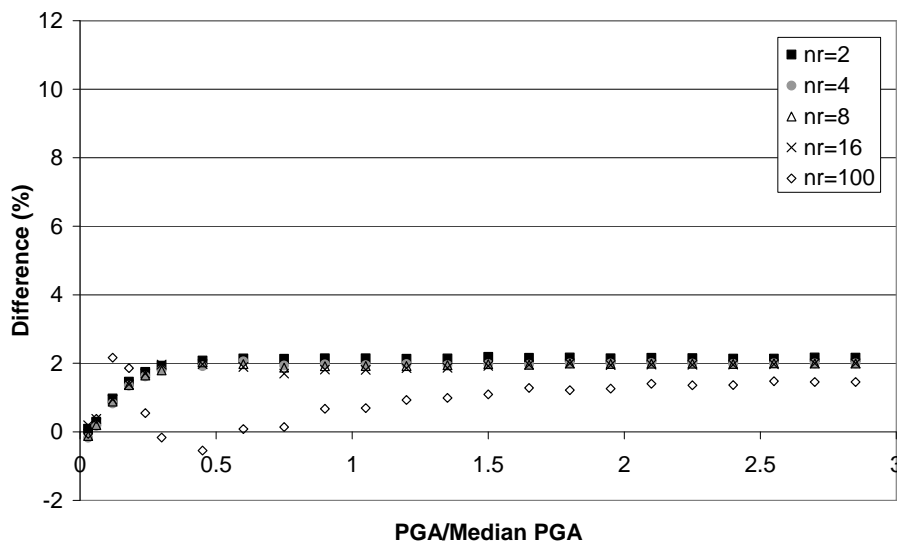


Figure A.1 The Variation of the Difference Between the Seismic Hazard Results Obtained by Ignoring Rupture Length Uncertainty and Considering it As a Function of Number of Rupture Lengths per Magnitude (Site 1a)

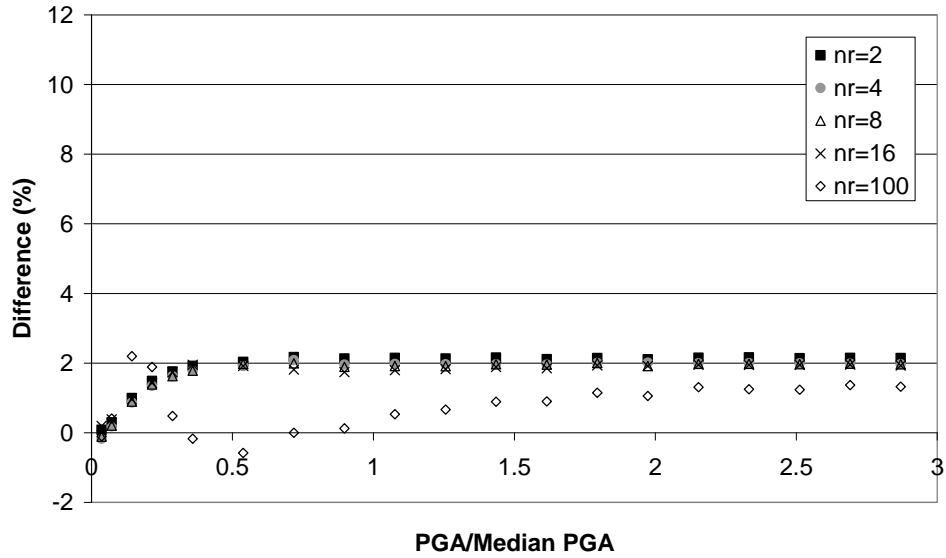


Figure A.2 The Variation of the Difference Between the Seismic Hazard Results Obtained by Ignoring Rupture Length Uncertainty and Considering it As a Function of Number of Rupture Lengths per Magnitude (Site5a)

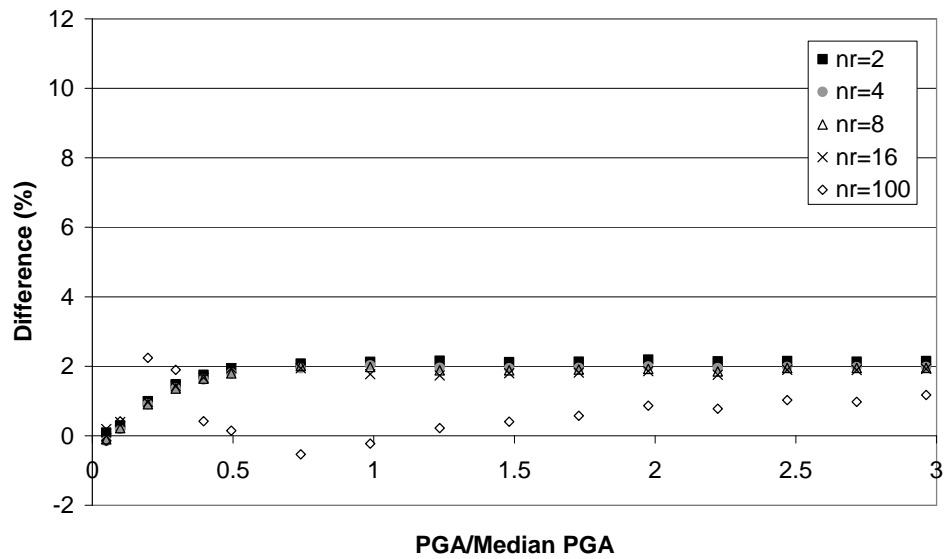


Figure A.3 The Variation of the Difference Between the Seismic Hazard Results Obtained by Ignoring Rupture Length Uncertainty and Considering it As a Function of Number of Rupture Lengths per Magnitude (Site10a)

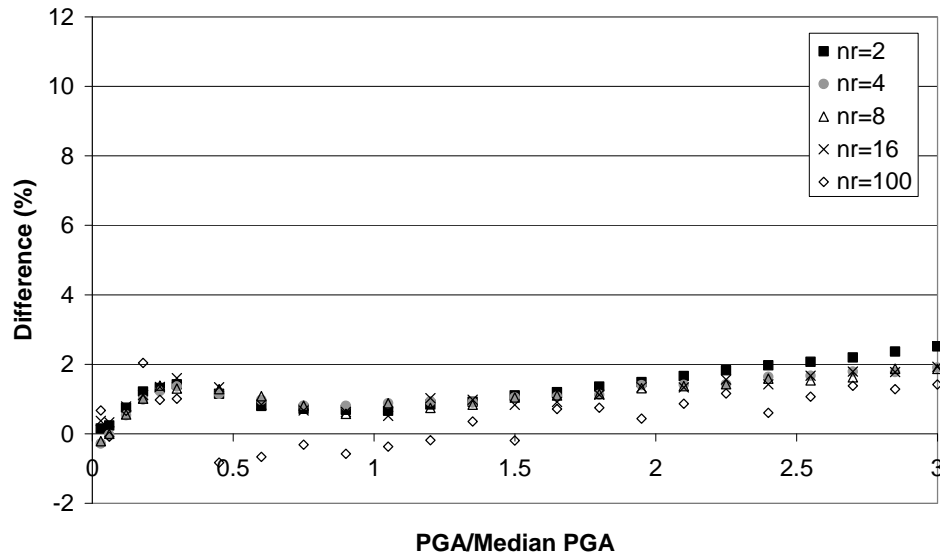


Figure A.4 The Variation of the Difference Between the Seismic Hazard Results Obtained by Ignoring Rupture Length Uncertainty and Considering it As a Function of Number of Rupture Lengths per Magnitude (Site1b)

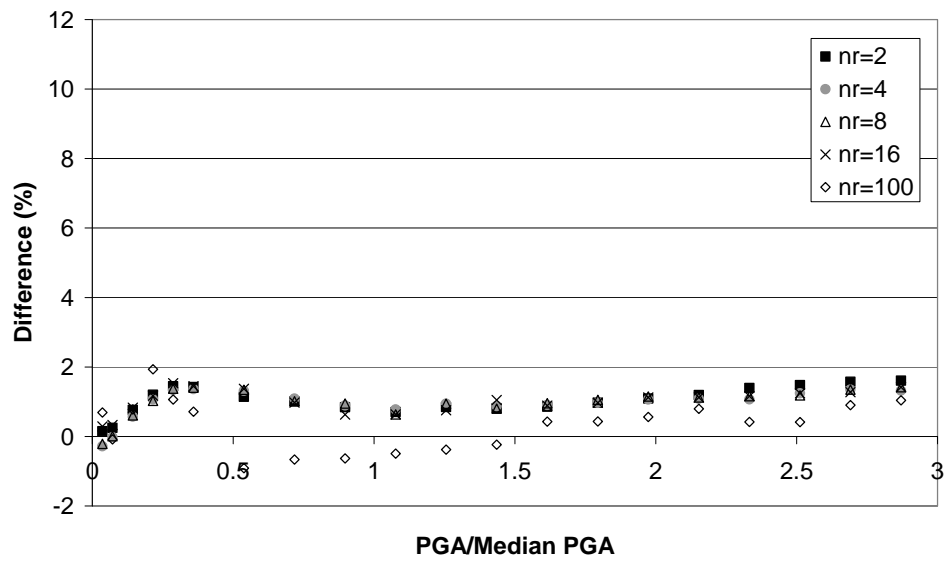


Figure A.5 The Variation of the Difference Between the Seismic Hazard Results Obtained by Ignoring Rupture Length Uncertainty and Considering it As a Function of Number of Rupture Lengths per Magnitude (Site5b)

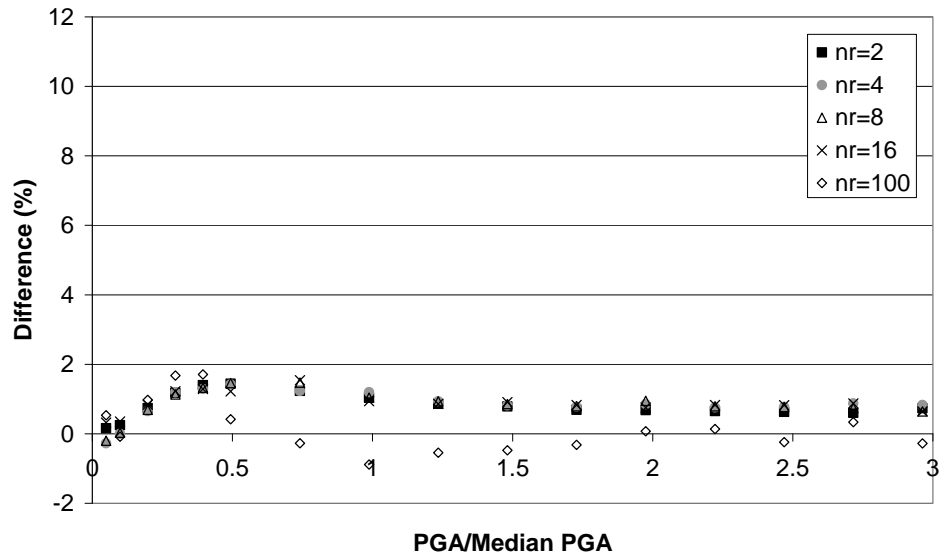


Figure A.6 The Variation of the Difference Between the Seismic Hazard Results Obtained by Ignoring Rupture Length Uncertainty and Considering it As a Function of Number of Rupture Lengths per Magnitude (Site10b)

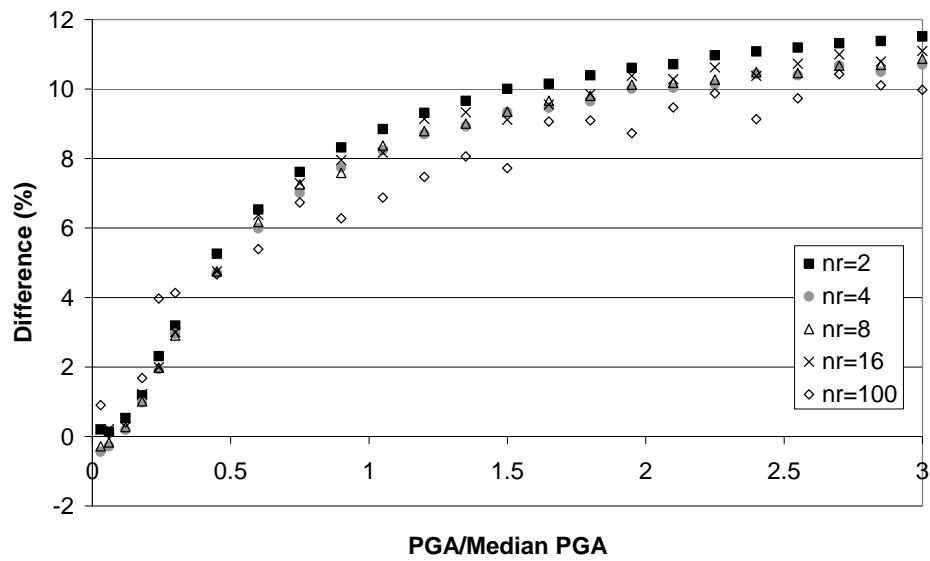


Figure A.7 The Variation of the Difference Between the Seismic Hazard Results Obtained by Ignoring Rupture Length Uncertainty and Considering it As a Function of Number of Rupture Lengths per Magnitude (Site1c)

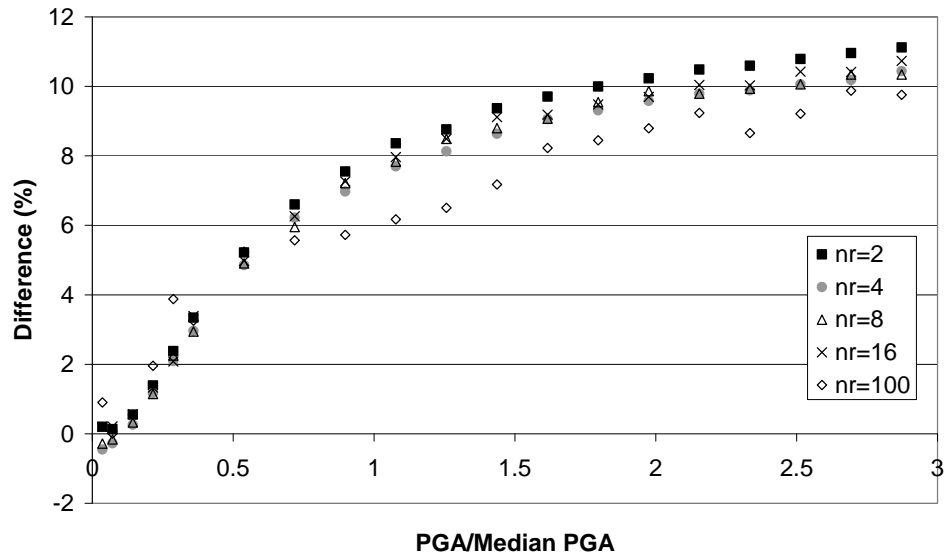


Figure A.8 The Variation of the Difference Between the Seismic Hazard Results Obtained by Ignoring Rupture Length Uncertainty and Considering it As a Function of Number of Rupture Lengths per Magnitude (Site 5c)

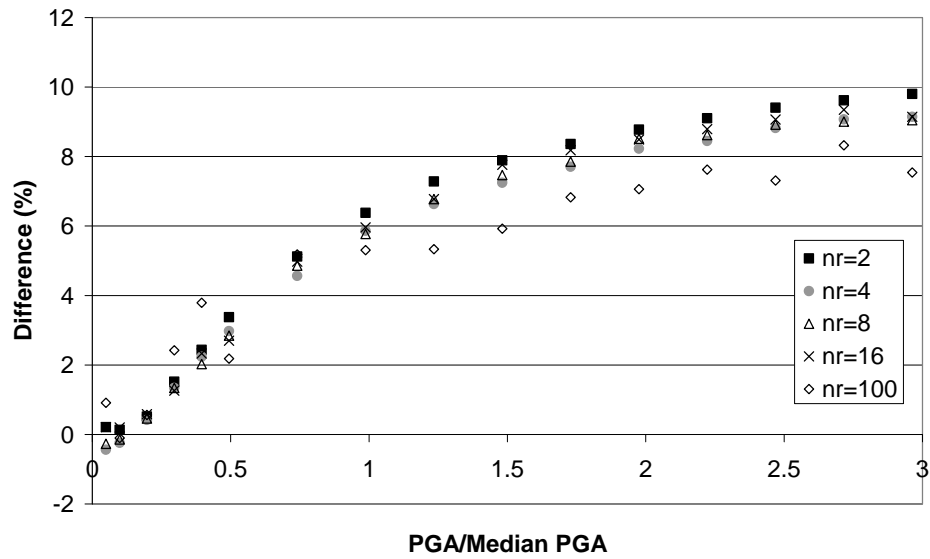


Figure A.9 The Variation of the Difference Between the Seismic Hazard Results Obtained by Ignoring Rupture Length Uncertainty and Considering it As a Function of Number of Rupture Lengths per Magnitude (Site 10c)

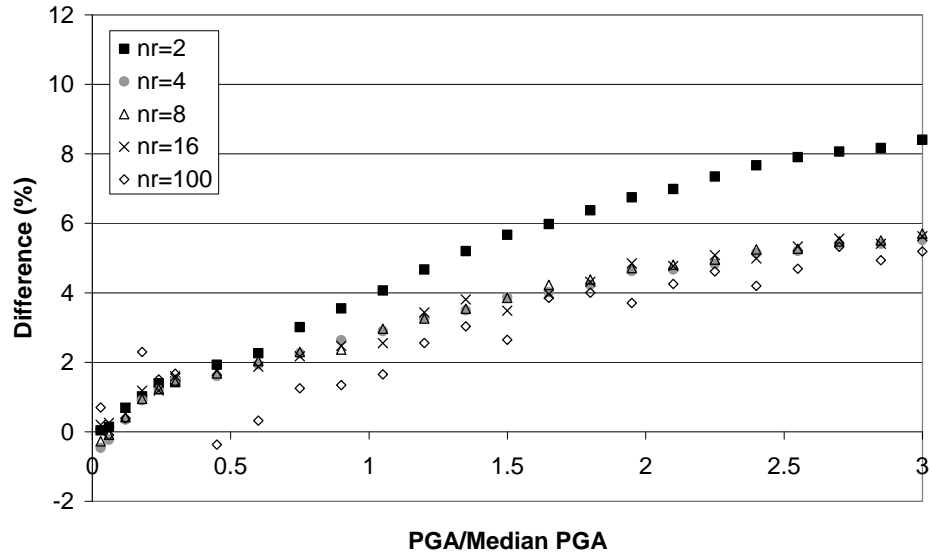


Figure A.10 The Variation of the Difference Between the Seismic Hazard Results Obtained by Ignoring Rupture Length Uncertainty and Considering it As a Function of Number of Rupture Lengths per Magnitude (Site1d)

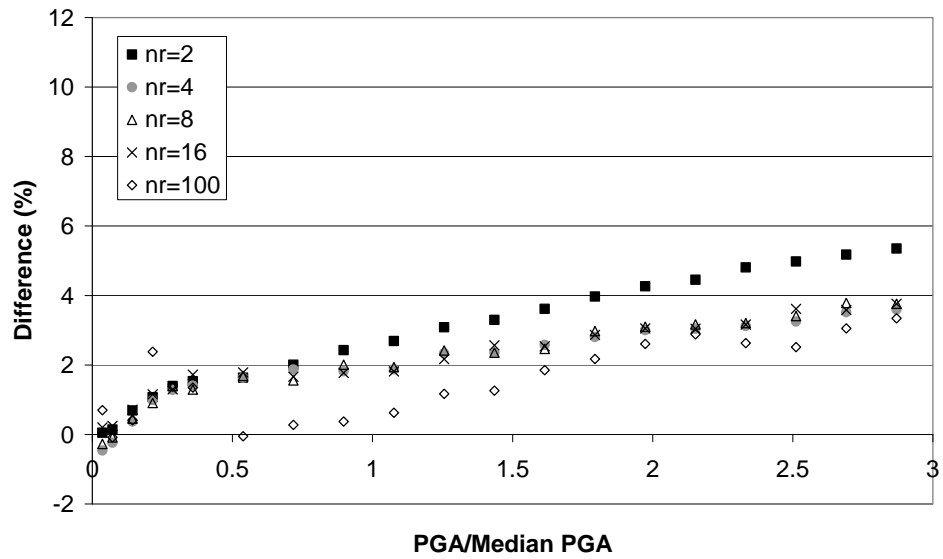


Figure A.11 The Variation of the Difference Between the Seismic Hazard Results Obtained by Ignoring Rupture Length Uncertainty and Considering it As a Function of Number of Rupture Lengths per Magnitude (Site5d)

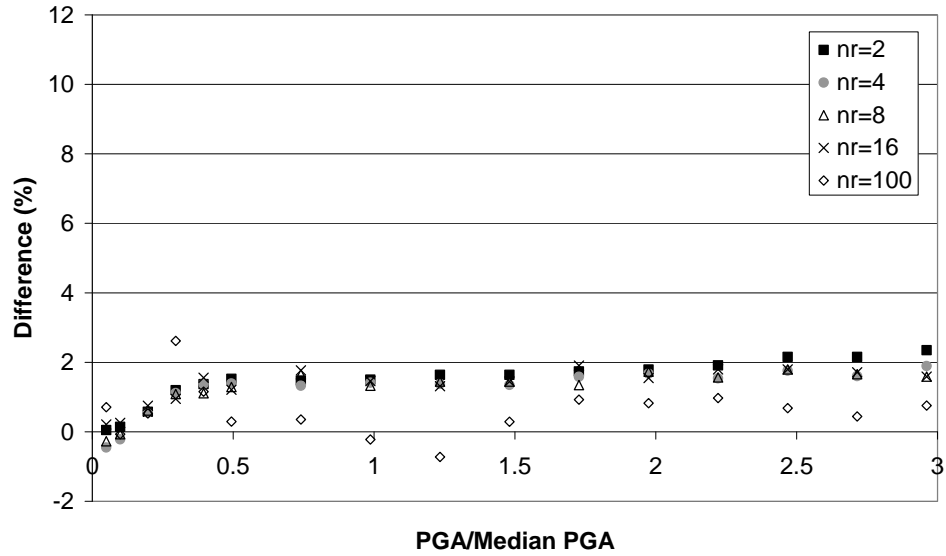


Figure A.12 The Variation of the Difference Between the Seismic Hazard Results Obtained by Ignoring Rupture Length Uncertainty and Considering it As a Function of Number of Rupture Lengths per Magnitude (Site10d)

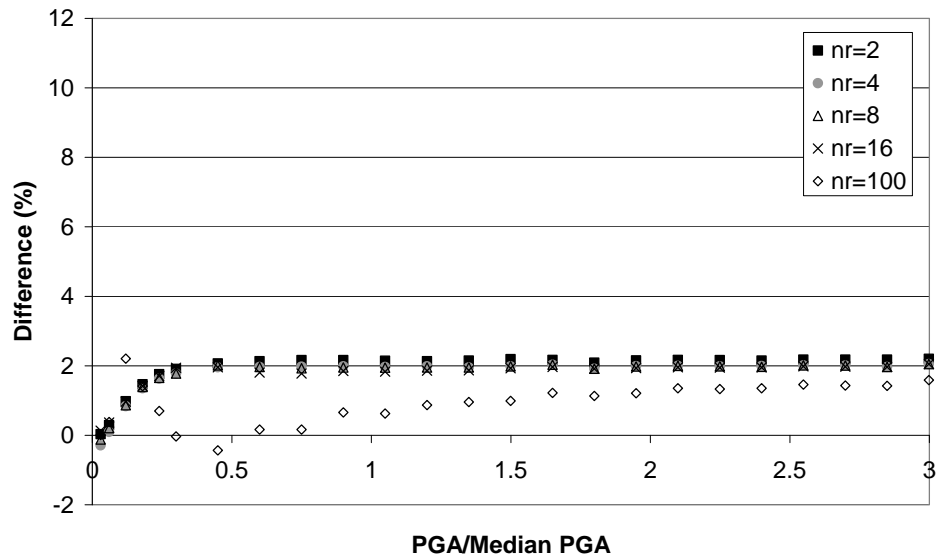


Figure A.13 The Variation of the Difference Between the Seismic Hazard Results Obtained by Ignoring Rupture Length Uncertainty and Considering it As a Function of Number of Rupture Lengths per Magnitude (Site1e)

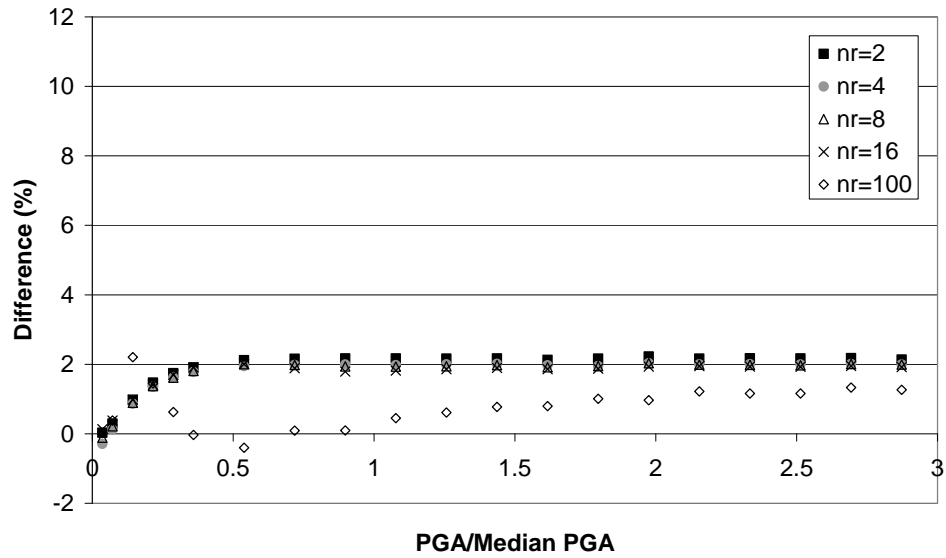


Figure A.14 The Variation of the Difference Between the Seismic Hazard Results Obtained by Ignoring Rupture Length Uncertainty and Considering it As a Function of Number of Rupture Lengths per Magnitude (Site5e)

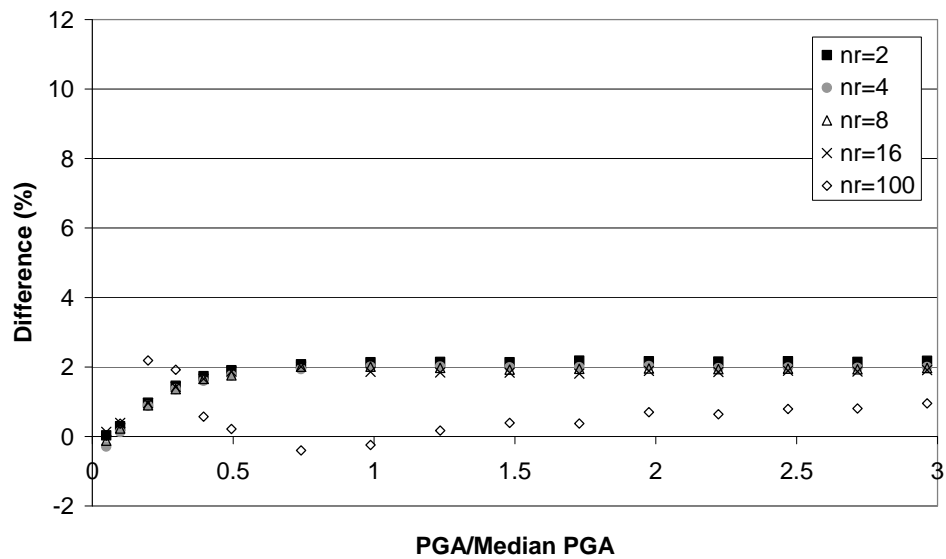


Figure A.15 The Variation of the Difference Between the Seismic Hazard Results Obtained by Ignoring Rupture Length Uncertainty and Considering it As a Function of Number of Rupture Lengths per Magnitude (Site10e)

APPENDIX B

EARTHQUAKE CATALOG PREPARED FOR JORDAN

There are 175 earthquakes treated as main shocks (independent events) with magnitudes (M_L) greater than or equal to 4.0 in this catalog.

Table B.1 Main Shocks in the Earthquake Catalog Prepared for Jordan

No	Year	Month	Day	Latitude (Degree)	Longitude (Degree)	Depth	M_s	M_b	M_L
1	1900	1	5	35.2000	33.2000			6.3	6.2
2	1903	3	29	32.2000	35.4000			5.25	5.5
3	1907	6	10	33.7000	35.4000			3.4	4.2
4	1907	7	22	33.7000	35.4000			3.4	4.2
5	1910	10	7	33.9000	36.2000	10		3.4	4.2
6	1918	9	29	35.2000	34.7000			6.7	6.5
7	1919	8	19	35.2000	34.7000			5.25	5.5
8	1921	4	20	34.0000	33.0000			5.6	5.75
9	1923	2	27	32.7000	35.4000			3.55	4.3
10	1924	2	18	34.5000	34.0000			6	6
11	1924	2	27	32.7000	36.2000	20		4.7	5.1
12	1924	9	13	30.8000	35.5000			4.4	4.9
13	1927	7	11	32.1000	35.5000			6	6
14	1927	7	11	32.0000	35.5000			6.5	6.3
15	1927	9	24	30.4000	35.1000	15		4.55	5
16	1927	12	12	34.5000	34.7000			5.25	5.5
17	1930	5	9	34.1000	32.2000			5.6	5.75
18	1930	5	21	32.0000	35.5000			3.5	4.3
19	1930	9	14	34.6000	36.6000			3.7	4.5
20	1937	10	12	31.5000	35.5000			3.4	4.2
21	1940	1	27	32.8000	35.1000			3.7	4.4
22	1940	7	24	34.5000	34.5000			5.7	5.8
23	1940	9	2	31.3000	35.6000			3.7	4.5
24	1941	1	20	35.5000	33.6000	100		6.5	6.6

Table B.1 (Continued) Main Shocks in the Earthquake Catalog Prepared for Jordan

No	Year	Month	Day	Latitude (Degree)	Longitude (Degree)	Depth	M _s	M _b	M _L
25	1942	9	28	34.4000	36.6000			3.4	4.2
26	1943	9	10	32.6000	35.4000			4.1	4.7
27	1944	10	7	32.7000	35.5000	10		3.55	4.3
28	1949	10	28	33.0000	33.5000			3.7	4.4
29	1951	1	30	32.4000	33.4000			5.55	5.7
30	1951	8	5	34.2000	36.0000			4.1	4.7
31	1952	3	22	27.2000	34.5000			4.55	5
32	1952	12	28	32.8000	35.4000			3.4	4.2
33	1953	2	1	33.5000	32.0000			4.55	5
34	1953	9	10	34.9000	32.2000			6.7	6.5
35	1953	11	3	32.0000	35.6000			3.25	4.1
36	1954	9	13	31.0000	35.4000	33		4.55	5
37	1956	3	16	33.6150	35.5100			5.25	5.5
38	1956	3	16	33.6150	35.5100			6	6
39	1956	12	18	31.6300	35.5200			5.15	5.4
40	1957	7	29	34.8000	36.9000			3.4	4.2
41	1957	11	3	32.5000	35.5000			3.8	4.5
42	1958	2	14	31.3000	35.6000			3.4	4.2
43	1959	6	13	34.9000	32.3900			5.3	5.5
44	1960	1	28	33.0000	35.5000			3.55	4.3
45	1961	9	15	34.9800	33.8300	33		6	6
46	1964	6	28	34.7700	32.3500	63	4.7	4.15	4.7
47	1964	9	23	34.2000	32.7000	67		4.3	4.8
48	1965	1	25	34.5600	32.8400	20	4.8	4.3	4.8
49	1965	3	17	34.6400	32.3000	52	4.6	4	4.6
50	1965	5	2	33.4000	35.5000			3.55	4.3
51	1965	6	8	34.0300	33.7000	33		3.4	4.2
52	1966	3	6	34.5000	32.7000			3.85	4.5
53	1967	4	17	34.5000	32.8400		4.6	4	4.6
54	1967	6	15	34.0900	32.4300	52	4.7	4.15	4.7
55	1968	3	26	34.0800	35.4700	37	4.8	4.3	4.8
56	1968	12	4	31.8000	35.6000			3.4	4.2
57	1969	3	31	27.6100	33.9100	33	6.1	6.1	6.1
58	1970	3	18	34.4200	32.4900	38		3.85	4.5
59	1970	9	29	33.2000	34.4000		4.1	3.3	4.1
60	1970	10	5	35.0400	39.0000	34	4.8	4.3	4.8
61	1970	10	8	31.7000	35.3000	10		4	4.6
62	1970	12	26	34.2000	33.7000		4.0	3.1	4
63	1971	4	16	33.6400	35.4300	10	4.5	3.85	4.5

Table B.1 (Continued) Main Shocks in the Earthquake Catalog Prepared for Jordan

No	Year	Month	Day	Latitude (Degree)	Longitude (Degree)	Depth	M _s	M _b	M _L
64	1971	7	8	27.5400	33.8170	35	4.8	4.3	4.9
65	1971	9	7	32.8000	35.6000			3.55	4.3
66	1971	11	8	33.3000	35.5000			3.4	4.2
67	1972	1	12	27.5490	33.8190	36	5.1	4.7	5.1
68	1972	6	28	27.6990	33.7990		5.5	5.5	5.5
69	1973	3	21	33.9490	32.3590		4.2	3.4	4.2
70	1973	9	2	32.7900	35.3000			3.4	4.2
71	1974	6	12	34.1000	37.2700		4.6	4	4.6
72	1974	7	20	33.3400	38.4300		4.2	3.4	4.2
73	1974	9	6	29.9000	35.5000			3.55	4.3
74	1975	1	28	34.5300	33.8100	35	4.7	4.1	4.7
75	1975	3	10	34.8700	33.4400	10	4.1	3.3	4.1
76	1975	5	12	27.7900	33.9500		4.2	3.4	4.2
77	1976	1	12	34.4300	32.6300	36	5.0	4.6	5
78	1976	10	4	34.1000	34.6000			3.55	4.3
79	1977	8	17	32.1000	35.3000			3.55	4.3
80	1978	1	30	34.6720	33.8350	38	4.5	3.85	4.5
81	1978	6	25	34.6700	33.3800	33	4.1	3.3	4.1
82	1979	4	23	31.1600	35.5100	10	5.1	4.7	5
83	1979	8	14	33.5900	34.5600	10	4.3	3.6	4.3
84	1980	5	3	29.5800	32.5600	33	4.2	3.45	4.2
85	1981	11	9	34.4060	35.9400	33	4.4	3.71	4.4
86	1981	11	24	33.0000	35.6600	8		3.55	4.3
87	1982	1	13	32.5780	35.6220	1		3.4	4.2
88	1982	3	11	33.1650	33.8320	15		3.25	4.1
89	1982	3	23	27.9560	34.3730	33	4.7	4.2	4.7
90	1982	5	23	31.5950	35.5490	21		4	4.6
91	1982	5	25	32.3580	35.5280	1		4	4.6
92	1982	10	30	27.6300	33.8200	10	4.6	4	4.6
93	1982	12	19	34.8900	34.0600	37	4.7	4.15	4.6
94	1983	1	31	29.9500	34.6300	20		3.4	4.2
95	1983	1	31	29.7780	34.8890	13		3.4	4.2
96	1983	1	31	28.5200	34.1700	10	4.3	3.6	4.5
97	1983	1	31	29.8200	33.8900	21	4.5	3.85	4.6
98	1983	2	1	29.5500	35.1200	1		3.4	4.2
99	1983	2	3	29.2600	34.7700	24	5.1	4.7	5.1
100	1983	2	5	29.8500	34.4900	1		3.4	4.2
101	1983	2	10	28.9000	35.6000		4.3	3.6	4.3
102	1983	6	3	33.8290	35.7480	8	4.6	3.9	4.9

Table B.1 (Continued) Main Shocks in the Earthquake Catalog Prepared for Jordan

No	Year	Month	Day	Latitude (Degree)	Longitude (Degree)	Depth	M _s	M _b	M _L
103	1983	6	12	28.5540	33.1300	29	5.0	4.8	5.2
104	1983	6	15	27.2200	34.4700	5		3.3	4.1
105	1983	7	19	29.0740	34.6510	2		3.3	4.1
106	1983	9	24	34.6240	33.3150	46	4.5	3.9	4.5
107	1983	9	28	34.8600	32.7200	58	4.2	3.4	4.2
108	1983	10	31	34.9000	33.6500	75	4.4	3.7	4.4
109	1984	3	2	28.7100	35.2340	1		3.3	4.1
110	1984	3	28	34.7500	33.5800	34	5.0	4.3	5
111	1984	3	29	30.2100	32.1900	8	4.8	4.3	4.8
112	1984	4	6	30.3800	33.9180	9		4	4.6
113	1984	4	7	33.7600	32.5110	27	4.5	3.85	4.4
114	1984	4	18	28.7200	33.2200	27		3.3	4.1
115	1984	5	23	32.2500	34.9900	1		3.3	4.1
116	1984	8	24	32.6910	35.1920	13	5.1	4.2	5.1
117	1984	9	7	27.1000	34.9600	2		3.45	4.2
118	1984	10	18	33.1600	35.6100	4			4.3
119	1984	11	5	32.1100	35.3650	4	4.4	3.45	4.2
120	1985	1	13	27.0500	34.6700	26		3.45	4.2
121	1985	1	25	31.8900	35.5900	18	4.6	4.4	4.9
122	1985	2	28	27.7200	33.7150	10	4.5	3.8	4.5
123	1985	4	26	34.0200	36.6900	18			4.3
124	1985	6	6	34.8500	32.6500	42	4.5	3.85	4.4
125	1985	11	16	35.0300	33.4000	41		3.55	4.3
126	1985	12	31	30.4100	35.0500	10			4.3
127	1985	12	31	29.1300	34.9000	9	4.8	4.3	5.1
128	1986	7	7	34.8050	33.6690	49	4.6	4	4.6
129	1986	7	30	34.6710	32.3070	37	4.9	4.1	5
130	1986	8	7	29.1540	34.7200			3.7	4.4
131	1987	1	2	30.4800	32.2210	24	5.0	4.55	5
132	1987	1	10	34.6590	33.2820	37	4.3	3.6	4.3
133	1987	2	18	34.9490	32.2940	49	4.6	4	4.6
134	1987	4	27	31.2500	35.5200	11	4.3	3.6	4.2
135	1987	10	18	29.5100	35.1870	10	4.4	3.7	4.7
136	1987	10	23	31.0000	35.5100	10	4.2	3.4	4.1
137	1987	11	9	34.7350	32.8770	26	4.5	3.85	4.5
138	1988	1	30	32.1900	35.4700	14			4.1
139	1988	6	5	27.9800	33.7300	10	4.6	4	4.8
140	1989	3	31	31.8700	37.5350	28	5.0	4.6	5.2
141	1989	10	4	28.0800	33.7300	10		3.7	4.4

Table B.1 (Continued) Main Shocks in the Earthquake Catalog Prepared for Jordan

No	Year	Month	Day	Latitude (Degree)	Longitude (Degree)	Depth	M _s	M _b	M _L
142	1989	12	18	28.4240	33.3330	10	4.4	3.7	4.4
143	1990	4	26	30.6880	35.6940	19.61			4.2
144	1990	9	13	32.0250	34.4910	13.16			4.45
145	1991	1	6	31.5610	35.6930	23.58			4.8
146	1991	8	4	34.6720	34.4690	17.98			4.08
147	1991	9	28	31.0860	35.5380	12.51			4.06
148	1993	1	1	34.7970	33.3380	5			4.96
149	1993	7	31	28.0420	34.6170	5.9			4.18
150	1993	8	2	31.4900	35.5360	26.17			4.05
151	1993	8	3	28.0240	33.9740	5			4.34
152	1993	8	3	29.7290	35.2890	5			4.91
153	1993	8	3	28.9380	34.7470	5			5.09
154	1993	8	6	28.2920	34.9340	0.26			4.26
155	1993	8	22	29.0770	37.0880	5			4.18
156	1993	8	28	32.8870	38.7620	0.07			4.14
157	1993	9	6	27.9660	35.4280	5			4.26
158	1993	9	6	27.6090	35.4850	7.75			4.44
159	1993	9	6	27.8960	32.9560	5			5.28
160	1993	9	12	28.3150	34.7350	7.61			4.35
161	1993	9	13	28.3240	35.5890	13.03			4.28
162	1993	9	25	28.2340	35.4530	5			4.09
163	1993	10	3	29.0410	37.2520	5			4.54
164	1993	10	18	27.4720	33.8700	5			4.65
165	1993	11	3	28.4770	34.3640	5			4.06
166	1993	12	4	28.5250	34.5560	5			4.4
167	1995	2	26	27.6290	34.5230	9.02			4.44
168	1995	5	14	28.3600	34.5050	5			4.79
169	1995	11	22	28.7580	34.6280	6.85			6.17
170	1996	9	4	30.2990	34.9070	5			4.52
171	1997	3	26	33.7660	35.6510	1.67			4.75
172	1997	12	17	32.7440	32.7560	5			4.6
173	1998	4	7	28.7810	34.5700	9.9			4.09
174	1998	4	17	28.8350	34.7480	1.26			4.19
175	1998	11	19	29.6420	34.4890	7.5			4.11

APPENDIX C

SEISMIC HAZARD MAPS FOR JORDAN BASED ON DIFFERENT MODELS

For the assumptions related to the different models (i.e. Model 1, 2, 3, 4) please refer to Section 3.3.2.

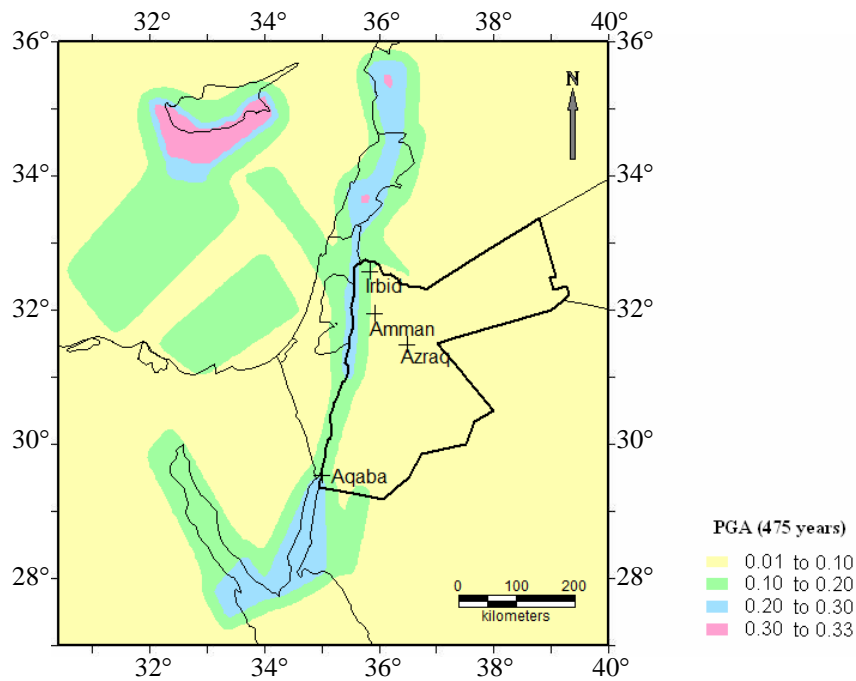


Figure C.1 Seismic Hazard Map Obtained from Model 1 for PGA at 10% Probability of Exceedance in 50 Years (475 Years Return Period)

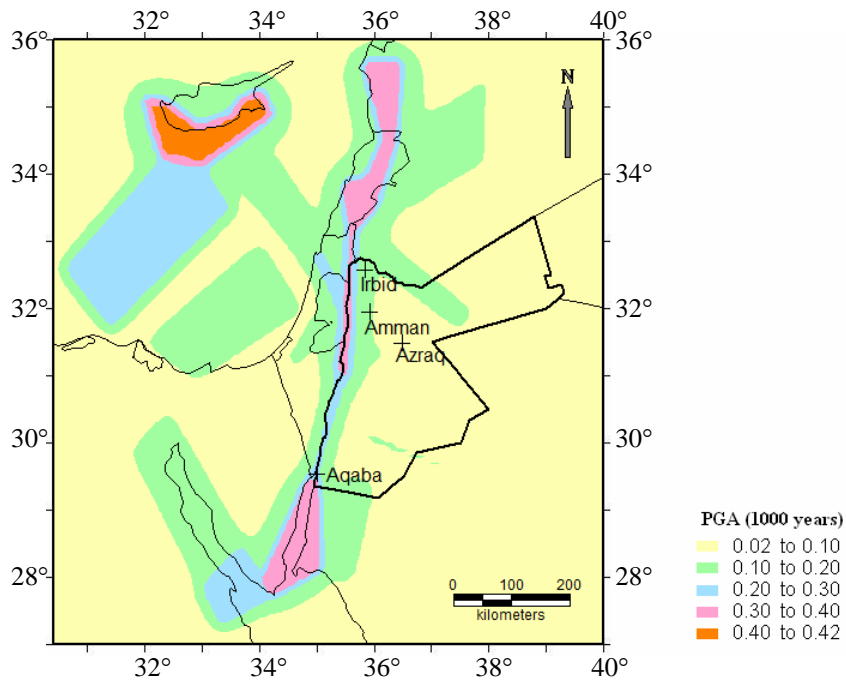


Figure C.2 Seismic Hazard Map Obtained from Model 1 for PGA at 5% Probability of Exceedance in 50 Years (1000 Years Return Period)

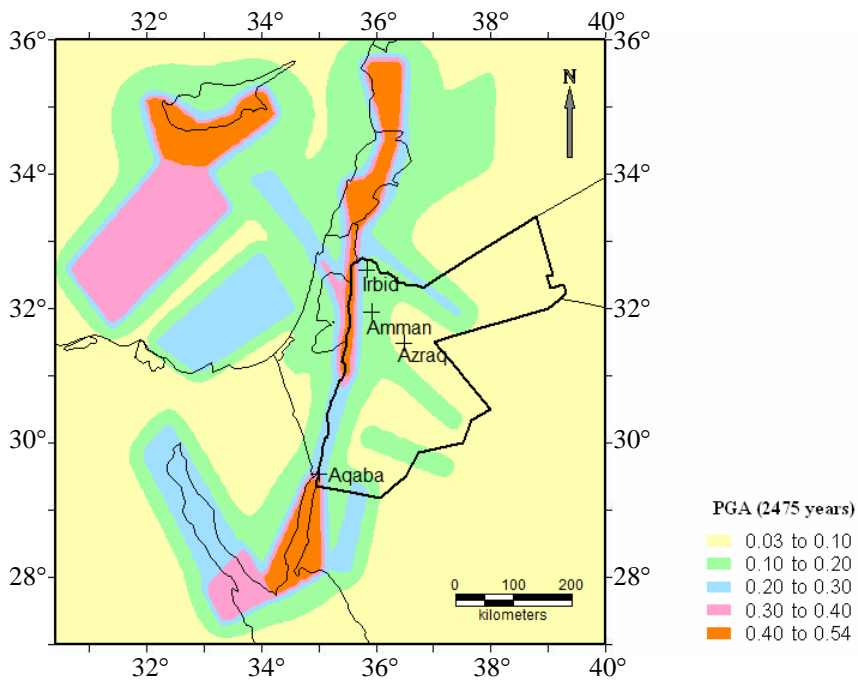


Figure C.3 Seismic Hazard Map Obtained from Model 1 for PGA at 2% Probability of Exceedance in 50 Years (2475 Years Return Period)

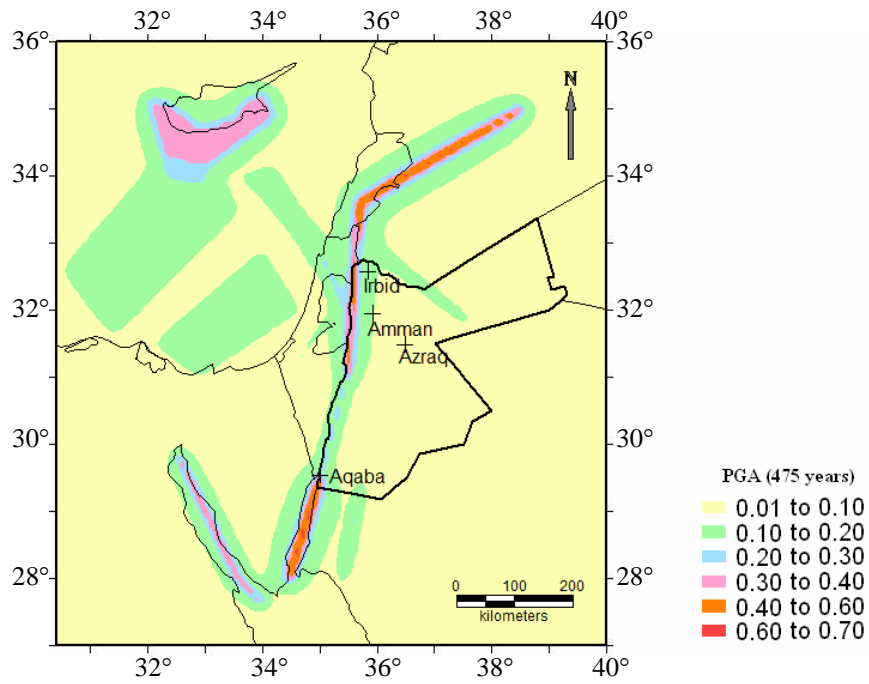


Figure C.4 Seismic Hazard Map Obtained from Model 2 for PGA at 10% Probability of Exceedance in 50 Years (475 Years Return Period)

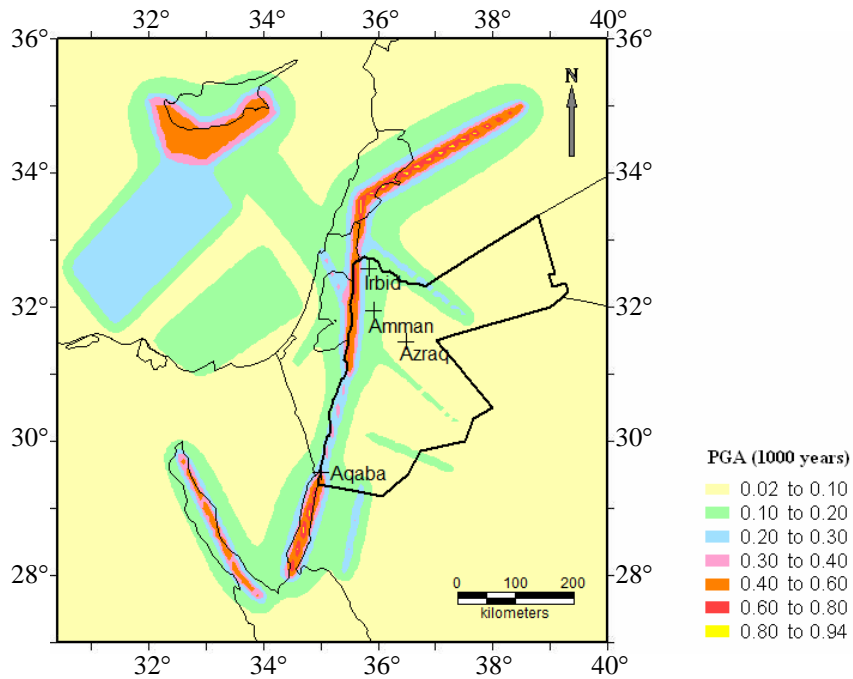


Figure C.5 Seismic Hazard Map Obtained from Model 2 for PGA at 5% Probability of Exceedance in 50 Years (1000 Years Return Period)

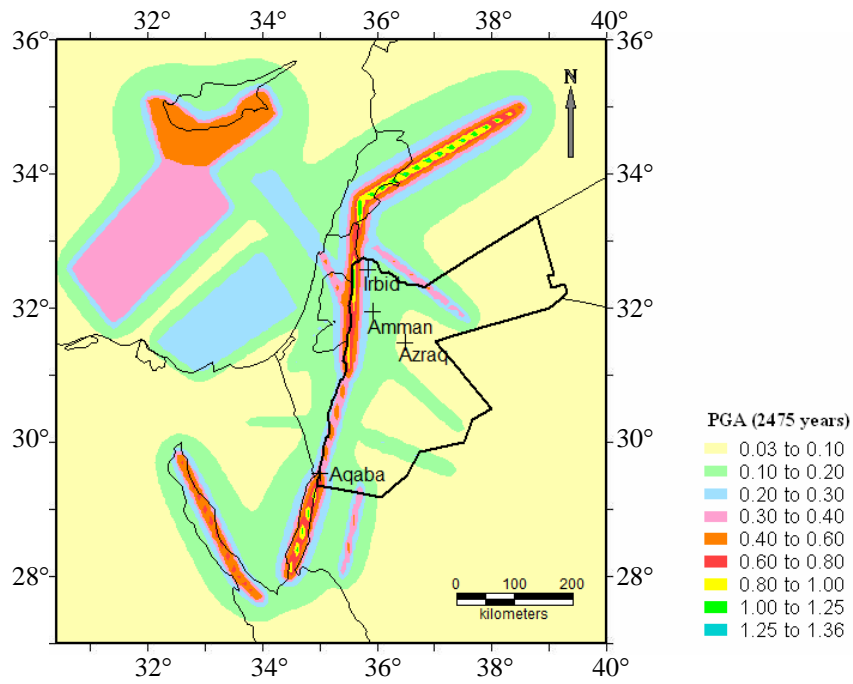


Figure C.6 Seismic Hazard Map Obtained from Model 2 for PGA at 2% Probability of Exceedance in 50 Years (2475 Years Return Period)

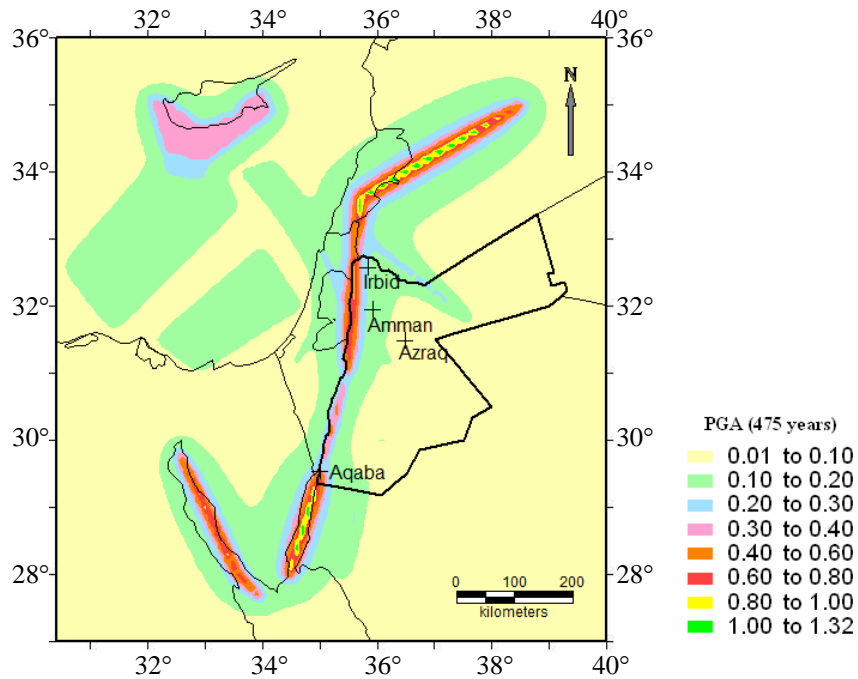


Figure C.7 Seismic Hazard Map Obtained from Model 3 for PGA at 10% Probability of Exceedance in 50 Years (475 Years Return Period)

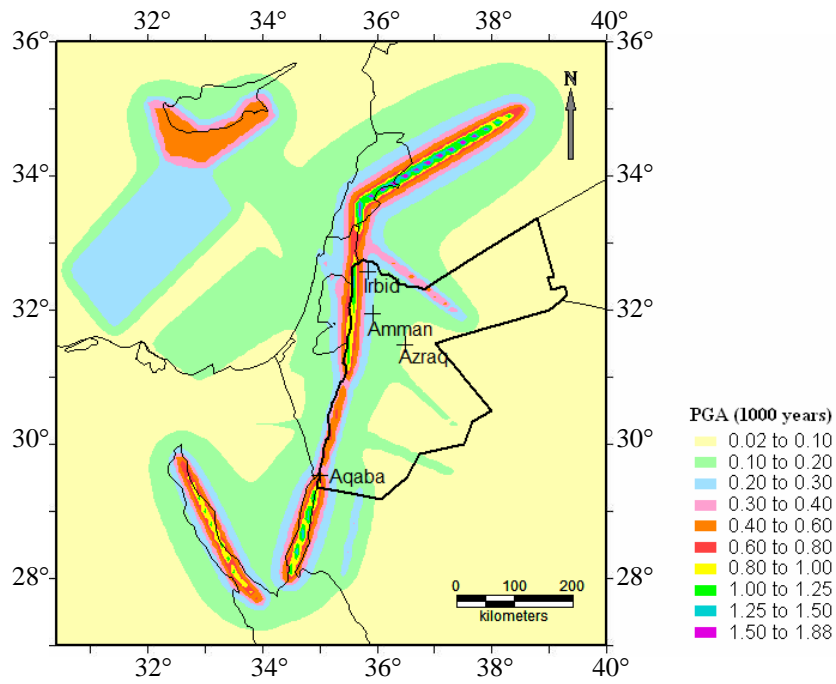


Figure C.8 Seismic Hazard Map Obtained from Model 3 for PGA at 5% Probability of Exceedance in 50 Years (1000 Years Return Period)

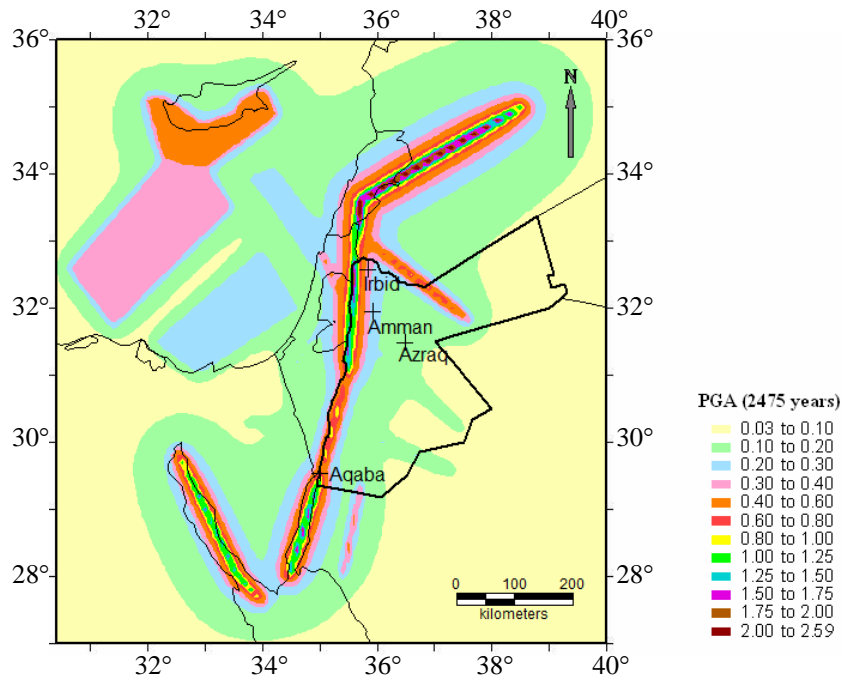


Figure C.9 Seismic Hazard Map Obtained from Model 3 for PGA at 2% Probability of Exceedance in 50 Years (2475 Years Return Period)

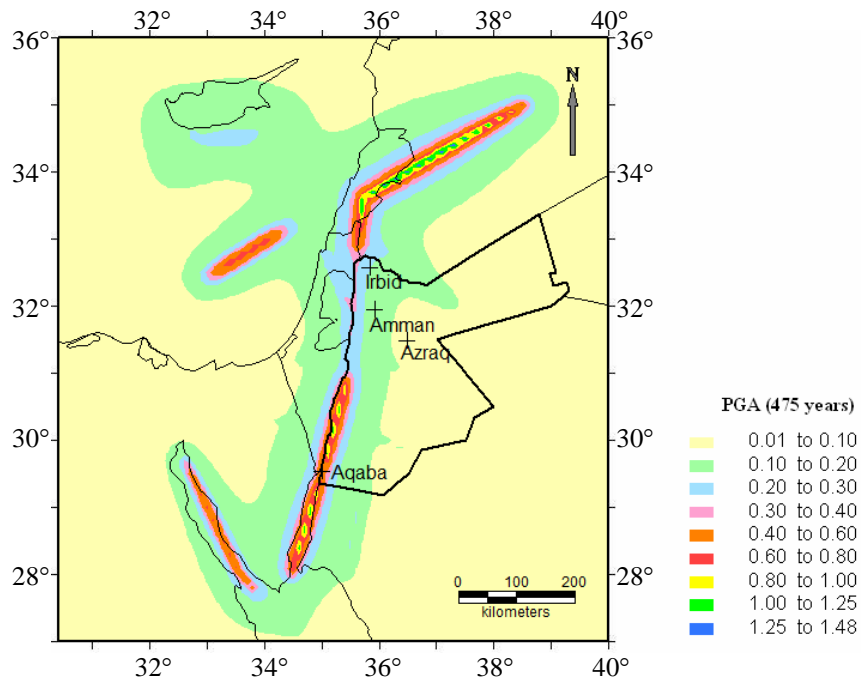


Figure C.10 Seismic Hazard Map Obtained from Model 4 for PGA at 10% Probability of Exceedance in 50 Years (475 Years Return Period)

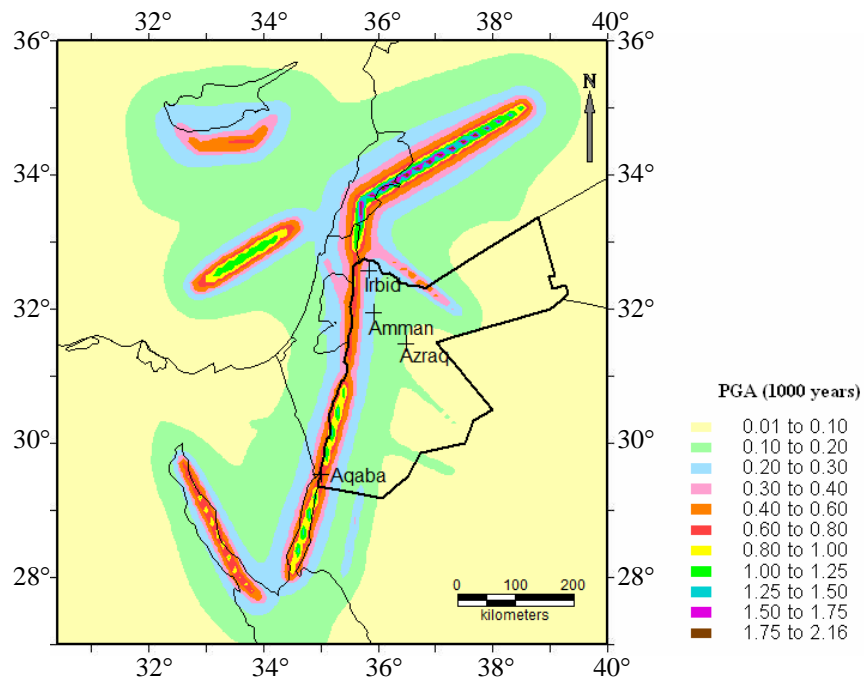


Figure C.11 Seismic Hazard Map Obtained from Model 4 for PGA at 5% Probability of Exceedance in 50 Years (1000 Years Return Period)

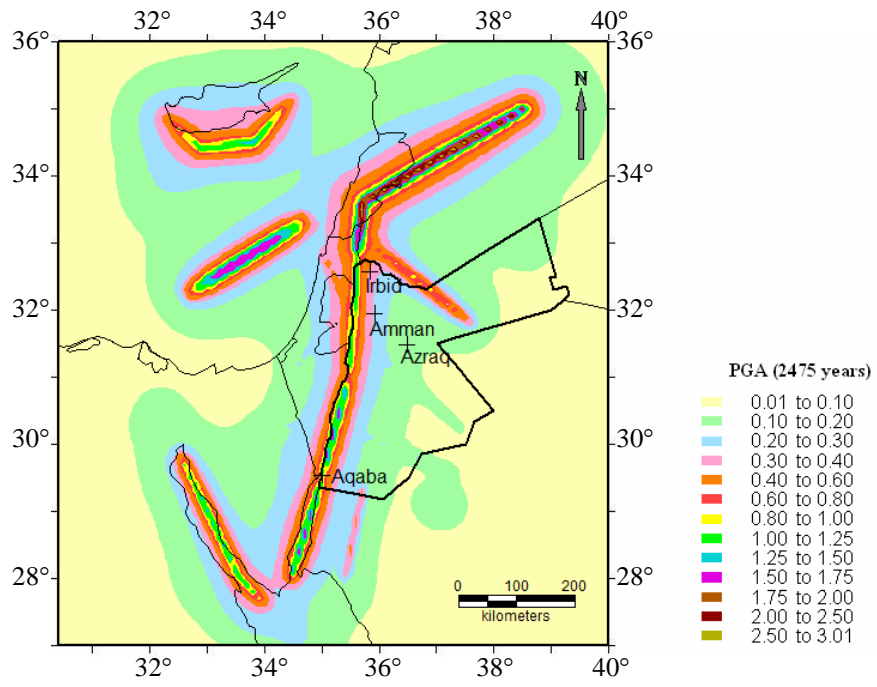


Figure C.12 Seismic Hazard Map Obtained from Model 4 for PGA at 2% Probability of Exceedance in 50 Years (2475 Years Return Period)

APPENDIX D

MAIN SEISMIC DATABASE COMPILED FOR BURSA FROM THE CATALOGS OF EARTHQUAKE RESEARCH DEPARTMENT, GENERAL DIRECTORATE OF DISASTER AFFAIRS

This seismic database contains earthquakes with moment magnitude (M_w) ≥ 4.5 occurred within the rectangular region bounded by 26.0°- 31.8° E longitudes and 38.8° - 42.0° N latitudes.

Table D.1 All Earthquakes in the Seismic Database Compiled for Bursa

No	Year	Month	Day	Longitude (Degree)	Latitude (Degree)	Depth (km)	$M_{w-(ave)}$
1	1901	5	12	30.5	39.8	15	5.5
2	1903	4	4	28	39	20	5.8
3	1905	1	11	27.9	39.6	15	5.5
4	1905	4	15	29	40.2	6	5.8
5	1905	4	30	30.5	39.8	22	5.7
6	1905	5	1	31.1	39.9		5.5
7	1905	10	22	31	41	27	5.6
8	1907	1	22	29	41	12	5.2
9	1907	8	21	30.1	40.7	15	5.8
10	1908	11	16	26.5	41.5	20	5.2
11	1912	8	9	27.2	40.6	16	6.8
12	1912	8	10	27.1	40.6	15	6.2
13	1912	8	10	27.1	40.6	15	5.7
14	1912	8	11	27.1	40.6	15	5.2
15	1912	8	11	27.2	40.6		5.5
16	1912	9	16	26.8	40.1		5.5
17	1912	10	21	27	40.5	15	5.2
18	1912	10	21	27	40.5	15	5.4
19	1914	3	22	26	40	15	5.2
20	1916	4	26	27	39.2	10	5.1
21	1917	4	10	27.1	40.6	15	5.7
22	1917	8	8	27	39	15	5.2

Table D.1 (Continued) All Earthquakes in the Seismic Database Compiled for Bursa

No	Year	Month	Day	Longitude (Degree)	Latitude (Degree)	Depth (km)	M _w (ave)
23	1917	12	27	26	40.5		5.5
24	1919	5	27	31.02	39.13	10	5.7
25	1919	10	13	28	41.5	12	5.2
26	1919	11	18	26.71	39.26	10	6.6
27	1920	1	9	26.2	41.8	20	5.6
28	1920	11	27	26.5	39.3	14	5.5
29	1921	7	24	26.5	38.8	22	5.6
30	1922	6	19	26	40.5		5.5
31	1923	5	29	30	41	25	5.8
32	1923	10	26	28.6	41.2	24	5.5
33	1924	1	22	28.4	39.51	80	5.7
34	1924	4	14	27.8	39	15	5.3
35	1924	12	22	27.7	39.6	15	5.7
36	1925	4	29	27.7	39.6	15	5.3
37	1925	6	10	29	41	8	5.2
38	1925	6	24	30.39	40.88	10	5.3
39	1925	9	14	31	39		5.5
40	1925	9	20	31	39		5.5
41	1926	11	13	26	39	20	5.1
42	1926	12	16	30.72	40.13	10	5.9
43	1926	12	20	31	39		5.5
44	1927	1	4	29.8	39.5	15	5.1
45	1928	1	24	30.86	40.99	10	5.7
46	1928	5	2	29.14	39.64	10	6.1
47	1928	5	3	26.8	40.8	4	5.1
48	1928	5	6	30.5	39.8	12	5.5
49	1929	4	5	31.23	41.61	10	5.4
50	1929	4	5	31.5	41.5	33	5.4
51	1929	4	27	31.43	40.51	70	5.4
52	1929	10	10	27.46	41.11	15	5.2
53	1931	7	12	26.34	39.15	10	5.7
54	1932	10	15	30.6	40.9	15	5.2
55	1933	2	5	31.5	41.5		5.2
56	1933	5	15	31.09	41.26	60	5.3
57	1934	7	14	26	39.5	10	5.1
58	1935	1	4	27.49	40.4	30	6.3
59	1935	1	4	27.65	40.12	12	5.3
60	1935	1	4	27.17	40.37	5	5.2
61	1935	1	4	27.45	40.3	20	6.2
62	1935	10	22	27.21	40.31	10	5.6
63	1938	7	2	27.88	40.17	10	5.5
64	1939	7	25	29.52	39.75	50	5.6
65	1939	7	31	29.6	39.8	10	5.4
66	1939	8	2	29.48	39.75	50	5.7
67	1939	8	3	29.68	39.75	50	5.8

Table D.1 (Continued) All Earthquakes in the Seismic Database Compiled for Bursa

No	Year	Month	Day	Longitude (Degree)	Latitude (Degree)	Depth (km)	M _w (ave)
68	1939	8	9	29.81	39.91	60	5.6
69	1939	9	15	29.56	39.76	20	5.9
70	1939	9	22	26.94	39.07	10	6.4
71	1939	10	19	29.5	39.82	10	5.7
72	1940	6	13	30.17	41.34	30	5.3
73	1940	8	19	30.09	40.13	40	5.2
74	1941	2	9	28.27	40.13	15	5.3
75	1942	2	5	29.8	38.9	17	5.7
76	1942	6	16	27.8	40.8	20	5.8
77	1942	8	12	27.64	39.13	50	5.4
78	1942	8	12	27.7	39.1	17	5.4
79	1942	10	28	28.19	39.27	10	5.7
80	1942	10	28	27.8	39.1	50	6
81	1942	10	28	27.79	39.46	10	5.8
82	1942	11	15	28.58	39.55	10	6.1
83	1943	4	14	29.64	39.62	40	5.5
84	1943	6	20	30.51	40.85	10	6.3
85	1943	6	20	30.73	40.84	10	5.8
86	1943	9	6	31.35	40.21	10	5.5
87	1943	9	8	30.4	40.7	5	5
88	1944	2	1	31.27	40.7	10	5.5
89	1944	2	2	31.44	40.74	40	5.6
90	1944	4	5	31.12	40.84	10	5.8
91	1944	6	25	29.55	38.97	57	5.8
92	1944	10	6	26.56	39.48	40	6.5
93	1944	10	6	26.5	39.3	18	5.5
94	1944	10	7	26.58	39.22	10	5.6
95	1945	2	9	31.2	40.5		5.5
96	1948	11	9	26.4	40.1	90	5.3
97	1948	11	13	29.02	40.23	60	5.8
98	1948	12	13	30	41	15	5.1
99	1949	1	4	27.9	38.9	14	5.2
100	1949	2	5	29.35	39.89	40	5.6
101	1949	11	28	30.9	40.6		5.3
102	1950	11	28	28.05	39.73	40	5.6
103	1951	3	12	31.8	42		5.3
104	1951	9	15	28.02	40.15	40	5.5
105	1952	1	22	30.4	40.8	15	5.1
106	1952	1	26	26.9	39.1	30	5.3
107	1952	3	13	28.14	41.02	11	5.5
108	1952	3	19	28.64	39.6	40	5.7
109	1953	3	18	27.36	39.99	10	6.7
110	1953	3	18	27.4	40	30	5.5
111	1953	3	18	27.83	40.02	10	5.3
112	1953	3	18	27.59	39.96	30	5.7

Table D.1 (Continued) All Earthquakes in the Seismic Database Compiled for Bursa

No	Year	Month	Day	Longitude (Degree)	Latitude (Degree)	Depth (km)	M _w (ave)
113	1953	3	18	27.4	40	30	5.4
114	1953	3	18	27.4	40		5.2
115	1953	3	19	27.3	40.1	48	5.4
116	1953	3	19	27.35	39.88	10	5.5
117	1953	3	22	27.3	40	26	5.1
118	1953	3	24	27.5	40	12	5.3
119	1953	3	26	27.48	39.94	10	5.3
120	1953	3	31	27.3	40.1	15	5.2
121	1953	4	1	27.45	39.97	20	5.7
122	1953	6	3	28.53	40.28	20	5.7
123	1953	6	9	28.21	39.34	20	5.3
124	1953	6	18	26.55	41.8	30	5.6
125	1953	7	22	28.43	39.24	10	5.6
126	1954	3	23	27.12	40.58	10	5.6
127	1954	10	24	27.53	40.46	10	5.4
128	1954	10	26	27.52	40.56	10	5.3
129	1956	1	6	26.29	40.39	10	5.8
130	1956	1	6	30.2	41	10	5.5
131	1956	2	20	30.49	39.89	40	6.3
132	1956	2	23	30.17	39.76	60	5.6
133	1956	7	14	30.9	40.32	40	5.3
134	1956	7	18	27.3	39.96	60	5.2
135	1956	8	28	29.93	41.08	80	5.3
136	1956	8	30	30.2	41	5	5
137	1956	11	20	26.4	39.36	70	5.7
138	1957	5	26	31	40.67	10	6.6
139	1957	5	26	30.74	40.6	40	5.7
140	1957	5	26	30.7	41.34	100	5.6
141	1957	5	26	31.09	41.42	10	5.5
142	1957	5	26	30.81	40.76	10	6
143	1957	5	27	31.19	41.14	80	5.1
144	1957	5	27	31.17	40.84	80	5.3
145	1957	5	27	30.65	41.13	70	5.3
146	1957	5	27	30.95	40.73	50	5.9
147	1957	5	28	30.53	40.58	50	5.4
148	1957	5	28	31.02	40.57	40	5.3
149	1957	5	29	31.04	40.72	20	5.3
150	1957	5	29	30.77	40.83	20	5.5
151	1957	5	30	31.78	40.62	10	5.1
152	1957	5	30	31.24	40.65	10	5.1
153	1957	6	1	30.86	40.75	50	5.5
154	1957	6	1	30.84	40.68	40	5.4
155	1957	6	2	30.78	40.71	10	5.4
156	1957	8	11	29.2	39.2		5.1
157	1957	10	11	28.19	39.32	10	5.5

Table D.1 (Continued) All Earthquakes in the Seismic Database Compiled for Bursa

No	Year	Month	Day	Longitude (Degree)	Latitude (Degree)	Depth (km)	M _w (ave)
158	1957	10	24	29.75	40.06	10	5.3
159	1957	12	26	29.72	40.83	10	5.6
160	1958	11	23	30.69	40.49	10	5.2
161	1959	4	2	29.41	40.5	20	5.3
162	1959	7	26	27.54	40.91	10	5.7
163	1959	8	6	29.2	40.4		5
164	1959	11	19	26.65	38.89	10	5.7
165	1960	3	6	26.5	41.3	22	5
166	1960	3	9	26.5	40.5		5
167	1961	3	28	30.19	39.82	10	5.5
168	1961	8	24	27.99	39.41	10	5.1
169	1961	11	28	26.1	39.99	80	5.6
170	1962	4	19	28.84	40.75	10	5.1
171	1962	9	14	28.17	39.57	40	5.2
172	1963	3	29	26.15	40.29	50	5.6
173	1963	4	28	27.82	39.32	30	5.3
174	1963	9	18	29.12	40.77	40	6.2
175	1963	9	24	28.9	40.84	10	5.4
176	1964	10	6	28.16	40.24	23	6
177	1964	10	6	28.23	40.3	34	7.4
178	1965	8	23	26.17	40.51	33	5.6
179	1966	8	21	27.4	40.33	12	4.7
180	1967	4	7	31	40		4.5
181	1967	7	22	30.69	40.67		7.4
182	1967	7	22	30.8	40.7	6	5.6
183	1967	7	22	30.53	40.73		4.7
184	1967	7	22	30.62	40.66	26	4.9
185	1967	7	22	30.51	40.72	35	5.3
186	1967	7	22	30.53	40.64	30	4.7
187	1967	7	22	30	41		4.8
188	1967	7	30	30.52	40.72	18	6
189	1968	2	19	26.4	39.8		5.6
190	1968	11	3	29.11	38.81	23	4.7
191	1969	3	3	27.5	40.08		6.5
192	1969	3	23	28.48	39.14	9	6.5
193	1969	3	24	28.51	39.11	30	5.1
194	1969	3	25	28.41	39.06	28	4.9
195	1969	3	25	28.44	39.25	37	6.2
196	1969	3	25	28	39		5.1
197	1969	3	25	28.49	39.17	34	4.7
198	1969	3	28	28.45	39.13	37	4.9
199	1969	4	30	28.52	39.12	8	5.1
200	1969	10	7	28.4	39.2	13	4.9
201	1969	10	7	28.54	39.16	49	4.9
202	1969	10	13	28.38	39.17	9	4.9

Table D.1 (Continued) All Earthquakes in the Seismic Database Compiled for Bursa

No	Year	Month	Day	Longitude (Degree)	Latitude (Degree)	Depth (km)	M _w -(ave)
203	1970	3	28	29.51	39.21	18	7.4
204	1970	3	28	29.46	39.28	17	4.7
205	1970	3	28	29.56	39.15	31	4.7
206	1970	3	28	29.76	39.07	32	5.1
207	1970	3	28	29.7	38.9		5.4
208	1970	3	28	30.3	39.5		5.6
209	1970	3	28	30.7	39.3		4.7
210	1970	3	28	30.7	39.5		4.5
211	1970	3	28	31.5	38.9		4.5
212	1970	3	28	31.1	39.5		4.5
213	1970	3	29	29.74	39.06	29	5.3
214	1970	3	30	29.26	39.34	16	5.3
215	1970	3	31	29.16	39.12	43	5.1
216	1970	3	31	30.1	39	15	4.5
217	1970	4	1	28.8	38.9	54	4.9
218	1970	4	1	29.27	39.32	35	4.7
219	1970	4	2	29.6	38.9	41	5.3
220	1970	4	4	30.3	38.9		4.6
221	1970	4	6	28.54	39.19	33	5.3
222	1970	4	7	29.61	39.07	33	6
223	1970	4	7	29.32	39.34	33	5.3
224	1970	4	16	29.91	39.02	31	6
225	1970	4	16	29.95	38.98	43	4.7
226	1970	4	19	29.76	39.03	18	6.2
227	1970	4	19	29.8	39.03	24	6
228	1970	4	19	30.9	40		5.2
229	1970	4	19	30.7	39.6		5.1
230	1970	4	19	30.7	39.6		5.6
231	1970	4	19	31	39.5		4.6
232	1970	4	20	31.5	39.9	256	5.8
233	1970	4	22	29.77	39.02	37	5.1
234	1970	4	23	30.01	38.94	32	4.9
235	1970	4	23	28.65	39.13	28	5.6
236	1970	4	24	29.85	39.01	32	4.7
237	1970	4	24	29.7	39.01	44	5.3
238	1970	4	27	29.58	38.96	33	4.7
239	1970	5	11	29.39	39.08		5.8
240	1970	5	14	29.1	39.02	38	5.3
241	1970	9	9	29.52	38.97		4.7
242	1970	12	20	29.24	39.36	26	5.1
243	1971	2	15	29.36	39.19	32	4.9
244	1971	2	23	27.32	39.62		5.1
245	1971	4	13	29.8	39.03	41	5.3
246	1971	5	25	29.71	39.05	16	6.7
247	1971	6	10	29.63	39.02	33	5.1

Table D.1 (Continued) All Earthquakes in the Seismic Database Compiled for Bursa

No	Year	Month	Day	Longitude (Degree)	Latitude (Degree)	Depth (km)	M _w (ave)
248	1971	11	6	29.78	39.02	16	5.1
249	1972	3	14	29.47	39.32	38	5.8
250	1972	4	26	26.36	39.43	18	5.1
251	1972	4	26	26.33	39.45	25	4.7
252	1972	5	28	30.04	38.96	29	4.7
253	1975	3	17	26.24	40.4	5	4.7
254	1975	3	17	26.08	40.48		5.1
255	1975	3	27	26.12	40.45		6.2
256	1976	5	8	29.1	39.33	33	4.7
257	1976	8	22	29.03	39.35	23	4.7
258	1978	6	15	27.68	40.79	28	4.6
259	1979	7	18	28.65	39.66	7	5.5
260	1980	8	2	27.42	38.93		5.8
261	1981	3	12	28.09	40.8		4.8
262	1981	12	26	28.74	40.15		4.9
263	1982	7	12	27.83	41	25	4.5
264	1982	12	26	28.26	39.32	5	4.9
265	1982	12	27	28.27	39.34	11	4.7
266	1983	2	1	28.94	40.2	3	4.7
267	1983	7	5	27.21	40.33	7	6.1
268	1983	10	21	29.35	40.14	12	5.3
269	1983	11	2	29.36	40.1	4	4.5
270	1983	11	6	29.32	39.33	14	4.6
271	1984	7	29	26	40.4	10	5
272	1985	3	29	26.57	38.8	26	4.7
273	1985	12	1	27.7	39.29	10	4.6
274	1985	12	18	26.17	39.2	17	5.3
275	1987	8	6	26.26	39.25	19	4.5
276	1988	4	24	28.24	40.88	11	5.3
277	1989	8	15	26.25	39.22	10	5.1
278	1991	2	12	28.82	40.8	10	5
279	1992	3	22	28.35	40.2	25	5
280	1993	3	31	28.04	39.14	2	4.5
281	1993	11	1	29.95	38.94	7	4.9
282	1993	12	12	28.79	41.55	28	4.9
283	1994	2	8	27.8	40.8	11	4.5
284	1995	4	13	27.65	40.85	27	4.5
285	1998	3	5	27.3	39.55	23	4.6
286	1999	7	24	27.98	39.31	10	4.6
287	1999	7	25	27.98	39.33	15.2	5.2
288	1999	8	17	29.96	40.76	17	7.3
289	1999	8	17	29.93	40.78	10	5.1
290	1999	8	17	29.11	40.68	7.4	5
291	1999	8	17	30.63	40.64	1.2	5.1
292	1999	8	17	30.06	40.78	11.3	5.1

Table D.1 (Continued) All Earthquakes in the Seismic Database Compiled for Bursa

No	Year	Month	Day	Longitude (Degree)	Latitude (Degree)	Depth (km)	M _w (ave)
293	1999	8	17	30.67	40.64	20.8	5.1
294	1999	8	17	30.41	40.69	12.6	4.7
295	1999	8	17	30.2	40.75	11	4.8
296	1999	8	17	31.09	40.72	10	5
297	1999	8	17	31.14	40.81	5.8	4.6
298	1999	8	19	30.66	40.61	10	4.6
299	1999	8	19	29.15	40.6	3.1	4.5
300	1999	8	19	29.14	40.63	12	5.1
301	1999	8	20	29.13	40.62	9.8	4.5
302	1999	8	22	30.7	40.69	13.9	4.8
303	1999	8	26	30.02	40.74	10	4.7
304	1999	8	31	29.13	40.56	10.4	4.5
305	1999	8	31	29.94	40.76	4	5.6
306	1999	8	31	29.95	40.73	5.9	4.6
307	1999	9	13	30.08	40.75	10.4	6.2
308	1999	9	18	29.21	40.6	9.5	4.7
309	1999	9	20	27.58	40.67	14.6	4.9
310	1999	9	29	29.33	40.74	12.2	5.1
311	1999	10	20	29.03	40.83	6.6	4.9
312	1999	11	7	30.72	40.7	7.4	4.9
313	1999	11	11	30.25	40.75	7.5	5.9
314	1999	11	12	31.25	40.87	9.6	5
315	1999	11	12	31.47	40.87	16.2	5
316	1999	11	12	31.19	40.81	10.4	7.3
317	1999	11	12	31.08	40.75	27.8	5.6
318	1999	11	12	31.47	40.7	11	5.1
319	1999	11	13	31.02	40.77	5.2	5.1
320	1999	11	16	31.59	40.73	5	5.2
321	1999	11	17	31.49	40.83	7	4.8
322	1999	11	19	31.02	40.83	5.3	4.9
323	2000	2	14	31.76	41.02	10	5.2
324	2000	8	23	30.72	40.68	15	6.4
325	2000	9	8	27.7	39.36	10	4.7
326	2001	6	22	27.91	39.31	10	5.2
327	2001	6	23	27.88	39.47	10	4.7
328	2001	8	26	31.57	40.95	7	5.7
329	2002	3	23	27.85	40.74	11.1	4.8
330	2002	3	23	28.81	39.49	1	4.8
331	2003	3	20	28.67	39.99	6.1	4.5
332	2003	6	9	27.91	40.17	13.9	5.2
333	2003	6	22	27.98	39.01	5.6	4.7
334	2003	7	6	26.25	40.49	11.6	5.5
335	2003	7	6	26.01	40.53	5.2	4.8
336	2003	12	16	26.74	38.88	11.2	4.7
337	2003	12	23	29.28	39.88	10.5	4.5

Table D.1 (Continued) All Earthquakes in the Seismic Database Compiled for Bursa

No	Year	Month	Day	Longitude (Degree)	Latitude (Degree)	Depth (km)	M_w(ave)
338	2004	6	27	26.01	40.9	10	4.6
339	2005	5	15	30.8254	39.6061	21.1	4.6
340	2005	12	24	27.7826	38.8446	6	4.6
341	2006	2	8	30.412	40.7082	6.8	4.5
342	2006	10	20	27.9792	40.2519	16.7	5.5
343	2006	10	24	28.9937	40.4221	7.9	5.3

APPENDIX E

MAIN SHOCK SEISMIC DATABASE COMPILED FOR BURSA FROM THE CATALOGS OF EARTHQUAKE RESEARCH DEPARTMENT, GENERAL DIRECTORATE OF DISASTER AFFAIRS

This seismic database contains only the main shocks that occurred within the rectangular region bounded by 26.0°- 31.8° E longitudes and 38.8°- 42.0° N latitudes.

Table E.1 Mainshocks in the Seismic Database Compiled for Bursa

No	Year	Month	Day	Longitude (Degree)	Latitude (Degree)	Depth (km)	M _w -(ave)
1	1901	5	12	30.5	39.8	15	5.5
2	1903	4	4	28	39	20	5.8
3	1905	1	11	27.9	39.6	15	5.5
4	1905	4	15	29	40.2	6	5.8
5	1905	4	30	30.5	39.8	22	5.7
6	1905	10	22	31	41	27	5.6
7	1907	1	22	29	41	12	5.2
8	1907	8	21	30.1	40.7	15	5.8
9	1908	11	16	26.5	41.5	20	5.2
10	1912	8	9	27.2	40.6	16	6.8
11	1912	8	10	27.1	40.6	15	6.2
12	1914	3	22	26	40	15	5.2
13	1916	4	26	27	39.2	10	5.1
14	1917	4	10	27.1	40.6	15	5.7
15	1917	8	8	27	39	15	5.2
16	1917	12	27	26	40.5		5.5
17	1919	5	27	31.02	39.13	10	5.7
18	1919	10	13	28	41.5	12	5.2
19	1919	11	18	26.71	39.26	10	6.6
20	1920	1	9	26.2	41.8	20	5.6
21	1921	7	24	26.5	38.8	22	5.6
22	1922	6	19	26	40.5		5.5

Table E.1 (Continued) Mainshocks in the Seismic Database Compiled for Bursa

No	Year	Month	Day	Longitude (Degree)	Latitude (Degree)	Depth (km)	M _w -(ave)
23	1923	5	29	30	41	25	5.8
24	1923	10	26	28.6	41.2	24	5.5
25	1924	1	22	28.4	39.51	80	5.7
26	1924	4	14	27.8	39	15	5.3
27	1924	12	22	27.7	39.6	15	5.7
28	1925	6	10	29	41	8	5.2
29	1925	6	24	30.39	40.88	10	5.3
30	1925	9	14	31	39		5.5
31	1926	11	13	26	39	20	5.1
32	1926	12	16	30.72	40.13	10	5.9
33	1926	12	20	31	39		5.5
34	1927	1	4	29.8	39.5	15	5.1
35	1928	1	24	30.86	40.99	10	5.7
36	1928	5	2	29.14	39.64	10	6.1
37	1928	5	3	26.8	40.8	4	5.1
38	1928	5	6	30.5	39.8	12	5.5
39	1929	4	5	31.23	41.61	10	5.4
40	1929	4	27	31.43	40.51	70	5.4
41	1929	10	10	27.46	41.11	15	5.2
42	1931	7	12	26.34	39.15	10	5.7
43	1932	10	15	30.6	40.9	15	5.2
44	1933	5	15	31.09	41.26	60	5.3
45	1934	7	14	26	39.5	10	5.1
46	1935	1	4	27.49	40.4	30	6.3
47	1935	1	4	27.45	40.3	20	6.2
48	1938	7	2	27.88	40.17	10	5.5
49	1939	9	15	29.56	39.76	20	5.9
50	1939	9	22	26.94	39.07	10	6.4
51	1940	6	13	30.17	41.34	30	5.3
52	1940	8	19	30.09	40.13	40	5.2
53	1941	2	9	28.27	40.13	15	5.3
54	1942	2	5	29.8	38.9	17	5.7
55	1942	6	16	27.8	40.8	20	5.8
56	1942	10	28	27.8	39.1	50	6
57	1942	11	15	28.58	39.55	10	6.1
58	1943	4	14	29.64	39.62	40	5.5
59	1943	6	20	30.51	40.85	10	6.3
60	1943	9	6	31.35	40.21	10	5.5
61	1944	4	5	31.12	40.84	10	5.8
62	1944	6	25	29.55	38.97	57	5.8
63	1944	10	6	26.56	39.48	40	6.5
64	1945	2	9	31.2	40.5		5.5
65	1948	11	9	26.4	40.1	90	5.3
66	1948	11	13	29.02	40.23	60	5.8
67	1948	12	13	30	41	15	5.1

Table E.1 (Continued) Mainshocks in the Seismic Database Compiled for Bursa

No	Year	Month	Day	Longitude (Degree)	Latitude (Degree)	Depth (km)	M _w -(ave)
68	1949	1	4	27.9	38.9	14	5.2
69	1949	11	28	30.9	40.6		5.3
70	1950	11	28	28.05	39.73	40	5.6
71	1951	3	12	31.8	42		5.3
72	1951	9	15	28.02	40.15	40	5.5
73	1952	1	22	30.4	40.8	15	5.1
74	1952	1	26	26.9	39.1	30	5.3
75	1952	3	13	28.14	41.02	11	5.5
76	1952	3	19	28.64	39.6	40	5.7
77	1953	3	18	27.36	39.99	10	6.7
78	1953	6	3	28.53	40.28	20	5.7
79	1953	6	18	26.55	41.8	30	5.6
80	1953	7	22	28.43	39.24	10	5.6
81	1956	1	6	26.29	40.39	10	5.8
82	1956	1	6	30.2	41	10	5.5
83	1956	2	20	30.49	39.89	40	6.3
84	1956	7	18	27.3	39.96	60	5.2
85	1956	8	28	29.93	41.08	80	5.3
86	1956	11	20	26.4	39.36	70	5.7
87	1957	5	26	31	40.67	10	6.6
88	1957	5	26	31.09	41.42	10	5.5
89	1957	5	26	30.81	40.76	10	6
90	1957	8	11	29.2	39.2		5.1
91	1957	10	11	28.19	39.32	10	5.5
92	1957	10	24	29.75	40.06	10	5.3
93	1957	12	26	29.72	40.83	10	5.6
94	1959	4	2	29.41	40.5	20	5.3
95	1959	7	26	27.54	40.91	10	5.7
96	1959	11	19	26.65	38.89	10	5.7
97	1960	3	6	26.5	41.3	22	5
98	1960	3	9	26.5	40.5		5
99	1961	3	28	30.19	39.82	10	5.5
100	1961	8	24	27.99	39.41	10	5.1
101	1961	11	28	26.1	39.99	80	5.6
102	1962	4	19	28.84	40.75	10	5.1
103	1962	9	14	28.17	39.57	40	5.2
104	1963	3	29	26.15	40.29	50	5.6
105	1963	4	28	27.82	39.32	30	5.3
106	1963	9	18	29.12	40.77	40	6.2
107	1964	10	6	28.16	40.24	23	6
108	1964	10	6	28.23	40.3	34	7.4
109	1965	8	23	26.17	40.51	33	5.6
110	1967	4	7	31	40		4.5
111	1967	7	22	30.69	40.67		7.4
112	1967	7	30	30.52	40.72	18	6

Table E.1 (Continued) Mainshocks in the Seismic Database Compiled for Bursa

No	Year	Month	Day	Longitude (Degree)	Latitude (Degree)	Depth (km)	M _w -(ave)
113	1968	2	19	26.4	39.8		5.6
114	1968	11	3	29.11	38.81	23	4.7
115	1969	3	3	27.5	40.08		6.5
116	1969	3	23	28.48	39.14	9	6.5
117	1969	3	25	28.44	39.25	37	6.2
118	1970	3	28	29.51	39.21	18	7.4
119	1970	3	28	31.5	38.9		4.5
120	1970	4	7	29.61	39.07	33	6
121	1970	4	16	29.91	39.02	31	6
122	1970	4	19	29.76	39.03	18	6.2
123	1970	4	19	29.8	39.03	24	6
124	1970	4	19	31	39.5		4.6
125	1971	2	23	27.32	39.62		5.1
126	1971	5	25	29.71	39.05	16	6.7
127	1972	4	26	26.36	39.43	18	5.1
128	1975	3	27	26.12	40.45		6.2
129	1976	5	8	29.1	39.33	33	4.7
130	1976	8	22	29.03	39.35	23	4.7
131	1978	6	15	27.68	40.79	28	4.6
132	1979	7	18	28.65	39.66	7	5.5
133	1980	8	2	27.42	38.93		5.8
134	1981	3	12	28.09	40.8		4.8
135	1981	12	26	28.74	40.15		4.9
136	1982	7	12	27.83	41	25	4.5
137	1982	12	26	28.26	39.32	5	4.9
138	1983	2	1	28.94	40.2	3	4.7
139	1983	7	5	27.21	40.33	7	6.1
140	1983	10	21	29.35	40.14	12	5.3
141	1983	11	6	29.32	39.33	14	4.6
142	1984	7	29	26	40.4	10	5
143	1985	3	29	26.57	38.8	26	4.7
144	1985	12	1	27.7	39.29	10	4.6
145	1985	12	18	26.17	39.2	17	5.3
146	1987	8	6	26.26	39.25	19	4.5
147	1988	4	24	28.24	40.88	11	5.3
148	1989	8	15	26.25	39.22	10	5.1
149	1991	2	12	28.82	40.8	10	5
150	1992	3	22	28.35	40.2	25	5
151	1993	3	31	28.04	39.14	2	4.5
152	1993	11	1	29.95	38.94	7	4.9
153	1993	12	12	28.79	41.55	28	4.9
154	1994	2	8	27.8	40.8	11	4.5
155	1995	4	13	27.65	40.85	27	4.5
156	1998	3	5	27.3	39.55	23	4.6
157	1999	7	25	27.98	39.33	15.2	5.2

Table E.1 (Continued) Mainshocks in the Seismic Database Compiled for Bursa

No	Year	Month	Day	Longitude (Degree)	Latitude (Degree)	Depth (km)	M _{w-(ave)}
158	1999	8	17	29.96	40.76	17	7.3
159	1999	9	13	30.08	40.75	10.4	6.2
160	1999	9	20	27.58	40.67	14.6	4.9
161	1999	11	12	31.19	40.81	10.4	7.3
162	2000	8	23	30.72	40.68	15	6.4
163	2000	9	8	27.7	39.36	10	4.7
164	2001	6	22	27.91	39.31	10	5.2
165	2002	3	23	27.85	40.74	11.1	4.8
166	2002	3	23	28.81	39.49	1	4.8
167	2003	3	20	28.67	39.99	6.1	4.5
168	2003	6	9	27.91	40.17	13.9	5.2
169	2003	6	22	27.98	39.01	5.6	4.7
170	2003	7	6	26.25	40.49	11.6	5.5
171	2003	12	16	26.74	38.88	11.2	4.7
172	2003	12	23	29.28	39.88	10.5	4.5
173	2004	6	27	26.01	40.9	10	4.6
174	2005	5	15	30.8254	39.6061	21.1	4.6
175	2005	12	24	27.7826	38.8446	6	4.6
176	2006	2	8	30.412	40.7082	6.8	4.5
177	2006	10	20	27.9792	40.2519	16.7	5.5
178	2006	10	24	28.9937	40.4221	7.9	5.3

CURRICULUM VITAE

PERSONAL INFORMATION

Surname, Name: Yılmaz Öztürk, Nazan

Nationality: Turkish (TC)

Date and Place of Birth: 10 October 1976, Samsun

Phone: +90 312 287 26 80/1549

email: nazany@deprem.gov.tr

EDUCATION

Degree	Institution	Year of Graduation
PhD	METU Civil Engineering	2008
MS	METU Civil Engineering	2001
BS	METU Civil Engineering	1998
High School	Samsun Ondokuzmayıs High School	1993

WORK EXPERIENCE

Year	Place	Enrollment
2006-present	Earthquake Research Department, General Directorate of Disaster Affairs, Ministry of Public Works and Settlement	Civil Engineer
2005-2006	Technical Department, General Directorate of Construction Affairs, Ministry of Public Works and Settlement	Civil Engineer
1998-2005	Civil Engineering Department, Middle East Technical University	Research Assistant

PUBLICATIONS

1. Yılmaz Öztürk N. and Yüçemen M. S. (2007). Comparison of Probabilistic and Deterministic Seismic Hazard Analysis Procedures, (in Turkish) *Structural Mechanics Seminar 2007*, Eskişehir, November 02.
2. Yüçemen M. S. and Yılmaz N. (2006). Comparison of Different Magnitude Recurrence and Earthquake Occurrence Models Used In Seismic Hazard Analysis, *Seventh International Congress on Advances in Civil Engineering*, İstanbul, Turkey, October 11-13.
3. Yüçemen M. S., Öztürk N. Y., and Deniz A. (2006). Probabilistic Seismic Loss Estimation for Eskişehir, Turkey, *2006 ECI Conference on Geohazards*, Farrokh Nadim, Rudolf Pöttler, Herbert Einstein, Herbert Klapperich, and Steven Kramer Eds, , Vol. P7.
4. Yüçemen M. S., Öztürk N. Y., Deniz A., Muaz S. M. H. (2005). Assessment of Seismic Hazard for Jordan, *Proceeding, The International Earthquake Engineering Conference*, Dead Sea, Jordan, November 21-24.
5. Yılmaz N., Yüçemen M. S. (2005). A Comparison of Stochastic Models Used in Seismic Hazard Analysis: A Case Study, *International Conference on Earthquake Engineering in the 21st Century*, CD-ROM, Skopje-Ohrid, Macedonia, August 27-September 1.
6. Yakut A., Yılmaz N., Bayılı S. (2003). Analytical Assessment of Seismic Capacity of RC Frame Buildings, *International Conference on Earthquake Engineering to Mark 40 Years from the Catastrophic 1963 Skopje Earthquake and Successful City Reconstruction, SE40EE*, CD-ROM, Skopje-Ohrid, Macedonia, August 26-29.
7. Öztürk N.Y. (2001). *Minimum Flexural Reinforcement Requirement of High Strength Concrete T-Beams with Flange in Tension*, MSc Thesis, Department of Civil Engineering, Middle East Technical University, Ankara, Turkey, December.

8. Yılmaz N., Ersoy U., Özcebe G. (2001). Minimum Flexural Reinforcement Requirement of High Strength Concrete T-Beams with Flange in Tension, (in Turkish), *I. Structural Mechanics Laboratories Meeting*, The Scientific and Technological Research Council of Turkey, Ankara, November.